TSINGHUA-PRINCETON-COMBUSTION INSTITUTE

2021 SUMMER SCHOOL ON COMBUSTION

Combustion Dynamics and Unsteady Combustion

Sébastien M. Candel

CentraleSupélec, University Paris-Saclay

July 11−17, 2021

Combustion Dynamics and Unsteady Combustion

Sébastien M. Candel

CentraleSupélec, University Paris-Saclay

July 11-17, 2021

Tsinghua-Princeton-Combustion Institute

2021 Summer School on Combustion

Contents

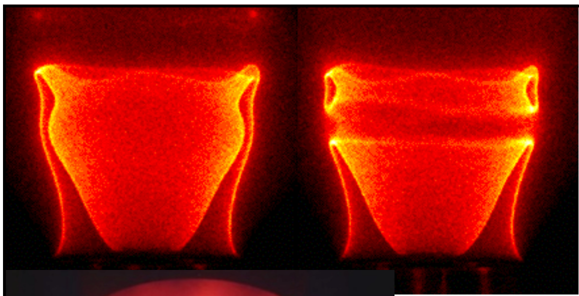

Combustion dynamics
Lecture 1a

S. Candel, D. Durox , T. Schuller

CentraleSupélec
Université Paris-Saclay, EM2C lab, CNRS

Tsinguha summer school, July 2021

1

Introductory comments

- Many thanks to Ed law for inviting me to give this course in this electronic setting. It is a pleasure to share ideas and some of our research with you
- The focus is on combustion dynamics with special attention to swirling flames and annular systems dynamics which are important for gas turbines. We'll try to cover fundamentals and practical applications
- Thanks to Nicolas Noiray, Paul Palies, Frédéric Boudy, Jean-François Bourgouin, Jonas Moeck, Kevin Prieur, Guillaume Vignat, Antoine Renaud and Davide Laera for their many contributions

2

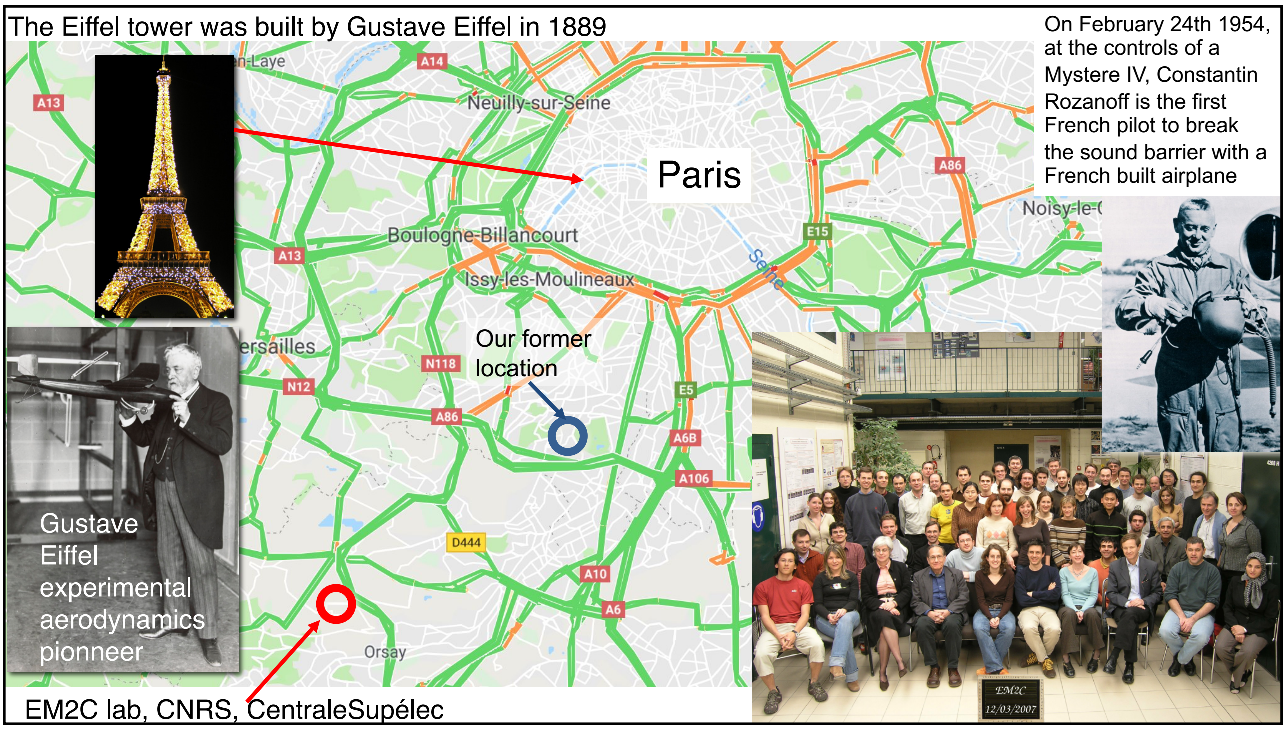

The beginnings of aeronautics

December 17, 1903 First motored flight of the Wright brothers Orville and Wilbur Wright at Kitty Hawk (North Carolina)

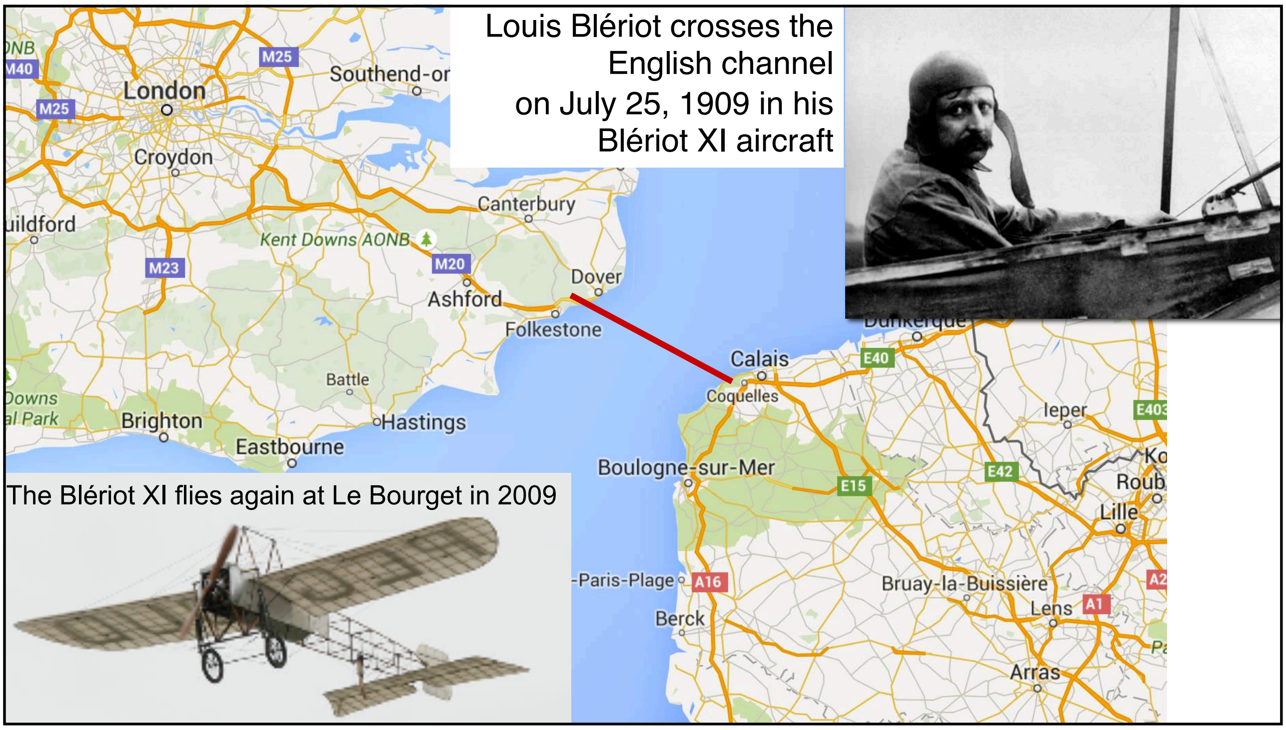

5

Contents

General introduction
Fundamental acoustics
Acoustics of reactive flows
Combustion noise

Simple instability model
Unified framework for combustion instability analysis
Sensitive time lag theory

Perturbed flames
Transfer function and describing function principles
Combustion control

Swirling flame dynamics

Chamber acoustics and modal identification
Annular combustion dynamics
Spinning and standing mode coupling

Computational flame dynamics (CFD)
Ignition dynamics

6

General introduction and background

- Introductory comments
- A few examples
- Why is combustion so susceptible to instabilities?
- Classification
- Combustion dynamics timeline
- Objectives

Thermo-acoustic instabilities

New technologies promote acoustic coupling problems

High pressure	Increased efficiency	High energy densities
Compact design	Gain in weight	Less well damped
Lean combustion	Low NOx	Stabilization issues

- Domestic boilers ~ 10 kW_{th}

- Process heaters ~ 1 MW_{th}

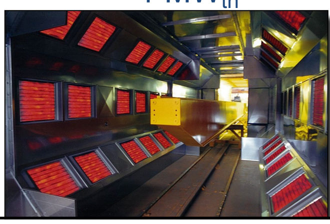

- Gas turbines ~ 100 MW_{th}

- Powerplants ~ 1 GW_{th}

Combustion instability mechanism

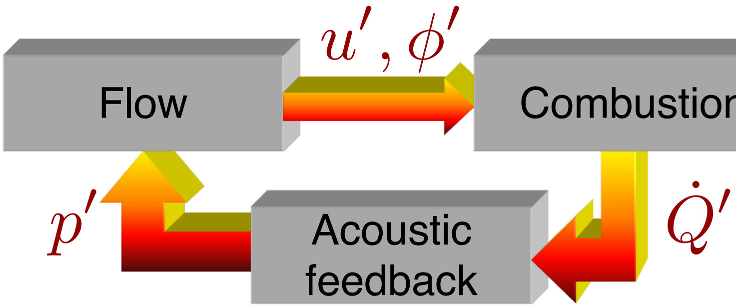

- Production of a flow perturbation
- This induces a combustion perturbation
- Acoustic feedback links the unsteady combustion process to flow perturbation
- The system is unstable if gain exceeds damping

9

Case 1

Domestic boiler

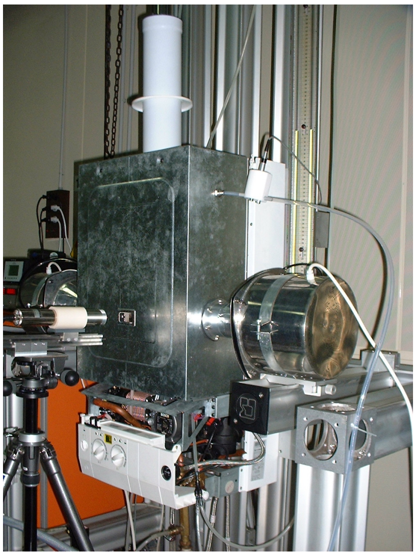

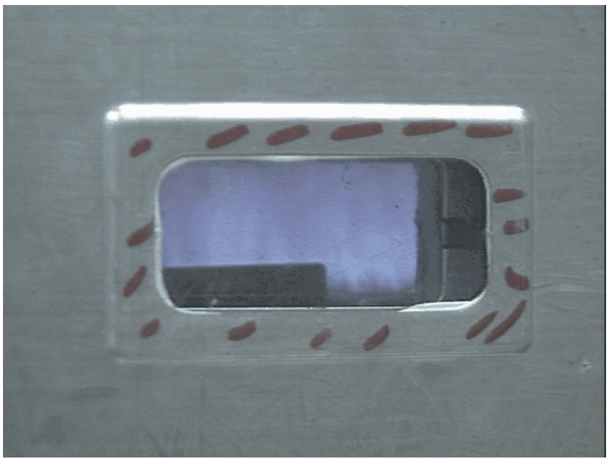

During unstable operation, lateral walls of this boiler are "breathing" highlighting large pressure oscillations within the system

10

Case 2 Combustion dynamics issues in gas turbines

Combustion dynamics degrades operation of many practical systems and in extreme cases leads to failure

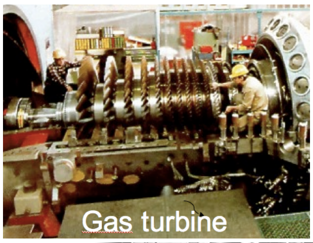

Challenges
(1) Gain an understanding of the processes driving and coupling combustion instabilities
(2) Develop models for the nonlinear dynamics observed in practice : limit cycles, triggering, mode switching, hysteresis…
(3) Derive predictive analytical and numerical tools for combustion dynamics
(4) Design novel instability control systems (passive, dynamical, active)

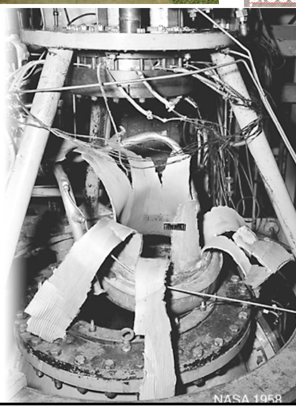

Liquid rocket engine after HF instability

Case 2 Combustion dynamics in modern gas turbines

Difficulties are related to the reduced stability of lean premixed combustors that are now widely used in gas turbines

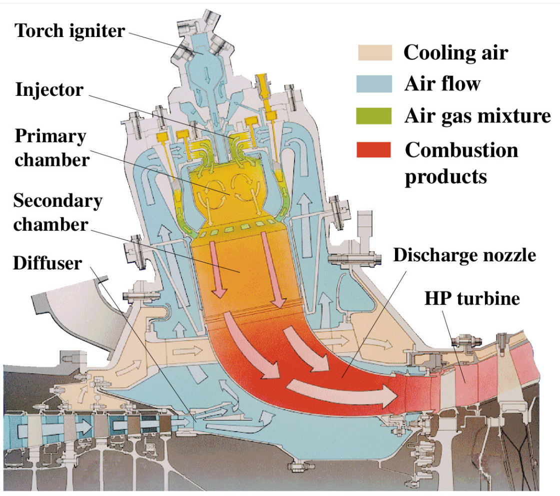

Premixed gas turbine combustor

Analysis
must take into account physical and geometrical complexities including
(1) A turbulent swirling flame,
(2) Resonant acoustic characteristics of the system,
(3) Reduced damping rates
(4) Complicated boundary conditions

Combustion dynamics issues in gas turbines

Lean premixed combustion generates low levels of NOx but is susceptible to pressure coupling and instability

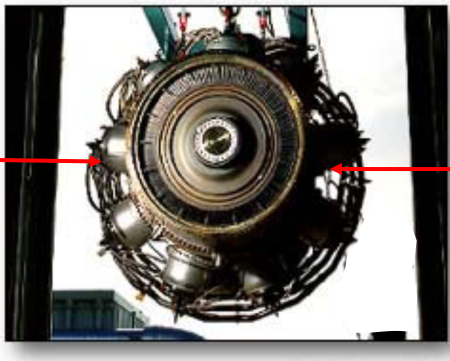

Predictive tools are needed to design stable combustors. Such tools are not available but their development is an objective for the future

Numerical simulation of instabilities has to deal with complex swirling injection configurations, turbulent flows, acoustic flame coupling, dynamics of upstream and downstream components

13

Thermoacoustic interactions in gas turbine combustors

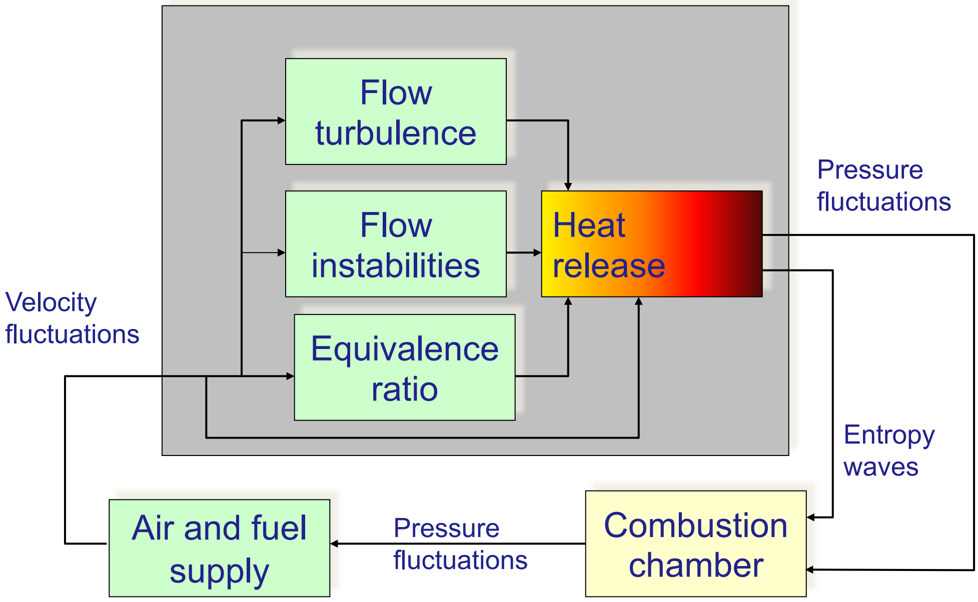

Adapted from Paschereit et al (1998)

14

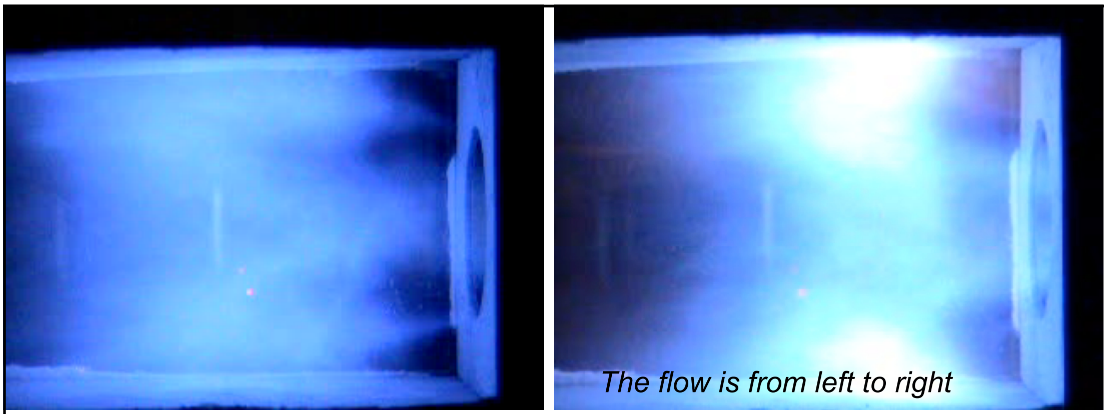

Case 3

Multipoint injection swirled burner

Barbosa, Scouflaire, Ducruix

Stable regime: the combustion zone (luminous region) features small stochastic fluctuations around its mean location due to turbulence. Radiated noise remains weak and broadband : “combustion roar”.

Unstable regime : Large synchronized motions with a strong harmonic content. Intensification of luminosity near the wall : enhanced heat fluxes to the boundaries. Oscillations induce flame flashback.

15

Basic interactions leading to combustion instabilities

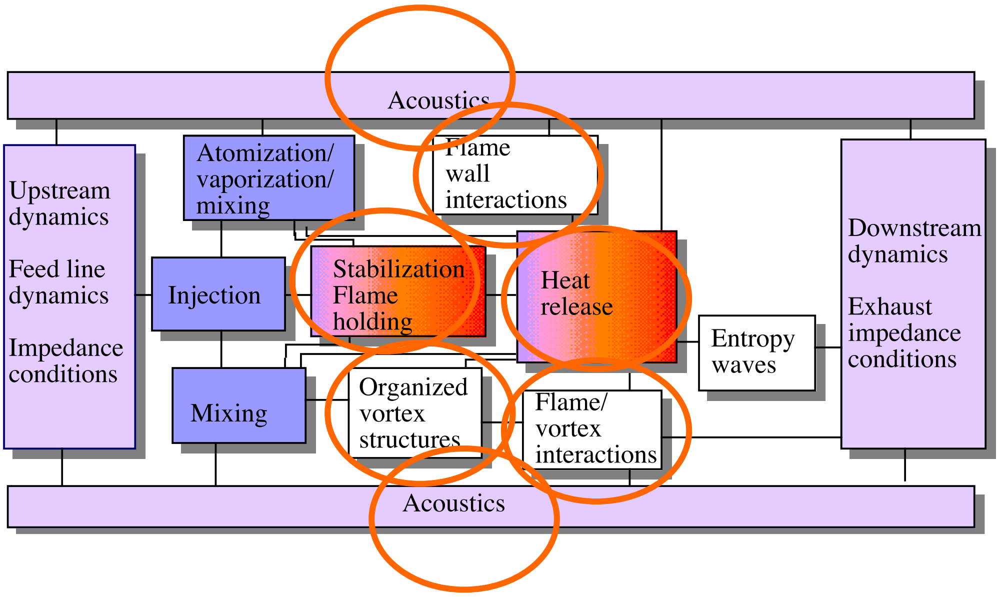

16

Organ pipe instabilities

Stable regime

Unstable regime

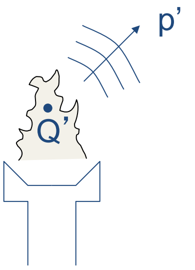

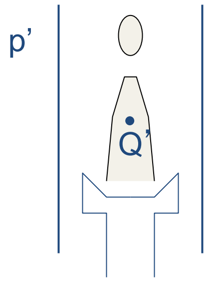

Turbulent fluctuations
Small amplitudes
Broadband noise
Combustion noise

High amplitude self-sustained cyclic oscillation. The frequency depends on:

- the flame position within the tube
- the tube length
- the boundary conditions

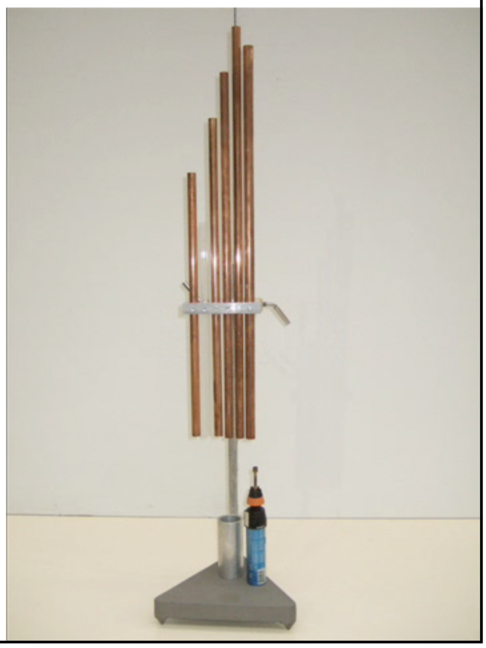

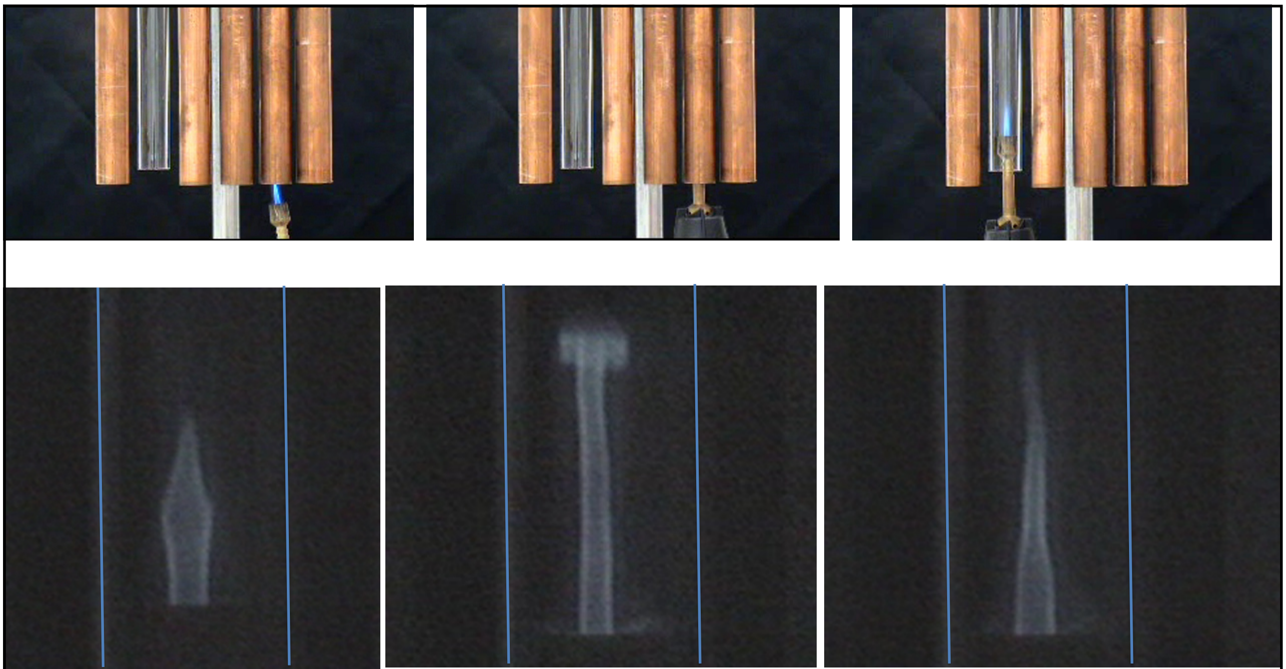

Flame dynamics in the Rijke tube

Case 4

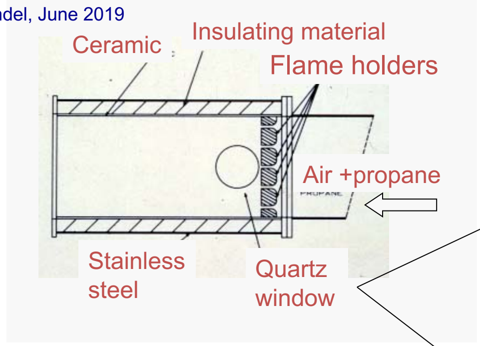

Stable operation

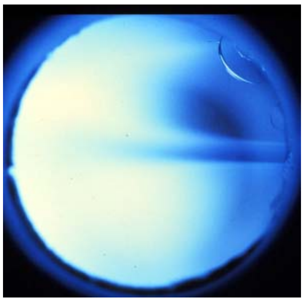

Unstable operation

Vortex driven instabilities in a premixed combustor (f=530 Hz)

T. Poinsot, A. Trouvé, D. Veynante, S.M. Candel and E. Esposito (1987) *Journal of Fluid Mechanics* **177**, 265-292. Vortex driven acoustically coupled combustion instabilities.

19

©Sebastien Candel, June 2019

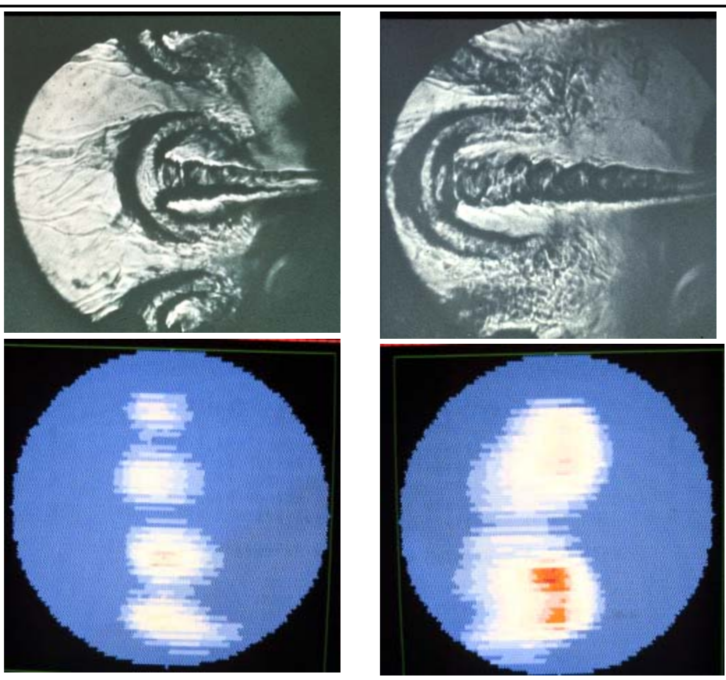

time t 1time t_1 time t 2time t_2

Schlieren images of the unsteady flow (flow from right to left)

Heat release rate distribution images (C_2 radical emission)

T. Poinsot, A. Trouvé, D. Veynante, S.M. Candel and E. Esposito (1987) *Journal of Fluid Mechanics* **177**, 265-292. Vortex driven acoustically coupled combustion instabilities.

20

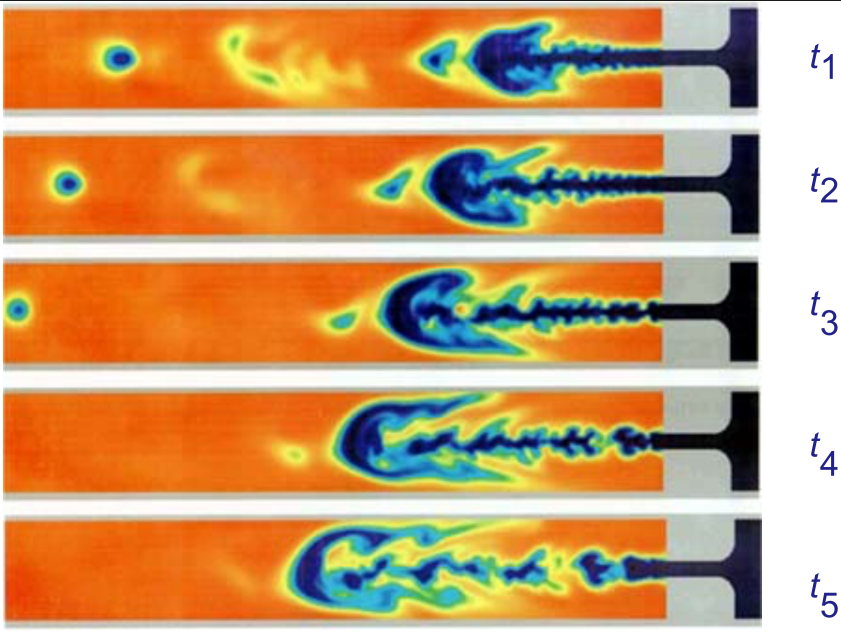

Numerical simulation of vortex driven instability. Flow from left to right (flame is thickened, flow is forced at the oscillation frequency f=530 Hz)

Angelberger et al (1999, 2001)

21

Experiment schlieren image of the flow (Poinsot et al. 1987)

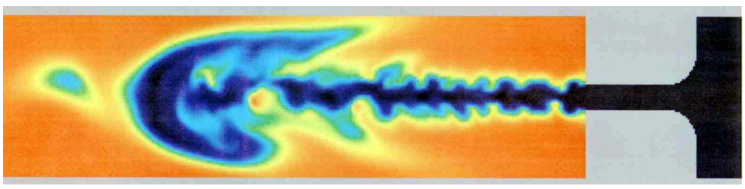

Simulation : temperature distribution

Vortex driven combustion instability

22

Turbulent flame response to acoustic waves

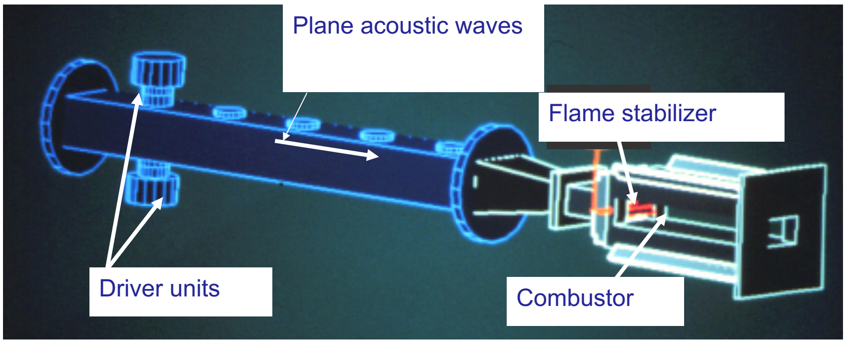

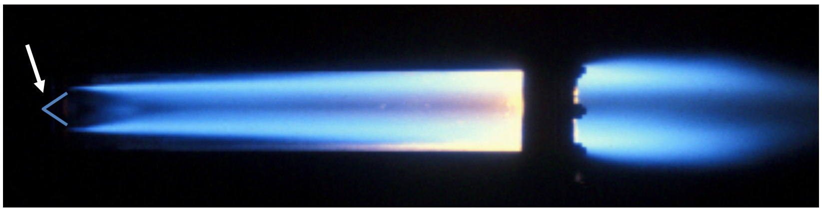

Turbulent premixed propane/air flame

23

Air/propane

Air/propane

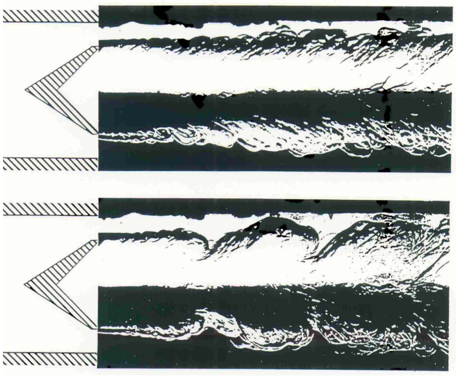

No acoustic modulation

With acoustic modulation
f=1210 Hz

K. Yu, A. Trouvé and S.M. Candel (1991) Combustion enhancement of a premixed flame by acoustic forcing with emphasis on role of large scale vortical structures. *AIAA Paper 91-0367. Aerospace Science Meeting*, Reno, Jan. 1991

Schlieren images of premixed turbulent ducted flame

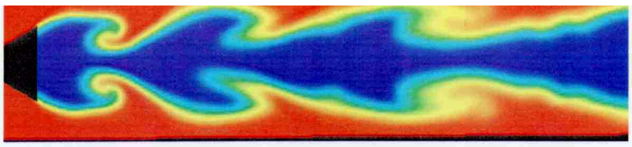

Computation
(C. Nottin, 1999)

Fuel mass fraction (external acoustic modulation)

24

Acoustically coupled combustion instabilities *(thermo-acoustic instabilities)*

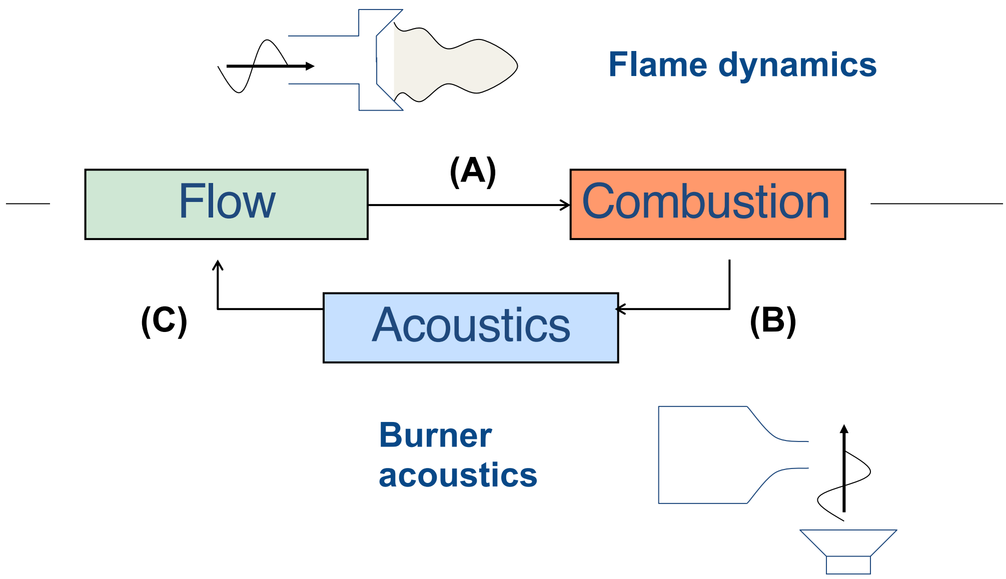

25

Why is combustion so succeptible to instabilities ? Some standard reasons :

(1) The power density associated with combustion is sizable.
A small fraction of this power is sufficient to drive the oscillations

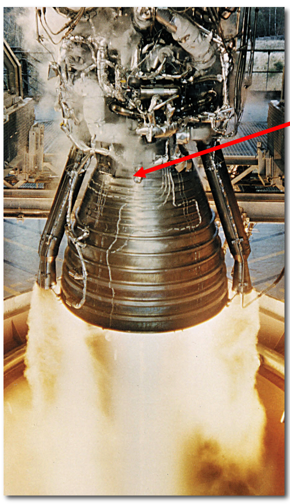

Vulcain engine (Ariane 5)

Power level : 2.5 GW

Power Density : $E_c \simeq 50\,\mathrm{GW\ m}^{-3}$

A fluctuation of 20% in pressure (about 2 MPa) corresponds to a power density

$$E_a \simeq 0.4\,\mathrm{MW\ m}^{-3}$$

The acoustic power is a small fraction of the thermal power

$$E_a/E_c \simeq 10^{-5}$$

26

(2) Combustion involves time lags. Reactants introduced in the chamber at one instant are converted into burnt gases at a later time

- Consider the following model including a restoring force with delay

$$\frac{d^2x}{dt^2} + 2\zeta\omega_0\frac{dx}{dt} + \omega_0^2 x(t-\tau) = 0$$

- Assume that the time lag is small and expand the last term in a Taylor series up to first order

$$\frac{d^2x}{dt^2} + (2\zeta - \omega_0\tau)\omega_0\frac{dx}{dt} + \omega_0^2 x = 0$$

- The model features a negative damping coefficient if

$$\boxed{2\zeta < \omega_0\tau}$$

The system is unstable when the time lag is sufficiently large

When the distance between the hot water tap and the shower cap is too long it introduces an excessive delay. This may give rise to growing oscillations in temperature resulting from the user lack of understanding of the situation

27

Sensitive time lag theory

Luigi Crocco (1909-1986) one of the founders of combustion instability theory, professor at Princeton for many years. He spent the later part of his life in Paris and was a Professor at Ecole Centrale Paris for a few years

H.S. Tsien (Tsien Hsue-Shen or Qian Xuesen) (1911-2009), went to study at Caltech under the supervision of von Karman, one of the founders of the Jet Propulsion Laboratory, and later « Father of China's Space Program »

$$\frac{d\tau}{dt} = n\frac{p(t-\tau) - p(t)}{\overline{p}}$$

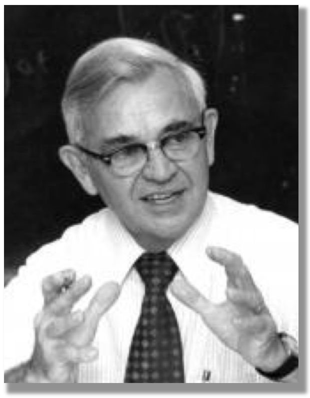

Frank Marble (1918-2014), professor at Caltech, jet propulsion pionneer

28

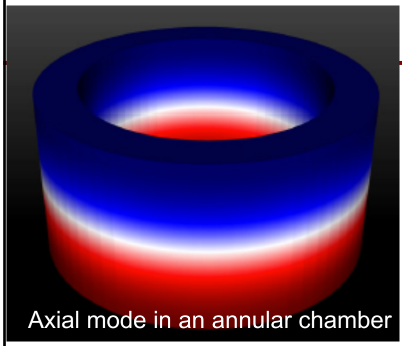

Axial mode in an annular chamber

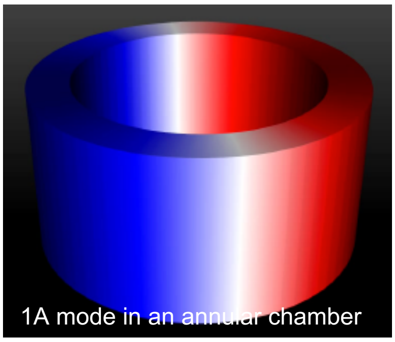

1A mode in an annular chamber

(3) Resonant interactions may readily occur in the weakly damped geometries used in modern combustors

- Among the possible coupling modes acoustics is dominant
- If the frequency is low

$$\lambda > d$$

wave propagation is longitudinal and this gives rise to system instabilities

- If the frequency is high

$$\lambda < d$$

the coupling may involve transverse modes giving rise to chamber instabilities

29

Classification

(Barrère and Williams, PCI 1969)

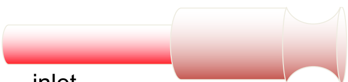

System Instabilities

- Involve the entire system
- Longitudinal wave propagation
- Low frequency range

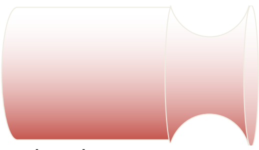

Chamber Instabilities

- Resonant modes of the chamber
- $\lambda \approx$ typical transverse dimension
- High frequency range

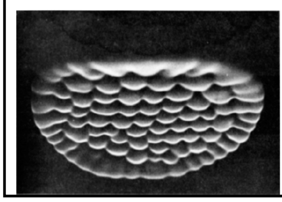

Intrinsic Instabilities

- Depend on the combustion process itself
- High frequency range

Georges Darrieus

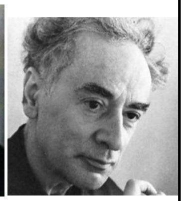

Lev Landau

30

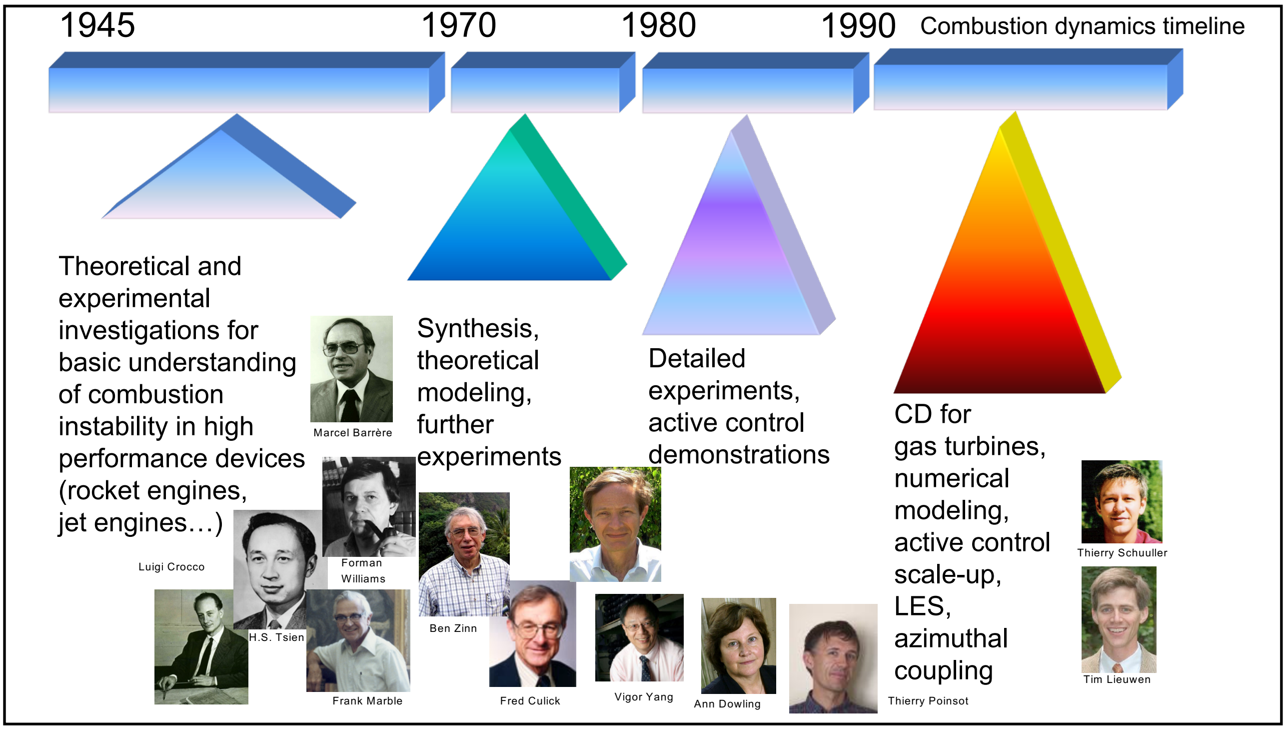

31

Objectives

1. Identify the main mechanisms governing combustion instabilities

2. Illustrate these mechanisms by experiments, that can also serve to validate predictions

1. Derive theoretical and modelling tools to analyze combustion dynamics.

2. Provide fundamental elements for the prediction of linear and nonlinear stability of combustors

32

Combustion dynamics
Lecture 1b

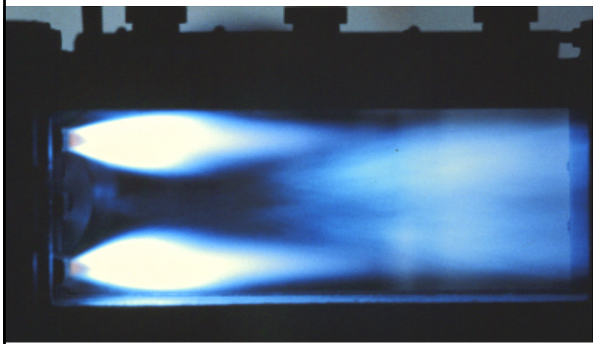

S. Candel, D. Durox , T. Schuller
CentraleSupélec
Université Paris-Saclay, EM2C lab, CNRS

Tsinghua summer school, June 2021

Elements of acoustics

- Basic equations of linear acoustics
- Plane waves in one dimension
- Harmonic waves
- Plane modes in a duct
- Harmonic spherical waves
- Acoustic energy balance

Balance equations

Mass

$$\frac{\partial \rho}{\partial t} + \nabla \cdot \rho v = 0$$

Momentum

$$\rho \frac{dv}{dt} = \rho g - \nabla p + \nabla \cdot \tau$$

Energy

$$\rho \frac{d}{dt}(e + \frac{1}{2}v^2) = \rho g \cdot v - \nabla \cdot (pv) + \nabla \cdot (\tau \cdot v) - \nabla \cdot q$$

Energy balance

$$\rho \frac{d}{dt}(e + \frac{1}{2}v^2) = \rho g \cdot v - \nabla \cdot (pv) + \nabla \cdot (\tau \cdot v) - \nabla \cdot q$$

$$\rho \frac{d}{dt}(\frac{1}{2}v^2) = \rho g \cdot v - v \cdot \nabla p + v \cdot (\nabla \cdot \tau)$$

$$\rho \frac{d}{dt}(e) = -p \nabla \cdot v + \tau : \nabla v - \nabla \cdot q$$

Other forms of the energy balance equation

$$e = h - p/\rho$$

$$\rho \frac{dh}{dt} = -\nabla \cdot q + \tau : \nabla v + \frac{dp}{dt}$$

$$\Downarrow$$

$$dh = Tds + \frac{1}{\rho} dp$$

$$\Downarrow$$

$$\rho T \frac{ds}{dt} = -\nabla \cdot q + \tau : \nabla v$$

Fundamentals of linear acoustics

Assumptions of the following analysis

- The thermodynamic state is determined by two thermodynamic variables
- The fluid is ideal so that its viscosity and heat conductivity may be taken equal to zero
- Chemical reactions are absent and there is no volumetric addition of mass or heat
- There are no volume forces (volume forces are negligible)

Using the previous assumptions one obtains an Euler set of equations

Mass

$$\frac{\partial \rho}{\partial t} + \boldsymbol{\nabla} \cdot \rho \boldsymbol{v} = 0$$

Momentum

$$\rho(\frac{\partial \boldsymbol{v}}{\partial t} + \boldsymbol{v} \cdot \boldsymbol{\nabla} \boldsymbol{v}) = -\boldsymbol{\nabla} p$$

Energy in entropy form

$$\rho T(\frac{\partial s}{\partial t} + \boldsymbol{v} \cdot \boldsymbol{\nabla} s) = 0$$

- Because the fluid is bivariant the entropy s may be expressed in terms of two other thermodynamic variables. For example $s = s(p, \rho)$ or equivalently one may write

$$p = p(\rho, s)$$

- For example, in the case of a perfect gas the state equation takes the forms

$$s = c_v \ln(p/p^\gamma) \quad \text{or} \quad p = \rho^\gamma e^{s/c_v}$$

where $\gamma = c_p/c_v$

- This equation indicates that $ds/dt = 0$ which is consistent with the fact that there is no entropy production associated with volumetric heat release, viscous dissipation and heat conduction

- If the medium is homogeneous its entropy is constant everywhere at the initial instant and because its material derivative is identically zero, the entropy will remain constant and equal to its initial value at all times. Hence, the acoustic disturbances will propagate in the medium at a constant entropy

$$s = s_0$$

and the state equation will take the form $p = p(\rho,\ s_0)$

- Now, consider a disturbance of the ambient state. The field variables may be cast in the form of a sum of the ambient value and a perturbation

$$p = p_0 + p_1, \quad \boldsymbol{v} = \boldsymbol{v}_0 + \boldsymbol{v}_1, \quad s = s_0 + s_1$$

- Here $\boldsymbol{v}_0 = 0$ and $p_0,\ \rho_0,\ s_0$ are constants linked by the state equation

$$p_0 = p(\rho_0,\ s_0)$$

- From the previous analysis of the balance equation for entropy one immediately deduces that the entropy perturbation vanishes identically

$$s_1 = 0$$

- One may now substitute the perturbed expressions into the balance equations of mass and momentum and in the equation of state

$$\frac{\partial}{\partial t}(\rho_0 + \rho_1) + \boldsymbol{\nabla} \cdot (\rho_0 + \rho_1)\boldsymbol{v}_1 = 0$$

$$(\rho_0 + \rho_1)(\frac{\partial}{\partial t} + \boldsymbol{v}_1 \cdot \boldsymbol{\nabla})\boldsymbol{v}_1 = -\boldsymbol{\nabla}(p_0 + p_1)$$

$$p_0 + p_1 = p(\rho_0 + \rho_1,\ s_0)$$

- For small perturbation in pressure, density and velocity, it is easy to distinguish terms of order zero, one and two. The terms of order zero vanish identically. The first order approximation obtained by neglecting higher order terms leads to the following equations

$$\frac{\partial}{\partial t}\rho_1 + \boldsymbol{\nabla}\cdot\rho_0\boldsymbol{v}_1 = 0$$

$$\rho_0\frac{\partial v_1}{\partial t} + \boldsymbol{\nabla}p_1 = 0$$

- A Taylor-series expansion of the state equation yields

$$p_0 + p_1 = p(\rho_0, s_0) + \left(\frac{\partial p}{\partial \rho}\right)_0 \rho_1 + \frac{1}{2}\left(\frac{\partial^2 p}{\partial \rho^2}\right)_0 \rho_1^2 + \dots$$

- Retaining only first order terms in this expansion one obtains

$$p_1 = c^2\rho_1 \quad \text{where} \quad c^2 = (\partial p/\partial\rho)_0$$

The derivative of pressure with respect to density at constant entropy has the dimensions of velocity square. From thermodynamics it can be shown that this quantity is positive. It will be shown later on that this derivative is actually the square of the speed of sound

- The linear acoustic equations take the form

$$\boxed{\begin{aligned} &\frac{\partial \rho_1}{\partial t} + \rho_0\boldsymbol{\nabla}\cdot\boldsymbol{v}_1 = 0 \\ &\rho_0\frac{\partial \boldsymbol{v}_1}{\partial t} + \boldsymbol{\nabla}p_1 = 0 \\ &p_1 = c^2\rho_1 \end{aligned}}$$

Determine the speed of sound in air at a temperature T=298.15 K

- For a perfect gas $p = \rho^\gamma e^{s/c_v}$

$$c^2 = (\gamma \rho^{\gamma-1}) \exp s/c_v \quad c^2 = \gamma p_0/\rho_0$$

Now the state equation for a perfect gas writes

$$p = \rho r T \qquad r = \mathcal{R}/W$$

- The speed of sound for a perfect gas is then given by

$$c = \left(\gamma r T_0\right)^{1/2} \qquad \mathcal{R} = 8314 \text{ J kmol}^{-1} \text{ K}^{-1} \qquad W = 29 \text{ kg kmol}^{-1}$$

Thus $r = 8314/29 = 287 \text{ J kg}^{-1} \text{ K}^{-1}$

and one finds that

$$\boxed{c = (1.4)(287)\left(298.15\right)^{1/2} = 346.1 \,\text{m s}^{-1}}$$

- There are other useful forms of the basic system of equations. It is first convenient to eliminate the density perturbation from the first equation by making use of the third relation. This yields

$$\boxed{\begin{aligned} &\frac{1}{c^2}\frac{\partial p_1}{\partial t} + \rho_0 \boldsymbol{\nabla} \cdot \boldsymbol{v}_1 = 0 \\ &\rho_0 \frac{\partial \boldsymbol{v}_1}{\partial t} + \boldsymbol{\nabla} p_1 = 0 \\ &p_1 = c^2 \rho_1 \end{aligned}}$$

- The acoustic problem is now specified by the first two equations. The third relation gives the density perturbation in terms of the pressure perturbation

Another system may be obtained by eliminating the velocity perturbation from the first two equations. This is achieved by taking the time derivative of the linearized mass balance and subtracting the divergence of the linearized momentum balance

$$\boxed{\begin{aligned}&\boldsymbol{\nabla}^2 p_1 - \frac{1}{c^2}\frac{\partial^2 p_1}{\partial t^2} = 0\\ &\rho_0 \frac{\partial \boldsymbol{v}_1}{\partial t} + \boldsymbol{\nabla} p_1 = 0\\ &p_1 = c^2 \rho_1\end{aligned}}$$

It is worth noting that the wave equation by itself does not allow the solution of most acoustic problems. It is in general necessary to use the linearized momentum equationto define the boundary conditions at the limits of the domain

Plane waves in one dimension

It is worth reviewing at this point the fundamental solution of the wave equation in one dimension. In this particular case the velocity perturbation has a single component and the set of linearized equations reduces to

$$\begin{aligned}&\frac{\partial p}{\partial t} + \rho_0 c^2 \frac{\partial v}{\partial x} = 0\\ &\rho_0 \frac{\partial v}{\partial t} + \frac{\partial p}{\partial x} = 0\\ &p = c^2 \rho\end{aligned}$$

Index 1 designating perturbed quantities has been eliminated from the previous equations. This simplified notation is not ambiguous and may be adopted from here-on

- The wave equation becomes in this case

$$\frac{\partial^2 p}{\partial x^2} - \frac{1}{c^2}\frac{\partial^2 p}{\partial t^2} = 0$$

D'Alembert's equation

$$\left(\frac{\partial}{\partial x} - \frac{1}{c}\frac{\partial}{\partial t}\right)\left(\frac{\partial}{\partial x} + \frac{1}{c}\frac{\partial}{\partial t}\right)p = 0$$

The factored form of the wave equation suggests the following change of variable

$$\xi = t - x/c, \quad \eta = t + x/c$$

- Introducing these relations in the wave equation yields

$$-\frac{4}{c^2}\frac{\partial^2 p}{\partial \xi \partial \eta} = 0$$

17

- The general solution of this partial differential equation takes the form of a sum

$$p = f(\xi) + g(\eta)$$

$$p = f(t - x/c) + g(t + x/c)$$

D'Alembert's solution

- It is a simple matter to show that the acoustic velocity corresponding to this pressure field takes the form

$$v(x,t) = \frac{1}{\rho_0 c}[f(t - x/c) - g(t + x/c)]$$

$f(t - x/c)$ represents a wave traveling to the right at the speed of sound

$g(t + x/c)$ represents a wave traveling to the left at the speed of sound

18

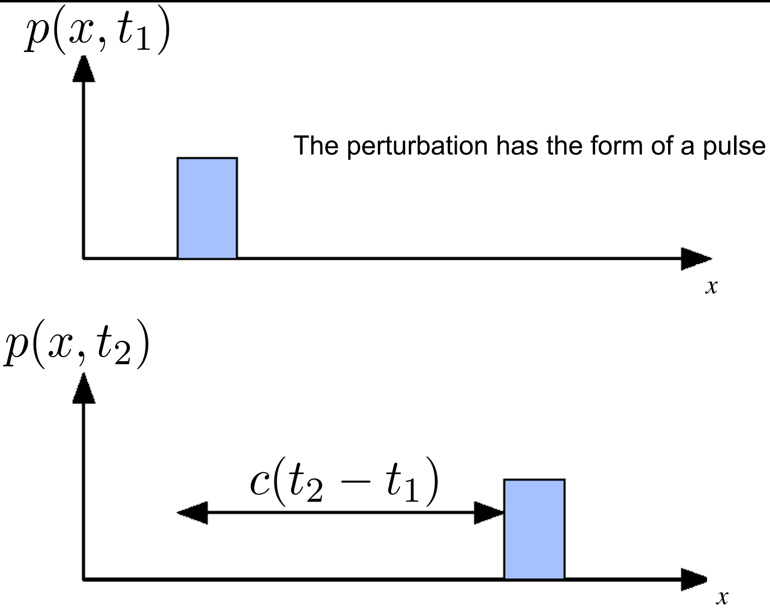

$f(t - x/c)$ represents a wave traveling to the right at the speed c.

19

$\rho_0 c$ is the specific acoustic impedance of the medium

$$\rho_0 c = (1.18)(346.1) = 408 \text{ kg m}^{-2} \text{ s}^{-1} = 408 \text{ Rayl}$$

The unit of acoustic impedance is the Rayl in honor of J.W. Strutt, Lord Rayleigh, one of the founders of modern acoustics

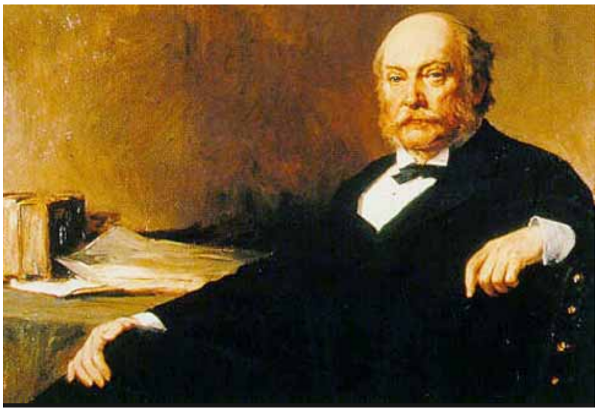

20

Harmonic waves

- Harmonic waves are such that their variation in time is of the form $e^{-i\omega t}$

$$p(\boldsymbol{x},t) = p_\omega(\boldsymbol{x})e^{-i\omega t}$$
$$\rho(\boldsymbol{x},t) = \rho_\omega(\boldsymbol{x})e^{-i\omega t}$$
$$\boldsymbol{v}(\boldsymbol{x},t) = \boldsymbol{v}_\omega(\boldsymbol{x})e^{-i\omega t}$$

- The complex number representation adopted for these waves follows the standard conventions. If one wishes to determine the actual pressure field at point and time it is sufficient to take the real part of the complex number which specifies the perturbation. For example :

$$p(\boldsymbol{x},t) = Re\{p_\omega(\boldsymbol{x})e^{-i\omega t}\}$$

- One may now derive the field equations governing harmonic disturbances. This is easily achieved by substituting the representation in the linearized acoustic equations obtained previously

- One finds that the time derivative $\partial/\partial t$ must be replaced by a factor $-i\omega$

- The common factor $e^{-i\omega t}$ may be dropped from all equations. This process yields

$$-i\omega p_\omega + \rho_0 c^2 \boldsymbol{\nabla}\cdot\boldsymbol{v}_\omega = 0$$
$$-\rho_0 i\omega \boldsymbol{v}_\omega + \boldsymbol{\nabla} p_\omega = 0$$
$$p_\omega = c^2\rho_\omega$$

- The wave equation is replaced by

$$\nabla^2 p_\omega + (\omega^2/c^2) p_\omega = 0$$

which is often written in the form

$$\nabla^2 p_\omega + k^2 p_\omega = 0 \qquad \text{where} \qquad k = \omega/c$$

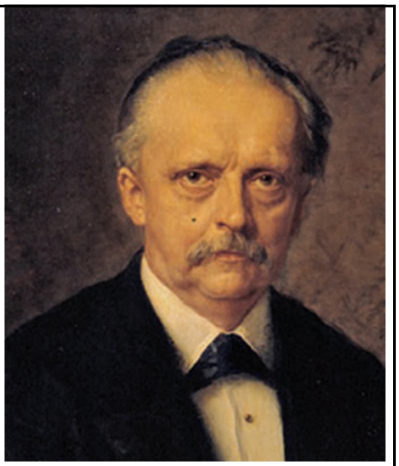

Herman von Helmholtz

- This Helmholtz equation specifies the spatial dependence of the complex field amplitude

Harmonic waves in one dimension

The set of equations for one dimensional wave propagation is

$$\frac{d^2 p}{dx^2} + k^2 p = 0$$

$$-i\omega v + \frac{dp}{dx} = 0$$

The pressure field is then a combination of two waves

$$p = A\exp(+ikx) + B\exp(-ikx)$$

and the velocity field is given by

$$v = \frac{1}{\rho_0 c}[A\exp(+ikx) - B\exp(-ikx)]$$

The first wave in the previous expressions propagates towards positive *x* while the second wave travels in the negative *x* direction

Problem 1 : Radiation in an infinite channel

A piston is placed at one end of an infinite duct and imposes an acoustic velocity of the form

$$v(0,t) = v_0 \cos \omega t$$

Find the acoustic field generated by the piston in this device

To deal with this problem it is convenient to work with complex representations

25

$$v(0,t) = \mathrm{Re}[v_0 \exp(-i\omega t)]$$

Since the duct is infinite there is only a traveling wave propagating away from the piston in the positive *x* direction

$$p(x,t) = \mathrm{Re}[A \exp(ikx - i\omega t)]$$

$$v(x,t) = \mathrm{Re}[\frac{A}{\rho_0 c} \exp(ikx - i\omega t)]$$

To satisfy the condition at the piston

$$v(0,t) = \mathrm{Re}[\frac{A}{\rho_0 c} \exp(-i\omega t)] = \mathrm{Re}[v_0 \exp(-i\omega t)]$$

26

As a consequence

$$A = \rho_0 c v_0$$

and the pressure field is given by

$$p(x,t) = \mathrm{Re}[\rho_0 c v_0 \exp(ikx - i\omega t)]$$

or

$$\boxed{p(x,t) = \rho_0 c v_0 \cos(kx - \omega t)}$$

Problem 2 : Plane modes in a duct

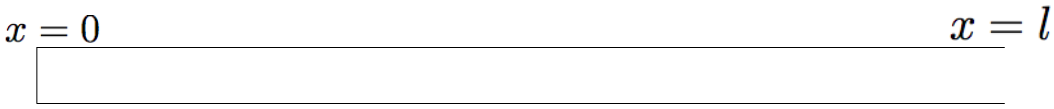

It is now interesting to examine plane modes in a duct. We consider a closed duct with an open end at *x= l*

The pressure field satisfies the Helmholtz equation

$$\frac{d^2p}{dx^2} + k^2 p = 0$$

subject to the following boundary conditions

$$\left(\frac{\partial p}{\partial x}\right)_0 = 0 \qquad\qquad p(l) = 0$$

The pressure field is of the form

$$p = A\exp(+ikx) + B\exp(-ikx)$$

The first condition is satisfied if

$$A = B$$

To fulfil the second condition

$$\exp(ikl) + \exp(-ikl) = 0$$

or equivalently

$$\cos(kl) = 0$$

This takes the form of a dispersion relation $\mathcal{D}(\omega) = 0$
that provides the eigennumbers of this system

$$k_n = (2n+1)\frac{\pi}{2l}$$

thus yielding the following eigenfrequencies

$$f_n = (2n+1)\frac{c}{4l}$$

and the corresponding eigenmodes

$$\psi_n(x) = \cos(k_n x)$$

The wavelength is given in this case by

$$\lambda_n = \frac{4l}{2n+1}$$

$$\lambda_0 = 4l \qquad \lambda_1 = \frac{4l}{3} \qquad \lambda_2 = \frac{4l}{5}$$

Problem 3 : Propagation in ducts with variable cross section

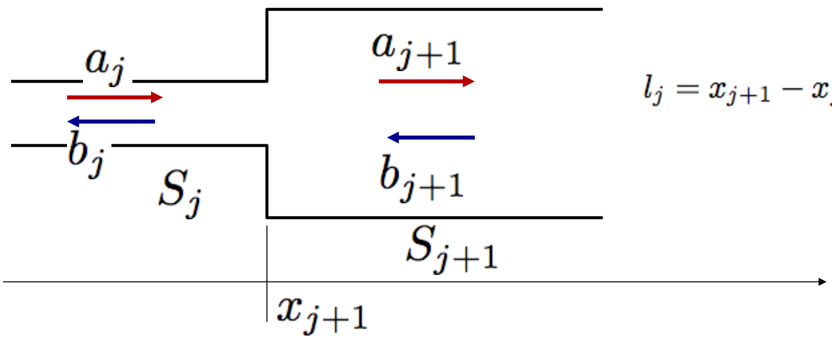

$$l_j = x_{j+1} - x_j$$

$$p_j = a_j \exp[ik_j(x - x_j)] + b_j \exp[-ik_j(x - x_j)]$$

$$v_j = \frac{a_j}{\rho_j c_j} \exp[ik_j(x - x_j)] - \frac{b_j}{\rho_j c_j} \exp[-ik_j(x - x_j)]$$

31

$$p_{j+1} = a_{j+1} \exp[ik_j(x - x_{j+1})] + b_{j+1} \exp[-ik_j(x - x_{j+1})]$$

$$v_{j+1} = \frac{a_{j+1}}{\rho_{j+1} c_{j+1}} \exp[ik_j(x - x_{j+1})] - \frac{b_{j+1}}{\rho_{j+1} c_{j+1}} \exp[-ik_j(x - x_{j+1})]$$

At the area change the pressure and volume flow rates are continuous :

$$p_j(x_{j+1}) = p_{j+1}(x_{j+1})$$

$$S_j v_j(x_{j+1}) = S_{j+1} v_{j+1}(x_{j+1})$$

This yields

$$a_j e^{ik_j l_j} + b_j e^{-ik_j l_j} = (a_{j+1} + b_{j+1})$$

$$\frac{S_j}{\rho_j c_j}(a_j e^{ik_j l_j} - b_j e^{-ik_j l_j}) = \frac{S_{j+1}}{\rho_{j+1} c_{j+1}}(a_{j+1} - b_{j+1})$$

32

Defining $$\beta_j = \frac{S_j}{S_{j+1}} \frac{\rho_{j+1} c_{j+1}}{\rho_j c_j}$$

the previous expressions become

$$a_{j+1} + b_{j+1} = a_j e^{ik_j l_j} + b_j e^{-ik_j l_j}$$
$$a_{j+1} - b_{j+1} = \beta_j (a_j e^{ik_j l_j} - b_j e^{-ik_j l_j})$$

and one obtains

$$\boxed{\begin{aligned} a_{j+1} &= \frac{1}{2}[(1+\beta_j) a_j e^{ik_j l_j} + (1-\beta_j) b_j e^{-ik_j l_j}] \\ b_{j+1} &= \frac{1}{2}[(1-\beta_j) a_j e^{ik_j l_j} + (1+\beta_j) b_j e^{-ik_j l_j}] \end{aligned}}$$

Harmonic spherical waves

We look for solutions of the Helmholtz equation in three dimensions which only depend on the radius

$$p = p(r)$$

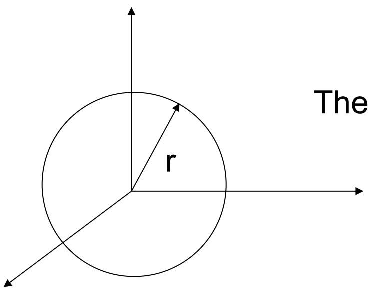

The pressure field satisfies

$$\frac{1}{r^2} \frac{d}{dr} (r^2 \frac{dp}{dr}) + k^2 p = 0$$

or equivalently $$\frac{d^2(rp)}{dr^2} + k^2 (pr) = 0$$

$$\frac{1}{r^2}\frac{d}{dr}(r^2\frac{dp}{dr}) + k^2 p = 0$$

$$\frac{d^2p}{dr^2} + \frac{2}{r}\frac{dp}{dr} + k^2 p = 0 \quad \text{or} \quad r\frac{d^2p}{dr^2} + 2\frac{dp}{dr} + k^2 pr = 0$$

Now $\frac{d^2}{dr^2}(pr) = \frac{d}{dr}(p + r\frac{dp}{dr}) = r\frac{d^2p}{dr^2} + 2\frac{dp}{dr}$

So that the Helmholtz equation in radial coordinates, for purely radial fields becomes

$$\frac{d^2}{dr^2}(pr) + k^2(pr) = 0$$

35

There are two solutions to this wave equation

$$p(r) = A\frac{1}{r}\exp(ikr) \quad \text{travels outwards}$$

$$p(r) = B\frac{1}{r}\exp(-ikr) \quad \text{travels inwards}$$

The acoustic velocity has only a radial component which is given by

$$\rho_0\frac{\partial v}{\partial t} + \frac{\partial p}{\partial r} = 0$$

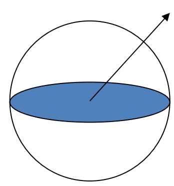

$p(r) = A\frac{1}{r}\exp(ikr)$

36

$$v = \frac{1}{\rho_0 i\omega}\frac{\partial p}{\partial r}$$

For the wave traveling outwards, the velocity is given by

$$v = \frac{1}{\rho_0 i\omega} A(ik - \frac{1}{r})\frac{\exp(ikr)}{r}$$

or equivalently $$v = \frac{1}{\rho_0 c} A(1 - \frac{1}{ikr})\frac{\exp(ikr)}{r}$$

In the farfield $$v \simeq \frac{1}{\rho_0 c} A\frac{\exp(ikr)}{r}$$

Problem 4 : Acoustic radiation by a pulsating sphere

A sphere of radius a pulsates harmonically. The acceleration of the surface of the sphere is specified

$$\ddot{w}(a,t) = \ddot{W}\exp(-i\omega t)$$

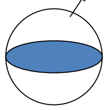

Determine the pressure radiated by this sphere

The pressure field is an outgoing spherical wave

$$p(r) = A\frac{1}{r}\exp(ikr)$$

On the sphere, the radial acceleration is specified and the linearized momentum equation must be satisfied

$$\rho_0 \frac{\partial v}{\partial t} + \frac{\partial p}{\partial r} = 0$$

Now
$$\ddot{w} = \frac{\partial v}{\partial t}$$

so that
$$\rho_0 \ddot{w} = -\frac{\partial p}{\partial r}$$

By imposing this condition at *r*=*a* one finds :

$$\rho_0 \ddot{W} = -A(ik - \frac{1}{a})\frac{\exp(ika)}{a}$$

39

$$A = \frac{\rho_0 \ddot{W} a^2}{(1-ika)} \exp(-ika)$$

$$\boxed{p(r,t) = \frac{\rho_0 \ddot{W} a^2}{(1-ika)} \frac{1}{r} \exp[ik(r-a) - i\omega t]}$$

It is convenient to introduce the volume acceleration

$$\ddot{Q} = 4\pi \ddot{W} a^2$$

$$p(r,t) = \frac{\rho_0 \ddot{Q}}{4\pi(1-ika)} \frac{1}{r} \exp[ik(r-a) - i\omega t]$$

40

If the radius of the sphere is small compared to the wavelength

$$ka << 1$$

this expression reduces to

$$\boxed{p(r,t) = \frac{\rho_0 \ddot{Q}}{4\pi r} \exp[ikr - i\omega t]}$$

This is the sound field radiated by a point source featuring a specified volume acceleration $\ddot{Q}$

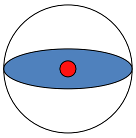

A point source with a specified volume acceleration

41

Acoustic energy density, flux and acoustic power

A conservation equation for the acoustic energy may be obtained from the linearized equations describing the acoustic field. One may start from

$$\frac{p_1}{\rho_0} \quad \Big| \quad \frac{1}{c^2}\frac{\partial p_1}{\partial t} + \rho_0 \boldsymbol{\nabla} \cdot \boldsymbol{v} = 0$$

$$+\boldsymbol{v}_1 \cdot \quad \Big| \quad \rho_0 \frac{\partial \boldsymbol{v}_1}{\partial t} + \boldsymbol{\nabla} p_1 = 0$$

$$\frac{p_1}{\rho_0}\left(\frac{1}{c^2}\frac{\partial p_1}{\partial t} + \rho_0 \boldsymbol{\nabla} \cdot \boldsymbol{v}_1\right) + \boldsymbol{v}_1 \cdot \left(\rho_0 \frac{\partial \boldsymbol{v}}{\partial t} + \boldsymbol{\nabla} p_1\right) = 0$$

42

This equation becomes

$$\frac{\partial}{\partial t}(\frac{1}{2}\rho_0 v_1^2 + \frac{1}{2}\frac{p_1^2}{\rho_0 c^2}) + \boldsymbol{\nabla}\cdot p_1 \boldsymbol{v}_1 = 0$$

$$\underbrace{\mathcal{E} = \frac{1}{2}\rho_0 v_1^2 + \frac{1}{2}\frac{p_1^2}{\rho_0 c^2}}_{\text{Acoustic energy density}} \qquad \underbrace{\boldsymbol{\mathcal{F}} = p_1 \boldsymbol{v}_1}_{\text{Acoustic energy flux}}$$

With these definitions the balance equation may be cast in the form

$$\frac{\partial \mathcal{E}}{\partial t} + \boldsymbol{\nabla}\cdot\boldsymbol{\mathcal{F}} = 0$$

This expression closely resembles to the balance equations of fluid dynamics. It is also in the same form as Pointing's theorem of electromagnetic theory.

43

Poynting's theorem

$$\boxed{\frac{\partial u}{\partial t} + \boldsymbol{\nabla}\cdot\boldsymbol{S} + \boldsymbol{J}\cdot\boldsymbol{E} = 0}$$

Electromagnetic energy flux vector (the Poynting vector)

$$\boldsymbol{S} = \boldsymbol{E}\times\boldsymbol{H}$$

Electromagnetic energy density

$$u = \frac{1}{2}\epsilon_0 \boldsymbol{E}\cdot\boldsymbol{E} + \frac{1}{2\mu_0}\boldsymbol{B}\cdot\boldsymbol{B}$$

$\boldsymbol{E}, \boldsymbol{B}, \boldsymbol{H}, \boldsymbol{J}$ are the electric and magnetic fields, the magnetic induction and current density

44

Sound pressure level(dB)

$$SPL = 20 \log_{10} \frac{p_{rms}}{p_{ref}}$$

$$p_{ref} = 2\ 10^{-5}\ Pa$$

Intensity level (dB)

$$IL = 10 \log_{10} \frac{I}{I_{ref}}$$

$$I_{ref} = 10^{-12}\ W m^{-2}$$

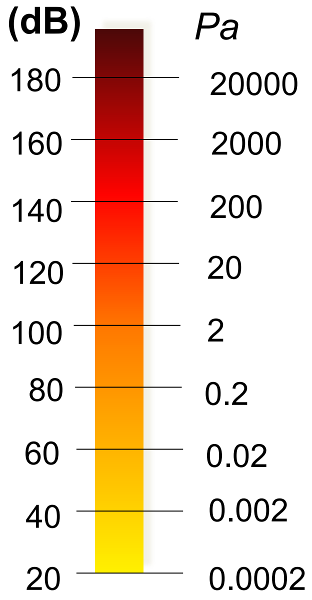

45

The sound intensity in the far field is given by

$$I = \frac{p^2}{\rho_0 c}$$

In air $\rho_0 c \simeq 400\,\mathrm{Rayl}$

and the sound intensity corresponding to the reference pressure used to define the sound pressure level is given by

$$I_{ref} = \frac{(2\,10^{-5})^2}{400} = 10^{-12}\,\mathrm{W\ m^{-2}}$$

Thus the sound pressure level and the intensity level are nearly equal

46

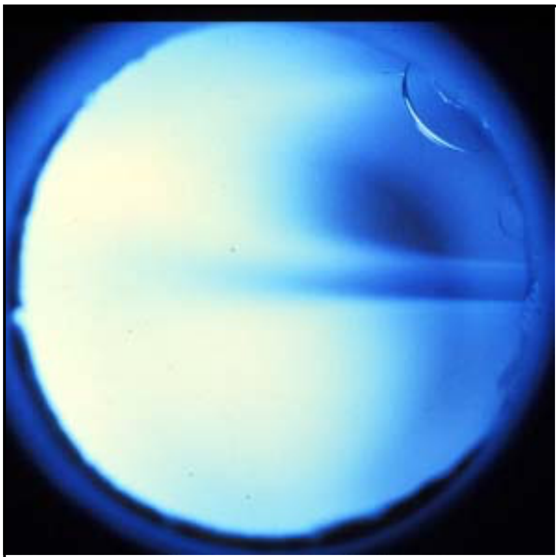

Combustion dynamics
Lecture 2a

S. Candel, D. Durox , T. Schuller

CentraleSupélec
Université Paris-Saclay, EM2C lab, CNRS

Tsinguha summer school, July 2021

Acoustics of reactive flows

Accounting for heat relase fluctuations
Compact flames
Acoustic energy balance
Equations of reactive flows

Acoustics of reactive flows

Consider the set of acoustic equations but this time including a nonsteady heat release source term in the energy balance

$$\frac{\partial \rho_1}{\partial t} + \rho_0 \boldsymbol{\nabla} \cdot \boldsymbol{v}_1 = 0$$

$$\rho_0 \frac{\partial \boldsymbol{v}_1}{\partial t} + \boldsymbol{\nabla} p_1 = 0$$

$$\rho_0 T_0 (\frac{\partial}{\partial t} s_1) = \dot{q}_1$$

The state equation $p = p(\rho, s)$ may be differentiated

$$dp = \left(\frac{\partial p}{\partial \rho}\right)_s d\rho + \left(\frac{\partial p}{\partial s}\right)_\rho ds$$

$$p_1 = \left(\frac{\partial p}{\partial \rho}\right)_s \rho_1 + \left(\frac{\partial p}{\partial s}\right)_\rho s_1$$

$$c^2 = \left(\frac{\partial p}{\partial \rho}\right)_s \quad \alpha = \left(\frac{\partial p}{\partial s}\right)_\rho$$

$$p_1 = c^2 \rho_1 + \alpha s_1$$

For a perfect gas $p = \rho^\gamma \exp(s/c_v)$

$$\boxed{c^2 = \frac{\gamma p}{\rho} = \gamma r T \qquad \alpha = \frac{p}{c_v} = (\gamma - 1)\rho T}$$

The density perturbation may be expressed in terms of pressure and entropy perturbations

$$\rho_1 = \frac{1}{c^2} p_1 - \frac{\alpha}{c^2} s_1$$

This relation may be introduced in the balance of mass

$$\frac{1}{c^2}\frac{\partial p_1}{\partial t} - \frac{\alpha}{c^2}\frac{\partial s_1}{\partial t} + \rho_0 \boldsymbol{\nabla} \cdot \boldsymbol{v}_1 = 0$$

Using the perturbed energy equation

$$\rho_0 T_0 \left(\frac{\partial}{\partial t} s_1\right) = \dot{q}_1$$

One obtains

$$\frac{1}{c^2}\frac{\partial p_1}{\partial t} + \rho_0 \boldsymbol{\nabla} \cdot \boldsymbol{v}_1 = \frac{\alpha}{\rho_0 T_0}\frac{1}{c^2}\dot{q}_1$$

The previous equation may be combined with the perturbed momentum balance

$$\begin{array}{c|c} \dfrac{\partial}{\partial t} & \dfrac{1}{c^2}\dfrac{\partial p_1}{\partial t} + \rho_0 \boldsymbol{\nabla} \cdot \boldsymbol{v}_1 = \dfrac{\alpha}{\rho_0 T_0}\dfrac{1}{c^2}\dot{q}_1 \\ -\boldsymbol{\nabla}\cdot & \rho_0 \dfrac{\partial \boldsymbol{v}_1}{\partial t} + \boldsymbol{\nabla} p_1 = 0 \\ \hline \end{array}$$

$$\frac{1}{c^2}\frac{\partial^2 p_1}{\partial t^2} - \boldsymbol{\nabla}^2 p_1 = \frac{\alpha}{\rho_0 T_0}\frac{1}{c^2}\frac{\partial \dot{q}_1}{\partial t}$$

$$\frac{\alpha}{\rho_0 T_0} = \frac{p_0}{\rho_0 c_v T_0} = \gamma - 1$$

One obtains a wave equation with a source term

$$\boxed{\frac{1}{c^2}\frac{\partial^2 p_1}{\partial t^2} - \boldsymbol{\nabla}^2 p_1 = \frac{\gamma - 1}{c^2}\frac{\partial \dot{q}_1}{\partial t}}$$

The compact flame case

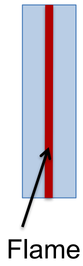

$$\frac{1}{c^2}\frac{\partial p_1}{\partial t} + \rho_0 \boldsymbol{\nabla}\cdot\boldsymbol{v}_1 = \frac{\alpha}{\rho_0 T_0}\frac{1}{c^2}\dot{q}_1$$

Now $$\frac{\alpha}{\rho_0 T_0} = \frac{p_0}{\rho_0 c_v T_0} = \gamma - 1$$

Thus $$\frac{1}{c^2}\frac{\partial p_1}{\partial t} + \rho_0 \boldsymbol{\nabla}\cdot\boldsymbol{v}_1 = \frac{\gamma-1}{c^2}\dot{q}_1$$

Or equivalently $$\frac{1}{\rho_0 c^2}\frac{\partial p_1}{\partial t} + \boldsymbol{\nabla}\cdot\boldsymbol{v}_1 = \frac{\gamma-1}{\rho_0 c^2}\dot{q}_1$$

Now $\rho_0 c^2 = \gamma p$ is essentially constant across the flame

7

Integrating the last expression on a volume including the flame

$$\int_V \frac{1}{\rho_0 c^2}\frac{\partial p_1}{\partial t}dV + \int_V \boldsymbol{\nabla}\cdot\boldsymbol{v}_1 dV = \int_V \frac{\gamma-1}{\rho_0 c^2}\dot{q}_1 dV$$

Or equivalently

$$\frac{1}{\rho_0 c^2}\int_V \frac{\partial p_1}{\partial t}dV + \int_V \boldsymbol{\nabla}\cdot\boldsymbol{v}_1 dV = \frac{\gamma-1}{\rho_0 c^2}\int_V \dot{q}_1 dV$$

If the flame is compact, the first term vanishes. The second term may be transformed using Green's theorem yielding

$$S_2 v_2' - S_1 v_1' = \frac{\gamma-1}{\rho_0 c^2}\dot{Q}' \quad \text{where} \quad \dot{Q}' = \int_V \dot{q}_1 dV$$

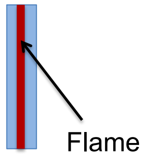

8

Assume that the surfaces on the upstream and downstream sides are equal

$$v_2' - v_1' = \frac{\gamma - 1}{\rho_0 c^2} \frac{1}{S} \dot{Q}'$$

From the definition of the flame transfer function

$$\mathcal{F}(\omega) = \frac{\dot{Q}'/\overline{\dot{Q}}}{v'/\overline{v}}$$

$$\dot{Q}' = \overline{\dot{Q}} \mathcal{F}(\omega) v'/\overline{v}$$

$$v_2' - v_1' = \frac{\gamma - 1}{\rho_0 c^2} \frac{\overline{\dot{Q}}}{S\overline{v}} \mathcal{F}(\omega) v_1'$$

Now $\overline{\dot{Q}} = \dot{m} c_p (T_b - T_u)$

and $\rho_0 c^2 S \overline{v} = \dot{m} \gamma r T_u$

$$\frac{\gamma - 1}{\rho_0 c^2} \frac{\overline{\dot{Q}}}{S\overline{v}} = \frac{\gamma - 1}{\gamma r} c_p \frac{T_b - T_u}{T_u} = \frac{T_b}{T_u} - 1$$

Hence

$$\boxed{v_2' - v_1' = (\frac{T_b}{T_u} - 1) \mathcal{F}(\omega) v_1'}$$

Acoustic energy balance

$$p_1 \quad \frac{1}{\rho_0 c^2}\frac{\partial p_1}{\partial t} + \boldsymbol{\nabla}\cdot\boldsymbol{v}_1 = \frac{\gamma-1}{\rho_0 c^2}\dot{q}_1$$

$$\boldsymbol{v}_1 \cdot \quad \rho_0 \frac{\partial \boldsymbol{v}_1}{\partial t} + \boldsymbol{\nabla} p_1 = 0$$

$$\frac{\partial}{\partial t}\left(\frac{1}{2}\frac{p_1^2}{\rho_0 c^2} + \frac{1}{2}\rho_0 v_1^2\right) + \boldsymbol{\nabla}\cdot p_1\boldsymbol{v}_1 = \frac{\gamma-1}{\rho_0 c^2}p_1\dot{q}_1$$

$$\mathcal{E} = \frac{1}{2}\frac{p_1^2}{\rho_0 c^2} + \frac{1}{2}\rho_0 v_1^2 \qquad \boldsymbol{\mathcal{F}} = p_1\boldsymbol{v}_1 \qquad \mathcal{S} = \frac{\gamma-1}{\rho_0 c^2}p_1\dot{q}_1$$

Acoustic energy density — Acoustic energy flux — Source term

$$\boxed{\frac{\partial \mathcal{E}}{\partial t} + \boldsymbol{\nabla}\cdot\boldsymbol{\mathcal{F}} = \mathcal{S}}$$

$$\mathcal{S} = \frac{\gamma-1}{\rho_0 c^2}p_1\dot{q}_1$$ Source term

The energy balance should include a term associated with damping processes and takes the final form

$$\boxed{\frac{\partial \mathcal{E}}{\partial t} + \boldsymbol{\nabla}\cdot\boldsymbol{\mathcal{F}} = \mathcal{S} - \mathcal{D}}$$

Taking the average of the energy balance over a period of oscillation one obtains

$$\frac{\partial E}{\partial t} + \boldsymbol{\nabla} \cdot \boldsymbol{F} = S - D$$

$$S = \frac{\gamma - 1}{\rho_0 c^2} \frac{1}{T} \int_T p_1 \dot{q}_1 dt$$

If the source term S is positive it tends to increase the acoustic energy density. However this energy density will grow locally if the source term is greater than the damping term and the acoustic energy flux leaving the local volume

D. Durox, T. Schuller, N. Noiray, A.L. Birbaud and S. Candel (2009) *Combustion and Flame*. **156**,106-119. The Rayleigh criterion and the acoustic energy balance in unconfined self excited oscillating flames.

The energy balance may be integrated over a volume V containing the reactive region :

$$\int_V \frac{\partial E}{\partial t} dV + \int_V \boldsymbol{\nabla} \cdot \boldsymbol{F} dV = \int_V S dV - \int_V D dV$$

Now $\int_V \boldsymbol{\nabla} \cdot \boldsymbol{F} dV = \int_A \boldsymbol{F} \cdot \boldsymbol{n} dA$

So that $\int_V \frac{\partial E}{\partial t} dV = \int_V S dV - \int_V D dV - \int_A \boldsymbol{F} \cdot \boldsymbol{n} dA$

The acoustic energy in the control volume increases if

$$\int_V S dV > \int_V D dV - \int_A \boldsymbol{F} \cdot \boldsymbol{n} dA$$

The Rayleigh criterion

A gain is obtained if pressure and heat-release fluctuations are in phase (Rayleigh, 1878)

$$\frac{1}{T}\int_0^T p'q'dt > 0$$

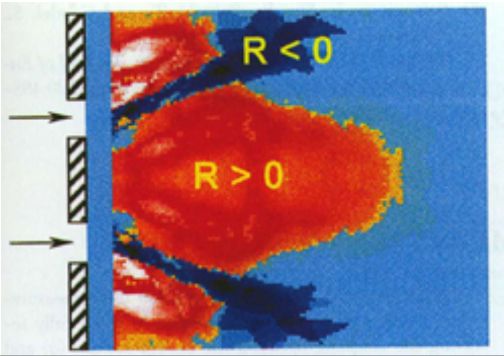

Local Rayleigh index in a lean premixed Combustor (Lee et al 2000)

driving (R>0) damping (R<0)

Equations of combustion acoustics

$$\frac{d\rho}{dt} = -\rho \boldsymbol{\nabla} \cdot \boldsymbol{v}$$ Mass

$$\rho \frac{d\boldsymbol{v}}{dt} = -\boldsymbol{\nabla} p + \boldsymbol{\nabla} \cdot \boldsymbol{\tau}$$ Momentum

$$\rho c_p \frac{dT}{dt} = \dot{Q} + \frac{dp}{dt} + \boldsymbol{\tau}:\boldsymbol{\nabla}\boldsymbol{v} - \boldsymbol{\nabla} \cdot \boldsymbol{J}^H$$ Energy

$$\rho \frac{dY_k}{dt} = \dot{\omega}_k - \boldsymbol{\nabla} \cdot \boldsymbol{J}_k^D$$ Species

$$\boldsymbol{J}_k^D = \rho Y_k \boldsymbol{V}_k^D \qquad \boldsymbol{J}^H = -\lambda \boldsymbol{\nabla} T + \sum_{k=1}^{N} \rho Y_k \boldsymbol{V}_k^D h_k$$ Diffusion and heat fluxes

$$\dot{Q} = -\sum_{k=1}^{N} h_k \dot{\omega}_k$$ Heat release rate

Starting from the state equation for the mixture

$$p = \rho r_g T, \text{ where } r_g = R/W \qquad \frac{1}{W} = \sum_{k=1}^{N} \frac{Y_k}{W_k}$$

one obtains

$$dT = \left(\frac{\partial T}{\partial p}\right)_{\rho, Y_k} dp + \left(\frac{\partial T}{\partial \rho}\right)_{p, Y_k} d\rho + \left(\frac{\partial T}{\partial Y_k}\right)_{\rho, p} dY_k$$

$$dT = \frac{T}{p} dp - \frac{T}{\rho} d\rho - T \sum_{k=1}^{N} \frac{W}{W_k} dY_k$$

- Combining the previous expression with the balance equations for energy and species one obtains

$$\frac{1}{\gamma p} \frac{dp}{dt} - \frac{1}{\rho} \frac{d\rho}{dt} = \frac{\dot{Q}}{\rho c_p T} + W \frac{d}{dt}\left(\frac{1}{W}\right)$$
$$+ \frac{1}{\rho c_p T} \left[\nabla \cdot \lambda \nabla T + \boldsymbol{\tau} : \nabla \boldsymbol{v} - \sum_{k=1}^{N} \rho Y_k c_{pk} \boldsymbol{V}_k^D \cdot \nabla T \right]$$

- Together with the balance of mass and momentum,

$$\frac{d\rho}{dt} = -\rho \nabla \cdot \boldsymbol{v} \quad \text{and} \quad \rho \frac{d\boldsymbol{v}}{dt} = -\nabla p + \nabla \cdot \boldsymbol{\tau}$$

this expression yields a wave equation for the logarithm of the pressure

Wave equation in a reactive flow

$$\nabla \cdot \left(\frac{c^2}{\gamma}\nabla \ln p\right) - \frac{d}{dt}\left(\frac{1}{\gamma}\frac{d}{dt}\ln p\right) = \nabla \cdot \left(\frac{1}{\rho}\nabla \cdot \tau\right)$$

$$-\frac{d}{dt}\left(\frac{1}{\rho c_p T}\left[\nabla \cdot \lambda \nabla T + \boldsymbol{\tau} : \nabla \boldsymbol{v} - \sum_{k=1}^{N} \rho Y_k c_{pk} \boldsymbol{V}_k^D \cdot \nabla T\right]\right)$$

$$-\frac{d}{dt}\left(\frac{\dot{Q}}{\rho c_p T}\right) - \frac{d}{dt}\left[W \frac{d}{dt}\left(\frac{1}{W}\right)\right] - \nabla \boldsymbol{v} : \nabla \boldsymbol{v}$$

Combustion noise source associated with nonsteady heat release

Combustion source associated with changes in molar composition

Aerodynamic noise source

19

Simplified wave equation

$$\boxed{\nabla \cdot \left(\frac{c^2}{\gamma}\nabla \ln p\right) - \frac{d}{dt}\left(\frac{1}{\gamma}\frac{d}{dt}\ln p\right) = -\frac{d}{dt}\left(\frac{\dot{Q}}{\rho c_p T}\right) - \frac{d}{dt}\left[W \frac{d}{dt}\left(\frac{1}{W}\right)\right] - \nabla \boldsymbol{v} : \nabla \boldsymbol{v}}$$

$$\dot{Q} = -\sum_{k=1}^{N} \dot{\omega}_k h_k = \left(-\Delta h_f^0\right)\dot{\omega}$$ Heat release rate

$\dot{Q}$ $[ML^{-1}T^{-3}]$

$\dot{\omega}$ $[ML^{-3}T^{-1}]$ Reaction rate

20

$$\frac{d}{dt}\left(\frac{\dot{Q}}{\rho c_p T}\right)$$

Combustion noise source associated with nonsteady heat release

$$\frac{d}{dt}\left[W\frac{d}{dt}\left(\frac{1}{W}\right)\right]$$

Combustion noise source associated with changes in molar composition

Truffaut and Searby (1998) propose an alternative expression for the second source term

$$\frac{d}{dt}\left(\frac{\dot{n}}{n}\right)$$

where n is the molar concentration

$$n = \sum_{k=1}^{N} n_k = \rho \sum_{k=1}^{N} Y_k / W_k$$

Using this expression one finds that

$$\frac{\dot{n}}{n} = \frac{1}{n}\frac{dn}{dt} = W\frac{d}{dt}\left(\frac{1}{W}\right) + \frac{1}{\rho}\frac{d\rho}{dt}$$

Extra term

which contains an extra term

21

Linearized wave equation

The previous wave equation may be linearized by writing

$$\ln p \simeq \frac{p'}{\overline{p}}$$

and assuming that the mean pressure is essentially constant (combustion is nearly isobaric). One obtains

$$\nabla \cdot (\overline{c}^2 \nabla p') - \frac{\partial^2 p'}{\partial t^2} = -\frac{\partial}{\partial t}\left[(\gamma - 1)\dot{Q}'\right] - \gamma \overline{p} \nabla \boldsymbol{v} : \nabla \boldsymbol{v} + \frac{\gamma \overline{p}}{\overline{W}} \frac{\partial^2 W'}{\partial t^2}$$

Nonsteady heat release source term

Aerodynamic sound

Changes in molar composition

22

An alternative formulation of the wave equation

Low Mach number limit $d/dt \sim \partial/\partial t$

By developing the logarithm of the pressure and using $\gamma p = \rho c^2$ one obtains

$$\nabla \cdot \left(\frac{1}{\rho}\nabla p\right) - \frac{\partial}{\partial t}\left(\frac{1}{\rho c^2}\frac{\partial}{\partial t}p\right) =$$

$$-\frac{\partial}{\partial t}\left(\frac{\dot{Q}}{\rho c_p T}\right) - \frac{\partial}{\partial t}\left[W\frac{\partial}{\partial t}\left(\frac{1}{W}\right)\right] - \nabla \boldsymbol{v} : \nabla \boldsymbol{v}$$

This expression can be rearranged by adding on both sides the left hand side terms where the density and the sound speed are replaced by their uniform ambient values

$$\nabla \cdot \left(\frac{1}{\rho_0}\nabla p\right) - \frac{\partial}{\partial t}\left(\frac{1}{\rho_0 c_0^2}\frac{\partial}{\partial t}p\right)$$

23

One obtains

$$\nabla^2 p - \frac{1}{c_0^2}\frac{\partial^2 p}{\partial t^2} =$$

$$\underbrace{\cancel{+\rho_0 \frac{\partial}{\partial t}\left[\left(\frac{1}{\rho c^2} - \frac{1}{\rho_0 c_0^2}\right)\frac{\partial p}{\partial t}\right]}}_{\simeq 0} - \rho_0 \nabla \cdot \left[\left(\frac{1}{\rho} - \frac{1}{\rho_0}\right)\nabla p\right]$$

Indirect noise source

$$-\rho_0 \nabla \mathbf{v} : \nabla \mathbf{v} \underbrace{- \rho_0 \frac{\partial}{\partial t}\left[W\frac{\partial}{\partial t}\left(\frac{1}{W}\right)\right] - \rho_0 \frac{\partial}{\partial t}\left(\frac{\dot{Q}}{\rho c_p T}\right)}_{\text{Combustion noise source}}$$

Aerodynamic noise source

The reasoning parallels that used by Lighthill in his theory of aerodynamic sound. This was used by Howe and by Dowling.

24

Noting that $$\frac{1}{\rho c_p T} = \frac{\gamma - 1}{\rho_0 c_0^2}$$

And only keeping the heat release source term and one finally obtains the following equation

$$\nabla^2 p - \frac{1}{c_0^2}\frac{\partial^2 p}{\partial t^2} = -\frac{\gamma - 1}{c_0^2}\frac{\partial \dot{Q}'}{\partial t}$$

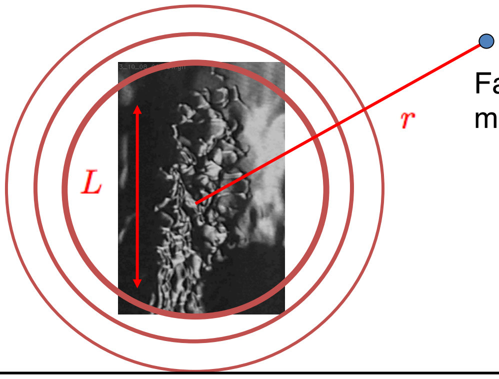

25

- Assuming that radiation takes place in an unconfined domain and only keeping the source term associated with perturbations in heat release one obtains

$$p'(\boldsymbol{r}, t) = \frac{\gamma - 1}{4\pi c_0{}^2}\int_V \frac{1}{|\boldsymbol{r} - \boldsymbol{r}_0|}\frac{\partial}{\partial t}\dot{Q}'(\boldsymbol{r}_0, t - |\boldsymbol{r} - \boldsymbol{r}_0|/c_0)dV(\boldsymbol{r}_0)$$

- When the observation point is in the farfield of a compact flame the previous expression becomes (Strahle (1985))

$$\boxed{p'(\boldsymbol{r}, t) = \frac{\gamma - 1}{4\pi c_0{}^2 r}\frac{\partial}{\partial t}\int_V \dot{Q}'(\boldsymbol{r}_0, t - r/c_0)dV(\boldsymbol{r}_0)}$$

26

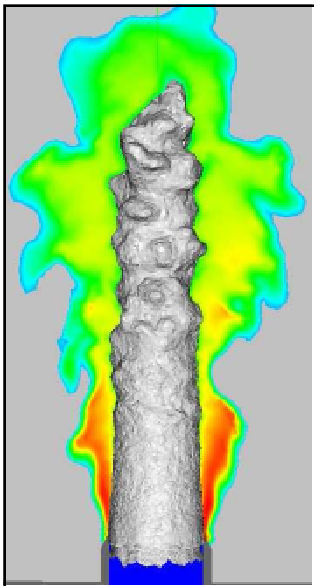

Combustion dynamics
Lecture 2b

S. Candel, D. Durox , T. Schuller

CentraleSupélec
Université Paris-Saclay, EM2C lab, CNRS

Tsinghua summer school, June 2021

1

Contents

- Introduction
- Combustion noise fundamentals and scaling
- Mechanisms of sound radiation from perturbed flames
- Confinement effects, noise and instabilities
- Computational combustion acoustics (CCA)

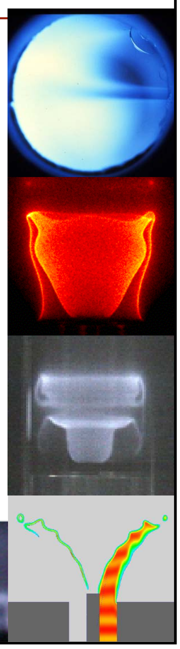

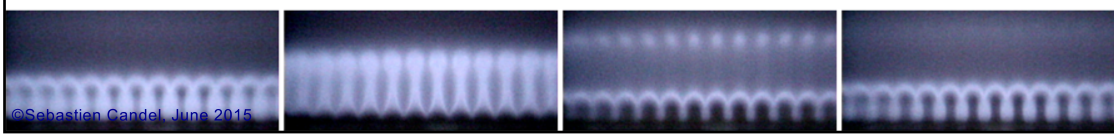

2

Noise radiation does not influence the flow	Noise radiation interacts with the flow leading to unstable oscillations

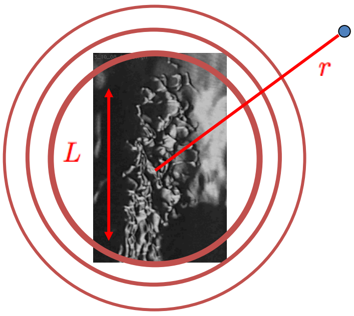

Flame dynamics
Noise sources
Radiated field
Scaling rules
Spectral content
Noise control

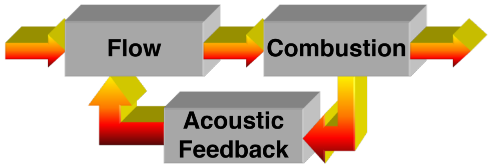

Flame dynamics
Coupling mechanisms
Conditions leading to instability
Level of oscillation
Prediction of instability
Passive and active control

3

The flow is not modified by the radiated sound

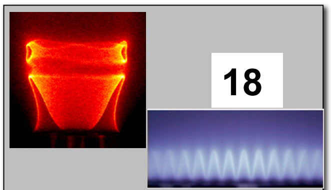

18

Direct noise weakly coupled

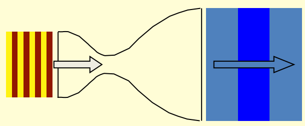

4

Indirect noise weakly coupled

The flow is modified by the radiated sound

Direct noise strongly coupled

7

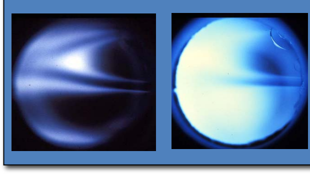

Indirect noise strongly coupled

0

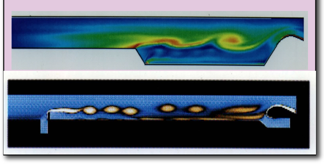

4

Indirect noise associated with entropy waves

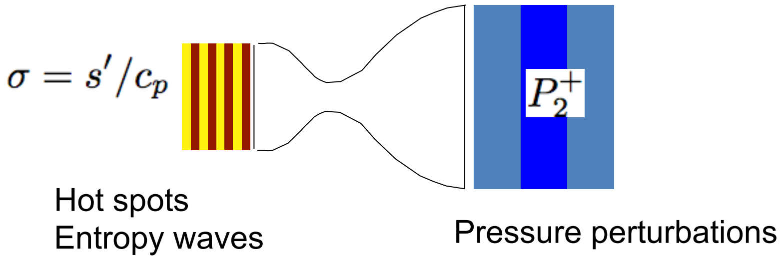

$$P_2^+ = \left(\frac{M_2 - M_1}{2}\right)\left[\frac{(1/2)\sigma}{1 + (1/2)(\gamma - 1)M_1}\right]$$

F.E. Marble and S.M. Candel (1977) Journal of Sound and Vibration **55**, 225-243. Acoustic disturbance from gas non-uniformities convected through a nozzle.

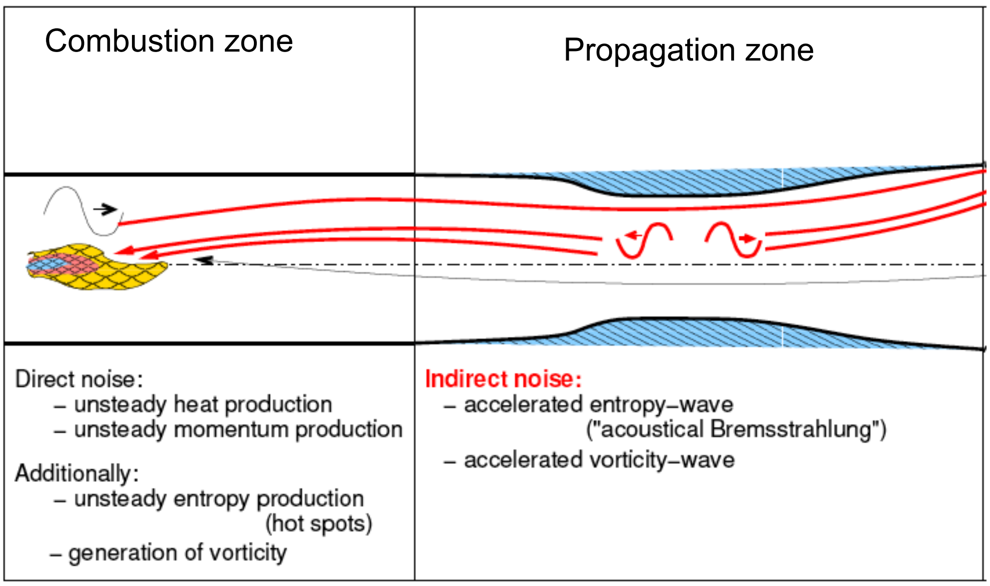

(from Schemel, Thiele, Bake, Lehmann and Michel (2004)

Interactions in combustion instabilities

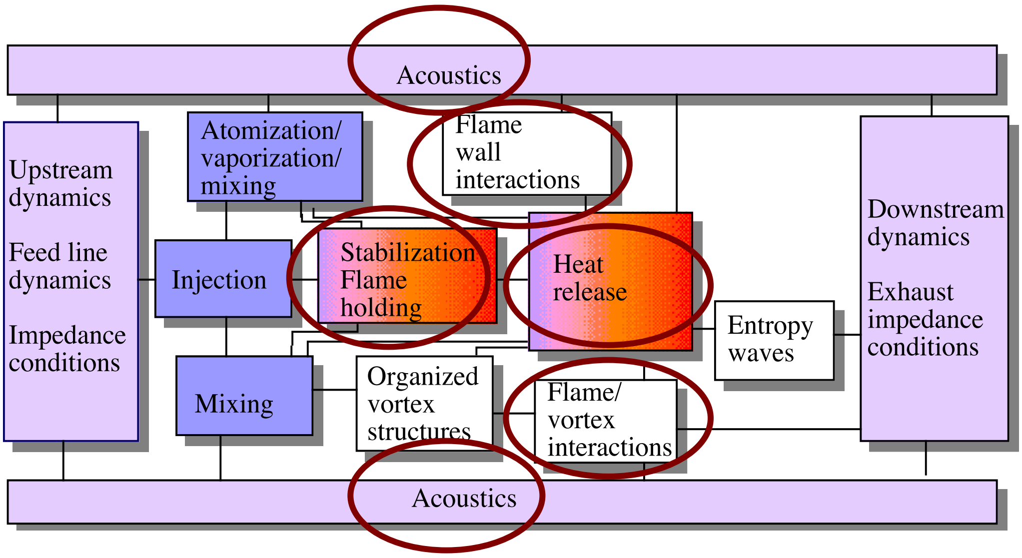

S. Candel (2002) *Proceedings of the Combustion Institute*, **29**. 1-28. Combustion dynamics and control : progress and challenges.

7

Early work on combustion noise

The soap bubble is filled with a mixture of fuel and air

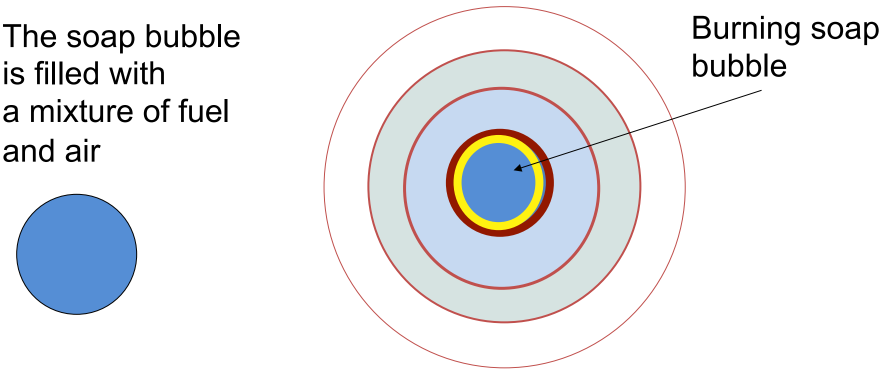

The farfield pressure field is due to the volume acceleration induced by non-steady combustion (Thomas and Williams 1966)

$$p'(\boldsymbol{r},t) = \frac{\rho_\infty}{4\pi r}\frac{d^2\Delta V}{dt^2}$$

The farfield can also be expressed in terms of the volumetric rate of consumption of reactants (Hurle et al. (1968), Price et al. (1968))

$$p'(\boldsymbol{r},t) = \frac{\rho_\infty}{4\pi r}\left(\frac{\rho_u}{\rho_b}-1\right)\left[\frac{dq}{dt}\right]_{t-\tau}$$

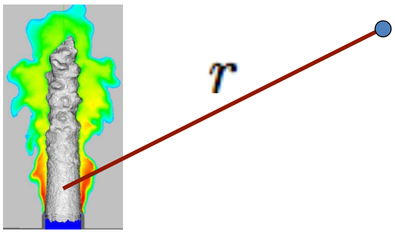

ρ_u/ρ_b is the volumetric expansion ratio

$\tau = r/c_0$ is the time required for acoustic propagation

q is the volumetric rate of consumption of reactants

For wrinkled flames, it is also possible to introduce the flame area (Abugov and Obrezkov(1978), Clavin and Siggia (1991))

$$p'(\boldsymbol{r},t) = \frac{\rho_\infty}{4\pi r}\left(\frac{\rho_u}{\rho_b}-1\right)S_L\left[\frac{dA}{dt}\right]_{t-\tau}$$

This is useful for theoretical analysis and has been employed to examine the spectral content of the radiated sound

The radiated power may be obtained from an estimate of the variance of the rate of change of flame surface area

$$W_a = \frac{\rho_\infty}{4\pi c_\infty}\left(\frac{1}{\rho_b}-\frac{1}{\rho_u}\right)^2(\rho_u S_L)^2\overline{\left(\frac{dA}{dt}\right)^2}$$

Strahle (1971, …1985) provides alternative expressions of the sound radiated by flames

$$p'(r,t) = c_0^2 \rho'(r,t) = -\frac{1}{4\pi r}\frac{\partial^2}{\partial t^2}\int_V \rho'_T\left(\boldsymbol{r}_0, t-\frac{r}{c_0}\right) dV(\boldsymbol{r}_0)$$

$$\rho'(r,t) = \frac{\bar{\rho}_1}{4\pi r}\int_{S_1} \frac{\partial \boldsymbol{v}_t}{\partial t}\left(\boldsymbol{r}_0, t-\frac{r}{c_0}\right)\cdot \boldsymbol{n}_0\, dS(\boldsymbol{r}_0)$$

$$p'(r,t) = \frac{\bar{\rho}_1}{4\pi r}\frac{\gamma-1}{\gamma \bar{p}}(-\Delta h_f^0)\int_{V_c} \frac{\partial \dot{\omega}}{\partial t}\left(\boldsymbol{r}_0, t-\frac{r}{c_0}\right) dV(\boldsymbol{r}_0)$$

$$\boxed{p'(\boldsymbol{r},t) = \frac{\gamma-1}{4\pi {c_0}^2}\int_V \frac{1}{|\boldsymbol{r}-\boldsymbol{r}_0|}\frac{\partial}{\partial t}\dot{Q}'(\boldsymbol{r}_0, t-|\boldsymbol{r}-\boldsymbol{r}_0|/c_0)dV(\boldsymbol{r}_0)}$$

11

Only keeping the heat release source term the following equation governs the noise emission from the flame

$$\boldsymbol{\nabla}^2 p - \frac{1}{c_0^2}\frac{\partial^2 p}{\partial t^2} = -\frac{\gamma-1}{c_0^2}\frac{\partial \dot{Q}'}{\partial t}$$

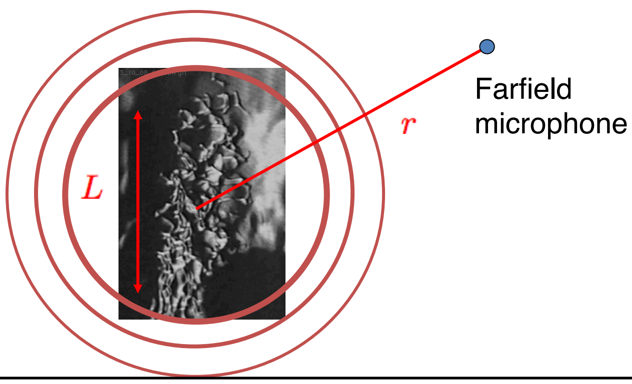

12

Assuming that radiation takes place in an unconfined domain and only keeping the source term associated with perturbations in heat release one obtains

$$p'(\boldsymbol{r},t) = \frac{\gamma-1}{4\pi {c_0}^2}\int_V \frac{1}{|\boldsymbol{r}-\boldsymbol{r}_0|}\frac{\partial}{\partial t}\dot{Q}'(\boldsymbol{r}_0, t-|\boldsymbol{r}-\boldsymbol{r}_0|/c_0)dV(\boldsymbol{r}_0)$$

When the observation point is in the farfield of a compact flame the previous expression becomes (Strahle (1985))

$$\boxed{p'(\boldsymbol{r},t) = \frac{\gamma-1}{4\pi {c_0}^2 r}\frac{\partial}{\partial t}\int_V \dot{Q}'(\boldsymbol{r}_0, t-r/c_0)dV(\boldsymbol{r}_0)}$$

The classical expression of Hurle and Price

$$p'(\boldsymbol{r},t) = \frac{\rho_\infty}{4\pi r}\left(\frac{\rho_u}{\rho_b}-1\right)\left[\frac{dq}{dt}\right]_{t-\tau}$$

is equivalent to that obtained previously

$$p'(\boldsymbol{r},t) = \frac{\gamma-1}{4\pi {c_0}^2 r}\frac{\partial}{\partial t}\int_V \dot{Q}'(\boldsymbol{r}_0, t-r/c_0)dV(\boldsymbol{r}_0)$$

when the flame is compact and is formed by premixed reactants. This is shown by noting that :

$$\rho_0\left(\frac{\rho_u}{\rho_b}-1\right)q = \rho_0\left(\frac{T_b}{T_u}-1\right)q = \frac{\gamma-1}{c_0^2}\int \dot{Q}' dV$$

Combustion noise scaling laws

The power radiated by the flame may be expressed as

$$W_a = \frac{\overline{p'^2}}{\rho_0 c_0} 4\pi r^2 = \frac{(\gamma-1)^2}{4\pi \rho_0 c_0^5} \int_V \overline{\frac{\partial \dot{Q}'}{\partial t}(\boldsymbol{r}'_0, t) \frac{\partial \dot{Q}'}{\partial t}(\boldsymbol{r}''_0, t) d\boldsymbol{r}'_0 d\boldsymbol{r}''_0}$$

Changing variables

$$\boldsymbol{r}'_0 = \boldsymbol{r}'_0$$

$$\xi_0 = \boldsymbol{r}''_0 - \boldsymbol{r}'_0$$

one obtains

$$W_a = \frac{\overline{p'^2}}{\rho_0 c_0} 4\pi r^2 = \frac{(\gamma-1)^2}{4\pi \rho_0 c_0^5} \int_V \overline{\frac{\partial \dot{Q}'}{\partial t}(\boldsymbol{r}'_0, t) \frac{\partial \dot{Q}'}{\partial t}(\boldsymbol{r}'_0 + \boldsymbol{\xi}_0, t) d\boldsymbol{r}'_0 d\boldsymbol{\xi}_0}$$

One obtains the following estimate

$$W_a = \frac{\overline{p'^2}}{\rho_0 c_0} 4\pi r^2 = \frac{(\gamma-1)^2}{4\pi \rho_0 c_0^5} f_c^2 \dot{Q}'^2_{max} V V_{cor}$$

where f_c is a characteristic frequency

$$\dot{Q}'_{max} = \eta \dot{m}_F h / V$$

$$\boxed{W_a = \frac{\overline{p'^2}}{\rho_0 c_0} 4\pi r^2 = \frac{(\gamma-1)^2}{4\pi \rho_0 c_0^5} f_c^2 \eta^2 (\dot{m}_F h)^2 \frac{V_{cor}}{V}}$$

f_c (Hz)

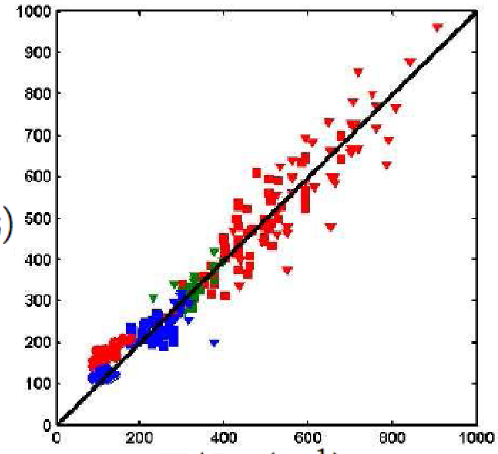

U/L_f (s^{-1})

$$f_c = U/L_f$$

Premixed combustion noise correlation established by Rajaram and Lieuwen (2006). (See also the work of Belliard and Truffaut)

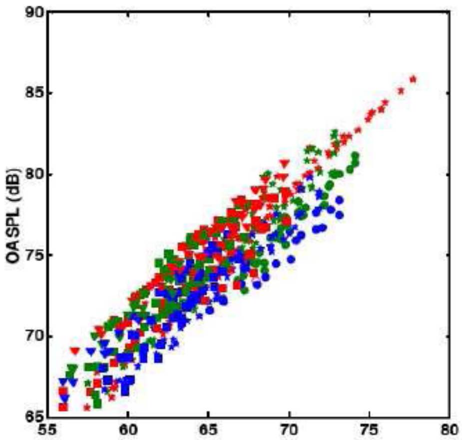

$10\log_{10}[f_c^2(\dot{m}_F h)^2]$

Premixed combustion noise correlation established by Rajaram and Lieuwen (2006)

Perturbed flame noise radiation

Compact premixed flame characterized by a thin reaction surface

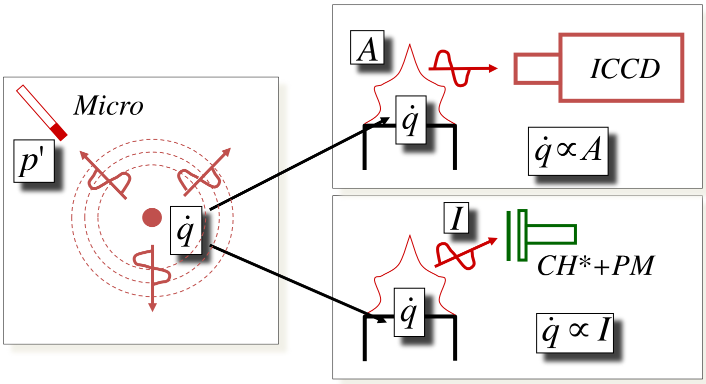

Heat realease rate is proportional to the flame surface area

Perturbed flame area is proportional to emission intensity from free radicals (CH*, OH*)

$$p_\infty(r,t) = k_1(r)\left[\frac{dI}{dt}\right]_{t-\tau} = k_2(r)\left[\frac{dA}{dt}\right]_{t-\tau}$$

k_1 and k_2 are known coefficients

19

Experimental setup

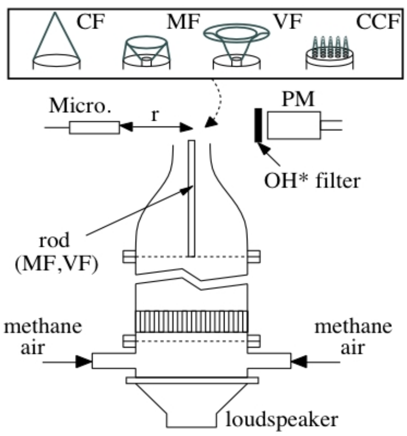

Flames stabilization

Burner rim	*conical and M flames*
Central rod	*V and M flames*
Perforated plate	*CCF*

Burner

Grid+ nozzle	*laminar flow*
Loudspeaker	*ac. Perturbation*
Axisymmetric	

Diagnostics *phased locked*

Microphone	*noise emission*
PM+ filter	*light emission*
LDV	*axial velocity*
PIV	*velocity field*
ICCD camera	*flame surface*

20

	Statio	(a)	(b)	(c)	(d)	(e)
Conical Flame (CF)						
M-flame						
V-flame						
Collection of conical flames						
Flame/ plate						

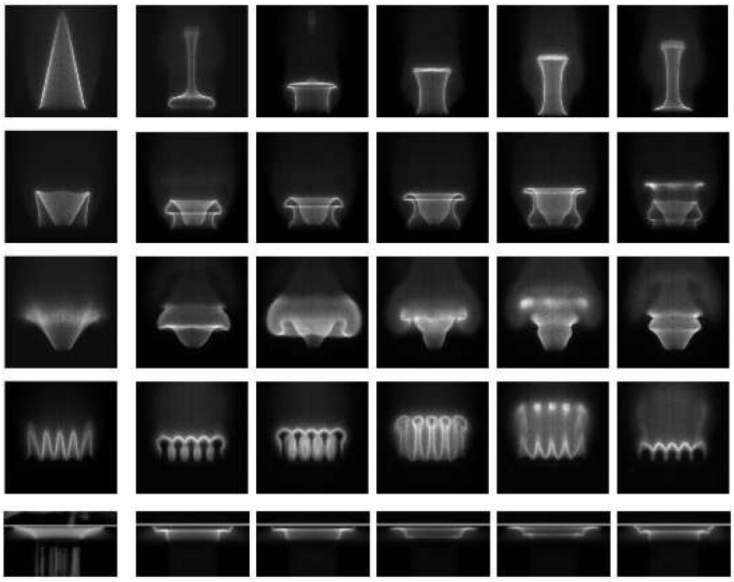

21

Perturbed conical flames

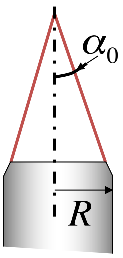

Low frequency modulation

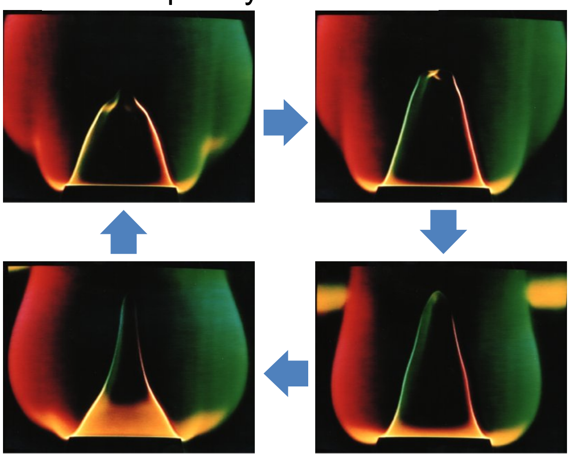

$$\omega_* = \frac{\omega R}{S_L \cos \alpha_0}$$

Methane-air flame, $\Phi = 0.95$, $v_0 = 0.96$ m.s^{-1}, $\omega_* = 5$

22

Perturbed conical flames

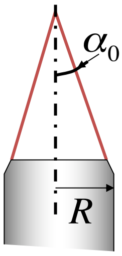

Intermediate frequency modulation

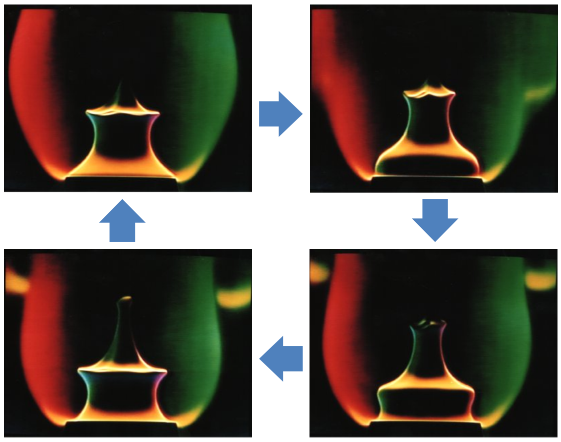

$$\omega_* = \frac{\omega R}{S_L \cos \alpha_0}$$

Methane-air flame, $\Phi = 0.95$, $v_0 = 0.96$ m.s^{-1}, $\omega_* = 15$

23

Noise emission from a conical flame

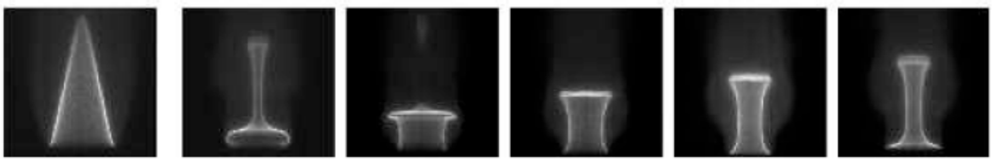

(a) (b) (c) (d) (e)

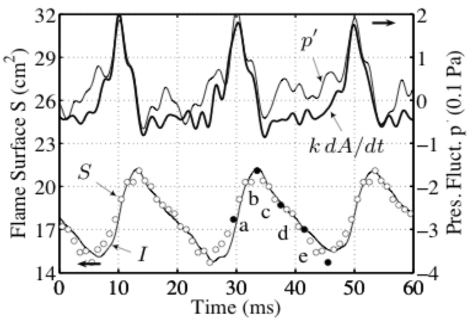

(a) **CF** : $f_e = 50\ Hz$, $\overline{v} = 1.7\ m\,s^{-1}$, $v_{rms} = 0.8\ m\,s^{-1}$, $\Phi = 1.11$

Conical flames

$\boxed{73\ \text{dB}}$

$v_{rms}/\overline{v} = 0.47$

$A_{rms}/\overline{A} = 0.11$

Strong harmonic forcing
Moderate level of noise generation

Maximum noise emission results from a *fast rate of production* of the flame surface area (a-b)

24

Mutual flame interaction noise radiation

Self-induced instability of a flame spreading from an annular burner

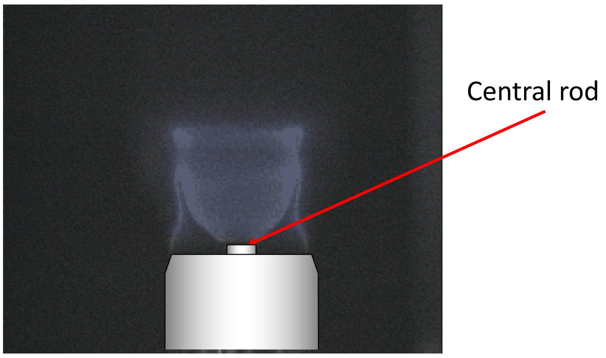

The M flame is stabilized both on the central rod and the burner rim

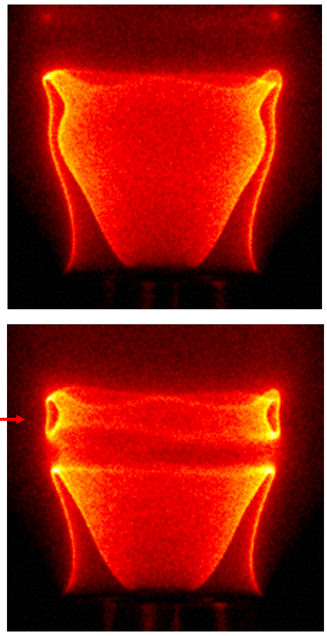

T. Schuller, D. Durox and S. Candel (2003) *Combustion and Flame*, **135**, 525-538. Self-induced combustion oscillations of laminar premixed flames stabilized on annular burners.

25

Noise emission from "*M*" flames

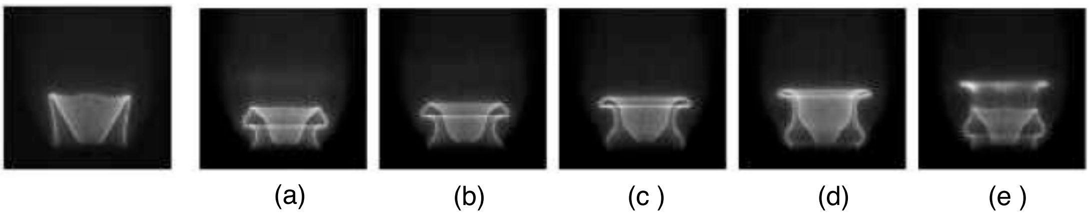

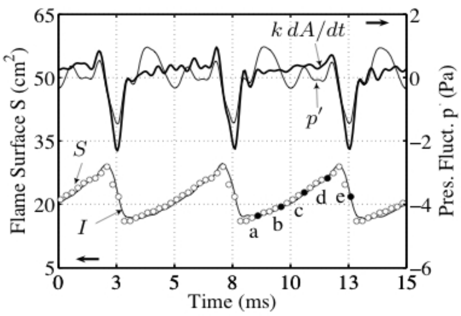

(b) **MF** : $f_e = 200\,Hz$, $\overline{v} = 2.3\,m\,s^{-1}$, $v_{rms} = 0.4\,m\,s^{-1}$, $\Phi = 1.11$

M flames

$\boxed{92\text{ dB}}$

$v_{rms}/\overline{v} = 0.17$

$A_{rms}/\overline{A} = 0.19$

Maximum noise emission corresponds to a *fast rate of destruction* of the flame surface area due to mutual annihilation of neighboring flame elements

26

Noise emission from "*M*"-flames

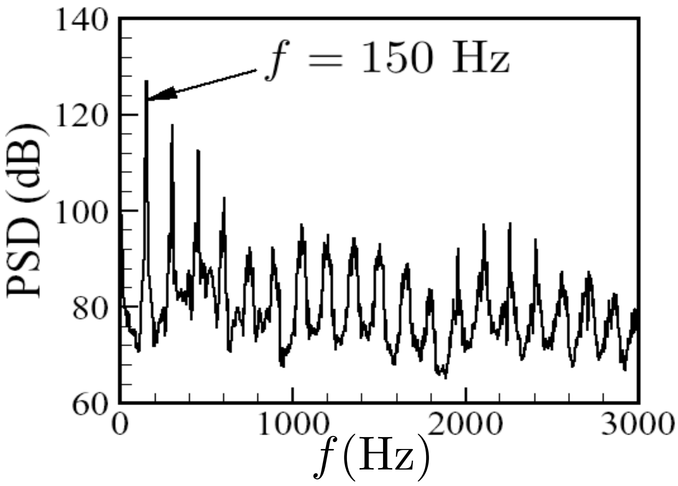

Power spectral density of acoustic pressure during flame/flame interaction

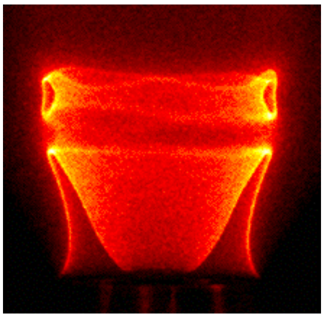

$\Phi = 1.13,\ v = 1.71\,\mathrm{m\ s^{-1}}, f = 150\,\mathrm{Hz},\ v' = 0.50\,\mathrm{m\ s^{-1}}$

$PSD(dB) = 10\log_{10}\left[PSD(Pa^2/Hz)\Delta f/p_{ref}^2\right]$

Flame vortex interactions

Visualization of the flame-vortex interaction (inverted conical flame) obtained by applying an Abel transform to direct images of light emission by the flame

Vorticity fields provided by phase averaged PIV

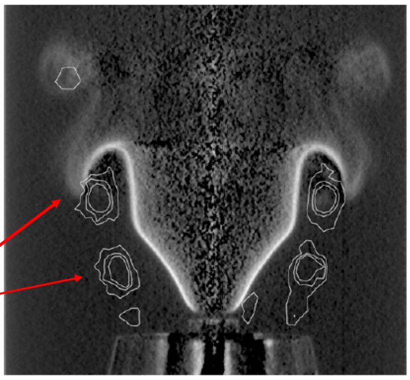

$\Phi = 0.8,\ v = 1.87\,\mathrm{m\ s^{-1}},\ f = 150\,\mathrm{Hz}, v' = 0.15\mathrm{m\ s^{-1}}$

D. Durox, T. Schuller and S. Candel (2005) *Proceedings of the Combustion Institute* **30**, 1717-1724. Combustion dynamics of inverted conical flames.

Flame vortex interactions

Visualization of the flame-vortex interaction (inverted conical flame) obtained by applying an Abel transform to direct images of light emission by the flame

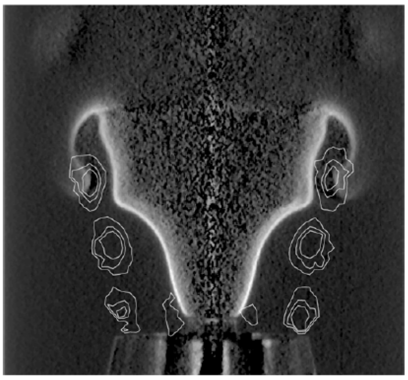

$$\Phi = 0.8,\ v = 1.87\,\mathrm{m\ s^{-1}},\ f = 150\,\mathrm{Hz}, v' = 0.15\mathrm{m\ s^{-1}}$$

D. Durox, T. Schuller and S. Candel (2005*) Proceedings of the Combustion Institute* **30**, 1717-1724. Combustion dynamics of inverted conical flames.

©Sebastien Candel, June 2019

Flame vortex interactions

Visualization of the flame-vortex interaction (inverted conical flame) obtained by applying an Abel transform to direct images of light emission by the flame

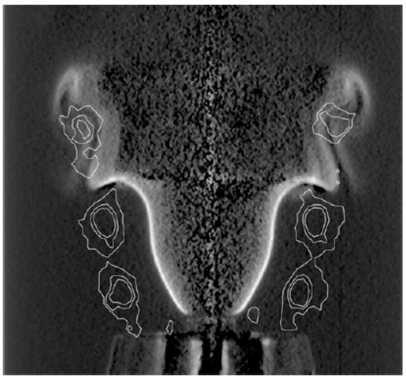

$$\Phi = 0.8,\ v = 1.87\,\mathrm{m\ s^{-1}},\ f = 150\,\mathrm{Hz}, v' = 0.15\mathrm{m\ s^{-1}}$$

D. Durox, T. Schuller and S. Candel (2005*) Proceedings of the Combustion Institute* **30**, 1717-1724. Combustion dynamics of inverted conical flames.

Flame vortex interactions

Visualization of the flame-vortex interaction (inverted conical flame) obtained by applying an Abel transform to direct images of light emission by the flame

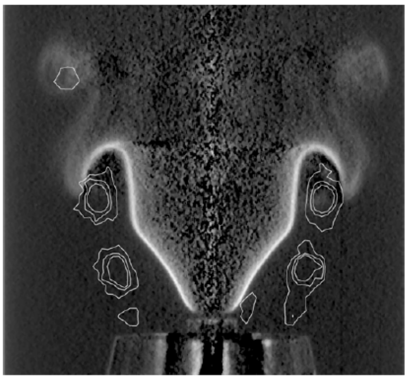

$$\Phi = 0.8,\ v = 1.87\,\mathrm{m\ s^{-1}},\ f = 150\,\mathrm{Hz}, v' = 0.15\mathrm{m\ s^{-1}}$$

D. Durox, T. Schuller and S. Candel (2005*) Proceedings of the Combustion Institute* **30**, 1717-1724. Combustion dynamics of inverted conical flames.

Noise emission from V-flame

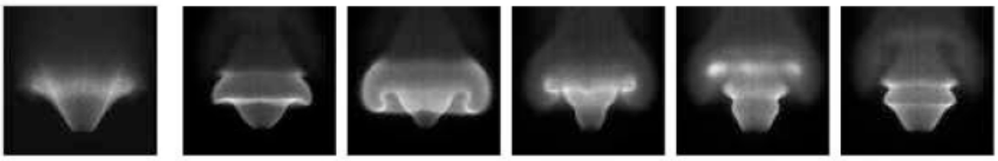

(a) (b) (c) (d) (e)

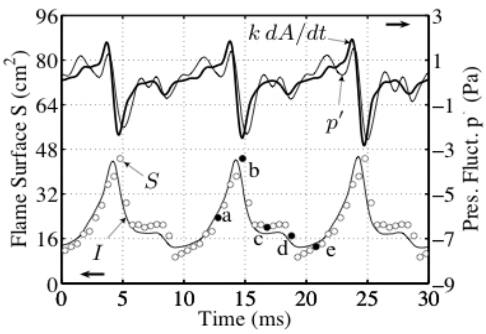

(c) **VF** : $f_e = 100\,Hz,\ \overline{v} = 2.3\,m\,s^{-1}$, $v_{rms} = 0.6\,m\,s^{-1}, \Phi = 1.11$

V flames $\boxed{96\text{ dB}}$

$v_{rms}/\overline{v} = 0.26$

$A_{rms}/\overline{A} = 0.43$

Maximum noise production corresponds to a *fast rate of destruction* of the flame surface area due to flame vortex interaction

D. Durox, T. Schuller and S. Candel (2005*) Proceedings of the Combustion Institute* **30**, 1717-1724. Combustion dynamics of inverted conical flames.

Noise emission from V flames

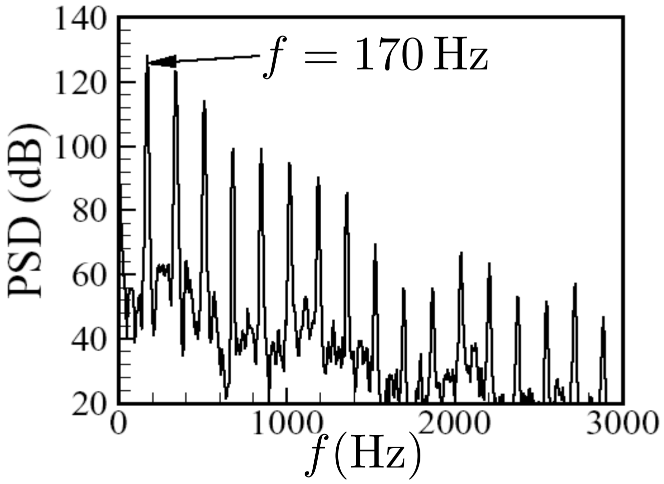

$\Phi = 0.92,\ v = 2.56\,\mathrm{m\ s^{-1}},\ f = 170\,\mathrm{Hz},\ v' = 0.30\,\mathrm{m\ s^{-1}}$

Power spectral density of acoustic pressure during flame vortex interaction

$$PSD(dB) = 10\log_{10}\left[PSD(Pa^2/Hz)\Delta f/p_{ref}^2\right]$$

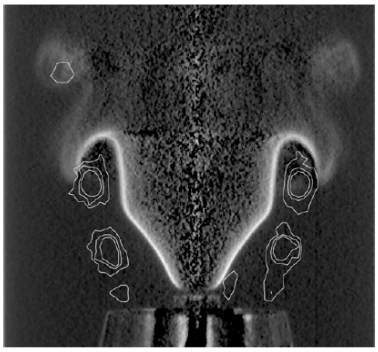

D. Durox, T. Schuller and S. Candel (2005) *Proceedings of the Combustion Institute* **30**, 1717-1724. Combustion dynamics of inverted conical flames.

Noise emission from a collection of small conical flames

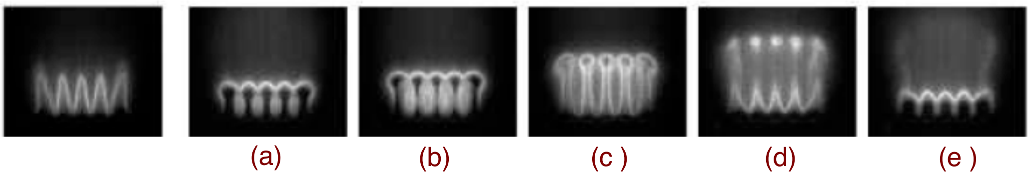

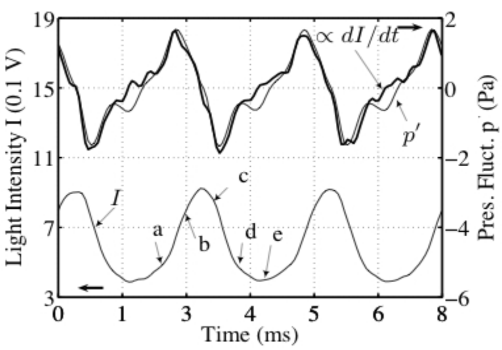

(d) **CSCF :** $f_e = 400\ Hz,\ \overline{v} = 5.0\ m\ s^{-1}$, $v_{rms} = 0.9\ m\ s^{-1},\ \Phi = 0.95$

Collection of conical flames

$v_{rms}/\overline{v} = 0.18$ $\boxed{96\ \mathrm{dB}}$

Maximum and minimum pressure peaks result from both *fast rates of production (a-b) and destruction (c-d)* of the flame surface area

N. Noiray, D. Durox, T. Schuller and S. Candel (2006) *Combustion and Flame.* **145**, 435-446. Self-induced instabilities of premixed flames in a multiple injection configuration.

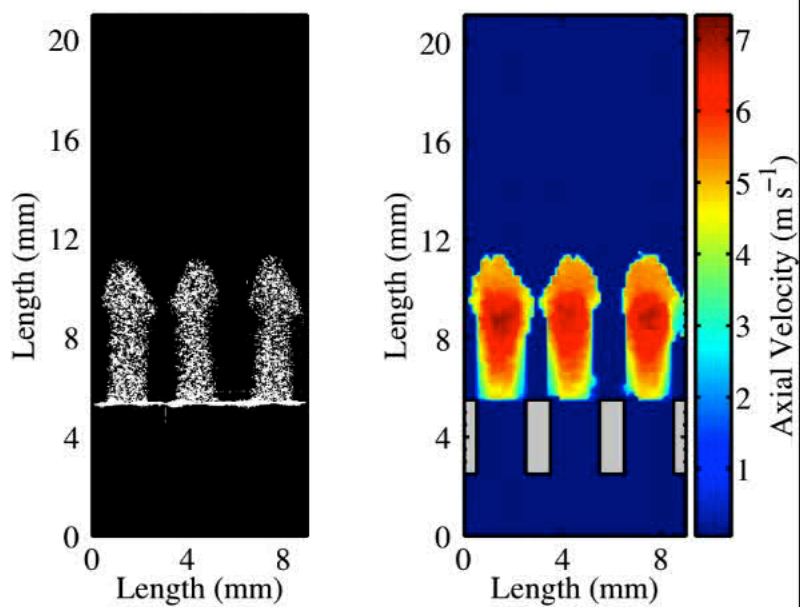

35

Flame interaction with solid boundaries

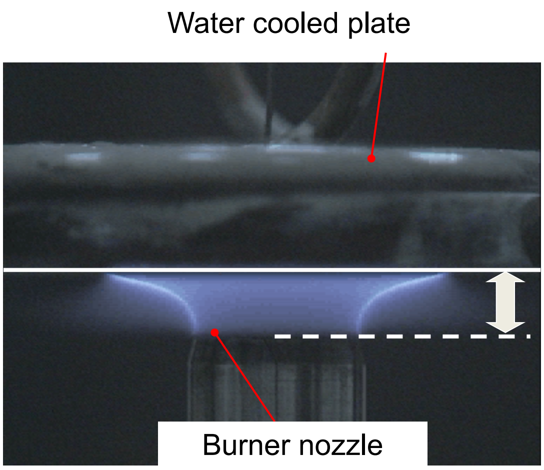

Self-induced oscillation occur as a function of plate to nozzle distance

Overall sound level as a function of modulation frequency

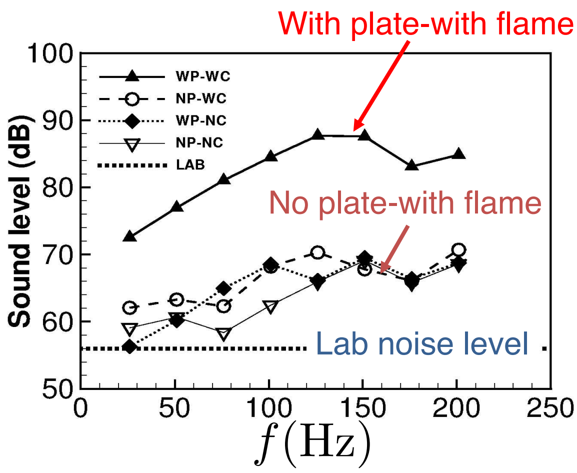

T. Schuller, D. Durox and S. Candel (2002) *Combustion and Flame*, **128**, 88-110. Dynamics of and noise radiated by a perturbed impinging premixed jet flame.

36

Confinement effects, noise and instabilities

- Most of the work on combustion noise concerns radiation from unconfined flames.
- In many applications combustion takes place in a confined environment and sound is radiated from the system inlet and exhaust
- Confinement induces interactions between the radiated field and the sources of sound

  (1) Weak coupling manifested by enhancement of sound by system resonances

  (2) Strong coupling in which energy fed in the burner eigenmodes destabilizes the reactive flow

37

The analysis may be carried out by expanding the perturbed field on a basis of eigenmodes (Zinn (1972), Culick(1980…))

$$p'(\boldsymbol{r},t) = \sum a_n(t)\psi_n(\boldsymbol{r})$$

The eigenmodes satisfy the homogeneous equation

$$\boldsymbol{\nabla}\cdot\bar{c}^2\boldsymbol{\nabla}\psi_n + \omega_n^2\psi_n = 0$$

The modal amplitudes are given

$$\frac{d^2 a_n}{dt^2} + \omega_n^2 a_n = F_n$$

where

$$F_n = \frac{\bar{c}^2}{\Lambda_n}\left[\int_V \frac{\gamma-1}{\bar{c}^2}\frac{\partial \dot{Q}'}{\partial t}\psi_n(\boldsymbol{r}_0)dV(\boldsymbol{r}_0) + \int_S f\psi_n(\boldsymbol{r}_0)dS(\boldsymbol{r}_0)\right]$$

Heat release rate　　　　Boundary effects

38

- Boundaries have two main effects :
  (1) They modify the reflection response of the system
  (2) They alter the flame dynamics
- The first item is treated in **S. Candel et al.** (2007) « Computational Flame Dynamics ». Invited lecture, ECCOMAS Computational Combustion. Delft
- The second item is illustrated by systematic variations of lateral confinement [Birbaud et al. (2007)]

$$\xi = \frac{d}{D} = \frac{\text{Injector diam}}{\text{Flame tube diam}}$$

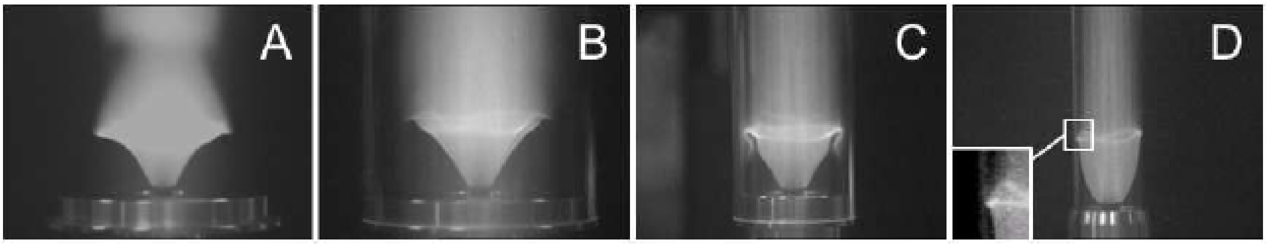

$\xi = 0.$ $\xi = 0.32$ $\xi = 0.64$ $\xi = 1.00$

39

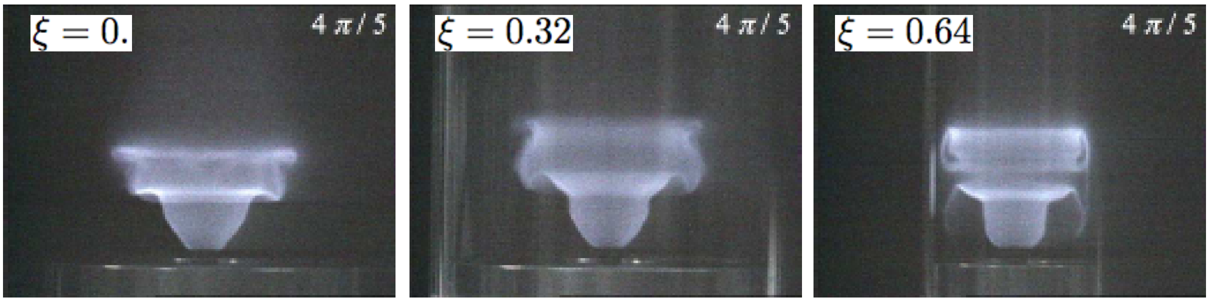

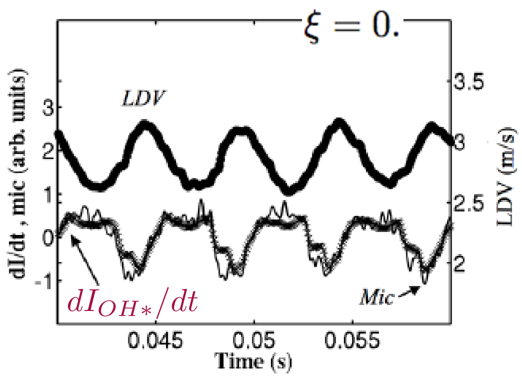

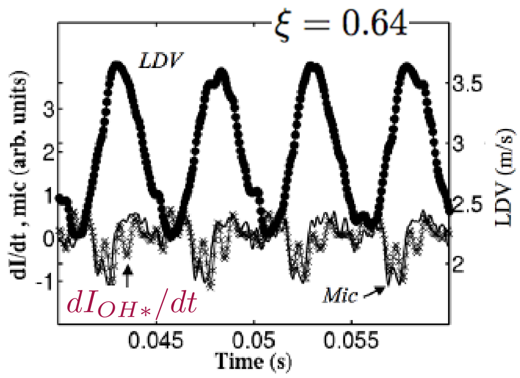

40

Conclusions and perspectives

- Progress in combustion noise has been quite substantial
- Sources of indirect combustion noise identified in the 70's are now the subject of further evaluation based on modern computational tools
- Direct combustion noise sources also identified during the same period have been studied in a series of detailed investigations of perturbed flames
- Basic expressions providing the sound field in terms of heat release rate fluctuations are now well validated in the premixed case
- Early correlations for the radiated sound power and spectral densities have been improved

41

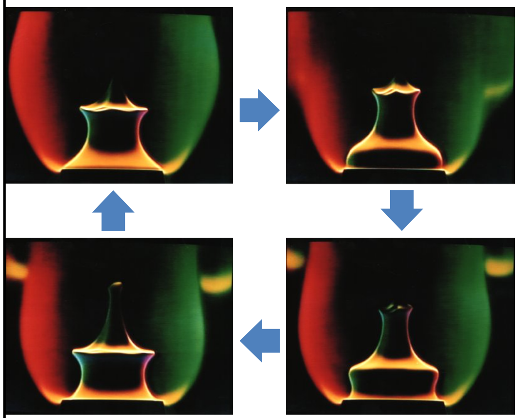

Combustion dynamics
Lecture 3a

S. Candel, D. Durox , T. Schuller

CentraleSupélec
Université Paris-Saclay, EM2C lab, CNRS

Tsinghua summer school, June 2021

1

Typical instability mechanism

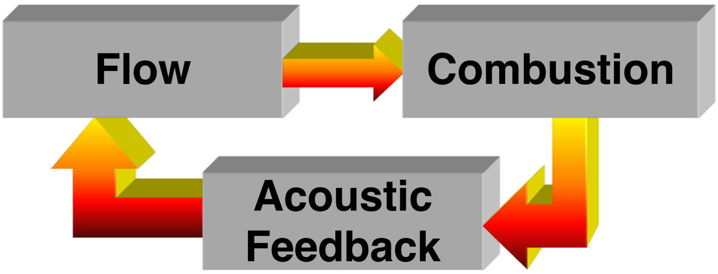

- Flow perturbation is produced
- This induces a combustion perturbation
- Acoustic feedback links the unsteady combustion process to flow perturbation
- The system is unstable if the gain exceeds the damping

2

A simplified instability model

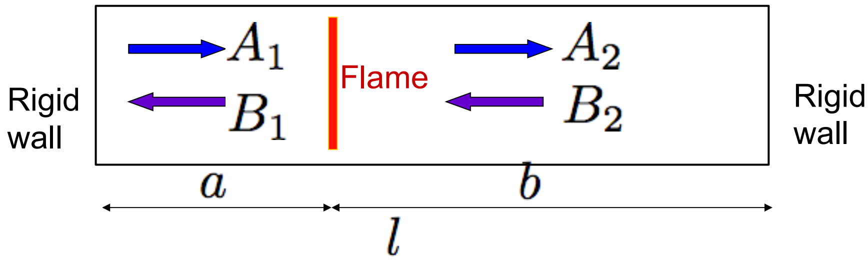

In region 1 (upstream of the flame)

$$p_1 = A_1 \exp(ikx) + B_1 \exp(-ikx)$$

$$v_1 = \frac{1}{\rho_0 c}[A_1 \exp(ikx) - B_1 \exp(-ikx)]$$

In region 2 (downstream ofthe flame)

$$p_2 = A_2 \exp(ikx) + B_2 \exp(-ikx)$$

$$v_2 = \frac{1}{\rho_0 c}[A_2 \exp(ikx) - B_2 \exp(-ikx)]$$

A simplified instability model

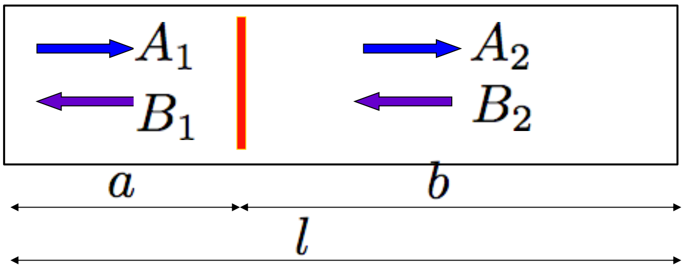

Across the flame, the pressure is continuous, the jump in velocity fluctuations is governed by fluctuations in heat release rate which caused by velocity fluctuations.

$$p_1 = p_2$$
$$v_2 - v_1 = \mathcal{F}(\omega) v_1$$

In this expression $\mathcal{F}(\omega)$ designates the flame transfer function multiplied by $(T_b/T_u) - 1$

The left and right conditions correspond to rigid walls $v_1(0) = 0 \; v_2(l) = 0$

Dispersion relation

$$\sin(kl) + \mathcal{F}(\omega)\cos(kb)\sin(ka) = 0$$

It is convenient to define

$$\mathcal{H}(\omega) = \sin(kl)$$
$$\mathcal{L}(\omega) = \sin(ka)\cos(kb)$$

In the absence of a flame, the resonant modes are given by

$$\mathcal{H}(\omega_0) = 0$$

The first root corresponds to

$$\omega_0 = \pi c/l \qquad f_0 = c/(2l) \qquad \lambda = 2l$$

Half wave mode

Assuming that the flame response is weak and expanding to first order one obtains

$$\mathcal{H}(\omega_0) + \left[\frac{d\mathcal{H}}{d\omega}\right]_{\omega_0} \omega_1 + \mathcal{F}(\omega_0)\mathcal{L}(\omega_0) = 0$$

Since $\mathcal{H}(\omega_0) = 0$

One obtains the first order estimate $\omega_1 = -\dfrac{\mathcal{F}(\omega_0)\mathcal{L}(\omega_0)}{[d\mathcal{H}/d\omega]_{\omega_0}}$

$$\mathcal{L}(\omega_0) = \sin(\pi a/l)\cos(\pi b/l)$$

$$[d\mathcal{H}/d\omega]_{\omega_0} = (l/c)\cos(\omega_0 l/c) = -(l/c)$$

- The sign of the imaginary part of the angular frequency defines the stability of this system. If the sign is positive, the system is unstable

$$\frac{\omega_{1i} l}{c} = G(\omega)\sin[\phi(\omega_0)]\sin(\pi a/l)\cos(\pi b/l)$$

In general $b/l > 1/2$ hence $\cos(\pi b/l) < 0$

and the first mode will be linearly unstable if

$\pi < \phi(\omega_0) < 2\pi$ modulo 2π

One may now consider a sitation where the duct is closed on the upstream side and open downstream

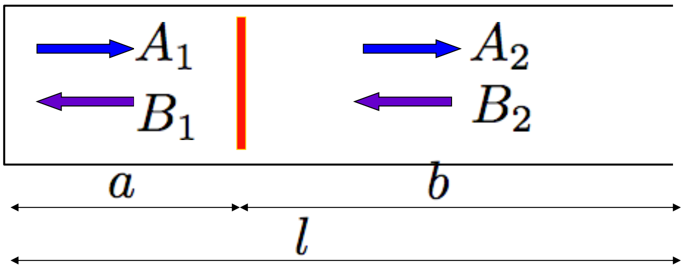

This case may be worked out as before. One has to change the boundary condition at *x=l*

The dispersion relation becomes

$$\mathcal{H}(\omega) = \cos kl - \mathcal{F}(\omega) \sin ka \sin kb = 0$$

In the absence of a flame the dispersion relation becomes

$$\cos kl = 0$$

The first root of this expression is given by

$$\omega_0 = \frac{\pi}{2}\frac{c}{l}$$ corresponding to $$f_0 = \frac{c}{4l}$$ $$\lambda = 4l$$

Quarter wave mode

Assuming that the flame response is weak and expanding to first order one obtains

$$\mathcal{H}(\omega_0) + \left[\frac{d\mathcal{H}}{d\omega}\right]_{\omega_0} \omega_1 + \mathcal{F}(\omega_0)\mathcal{L}(\omega_0) = 0$$

where $\mathcal{L}(\omega) = -\sin ka \sin kb$

- Since $\mathcal{H}(\omega_0) = 0$

  One obtains the first order estimate $\omega_1 = -\dfrac{\mathcal{F}(\omega_0)\mathcal{L}(\omega_0)}{\left[d\mathcal{H}/d\omega\right]_{\omega_0}}$

- This yields after some calculations

$$\omega_1 = -\frac{c}{l}\mathcal{F}(\omega_0)\sin k_0 a \sin k_0 b$$

- The imaginary part of the angular frequency perturbation is given by

$$\omega_{1i} = -\frac{c}{l}G(\omega_0)\sin\phi \sin\frac{\pi a}{2l}\sin\frac{\pi b}{2l}$$

The system is unstable if $\pi < \phi < 2\pi$ modulo 2π

Combustion dynamics
Lecture 3b

S. Candel, D. Durox , T. Schuller

CentraleSupélec
Université Paris-Saclay, EM2C lab, CNRS

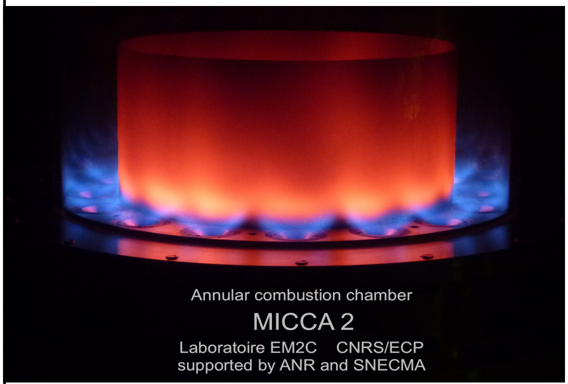

Tsinghua summer school, June 2021

1

A unified dynamical modeling of combustion instabilities

Expansion on system eigenmodes
General formulation
Coupled cavity modeling

2

- Low order modeling of combustion dynamics may be carried out by expanding the state variables in terms of the system modes
- Pressure fluctuations are expanded on the system eigenmodes, a method introduced by Ben Zinn and explored by Culick and his coworkers

$$p'(t,\mathbf{x}) = \sum_{m=1}^{N} \eta_m(t)\Psi_m(\mathbf{x})$$

- Where Ψ_n are the eigenfunctions corresponding to the eigenfrequencies ω_n

$$\frac{\omega_n^2}{\overline{c}^2}\Psi_n + \overline{\rho}\nabla\cdot\left(\frac{1}{\overline{\rho}}\nabla\Psi_n\right) = 0$$

$$\kappa_1\Psi_n|_S + \kappa_2\nabla\Psi_n\cdot\mathbf{n}|_S \quad = 0$$

B. T. Zinn and E.A. Powell (1970) Application of the Galerkin method in the solution ofCombustion instability problems. Proc. 19th International Astronautical Congress on Propulsion, Re-entry physics Vol. 3, 59-73 (p.99), Pergamon press, Oxford

Zinn, B. T. & Lores, M. E. (1972) Combust. Sci. Technol. 4, 269. Application of galerkin method in solution of nonlinear axial combustion instability problems in liquid rockets.

F.E.C. Culick (1971) Nonlinear growth and limiting amplitude of acoustic waves in combustion chambers. *Combustion Science and Technology* 3 (1) p. 16.

- The eigenmodes are orthogonal

$$\int_V \Psi_m\Psi_n dV = 0,\ m \neq n \qquad \Lambda_n = \int_V \Psi_n^2 dV$$

- The modal expansion is inserted in the wave equation

$$\frac{\partial^2 p'}{\partial t^2} + \alpha\frac{\partial p'}{\partial t} - \bar{\rho}\bar{c}^2\nabla\cdot\left(\frac{1}{\bar{\rho}}\nabla p'\right) = (\gamma-1)\frac{\partial \dot{q}'}{\partial t}$$

- After multiplication by Ψ_n and integration over the control volume *V*

$$\frac{d^2\eta_n}{dt^2} + \alpha\frac{d\eta_n}{dt} + \omega_n^2\eta_n = \frac{1}{\Lambda_n}(\gamma-1)\int_V \frac{\partial\dot{q}'}{\partial t}\Psi_n dV$$

$$+\frac{1}{\Lambda_n}\underbrace{\int_S \bar{c}^2(\Psi_n\nabla p' - p'\nabla\Psi_n)\cdot\mathbf{n}dS}_{\text{Surface source term}}$$

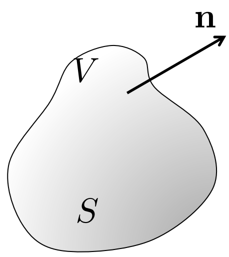

- Assuming that the pressure field and the modes satisfy the same homogeneous boundary conditions

$$\kappa_1 p' + \kappa_2 \nabla p' \cdot \mathbf{n} = 0 \qquad \kappa_1 \Psi_n + \kappa_2 \nabla \Psi_n \cdot \mathbf{n} = 0$$

- The surface term vanishes and the normal modes amplitudes satisfy a set of differential equations featuring on their right hand sides the projection of the time derivatives of the heat release rates

$$\frac{d^2\eta_n}{dt^2} + \alpha \frac{d\eta_n}{dt} + \omega_n^2 \eta_n = \frac{1}{\Lambda_n}(\gamma - 1) \int_V \frac{\partial \dot{q}'}{\partial t} \Psi_n dV$$

- These equations describe the dynamics of the system if the heat release rate can be linked to the state variables so that the right hand side can be determined

Formulation for coupled cavities

- Model derivation (variant for coupled cavities)
  - Application of the modal amplitude equations to the plenum

$$\frac{d^2\eta_{n,pl}}{dt^2} + \alpha \frac{d\eta_{n,pl}}{dt} + \omega_{n,pl}^2 \eta_{n,pl} = -\frac{\overline{\rho}_u \overline{c}_u^2}{\Lambda_{n,pl}} \sum_{x_s} A(x_s) \Psi_{n,pl}(x_s) \frac{du'_{pl}(x_s)}{dt}$$

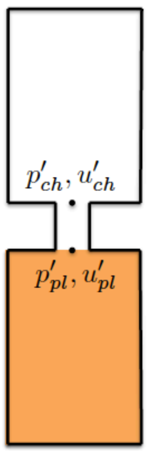

Formulation for coupled cavities

- **Model derivation**
  - Application of the modal amplitude equations to the plenum

$$\frac{d^2\eta_{n,pl}}{dt^2} + \alpha\frac{d\eta_{n,pl}}{dt} + \omega_{n,pl}^2\eta_{n,pl} = -\frac{\overline{\rho}_u\overline{c}_u^2}{\Lambda_{n,pl}}\sum_{x_s} A(x_s)\Psi_{n,pl}(x_s)\frac{du'_{pl}(x_s)}{dt}$$

  - Application of the modal amplitude equations to the chamber

$$\frac{d^2\eta_{n,ch}}{dt^2} + \alpha\frac{d\eta_{n,ch}}{dt} + \omega_{n,ch}^2\eta_{n,ch} = -\frac{\overline{\rho}_u\overline{c}_u^2}{\Lambda_{n,ch}}\sum_{x_s} A(x_s)\Psi_{n,ch}(x_s)\frac{du'_{ch}(x_s)}{dt}$$

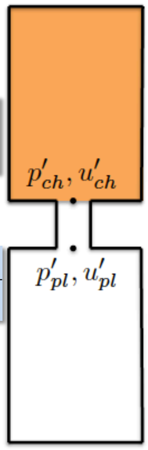

Formulation for coupled cavities

- **Model derivation**
  - Application of the modal amplitude equations to the plenum

$$\frac{d^2\eta_{n,pl}}{dt^2} + \alpha\frac{d\eta_{n,pl}}{dt} + \omega_{n,pl}^2\eta_{n,pl} = -\frac{\overline{\rho}_u\overline{c}_u^2}{\Lambda_{n,pl}}\sum_{x_s} A(x_s)\Psi_{n,pl}(x_s)\frac{du'_{pl}(x_s)}{dt}$$

  - Application of the modal amplitude equations to the chamber

$$\frac{d^2\eta_{n,ch}}{dt^2} + \alpha\frac{d\eta_{n,ch}}{dt} + \omega_{n,ch}^2\eta_{n,ch} = -\frac{\overline{\rho}_u\overline{c}_u^2}{\Lambda_{n,ch}}\sum_{x_s} A(x_s)\Psi_{n,ch}(x_s)\frac{du'_{ch}(x_s)}{dt}$$

  - Injector representation to close the model

$$\begin{pmatrix} u'_{ch} \\ u'_{pl} \end{pmatrix} = [Y]\begin{pmatrix} p'_{ch} \\ p'_{pl} \end{pmatrix}$$

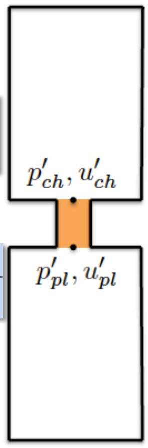

Main steps in the derivation

The starting point is the wave equation for the pressure perturbation

$$\frac{\partial^2 p'}{\partial t^2} + \alpha \frac{\partial p'}{\partial t} - \bar{\rho}\bar{c}^2 \nabla . \left(\frac{1}{\bar{\rho}} \nabla p' \right) = (\gamma - 1) \frac{\partial q'}{\partial t}$$

$$\kappa_1 p'|_S + \kappa_2 \nabla p' \cdot \mathbf{n}|_S = 0 \ \text{ where } \nabla p' \cdot \mathbf{n}|_S = -\bar{\rho} \left. \frac{\partial u'}{\partial t} \right|_S$$

Multiplying by the *n*-th eigenfunction

$$\Psi_n [\frac{\partial^2 p'}{\partial t^2} + \alpha \frac{\partial p'}{\partial t} - \overline{\rho}\, \overline{c}^2 \nabla \cdot (\frac{1}{\overline{\rho}} \nabla p')] = \Psi_n (\gamma - 1) \frac{\partial q'}{\partial t}$$

and integrating over the volume one gets

$$\int_V \Psi_n [\frac{\partial^2 p'}{\partial t^2} + \alpha \frac{\partial p'}{\partial t} - \overline{\rho}\, \overline{c}^2 \nabla \cdot (\frac{1}{\overline{\rho}} \nabla p')] dV = \int_V \Psi_n (\gamma - 1) \frac{\partial q'}{\partial t} dV$$

Main steps in the derivation

$$\int_V \nabla \cdot \left(\frac{1}{\bar{\rho}} \nabla p' \right) \Psi_n dV = \int_V \nabla \cdot \left(\frac{1}{\bar{\rho}} \nabla \Psi_n \right) p' dV + \int_S \frac{1}{\bar{\rho}} (\Psi_n \nabla p' - p' \nabla \Psi_n) \cdot \boldsymbol{n} dS$$

Since $\frac{\omega_n^2}{\overline{c}^2} \Psi_n + \overline{\rho} \nabla \cdot (\frac{1}{\overline{\rho}} \nabla \Psi_n) = 0$ one has:

$$\int_V \nabla \cdot \left(\frac{1}{\bar{\rho}} \nabla p' \right) \Psi_n dV = \int_V -\frac{\omega_n^2}{\bar{\rho}\bar{c}^2} \Psi_n p' dV + \int_S \frac{1}{\bar{\rho}} (\Psi_n \nabla p' - p' \nabla \Psi_n) \cdot \boldsymbol{n} dS$$

Since $\int_V \Psi_m \Psi_n dV = 0$ for $m \neq n$ $\Lambda_n = \int_V \Psi_n^2 dV$ one obtains:

$$\int_V \nabla \cdot \left(\frac{1}{\bar{\rho}} \nabla p' \right) \Psi_n dV = -\Lambda_n \frac{\omega_n^2}{\bar{\rho}\bar{c}^2} \eta_n + \int_S \frac{1}{\bar{\rho}} (\Psi_n \nabla p' - p' \nabla \Psi_n) \cdot \boldsymbol{n} dS$$

Main steps in the derivation

Introducing the modal expansion $p' = \sum_m \eta_m \Psi_m$
one obtains

$$\frac{d^2\eta_n}{dt^2} + \alpha\frac{d\eta_n}{dt} + \omega_n^2\eta_n = \frac{\gamma-1}{\Lambda_n}\int_V \frac{d\dot{q}'}{dt}\Psi_n dV - \frac{\overline{\rho}_u\overline{c}_u^2}{\Lambda_n}\sum_{x_s} A(x_s)\Psi_n(x_s)\frac{du'(x_s)}{dt}$$

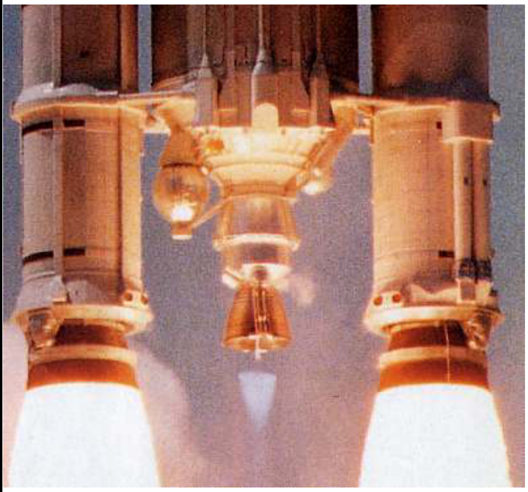

Combustion dynamics Lecture 4a

S. Candel, D. Durox , T. Schuller
CentraleSupélec
Université Paris-Saclay, EM2C lab, CNRS

Tsinghua summer school, June 2021

Sensitive time lag concepts

Time lag analysis
An equation for the sensitive time lag
Heat release rate fluctuations
Intrinsic low frequency instability analysis of rocket engines

Time lag analysis

Luigi Crocco (1909-1986) one of the founders of combustion instability theory, was a professor at Princeton for many years. He spent the later part of his life in Paris and was a Professor at Ecole Centrale Paris for a few years

H.S. Tsien (Tsien Hsue-Shen or Qian Xuesen) (1911-2009) one of rocket propulsion pioneers, went to study at Caltech under the supervision of Theodore von Karman, he was one of the founders of the Jet Propulsion Laboratory, and later "Father of China's Space Program"

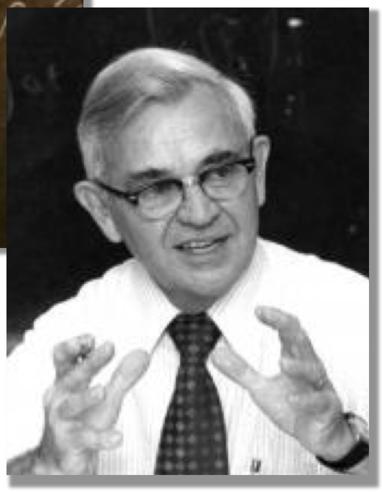

Frank Marble (1918-2014) jet propulsion pionneer and eminent adviser

Rocket motor

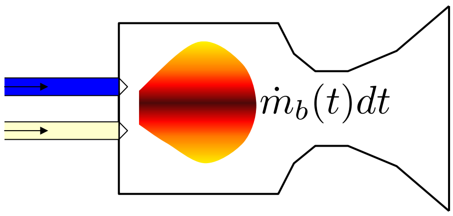

Consider a mass of propellant burning between times *t* and *t+dt*

$$\dot{m}_b(t)dt$$

This mass must be equal to the mass injected from $t-\tau$ to $t-\tau+d(t-\tau)$

Thus

$$\dot{m}_b(t)dt = \dot{m}_i(t-\tau)d(t-\tau)$$

- This yields a relation between the mass rate of burning and the mass rate of propellants injected in the chamber

$$\dot{m}_b(t) = \dot{m}_i(t-\tau)(1-\frac{d\tau}{dt})$$

- If the time lag is constant the last term vanishes and the mass rate of burning reflects the mass rate of injected propellants with a delay

$$\dot{m}_b(t) = \dot{m}_i(t-\tau)$$

- In general the delay is not constant but is sensitive to the values of the state variables governing the conversion rate of propellants in the chamber

An equation for the sensitive time lag

- An equation for the time lag may be derived by considering the process involved in the conversion of propellants into combustion products. Consider a function $f(p, T_g)$ which globally describes this process.

- This function will depend on pressure and gas temperature and may also depend on other parameters. To fix the ideas this function may be considered to represent the rate of heat transfer to the propellant. Vaporization of the liquid propellant will be achieved when a certain amount of heat designated by *C* will have been transferred to the liquid. This may be described by stating that the sum of this function over the time lag will have to be equal to *C*

$$\int_{t-\tau}^{t} f(p, T_g)dt' = C = \text{const.}$$

- The dependence of the time lag with respect to the state parameters is made more explicit by differentiating the previous equation with respect to time

$$f[p(t), T_g(t)] - f[p(t-\tau), T_g(t-\tau)](1 - \frac{d\tau}{dt}) = 0$$

- Assuming that pressure and temperature remain close to their mean values, the function *f* may be expanded in a Taylor series

$$f[p(t),\, T_g(t)] = f(\overline{p},\, \overline{T}_g) + \frac{\partial f}{\partial p}(p - \overline{p}) + \frac{\partial f}{\partial T_g}(T_g - \overline{T}_g)$$

$$f[p(t-\tau),\, T_g(t-\tau)] = f(\overline{p},\, \overline{T}_g) + \frac{\partial f}{\partial p}(p(t-\tau) - \overline{p}) + \frac{\partial f}{\partial T_g}(T_g(t-\tau) - \overline{T}_g)$$

- Inserting these expressions in the previous relation one finds that

$$\frac{d\tau}{dt} = \frac{\partial \ln f}{\partial \ln p}\frac{p(t-\tau) - p(t)}{\overline{p}} + \frac{\partial \ln f}{\partial \ln T_g}\frac{T_g(t-\tau) - T_g(t)}{\overline{T}_g}$$

- The dependence of the time lag on the gas pressure and temperature in the chamber now appears explicitly.

- It is convenient to define two interaction indices

$$n = \frac{\partial \ln f}{\partial \ln p}, \qquad q = \frac{\partial \ln f}{\partial \ln T_g}$$

- One obtains the following expression for the rate of change of the time lag

$$\frac{d\tau}{dt} = n\frac{p(t-\tau) - p(t)}{\overline{p}} + q\frac{T_g(t-\tau) - T_g(t)}{\overline{T}_g}$$

- It is often considered that the burnt gas temperature remains essentially constant so that the second term vanishes. The rate of change of the time lag then becomes

$$\frac{d\tau}{dt} = n\frac{p(t-\tau) - p(t)}{\overline{p}}$$

- It is now possible to combine the two expressions obtained previously

$$\dot{m}_b(t) = \dot{m}_i(t-\tau)(1-\frac{d\tau}{dt})$$

$$\frac{d\tau}{dt} = n\frac{p(t-\tau)-p(t)}{\overline{p}}$$

- One considers fluctuations around the mean value and one finds after a few calculations

$$\frac{\dot{m}_b'(t)}{\overline{\dot{m}}} = \frac{\dot{m}_i'(t-\tau)}{\overline{\dot{m}}} - \frac{d\tau}{dt}$$

- If the injected mass flow rate is constant, the fluctuation in burnt gas flow rate is given by

$$\frac{\dot{m}_b'(t)}{\overline{\dot{m}}} = n\frac{p(t)-p(t-\tau)}{\overline{p}}$$

Heat release rate fluctuations

- This result may be interpreted in terms of relative heat release fluctuations by noting that

$$\frac{\dot{m}_b'(t)}{\overline{\dot{m}}} = \frac{\dot{q}'(t)}{\overline{\dot{q}}}$$

One obtains

$$\frac{\dot{q}'(t)}{\overline{\dot{q}}} = n\frac{p(t)-p(t-\tau)}{\overline{p}}$$

- An expression which is often used in analytical studies of instabilities coupled by longitudinal modes involves a delayed velocity perturbation impinging on the flame

$$\frac{\dot{q}'(t)}{\overline{\dot{q}}} = n\frac{u'(t-\tau)}{\overline{u}}$$

- This corresponds to a transfer function

$$\mathcal{F}(\omega) = \frac{\dot{q}'/\overline{\dot{q}}}{u'/\overline{u}} = n e^{i\omega\tau}$$

- The gain is constant and the phase depends linearly on frequency. This is a simplified description of what is found experimentally and theoretically but may be used to simplify the analysis

Low frequency instability of rocket motors

As a first application of the time lag concept let us consider the low frequency instabilities (chugging instabilities) of rocket motors

(1) The gas temperature in the chamber is constant and uniform even in the presence of pressure oscillations.
(2) The gas pressure is uniform in the combustion chamber and that it oscillates with a small amplitude around its mean value
(3) The time lag between injection and combustion exhibits the dependence described previously

A balance of mass written for the thrust chamber indicates that

$$\frac{dM_g}{dt} = \dot{m}_b - \dot{m}_e$$

Now, in the steady state the gas mass in the chamber is constant and the mass rates of burning and ejection are equal

$$\overline{\dot{m}}_b = \overline{\dot{m}}_e = \overline{\dot{m}}$$

Introducing the fractional burning and discharge rates

$$\mu_b = (\dot{m}_b - \overline{\dot{m}})/\overline{\dot{m}}$$
$$\mu_e = (\dot{m}_e - \overline{\dot{m}})/\overline{\dot{m}}$$

The mass balance equation becomes

$$\theta_g \frac{d}{dt}\left(\frac{M_g}{\overline{M}_g}\right) = \mu_b - \mu_e \qquad \theta_g = \frac{\overline{M}_g}{\overline{\dot{m}}}$$

θ_g represents the average residence time that the burned gas spends in the chamber

It is convenient to introduce a dimensionless time $z = t/\theta_g$

$$\frac{d}{dz}\left(\frac{M_g}{\overline{M}_g}\right) = \mu_b - \mu_e$$

and define a dimensionless time lag as well $\tilde{\tau} = \tau/\theta_g$

To simplify the notation the tilde will be deleted in what follows

The relative rate of burning obtained previously is first substituted in the mass balance

$$\frac{d}{dz}\left(\frac{M_g}{\overline{M}_g}\right) = n[\varphi(z) - \varphi(z-\tau)] + \mu_i(z-\tau) - \mu_e(z)$$
$$\varphi = (p - \overline{p})/\overline{p}$$

Now consider the mass of gas stored in the chamber

$$M_g = \int_V \rho_g dV = \int_V \frac{p}{RT_g} dV$$

Because the pressure and temperature are both uniform in the chamber

$$M_g = \frac{p}{R\overline{T}_g}\int_V dV = \frac{pV}{R\overline{T}_g}$$

$$M_g/\overline{M}_g = p/\overline{p} = 1 + \varphi$$

$$\frac{d\varphi}{dz} = n[\varphi(z) - \varphi(z-\tau)] + \mu_i(z-\tau) - \mu_e(z)$$

Consider the fractional variation of the mass flow rate ejected through the nozzle

$$\mu_e(z) = (\dot{m}_e - \overline{\dot{m}})/\overline{\dot{m}}$$

In the low frequency range, the nozzle behaves as a compact element and it may be described in terms of a succession of equilibrium flows

$$\dot{m}_e = Kp/(T_g)^{1/2}$$

Since the temperature is constant in the chamber one finds that

$$\frac{\dot{m}_e}{\overline{\dot{m}}_e} = \frac{p}{\overline{p}} \qquad \text{and} \quad \mu_e(z) = \varphi(z)$$

The mass balance equation finally becomes

$$\boxed{\frac{d\varphi}{dz} = n[\varphi(z) - \varphi(z-\tau)] - \varphi(z) + \mu_i(z-\tau)}$$

This equation governs the low frequency instabilities of a monopropellant engine

If the injection rate is constant in time, and in particular if it is not influenced by the processes taking place in the chamber the dynamic behavior of the system is governed by

$$\frac{d\varphi}{dz} + (1-n)\varphi(z) + n\varphi(z-\tau) = 0$$

$$z = t/\theta_g,\ \theta_g = M_g/\overline{\dot{m}} \qquad n = \left(\frac{\partial \ln f}{\partial \ln p}\right)_{\overline{p},\overline{T}_g}$$

To examine the stability of this system one may take the Laplace transform of this equation or equivalently set the relative pressure fluctuation in the form

$$\varphi(z) = Ae^{sz}$$

This yields the following characteristic equation

$$s + (1-n) + ne^{-s\tau} = 0$$

One may solve the characteristic equation and discuss the sign of the real part of the roots obtained to determine the regions of stability. For this it is convenient to write

$$s = \Lambda + i\Omega$$

This yields the following set of equations

$$\Lambda + (1-n) + ne^{-\Lambda\tau}\cos\Omega\tau = 0$$
$$\Omega - ne^{-\Lambda\tau}\sin\Omega\tau = 0$$

Neutral stability is achieved when Λ=0

$$1 - n + n\cos\Omega_*\tau_* = 0$$
$$\Omega_* - n\sin\Omega_*\tau_* = 0$$

τ_* designates the time delay for neutral oscillation

The angular frequency of neutral oscillations is easily determined from these expressions

$$(1-n)^2 + \Omega_*^2 = n^2 \quad \text{and hence} \quad \boxed{\Omega_*^2 = 2n - 1}$$

Because this angular frequency must be real it turns out that no neutral oscillations may exist if 0<*n*<1/2. When *n*>1/2, the stability boundary may be odeduced from the previous equation

$$\Omega_* \tau_* = \cos^{-1}[(n-1)/n)]$$

$$n = 1/(1 - \cos \Omega_* \tau_*)$$

19

Stability diagram

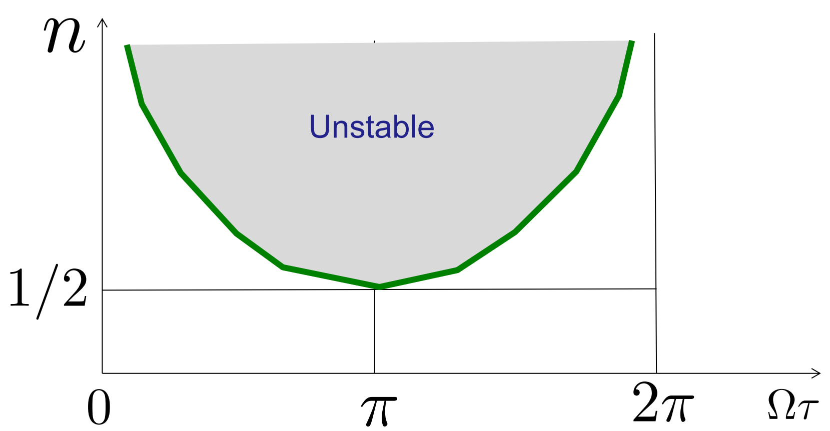

20

Combustion dynamics
Lecture 4b

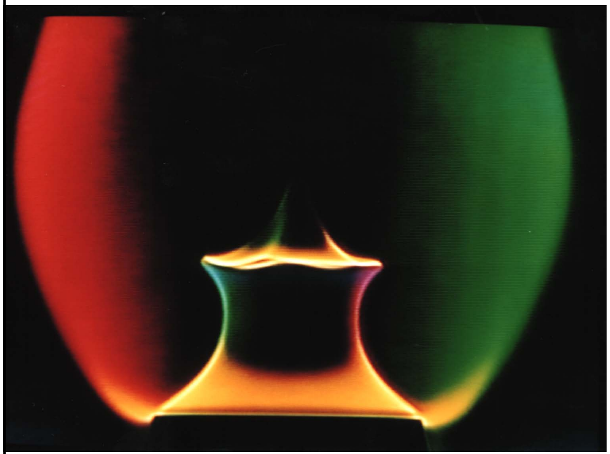

S. Candel, D. Durox , T. Schuller
CentraleSupélec
Université Paris-Saclay, EM2C lab, CNRS

Tsinghua summer school, June 2021

Perturbed flames

- Experiments on conical flames
- Mutual interactions of flame sheets
- Representing the flame dynamics using the G-equation
- Flame transfer function concepts
- Effects of equivalence ratio perturbations

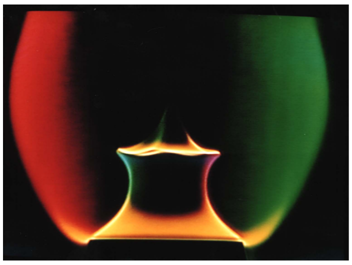

Acoustically coupled combustion instabilities *(thermo-acoustic instabilities)*

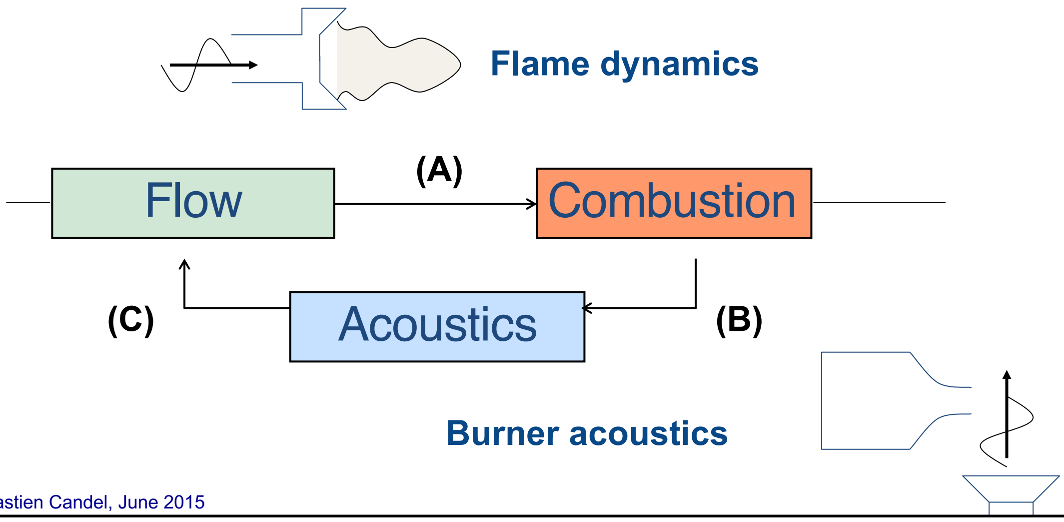

Sensitivity of flames to acoustic waves

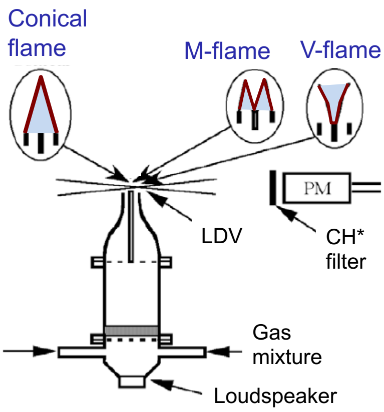

The flame can be stabilized in three different configurations. (film by Daniel Durox, EM2C)

Experiments indicate that flames are sensitive to perturbations and that their response depends on the flame geometry, modulation frequency, type of perturbation and amplitude

D. Durox, T. Schuller, N. Noiray and S. Candel (2009) *Proceedings of the Combustion Institute.* 32, 1391-1398. Experimental analysis of flame transfer functions nonlinearities.

Interactions leading to heat release rate disturbances

LES of the unsteady flow in a combustion chamber featuring a self-sustained oscillation

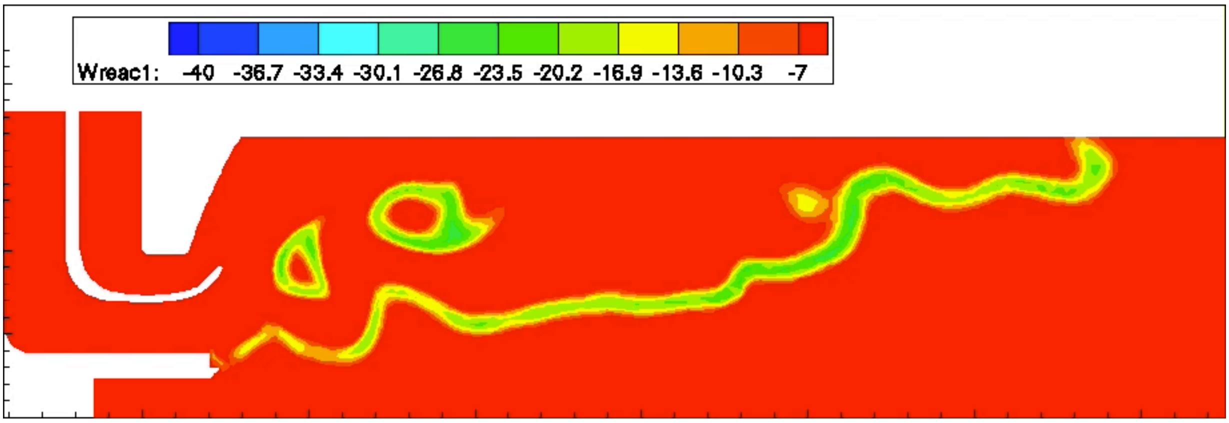

S. Ducruix, T. Poinsot and S. Candel (2002) Large eddy simulation of combustion instabilities in a swirled combustor. In *Turbulent mixing and combustion*, A. Pollard and S. Candel, eds. Kluwer, Dodrecht, Chapter 31, pp. 357-366.

Interactions leading to heat release rate disturbances

1. Flame interactions with the flow

A. Velocity and mixture composition disturbances

B. Mutual flame annihilation leading to destruction of flame surface area

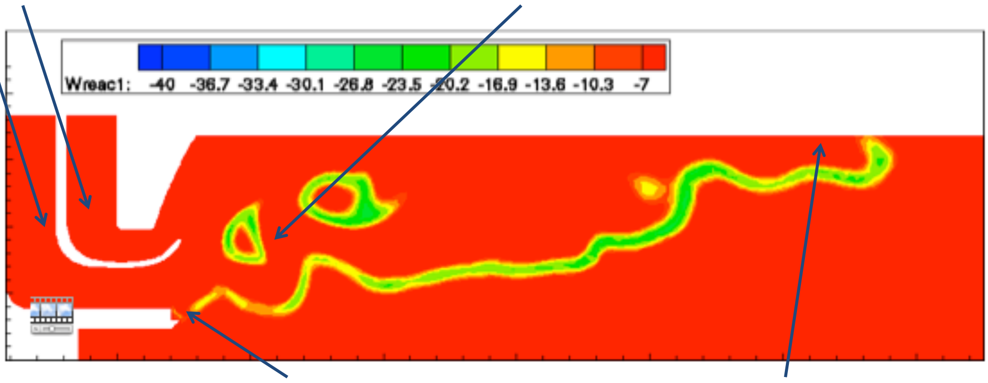

C. Anchoring devices used to stabilize the flame

D. Combustion chamber walls confining the flame

2. Flame interactions with solid boundaries

Flame transfer functions

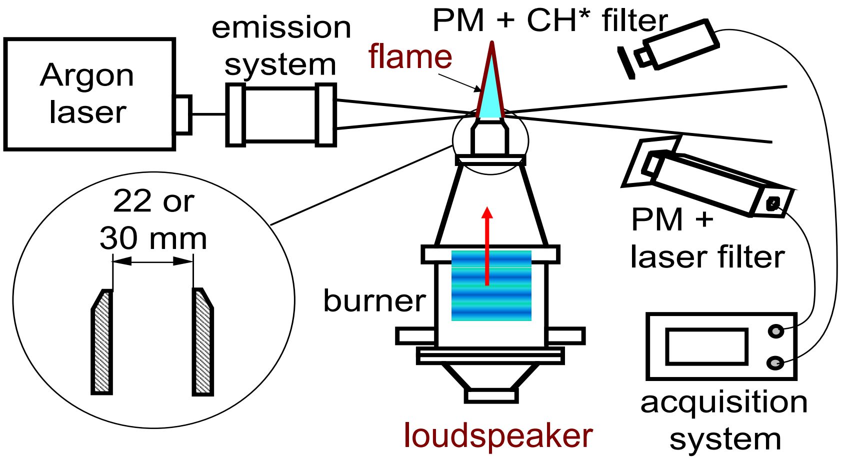

It is instructive to examine simple situations before dealing with the more complex practical configurations. This is exemplified by experiments on the flame response to acoustic modulations generated in the fresh mixture

 Blackshear (1953), De Soete (1964), Matsui (1981), Baillot& al (1992),Ducruix & al (2000)

7

Steady conical flame | Perturbed conical flame

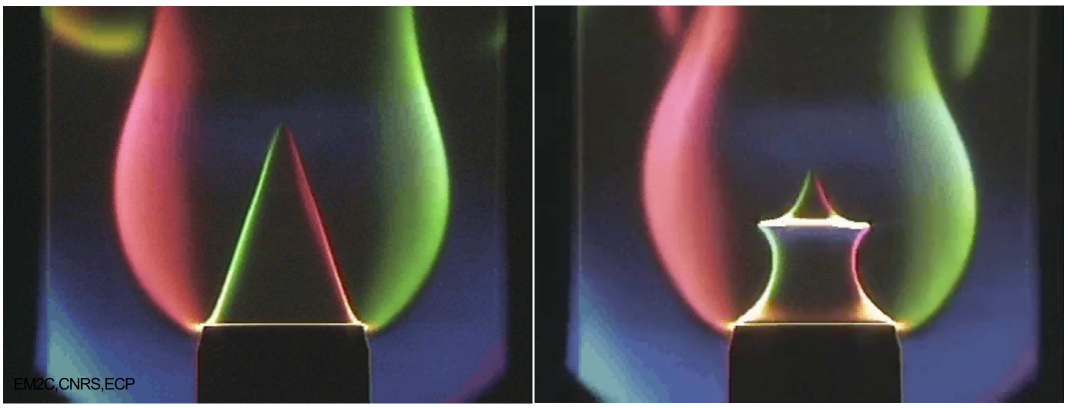

Methane-air flame perturbed by upstream acoustic modulations
$\phi = 0.95 \quad f = 75$ Hz

S. Ducruix, D. Durox and S. Candel (2000) *Proceedings of the Combustion Institute,* 28, 765-773.
Theoretical and experimental determinations of the transfer function of a laminar premixed flame.

8

Flame front motion

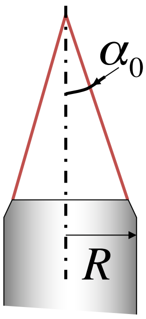

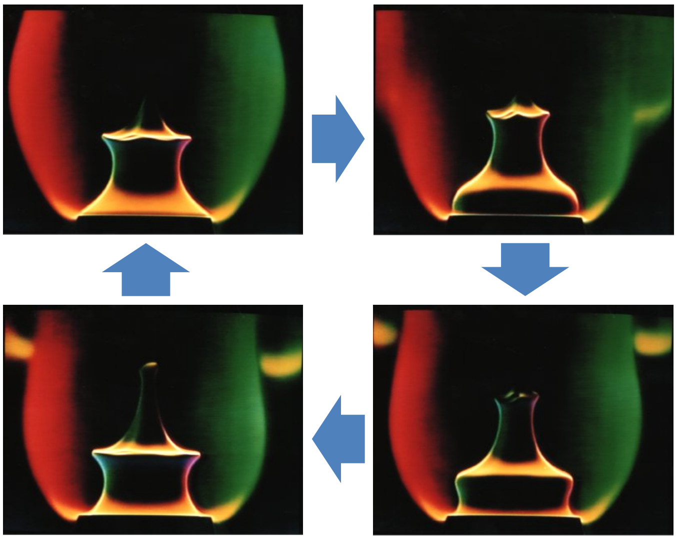

$$\omega_* = \frac{\omega R}{S_L \cos \alpha_0}$$

Methane-air flame $\Phi = 0.95$, $v_0 = 0.96$ m.s^{-1}, $\omega_* = 15$

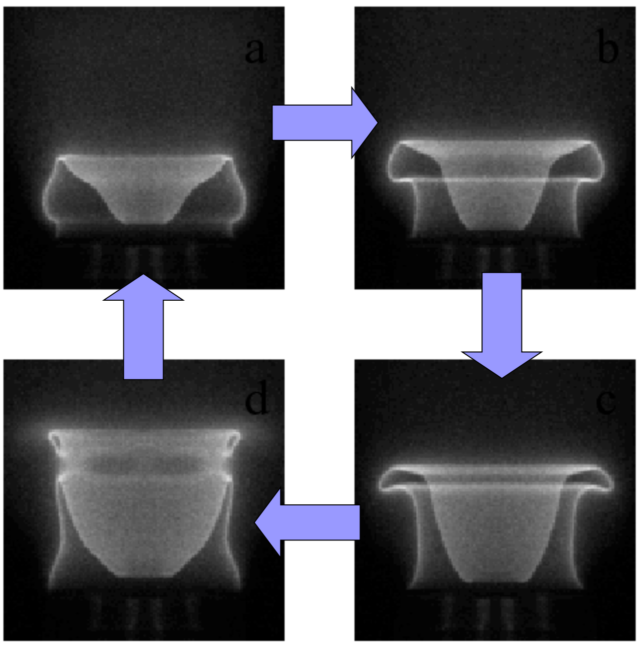

Cyclic flame motion during flame/flame interaction

$$\Phi = 1.13,\ v = 1.71\,\mathrm{m\ s^{-1}},\ f = 150\,\mathrm{Hz},\ v' = 0.5\,\mathrm{m\ s^{-1}}$$

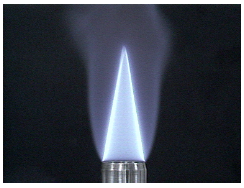

Conical flame

Cylindrical flame

V-flame

Swirling flame

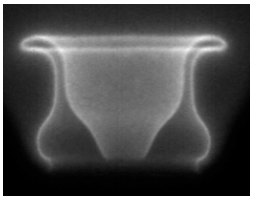

M-flame

Many types of interactions have been identified by considering different flame geometries

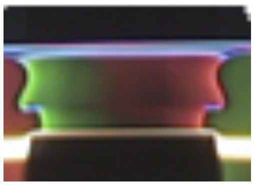

Flame on a wall

Lateral confinement effects on dynamics of inverted flames $\xi = d/D$

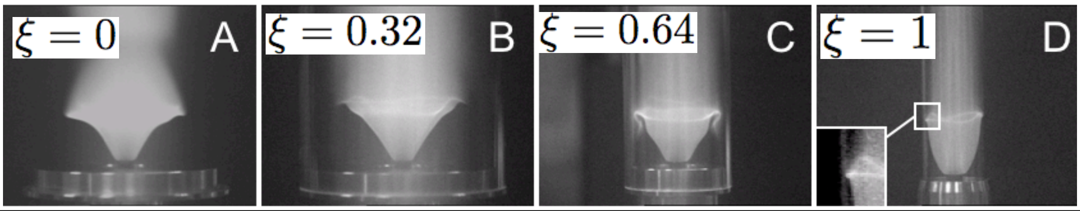

The G-equation and its perturbation

The flame is described by a level set. One level corresponds to the flame position

$$G(\boldsymbol{x}, t) = G_0$$

This expression may be differentiated with respect to time

$$\frac{dG(\boldsymbol{x}, t)}{dt} = \frac{\partial G}{\partial t} + \boldsymbol{w} \cdot \boldsymbol{\nabla} G = 0$$

The unit normal vector is directed towards the fresh stream

$$\boldsymbol{n} = -\boldsymbol{\nabla} G / |\boldsymbol{\nabla} G|$$

$$\boldsymbol{w} = \boldsymbol{v} + S_d \boldsymbol{n}$$

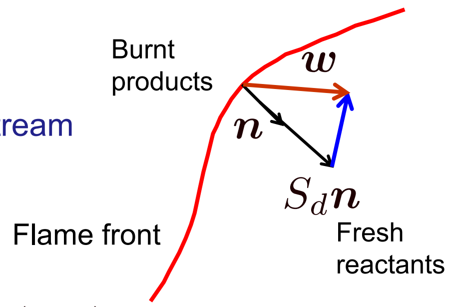

$$G(\boldsymbol{x}, t) = G_0$$

Using the previous expressions for the normal and the absolute flame velocity one obtains

$$\boxed{\frac{\partial G}{\partial t} + \boldsymbol{v} \cdot \boldsymbol{\nabla} G = S_d |\boldsymbol{\nabla} G|}$$

This expression can now linearized by introducing small perturbations around the mean value

$$G = G_0 + G_1$$
$$\boldsymbol{v} = \boldsymbol{v}_0 + \boldsymbol{v}_1$$
$$S_d = S_{d0} + S_{d1}$$

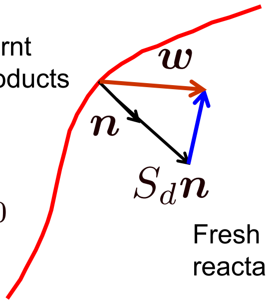

Retaining only terms up to first order one finds that

$$|\boldsymbol{\nabla} G_0 + \boldsymbol{\nabla} G_1| = |\boldsymbol{\nabla} G_0| + \boldsymbol{n}_0 \cdot \boldsymbol{\nabla} G_1$$

$$\frac{\partial G_1}{\partial t} + \boldsymbol{v}_0 \cdot \boldsymbol{\nabla} G_0 + \boldsymbol{v}_1 \cdot \boldsymbol{\nabla} G_0 + \boldsymbol{v}_0 \cdot \boldsymbol{\nabla} G_1 =$$
$$(S_{d0} + S_{d1})(|\boldsymbol{\nabla} G_0| + \boldsymbol{n}_0 \cdot \boldsymbol{\nabla} G_1)$$

(1) - Transport equation for the mean G_0 field

$$\boldsymbol{n}_0 = -\frac{\boldsymbol{\nabla} G}{|\boldsymbol{\nabla} G|} \qquad \boldsymbol{v}_0 \cdot \boldsymbol{\nabla} G_0 = S_{d0} |\boldsymbol{\nabla} G_0|$$

$$\boxed{S_{d0} - \boldsymbol{v}_0 \cdot \boldsymbol{n}_0 = 0}$$

(2) -Transport equation for the perturbed G_1 field

$$\frac{\partial G_1}{\partial t} + \boldsymbol{v}_1 \cdot \boldsymbol{\nabla} G_0 + \boldsymbol{v}_0 \cdot \boldsymbol{\nabla} G_1 = S_{d0} \boldsymbol{n}_0 \cdot \boldsymbol{\nabla} G_1 + S_{d1} |\boldsymbol{\nabla} G_0|$$

which may be rearranged in the form

$$\frac{\partial G_1}{\partial t} + (\boldsymbol{v}_0 - S_{d0} \boldsymbol{n}_0) \cdot \boldsymbol{\nabla} G_1 = -\boldsymbol{v}_1 \cdot \boldsymbol{\nabla} G_0 + S_{d1} |\boldsymbol{\nabla} G_0|$$

Making use of the result obtained at zero-th order one may write

$$\boldsymbol{v}_0 - S_{d0} \boldsymbol{n}_0 = \boldsymbol{v}_0 - (\boldsymbol{v}_0 \cdot \boldsymbol{n}_0) \boldsymbol{n}_0 = \boldsymbol{v}_{0t}$$

This is the velocity vector projected on the plane tangent to the flame

$$\frac{\partial G_1}{\partial t} + \boldsymbol{v}_{0t} \cdot \boldsymbol{\nabla} G_1 = -\boldsymbol{v}_1 \cdot \boldsymbol{\nabla} G_0 + S_{d1} |\boldsymbol{\nabla} G_0|$$

Recalling that $S_{d0} = \boldsymbol{v}_0 \cdot \boldsymbol{n}_0$

The right hand side of the previous equation may be written in the form

$$-\boldsymbol{v}_1 \cdot \boldsymbol{\nabla} G_0 + S_{d1} |\boldsymbol{\nabla} G_0| = \left(\boldsymbol{v}_1 - \frac{S_{d1}}{S_{d0}} \boldsymbol{v}_0\right) \cdot \boldsymbol{n}_0 |\boldsymbol{\nabla} G_0|$$

One obtains in this way the following equation

$$\boxed{\frac{\partial G_1}{\partial t} + \boldsymbol{v}_{0t} \cdot \boldsymbol{\nabla} G_1 = \left(\boldsymbol{v}_1 - \frac{S_{d1}}{S_{d0}} \boldsymbol{v}_0\right) \cdot \boldsymbol{n}_0 |\boldsymbol{\nabla} G_0|}$$

Burning velocity and velocity perturbations generate disturbances of the flame position in the normal direction, which are then convected along the flame front by the component of the mean local flow velocity $\boldsymbol{v}_{0t}$ parallel to the mean flame front.

Flame transfer function concepts

The flame response can be characterized in terms of a transfer function

$$\frac{u'}{\overline{U}} \longrightarrow \boxed{\text{Combustion}} \xrightarrow{\dot{Q}'/\overline{\dot{Q}}}$$

$$\mathcal{F}(\omega) = \frac{\dot{Q}'/\overline{\dot{Q}}}{u'/\overline{U}}$$

But the flame transfer function (FTF) only provides the linear growth rate in the analysis of instabilities,

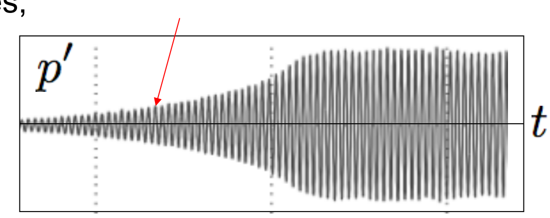

Flowrate disturbances

Experiments carried out at a fixed mixture composition when the flame is submitted to harmonic flowrate modulations.

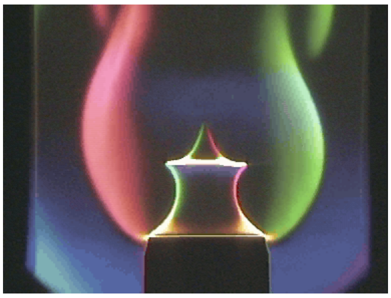

f = 75 Hz

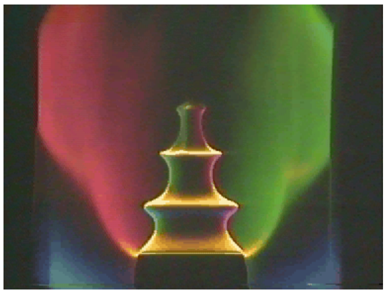

f = 150 Hz

Methane/air
Φ =0.95,
u'/u~0.3,
u~1 m/s

$$\frac{\dot{Q}_1}{\dot{Q}_0} = \int_A \frac{dA_1(\cancel{\Phi}, v)}{A_0}$$

Heat release rate fluctuations

flame surface area fluctuations

Flame surface wrinkles produce heat release rate disturbances

19

Mixture composition disturbances

DNS of a V-flame submitted to mixture composition oscillations

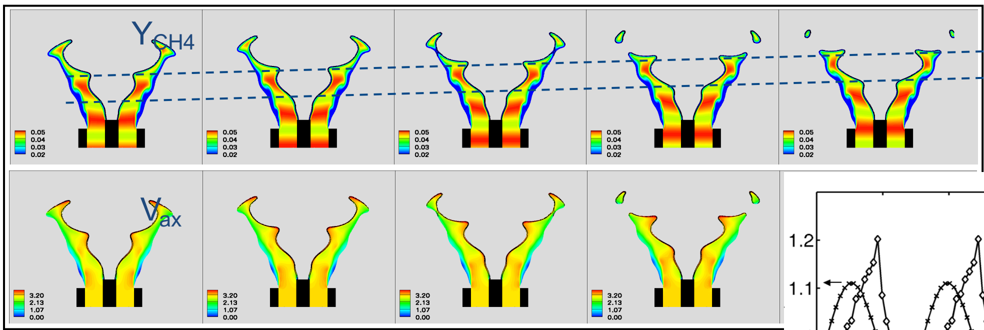

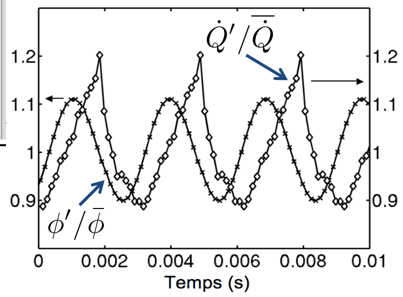

Harmonic mixture composition oscillations are convected and wrinkle the flame (no acoustic forcing):
(1) Fluctuations in the burning rate
(2) Flame surface area disturbances
(3) Feedback on the flow field
giving rise to large heat release rate nonlinear oscillations

A.L. Birbaud, S. Ducruix, D . Durox and S. Candel (2008) *Combustion and Flame*, 154, 356-367. The nonlinear response of inverted « V »-flames submitted to equivalence ratio nonuniformities.

20

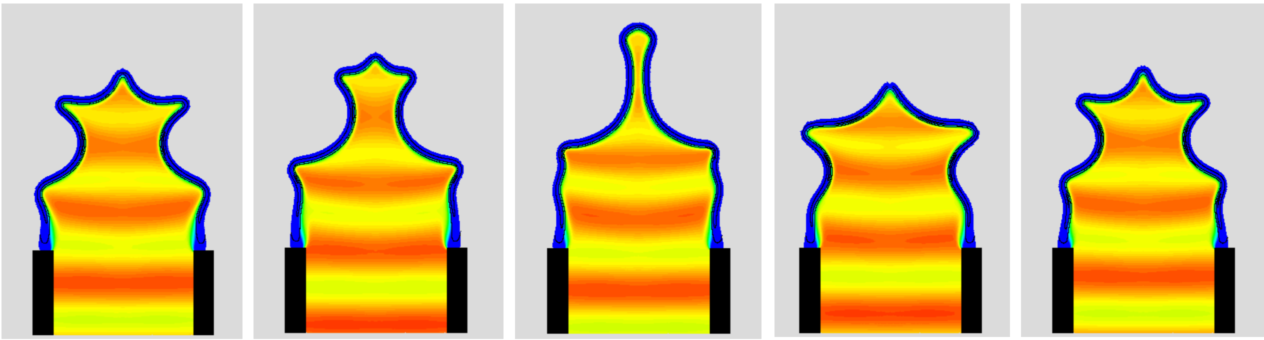

A conical methane air flame pertubed by a convective equivalence ratio perturbation

Heat release rate fluctuations

Volumetric heat release rate controlled by the fuel supply (only lean flames are considered)

$$\dot{Q} = \int_A \underline{Y_F \rho S_d} \, \underline{dA(\phi, \mathbf{v})} \, \underline{(-\Delta h_f^0)}$$

$-\Delta h_f^0$ Fuel heating value (J/kg) is constant

$$\dot{m}_f = \underline{Y_F \rho S_d}$$

Fuel mass burning rate
- ❑ equivalence ratio
- ❑ ~~stretch effects~~

$\underline{dA(\Phi, \mathbf{v})}$ Flame surface area
- equivalence ratio
- velocity

$$\frac{\dot{Q}_1}{\dot{Q}_0} = \frac{\int \dot{m}_{f1}(\phi, \epsilon) dA_0}{\dot{m}_{f0} \int dA_0} + \frac{\int dA_1(\Phi, \mathbf{v})}{\int dA_0}$$

Heat release rate fluctuations

Mass burning rate fluctuations averaged over the flame surface area

Flame surface area fluctuations

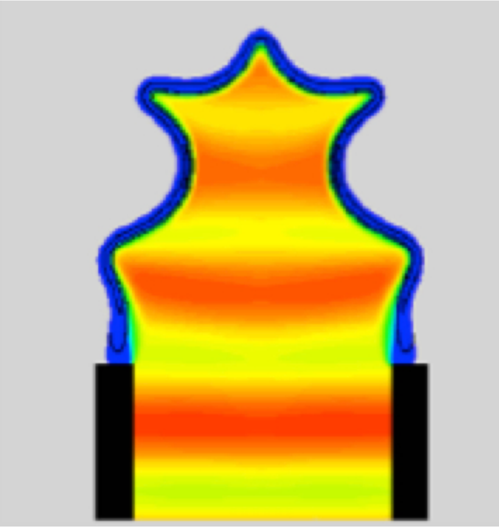

Combustion dynamics Lecture 5a

S. Candel, D. Durox , T. Schuller

CentraleSupélec
Université Paris-Saclay, EM2C lab, CNRS

Tsinguha summer school, July 2021

1

Instrinsic flame instabilities will not be considered

Darrieus-Landau instabilities

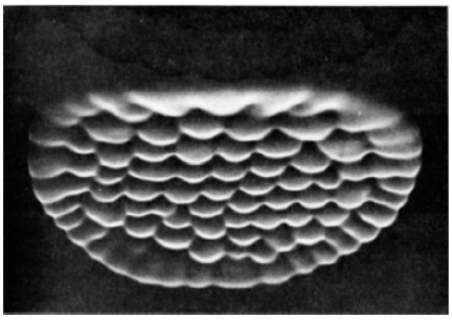

Thermo-diffusive instabilities

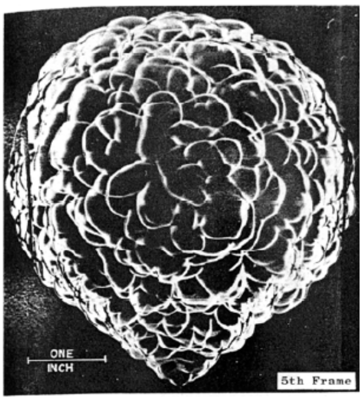

Markstein (1964)
Clavin et al. (1990)
Buckmaster and Ludford (1982)
Sivashinski (1976…)
Law (2008)
Clanet & Searby (1998)
Searby et al. (2001)

Growth rates are relatively weak : in many applications (but not all!) other mechanisms dominate

Exceptions : Oxy-fuel welding torch is notably influenced by D-L instability

2

First example

Domestic boiler

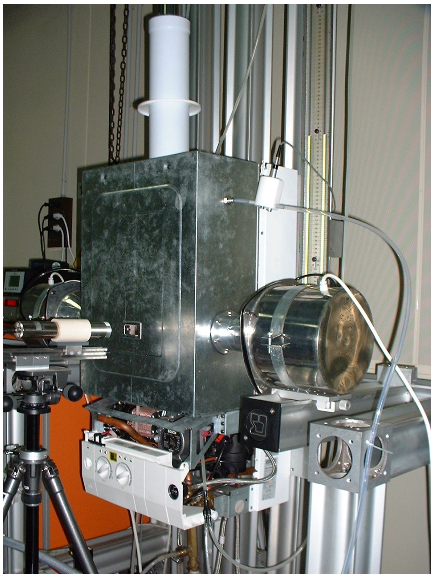

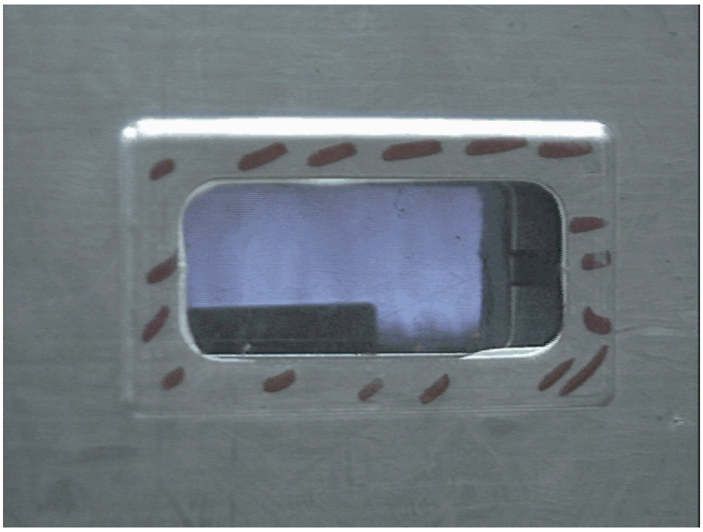

During unstable regime, walls are "breathing" highlighting large pressure oscillations within the combustion

Second example

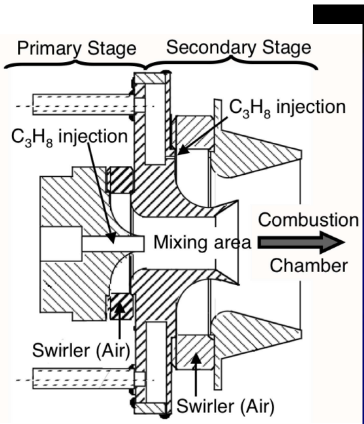

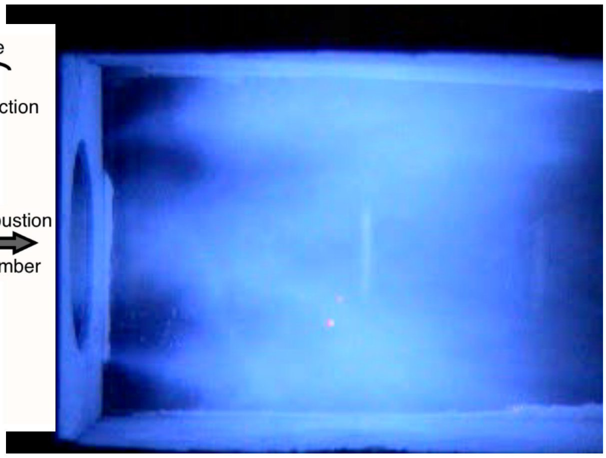

Multipoint injection swirled injector

Stable regime: the combustion zone (luminous zone) features small stochastic fluctuations around its mean location (effects of turbulence). Radiated noise is weak and broad band : "combustion roar".
Unstable regime : Large synchronized motion featuring peak noise emission. Intensification of luminosity near the wall : higher heat fluxes to the boundary. Induces flame flashback.

S. Barbosa, P. Scoufflaire, S. Ducruix, "Time resolved flowfield, flame structure and acoustic characterization of a staged multi-injection burner", *Proceedings of the Combustion Institute*, 32 : 265-2972 (2009)

Azimuthally coupled instabilities in an annular combustor equipped with 16 matrix burners

Third example

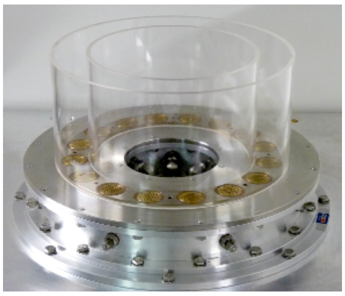

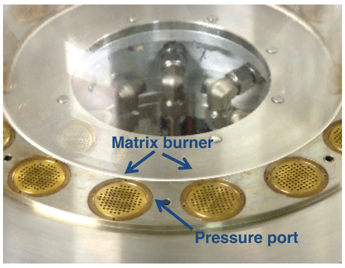

Spinning mode @ f= 498 Hz

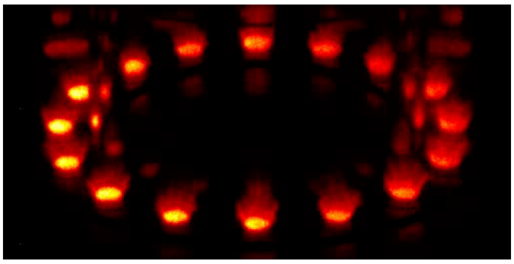

Standing mode @ f=380 Hz

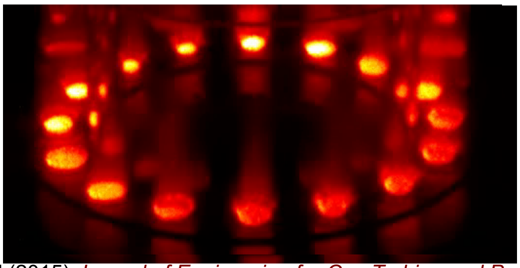

J.F. Bourgouin, D. Durox, J.P. Moeck, T. Schuller, and S. Candel (2015) *Journal of Engineering for Gas Turbine and Power (ASME)*. 137, 021503. Characterization and modeling of a spinning thermoacoustic instability in an annular combustor equipped with multiple matrix injectors.

Acoustically induced combustion Instabilities *(thermo-acoustic instabilities)*

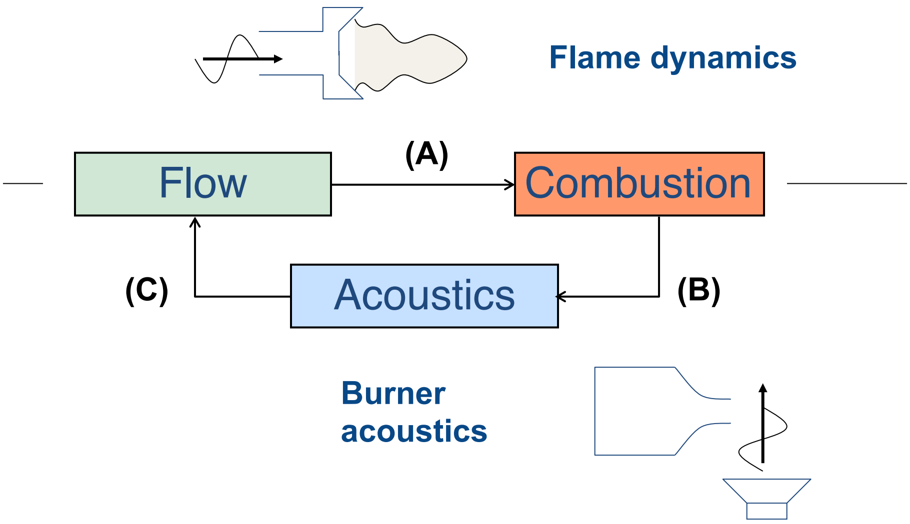

Flowrate disturbances

Experiments with a fixed mixture composition when the flame is submitted to harmonic flowrate modulations

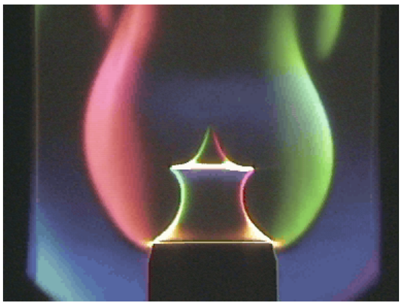

f = 75 Hz

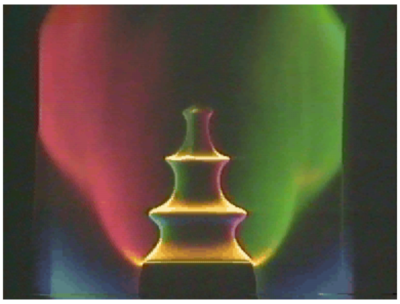

f = 150 Hz

$$\frac{\dot{Q}_1}{\dot{Q}_0} = \int_A \frac{dA_1(\cancel{\Phi}, v)}{A_0}$$

Flame surface area fluctuations

Flame surface wrinkles produce heat release rate disturbances

Methane/air

$\phi = 0.95$, *u'/u*~0.3, *u*~1 m/s

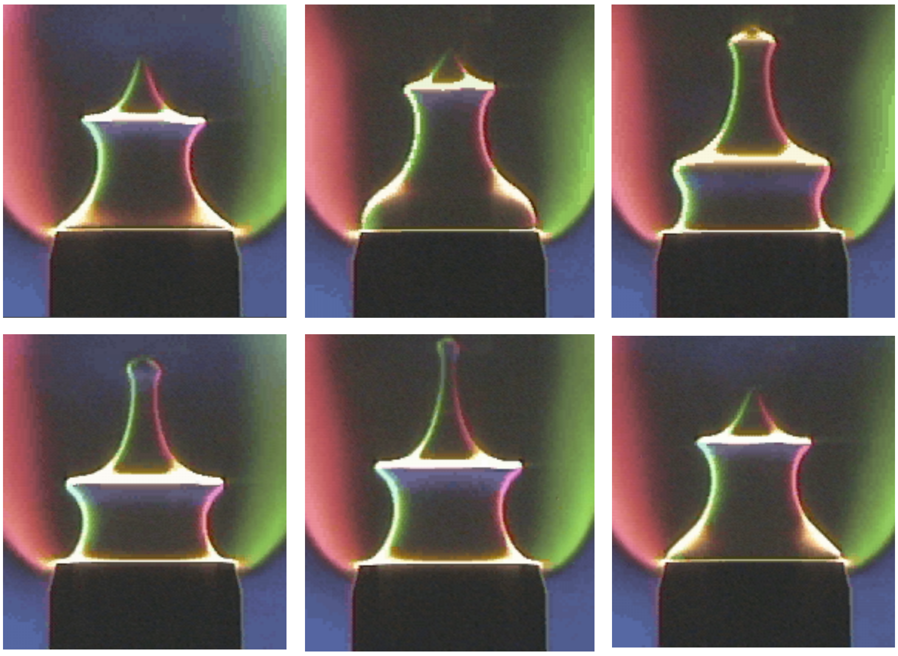

Premixed conical flame submitted to velocity modulations at 75 Hz

Equivalence ratio inhomogeneities

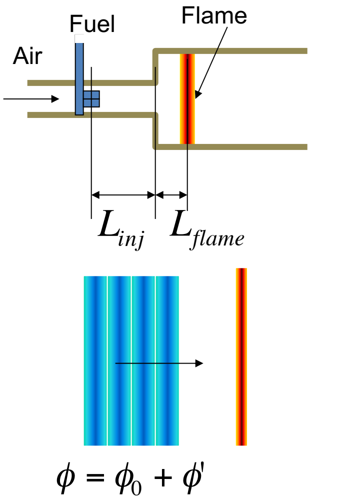

Equivalence ratio perturbations

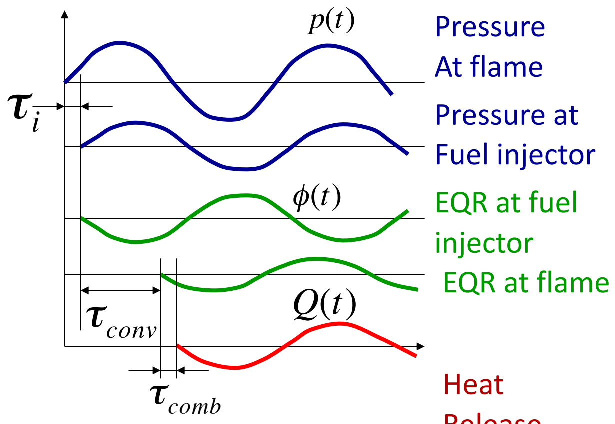

$$\tau_i + \tau_{conv} + \tau_c = (2n-1)\frac{T}{2}$$

T. Lieuwen and B. Zinn (1998) Proc. Combusti. Inst., 27(2) 1809-1816. The role of equivalence ratio oscillations in driving combustion instabilities in low NO_x gas turbines

9

Combustion dynamics of flames interacting with equivalence ratio perturbations

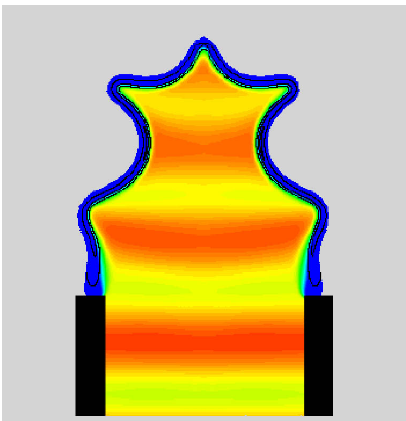

Conical flame perturbed by equivalence ratio modulations

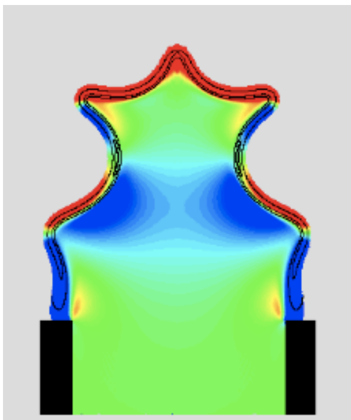

Velocity field induced on the upstream side of the flame by interactions with equivalence ratio modulations

A.L. Birbaud, S. Ducruix, D . Durox and S. Candel (2008) *Combustion and Flame.* 154, 356-367. The nonlinear response of inverted « V »-flames submitted to equivalence ratio nonuniformities.

10

Combustion dynamics of flames interacting with equivalence ratio perturbations

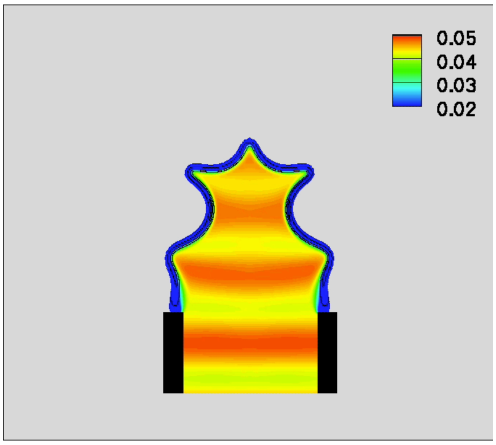

Conical flame perturbed by equivalence ratio modulations

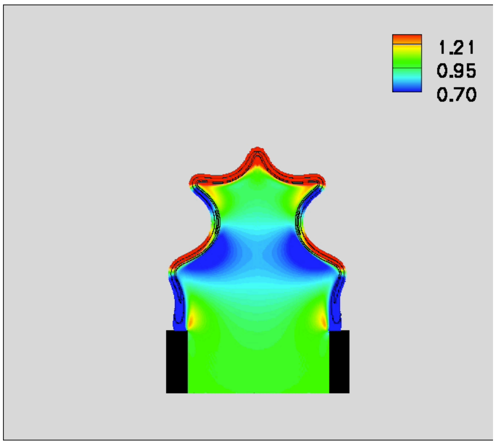

Velocity field induced on the upstream side of the flame by interactions with equivalence ratio modulations

A.L. Birbaud, S. Ducruix, D . Durox and S. Candel (2008) *Combustion and Flame.* 154, 356-367. The nonlinear response of inverted « V »-flames submitted to equivalence ratio nonuniformities.

Inverted flame perturbed by equivalence ratio oscillations

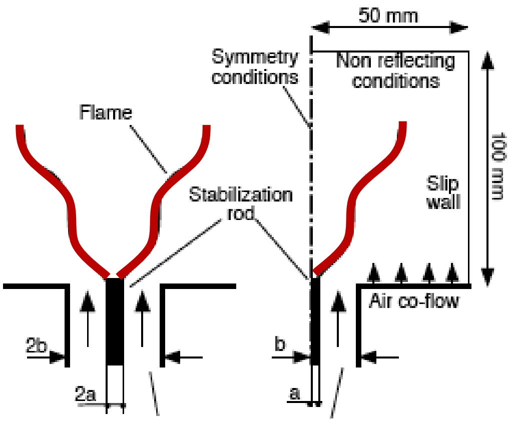

Premixed flow with equivalence ratio perturbations

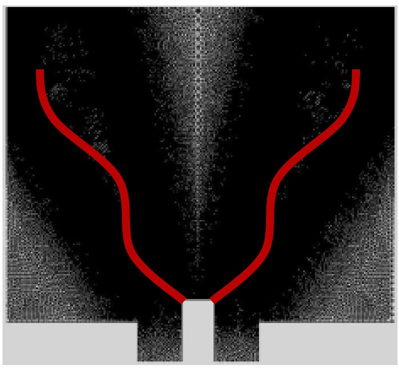

Computational mesh

$$\phi(t) = \phi_0 + \phi_1 \sin \omega t \qquad \phi_0 = 0.8 \text{ and } \phi_1 = 0.1$$

Mixture composition disturbances

DNS of a V-flame submitted to mixture composition oscillations

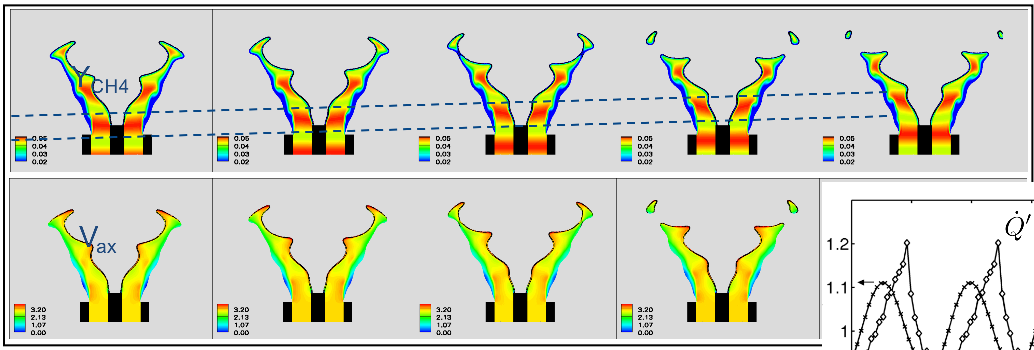

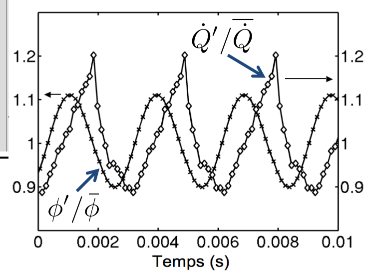

Harmonic mixture composition oscillations are convected and wrinkle the flame (no acoustic forcing):

(1) Fluctuations in the burning rate
(2) Flame surface area disturbances
(3) Feedback on the flow field

Result in large heat release rate oscillations (nonlinear)

A.L. Birbaud, S. Ducruix, D . Durox and S. Candel (2008) *Combustion and Flame.* 154, 356-367. The nonlinear response of inverted « V »-flames submitted to equivalence ratio nonuniformities.

Heat release rate fluctuations

Volumetric heat release rate controlled by the fuel supply
Only lean flames are considered

$$\dot{Q} = \int_A \underline{Y_F \rho S_d} \underline{dA(\phi, \mathbf{v})} \underline{(-\Delta h_f^0)}$$

$\underline{-\Delta h_f^0}$ Fuel heating value (J/kg) is constant

$\dot{m}_f = \underline{Y_F \rho S_d}$ Fuel mass burning rate

- equivalence ratio
- ~~stretch effects~~

$\underline{dA(\Phi, \mathbf{v})}$ Flame surface area
- equivalence ratio
- velocity

$$\frac{\dot{Q}_1}{\dot{Q}_0} = \frac{\int \dot{m}_{f1}(\phi, \epsilon) dA_0}{\dot{m}_{f0} \int dA_0} + \frac{\int dA_1(\Phi, \mathbf{v})}{\int dA_0}$$

Heat release rate fluctuations

Mass burning rate fluctuations averaged over the flame surface area

Flame surface area fluctuations

Fuel mass burning rate oscillations

Mixture composition disturbances lead to fuel mass burning rate perturbations

$$\frac{\int \dot{m}_{f1}(\phi,\cancel{\kappa})dA_0}{\dot{m}_{f0}\int dA_0} = m(\phi_0)\frac{\int \phi_1 dA_0}{\phi_0 \int dA_0} \qquad \dot{m}_f = Y_F \rho S_d$$

$$m(\phi_0) = \left[\underbrace{\frac{\partial(\rho/\rho_0)}{\partial(\phi/\phi_0)}}_{<<1} + \underbrace{\frac{\partial(Y_f/Y_{f0})}{\partial(\phi/\phi_0)}}_{\sim 1} + \underbrace{\frac{\partial(S_L/S_{L0})}{\partial(\phi/\phi_0)}}_{a}\right]_{\phi=\phi_0}$$

$$m(\phi_0) \simeq 1 + a$$

Example : CH_4/air

$$\phi_0 = 0.8 \quad a = \frac{\partial(S_L/S_{L0})}{\partial(\phi/\phi_0)} = 2.30$$

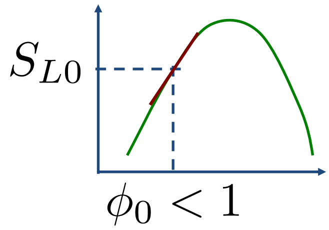

Burning velocity disturbances

Fluctuations of the flame displacement speed $\qquad S_d = S_L(1 + \cancel{\mathcal{L}_a}\kappa)$

Mixture composition oscillations

$$\phi = \phi_0 + \phi_1(t)$$

$$\phi_1(t) = \Phi \exp(-i\omega t)$$

Laminar burning velocity

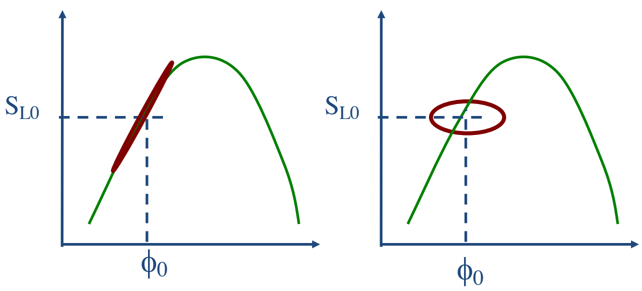

Low frequency — High frequency

The burning velocity describes (twisted) cycles around steady conditions for increasing modulation frequencies

Lauvergne & Egolfopoulos (2000)

Response of lean premixed flames to mixture composition disturbances

$$\phi_0 < 1 \quad \dot{m}_f = Y_F \rho S_d$$

$$\frac{\dot{Q}_1}{\dot{Q}_0} = m(\phi_0)\frac{\int \phi_1 dA_0}{\phi_0 \int dA_0} + \frac{\int dA_1(\Phi, \mathbf{v})}{\int dA_0}$$

Heat release rate fluctuations

Mass burning rate fluctuations averaged over the flame surface area

Flame surface area fluctuations

$$\boxed{m(\phi_0) \simeq 1 + a}$$

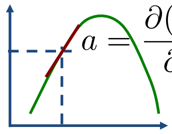

$$a = \frac{\partial(S_L/S_{L0})}{\partial(\phi/\phi_0)}$$

Heat release rate fluctuations result from fuel mass burning rate (function of ϕ and mean flame surface area) and flame surface area fluctuations (function of ϕ, *v* and mean flame surface area).

Flame surface area fluctuations

Kinematic description of the flame sheet (*G*=0) separating the burnt gases (*G*>0) from the fresh reactants (*G*<0)

$$\frac{\partial G}{\partial t} + \boldsymbol{v} \cdot \boldsymbol{\nabla} G = S_d |\boldsymbol{\nabla} G|$$

$$S_d(\phi, \epsilon, \kappa, t) \simeq S_L(\phi)$$

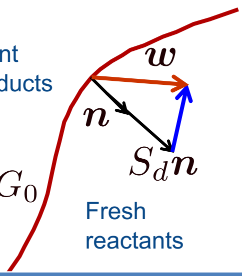

Flame type	Some references
Conical flames	Baillot et al. (1992, 1996), Fleifil et al. (1996), Ducruix (2000), Schuller et al. (2003)
V-flames	Boyer & Quinard (1990), Dowling (1999), Schuller et al. (2003)
Nonlinear response	Schuller (2002), Lieuwen (2005), Preetham et al. (2008)
Turbulent flames	Preetham & Lieuwen (2007), Hemchandra & Lieuwen (2010)
Swirling flames	Palies et al. (2011), Acharya et al. (2012)

The G-equation

The flame is described by a level set. One level corresponds to the flame position

$$G(\boldsymbol{x}, t) = G_0$$

This expression may be differentiated with respect to time

$$\frac{dG(\boldsymbol{x}, t)}{dt} = \frac{\partial G}{\partial t} + \boldsymbol{w} \cdot \boldsymbol{\nabla} G = 0$$

$$\boldsymbol{n} = -\boldsymbol{\nabla} G / |\boldsymbol{\nabla} G|$$

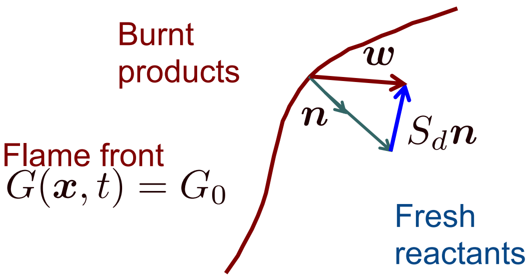

19

Using the previous expressions for the normal and the absolute flame velocity one obtains

$$\boxed{\frac{\partial G}{\partial t} + \boldsymbol{v} \cdot \boldsymbol{\nabla} G = S_d |\boldsymbol{\nabla} G|}$$

This expression can now linearized by introducing small perturbations around the mean value

$$G = G_0 + G_1$$
$$\boldsymbol{v} = \boldsymbol{v}_0 + \boldsymbol{v}_1$$
$$S_d = S_{d0} + S_{d1}$$

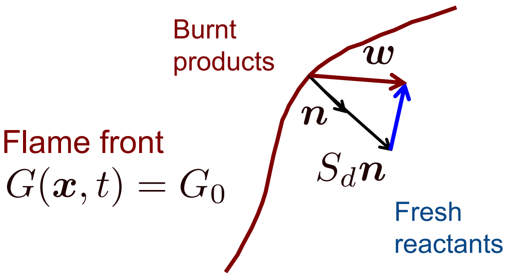

20

Retaining only terms up to first order one finds that

$$|\nabla G_0 + \nabla G_1| = |\nabla G_0| + \boldsymbol{n}_0 \cdot \nabla G_1$$

$$\frac{\partial G_1}{\partial t} + \boldsymbol{v}_0 \cdot \nabla G_0 + \boldsymbol{v}_1 \cdot \nabla G_0 + \boldsymbol{v}_0 \cdot \nabla G_1 = (S_{d0} + S_{d1})(|\nabla G_0| + \boldsymbol{n}_0 \cdot \nabla G_1)$$

(1) - Transport equation for the mean G_0 field

$$\boldsymbol{n}_0 = -\frac{\nabla G}{|\nabla G|} \qquad \boldsymbol{v}_0 \cdot \nabla G_0 = S_{d0}|\nabla G_0|$$

$$\boxed{S_{d0} - \boldsymbol{v}_0 \cdot \boldsymbol{n}_0 = 0}$$

21

(2) -Transport equation for the perturbed G_1 field

$$\frac{\partial G_1}{\partial t} + \boldsymbol{v}_1 \cdot \nabla G_0 + \boldsymbol{v}_0 \cdot \nabla G_1 = S_{d0}\boldsymbol{n}_0 \cdot \nabla G_1 + S_{d1}|\nabla G_0|$$

which may be rearranged in the form

$$\frac{\partial G_1}{\partial t} + (\boldsymbol{v}_0 - S_{d0}\boldsymbol{n}_0) \cdot \nabla G_1 = -\boldsymbol{v}_1 \cdot \nabla G_0 + S_{d1}|\nabla G_0|$$

Making use of the result obtained at zero-th order one may write

$$\boldsymbol{v}_0 - S_{d0}\boldsymbol{n}_0 = \boldsymbol{v}_0 - (\boldsymbol{v}_0 \cdot \boldsymbol{n}_0)\boldsymbol{n}_0 = \boldsymbol{v}_{0t}$$

This is the velocity vector projected on the plane tangent to the flame

$$\frac{\partial G_1}{\partial t} + \boldsymbol{v}_{0t} \cdot \nabla G_1 = -\boldsymbol{v}_1 \cdot \nabla G_0 + S_{d1}|\nabla G_0|$$

22

Recalling that $S_{d0} = \boldsymbol{v}_0 \cdot \boldsymbol{n}_0$

The right hand side of the previous equation may be written in the form

$$-\boldsymbol{v}_1 \cdot \boldsymbol{\nabla} G_0 + S_{d1}|\boldsymbol{\nabla} G_0| = \big(\boldsymbol{v}_1 - \frac{S_{d1}}{S_{d0}}\boldsymbol{v}_0\big) \cdot \boldsymbol{n}_0|\boldsymbol{\nabla} G_0|$$

One obtains in this way the following equation

$$\boxed{\frac{\partial G_1}{\partial t} + \boldsymbol{v}_{0t} \cdot \boldsymbol{\nabla} G_1 = \big(\boldsymbol{v}_1 - \frac{S_{d1}}{S_{d0}}\boldsymbol{v}_0\big) \cdot \boldsymbol{n}_0|\boldsymbol{\nabla} G_0|}$$

Burning velocity and velocity perturbations generate disturbances of the flame position in the normal direction, which are then convected along the flame front by the component of the mean local flow velocity $\boldsymbol{v}_{0t}$ parallel to the mean flame front.

Equivalence ratio perturbations

Equivalence ratio perturabtions induce changes in the local displacement velocity

$$S_d = S_{d0} + S_{d1}$$

such that

$$S_{d1} = S_{d0}(1 + a\frac{\phi_1}{\phi_0}) \quad \text{where} \quad a = \frac{\phi_0}{S_{d0}}\left(\frac{\partial S_d}{\partial \phi}\right)_{\phi=\phi_0}$$

(1) - Transport equation for the mean G_0 field

$$\mathbf{n}_0 = -\frac{\nabla G_0}{|\nabla G_0|} \qquad \mathbf{v}_0 \cdot \nabla G_0 = S_{d0}|\nabla G_0|$$

$$\boxed{S_{d0} - \mathbf{v}_0 \cdot \mathbf{n}_0 = 0}$$

Perturbed flame position

(2) -Transport equation for the perturbed G_1 field

$$\mathbf{n}_0 = -\frac{\nabla G_0}{|\nabla G_0|}$$

$$\frac{\partial G_1}{\partial t} + \left[\mathbf{v}_0 - S_{d0}\frac{\nabla G_0}{|\nabla G_0|}\right]\cdot \nabla G_1 = -\mathbf{v}_1 \cdot \nabla G_0 + aS_{d0}|\nabla G_0|\frac{\phi_1}{\phi_0}$$

$$\boxed{\frac{\partial G_1}{\partial t} + \mathbf{v}_0^t \cdot \nabla G_1 = \left(\mathbf{v}_1 - a\frac{\phi_1}{\phi_0}\mathbf{v}_0\right)\cdot \mathbf{n}_0|\nabla G_0|}$$

$\mathbf{v}_0^t = \mathbf{v}_0 - (\mathbf{v}_0 \cdot \mathbf{n}_0)\mathbf{n}_0$ mean flow velocity parallel to the mean flame front.

Composition and velocity disturb the flame position in the normal direction, These disturbances are convected along the flame front by the component of the mean local flow velocity $\boldsymbol{v}_{0t}$ parallel to the mean flame front.

25

Application to inclined flames

Inclined flames

Many flames are stabilized in a flow featuring a principal direction. The flame sheet then forms an angle with this direction.

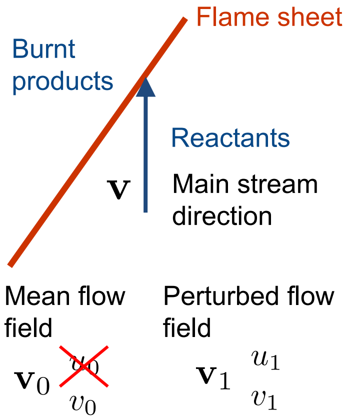

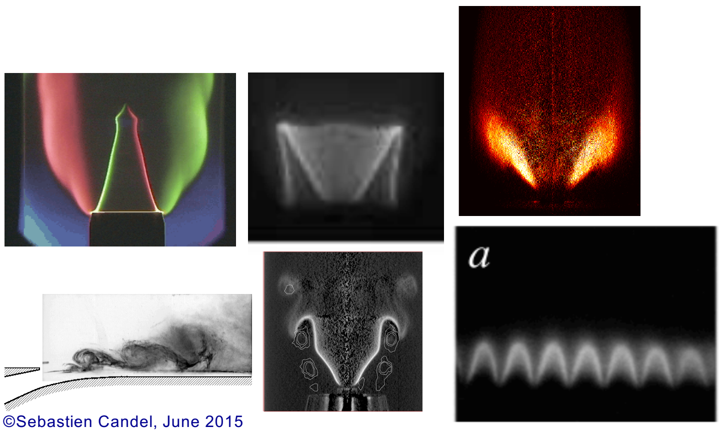

26

Calculation of inclined flame response

The flame motion is easier to analyze in a reference frame attached to the flame front

$$G(X,Y;t) = Y - \xi(X;t) = 0$$

$$\boxed{\begin{gathered}\frac{\partial \xi}{\partial t} + U_0 \frac{\partial \xi}{\partial X} = V_1(X;t) \\ \xi(0,t) = \xi_0(t)\end{gathered}}$$

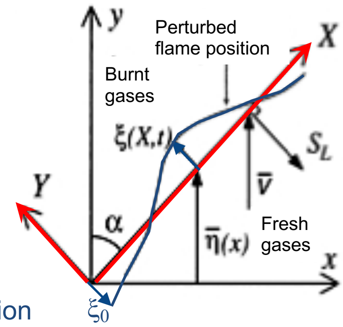

ξ normal flame front displacement with respect to the mean position

U_0 mean flow velocity along the flame front

V_1 velocity fluctuation normal to the flame front

ξ_0 normal flame front displacement at the flame base

T. Schuller, D. Durox and S. Candel (2003) *Combustion and flame*, **134**, 21-34. A unified model for the prediction of flame transfer functions : comparison between the conical and V-flame dynamics.

27

Normal flame displacement

Solution for normal flame sheet displacement

$$\boxed{\xi(X,t) = \underbrace{\frac{1}{U_0}\int_0^X V_1\left(X', t - \frac{X - X'}{U_0}\right) dX'}_{\text{Perturbed velocity field contribution}} + \underbrace{\xi_0\left(t - \frac{X}{U_0}\right)}_{\text{Anchoring point dynamics}}}$$

Interference integral for flame front perturbations

Boyer & Quinard (1990), Schuller et al. (2003), Lee & Lieuwen (2009), Borghesi et al. (2009)

Wrinkles (i.e. normal flame displacement *ξ(X,t)*) appear as convected by the mean flow with a wavelength $\lambda = U_0/f$.

This convective wave is modulated by a complex amplitude given by the integral term

28

Anchoring point dynamics

Ring modulation and acoustic waves produce the same type of wrinkles along the flame front

Vibrating rod

Petersen & Emmons (1961)

Acoustic modulation

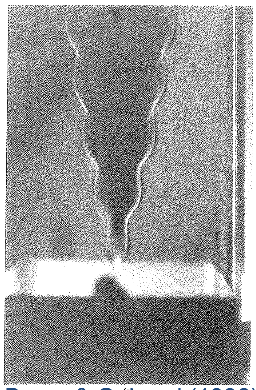

Boyer & Quinard (1996)

Ring modulation / Acoustic modulation

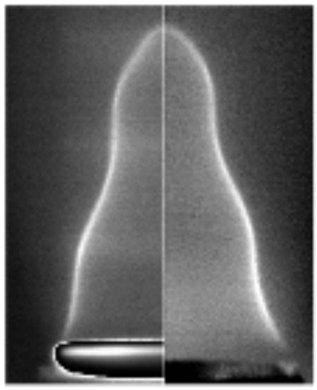

Kornilov et al. (2007)

29

Impact of flow perturbation model

Compact flame submitted to low frequency acoustic forcing

$$\lambda = \frac{c}{f} \gg L$$

Forcing conditions :
f=62.5 Hz, v'/v_0=0.20

Operating conditions
Φ=1.05, v_0=0.97 m/s

- - - Predictions with a uniform flow modulation

—— Predictions with a convective wave perturbation

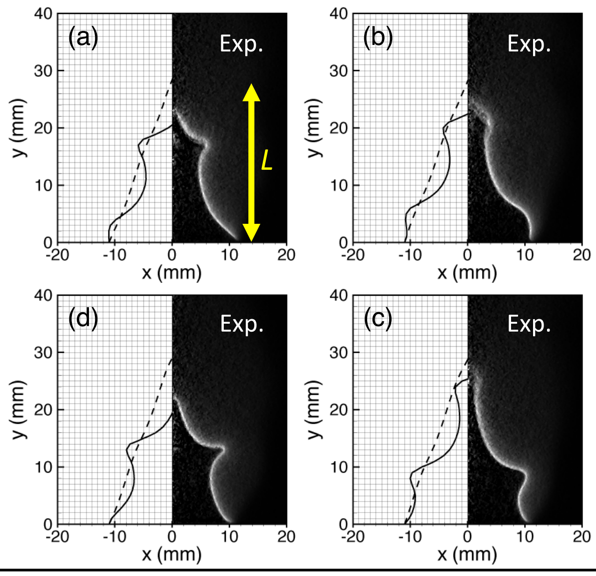

30

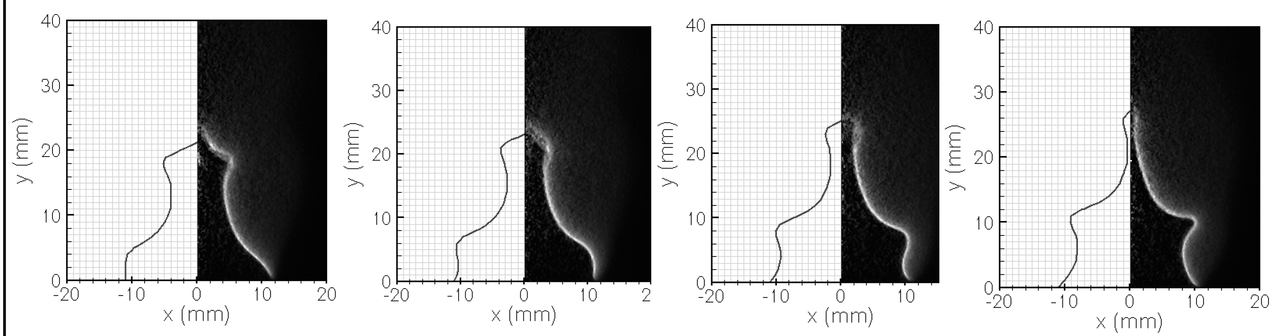

Prediction of flame response using the G-equation and a convective model for the incident velocity perturbation

T. Schuller, S. Ducruix, D. Durox and S. Candel (2002) *Proceedings of the Combustion Institute*, **29**. 107-114. Modeling tools for the prediction of premixed flame transfer functions.

31

Incident flow perturbations determine the time lag of the flame response

Flow perturbations

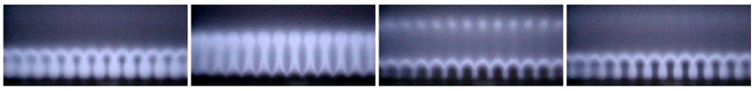

Φ= 0.85, V_d = 5.2 m/s, v'= 1.35 m/s, f = 500 Hz

$kL \sim 1$ $\quad k = \omega / u_0$

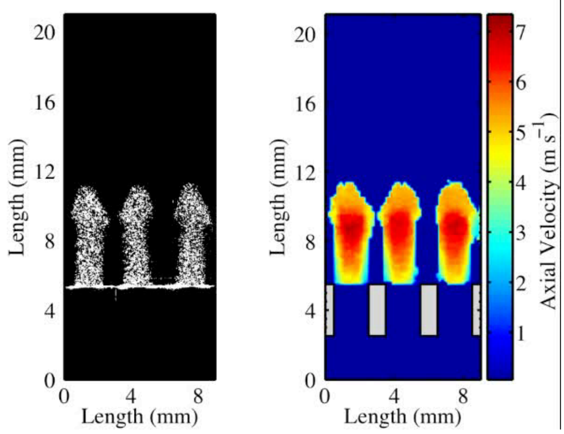

$$\boxed{\begin{aligned} v_1 &= \tilde{v}_1 \cos(\omega t - ky) \\ \nabla \cdot \mathbf{v}_1 &= 0 \end{aligned}}$$

Flow perturbations are convected by the mean flow and are of hydrodynamic type (incompressible)

De Soete (1964), Baillot et al. (1992), Schuller et al. (2002), Birbaud et al. (2006), Noiray et al. (2006)

32

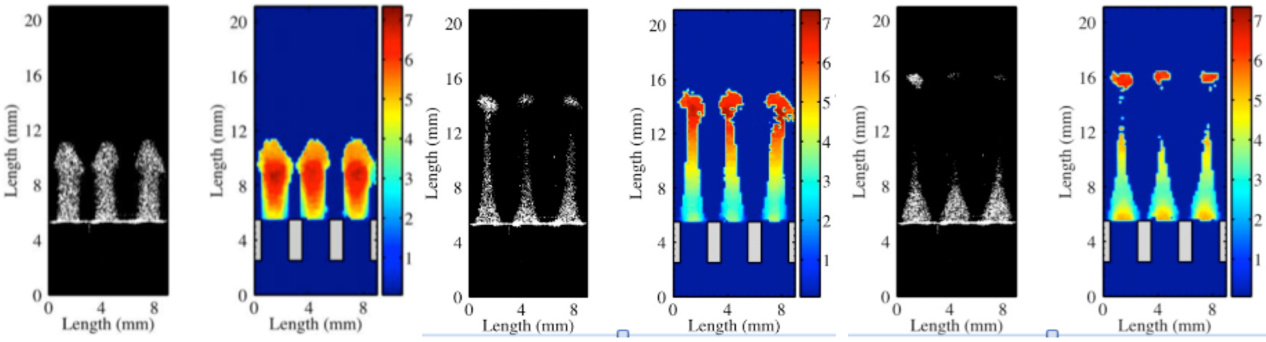

Three instants during a cycle of oscillation of multiple conical flames formed by a matrix injection plate. The flames are modulated by an acoustic wave. This induces a hydrodynamic velocity perturbation convected by the flow and Impinging on the flame. The color scale gives the axial velocity in m/s

Flame Transfer Function (FTF)

The Flame Transfer Function (FTF) describes the flame frequency response in terms of heat release rate disturbances due to the acoustic forcing

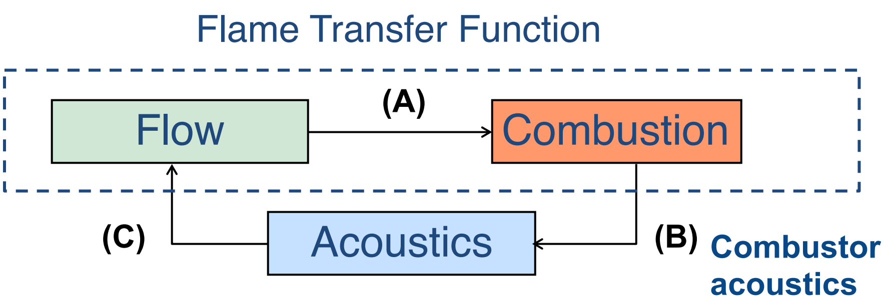

The objective is to decouple the analysis of flow and combustion dynamics (nonlinear problem) from the analysis of the combustor acoustics (linear problem).

FTF determination

The FTF or Flame Impulse Response (FIR) are determined from DNS, LES, low-order models or experiments

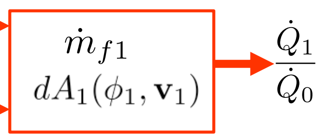

$$\frac{\dot{Q}_1}{\dot{Q}_0} = F_v \frac{v_1}{v_0} + F_\phi \frac{\phi_1}{\phi_0}$$

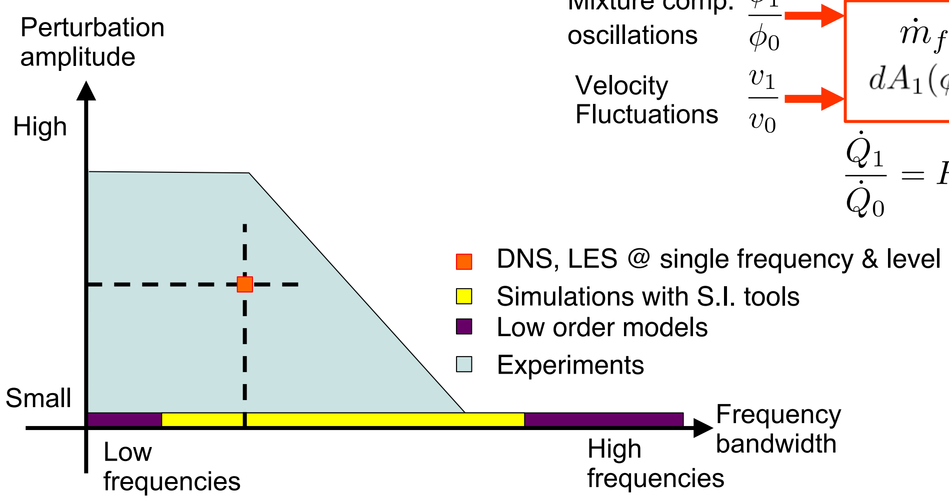

35

Experimental FTF determination

Premixed conical flame FTF submitted to harmonic incoming velocity perturbations in
a CH4/air mixture

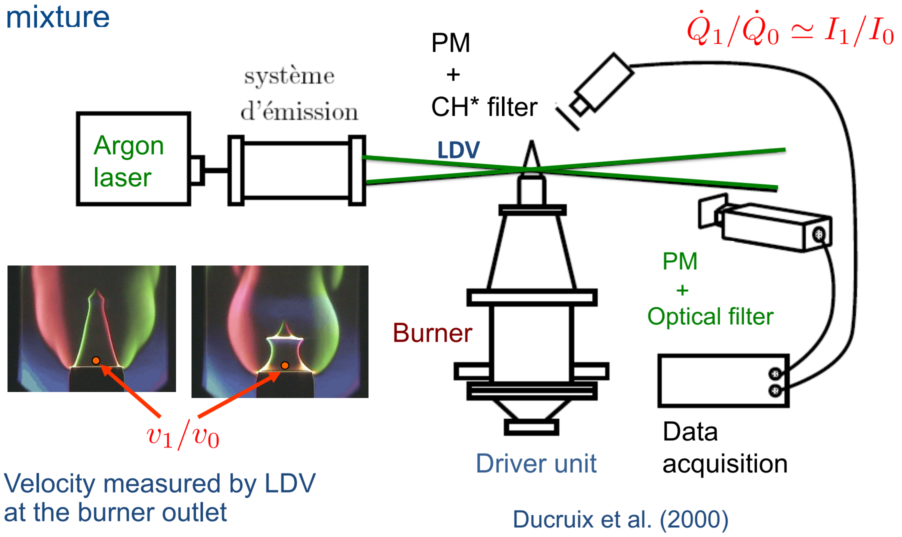

Ducruix et al. (2000)

36

Typical signals

Mixture kept at constant equivalence ratio
Modulation level kept constant

Φ=0.95, v_0=1.20 m/s, v_{1rms}=0.19 m/s, v_{1rms}/v_0=0.16

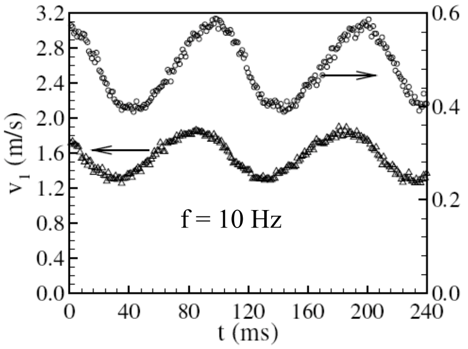

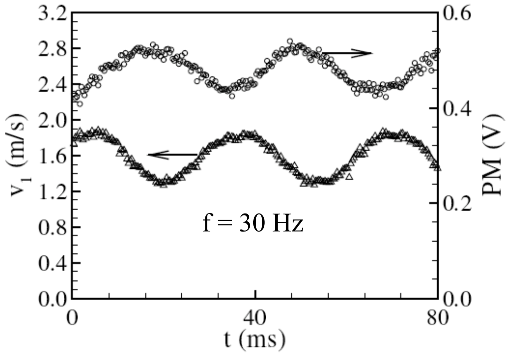

The velocity input is harmonic and the flame response (heat release rate fluctuation) remains also harmonic at these two forcing frequencies

37

FTF determination

The FTF is deduced from cross-spectral power analysis of the input and output signals

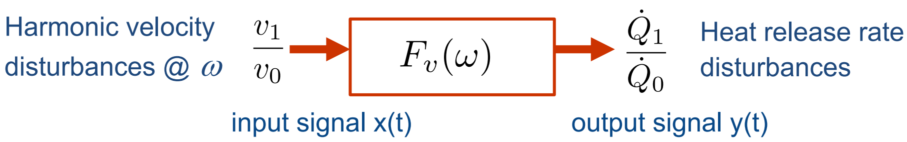

$$F_v(\omega) = \frac{S_{xy}(\omega)}{S_{xx}(\omega)}$$

Cross-power spectral density of *x(t)* and *y(t)* examined at the forcing frequency

Power spectral density of *x(t)* examined at the forcing frequency

A periodogram method helps to improve the signal to noise ratio. Statistical convergence requires a large number of periods (typically more than 100).

38

Conical Flame Transfer Function

$$\frac{\dot{Q}_1}{\dot{Q}_0} \simeq \frac{I_1}{I_0} = F_v \frac{v_1}{v_0}$$

$$F_v = G(\omega)\exp(i\varphi)$$

Gain :

- relative fluctuation amplitude
- G>1 amplification
- G<1 attenuation
- Low pass filter

Phase :

- time lag $\boxed{\varphi = \omega\tau}$
- convective at low frequencies
- saturation at high frequencies

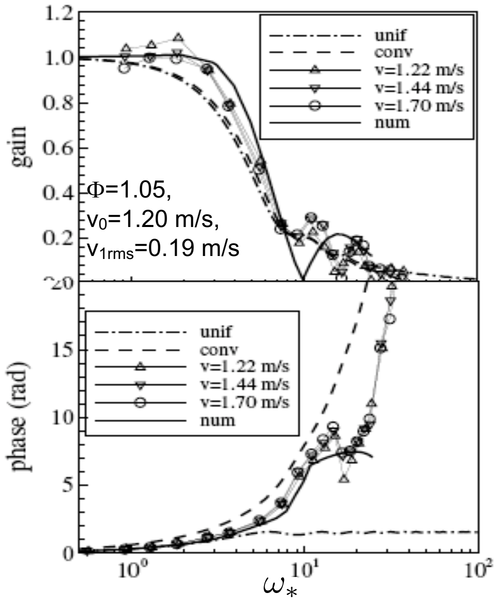

39

V- flame response

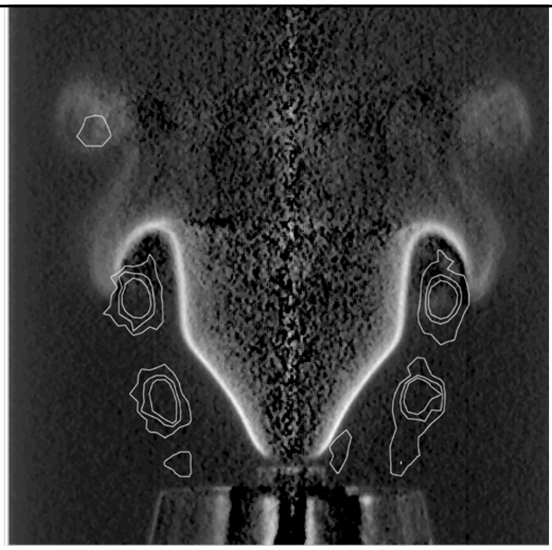

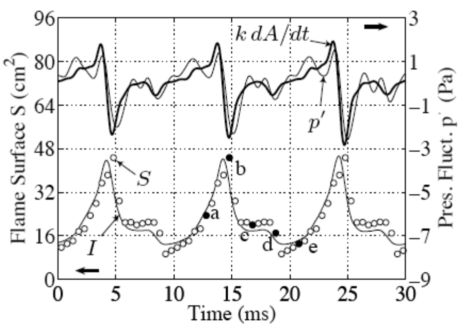

(c) **VF** : $f_e = 100\,Hz$, $\overline{v} = 2.3\,m\,s^{-1}$, $v_{rms} = 0.6\,m\,s^{-1}$, $\Phi = 1.11$

Acoustic forcing synchronizes large vortices generated in shear layers that are responsible of rapid flame surface destruction when impacting the flame periphery.

Durox et al. (2005)

40

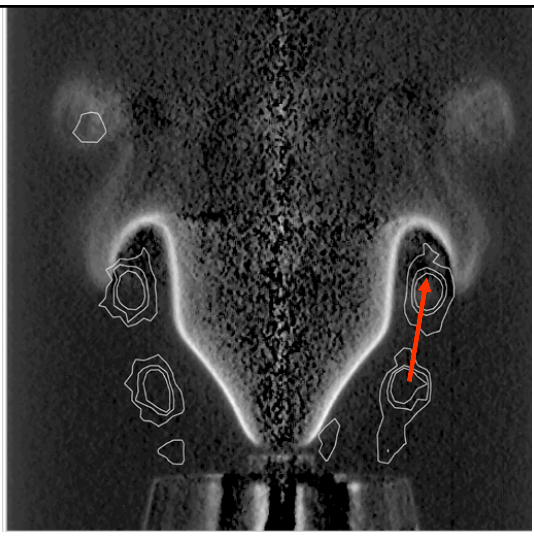

Vortex / flame interactions

$\Phi = 0.8$, $V_d = 1.87$ m/s
$v'_1 = 0.15$ m/s , $f = 150$ Hz

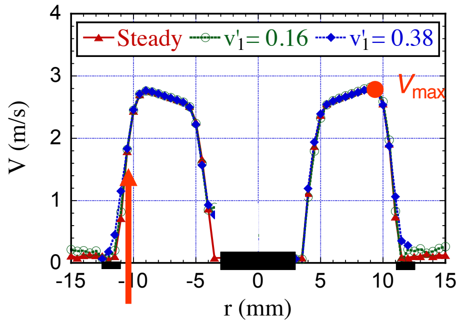

The flame front motion is controlled by the shear layer dynamics. The time lag corresponds to the travel time taken by a vortex to impinge the flame front (convected at about 0.5 V_{max}). This time lag is barely affected by the input level.

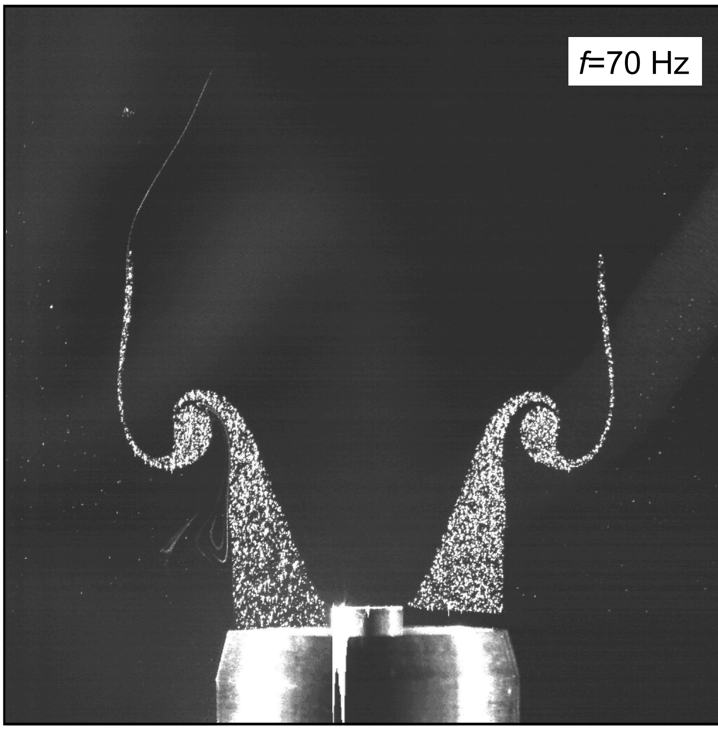

Vortex / flame interactions

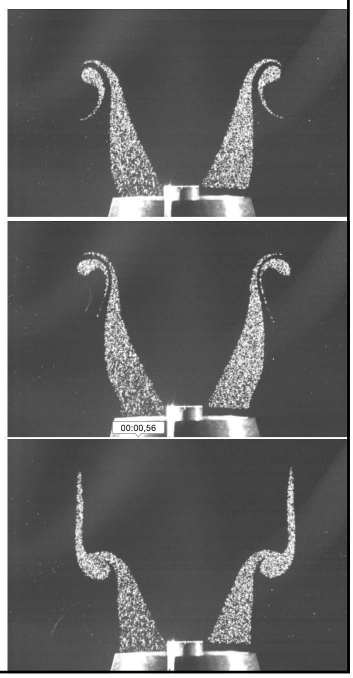

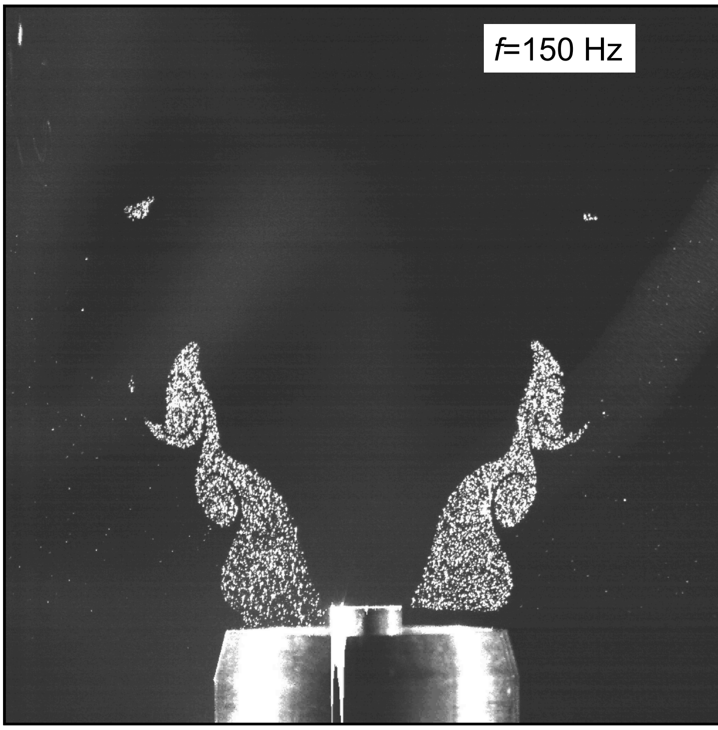

Vortex / flame interactions

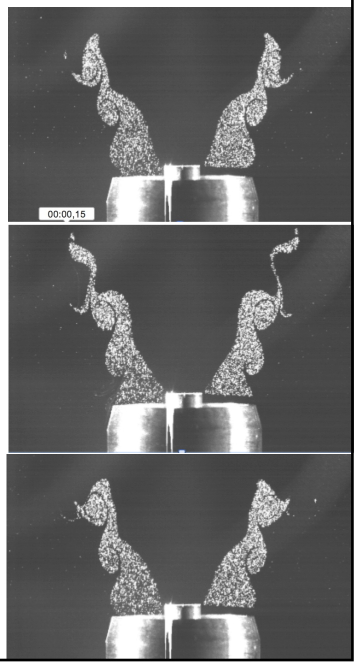

Effects of the modulation level

The perturbation level modifies the response of the flame operated at the same conditions

V_{rms}= 0.14 m/s

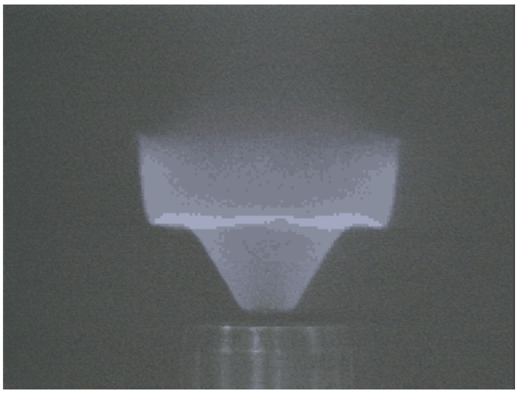

V_{rms}= 0.38 m/s

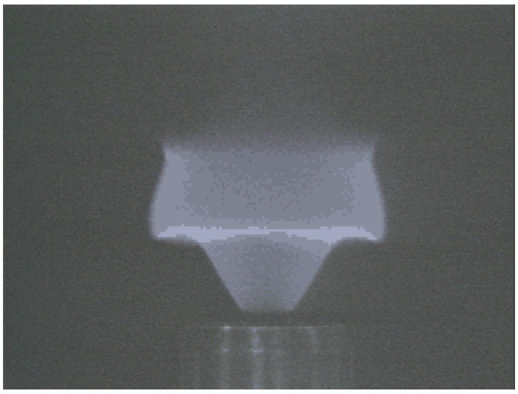

When the perturbation level increases saturation occurs : energy is transferred to higher harmonics and the gain examined at the forcing frequency drops.

V- Flame Transfer Function

$$\frac{\dot{Q}_1}{\dot{Q}_0} \simeq \frac{I_1}{I_0} = F_v \frac{v_1}{v_0}$$

$$F_v = G(\omega) \exp(i\varphi)$$

Gain :

- relative fluctuation amplitude
- Large overshoot G>1
- Gain reduces with increasing v_1
- Low pass filter

Phase :

- time lag $\varphi = \omega\tau$
- convective time lag independent of the input level

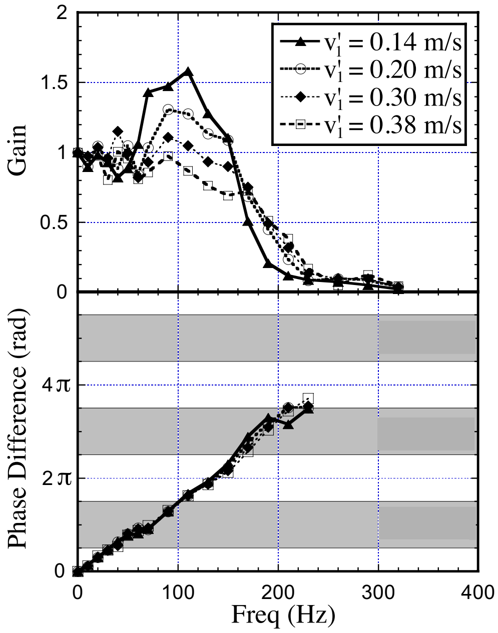

Durox et al. (2005)

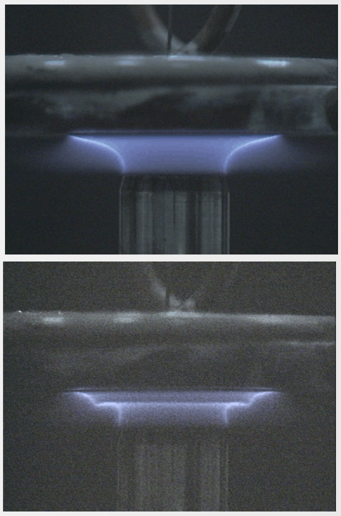

Combustion dynamics
Lecture 5b

S. Candel, D. Durox , T. Schuller

CentraleSupélec
Université Paris-Saclay, EM2C lab, CNRS

Tsinghua summer school, July 2021

Self-induced instability of a premixed jet flame impinging on a plate

Δv or Δp ⇒ ΔQ transfer function

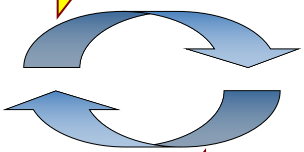

Δp or Δv ⇐ ΔQ

The Rayleigh criterion is often satisfied

$$\int_T p'(t)\dot{q}'(t)dt > 0$$

Match of frequencies and proper phase difference ⇒ Instabilities

Instabilities are also observed in the case of unconfined flames

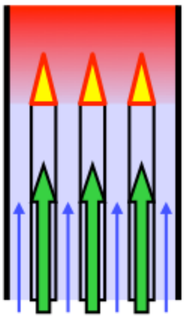

In domestic burners

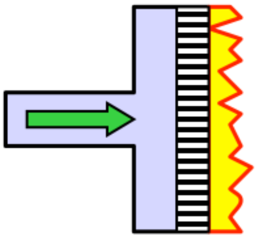

In radiant burners

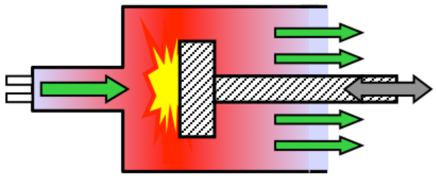

When the distance of the piston is varied Schäfer et al. (2000)

The coupling between acoustics and combustion differs from the case of confined flames and it is not well understood

Experimental set-up

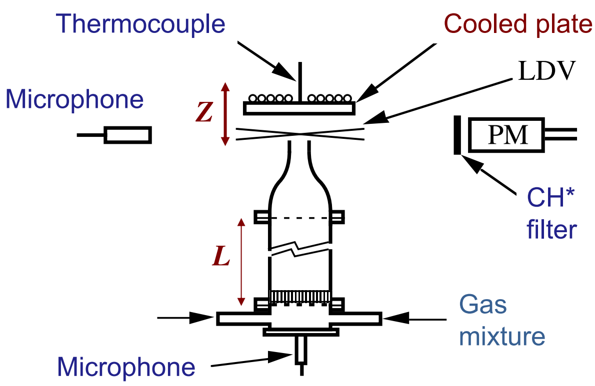

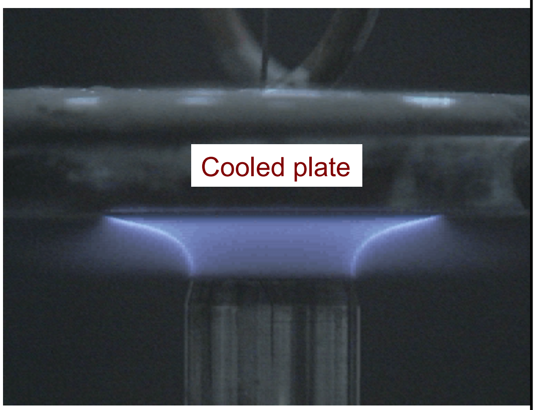

Outlet diameter : 22 mm, L = 100, 164 or 228 mm
CH_4 – air, Equivalence ratio : 0.95
Mean flow velocities : 1.20, 1.44 or 1.68 m/s

Zhang & Bray classification (1999)

Cool central core flame

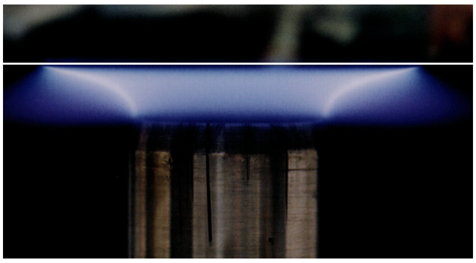

Envelope flame

Envelope flame

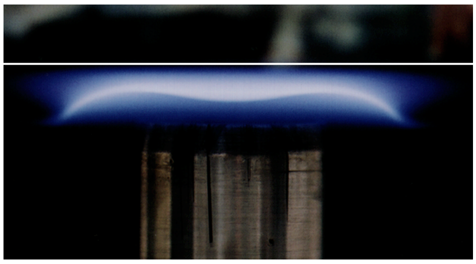

Disk flame

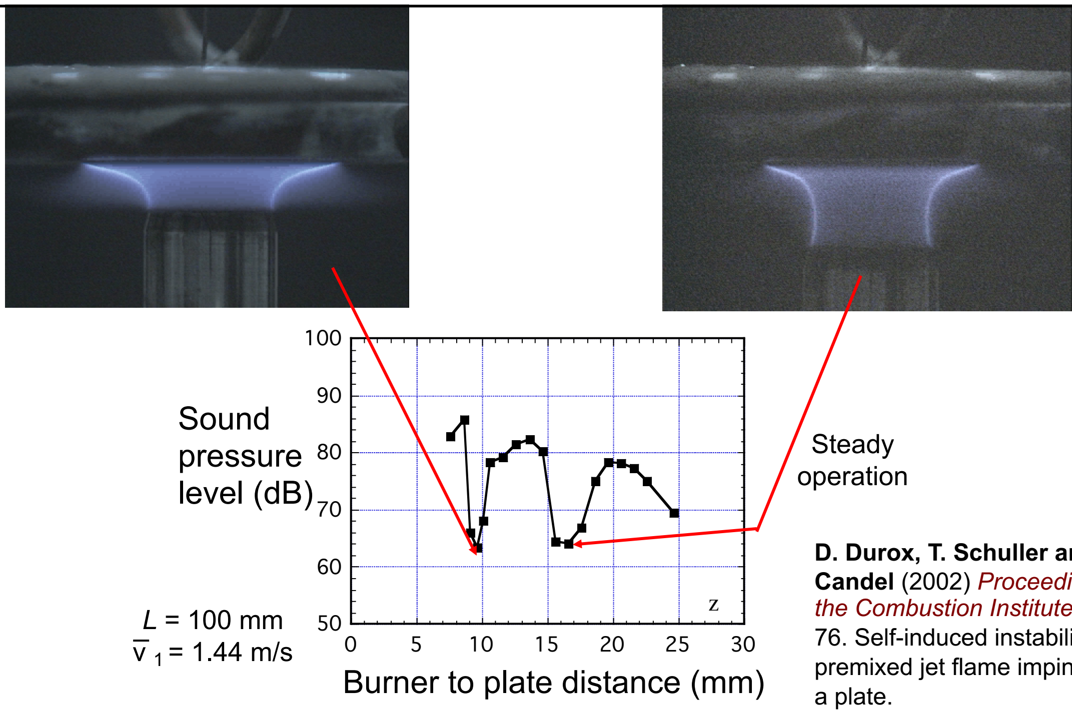

D. Durox, T. Schuller and S. Candel (2002) *Proceedings of the Combustion Institute,* **29**. 69-76. Self-induced instability of a premixed jet flame impinging on a plate.

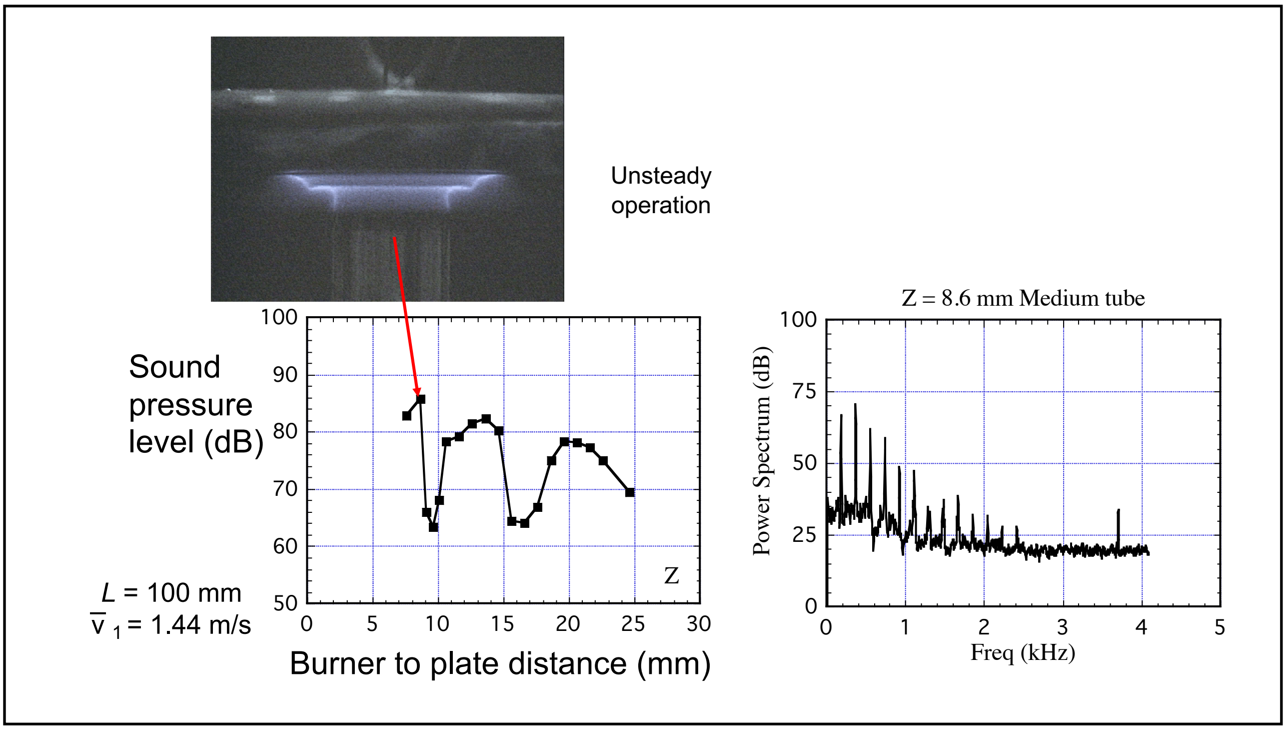
Unsteady operation
Z = 8.6 mm Medium tube
Sound pressure level (dB)
L = 100 mm
$\bar{v}_1$ = 1.44 m/s
Burner to plate distance (mm)
Z
Power Spectrum (dB)
Freq (kHz)

7

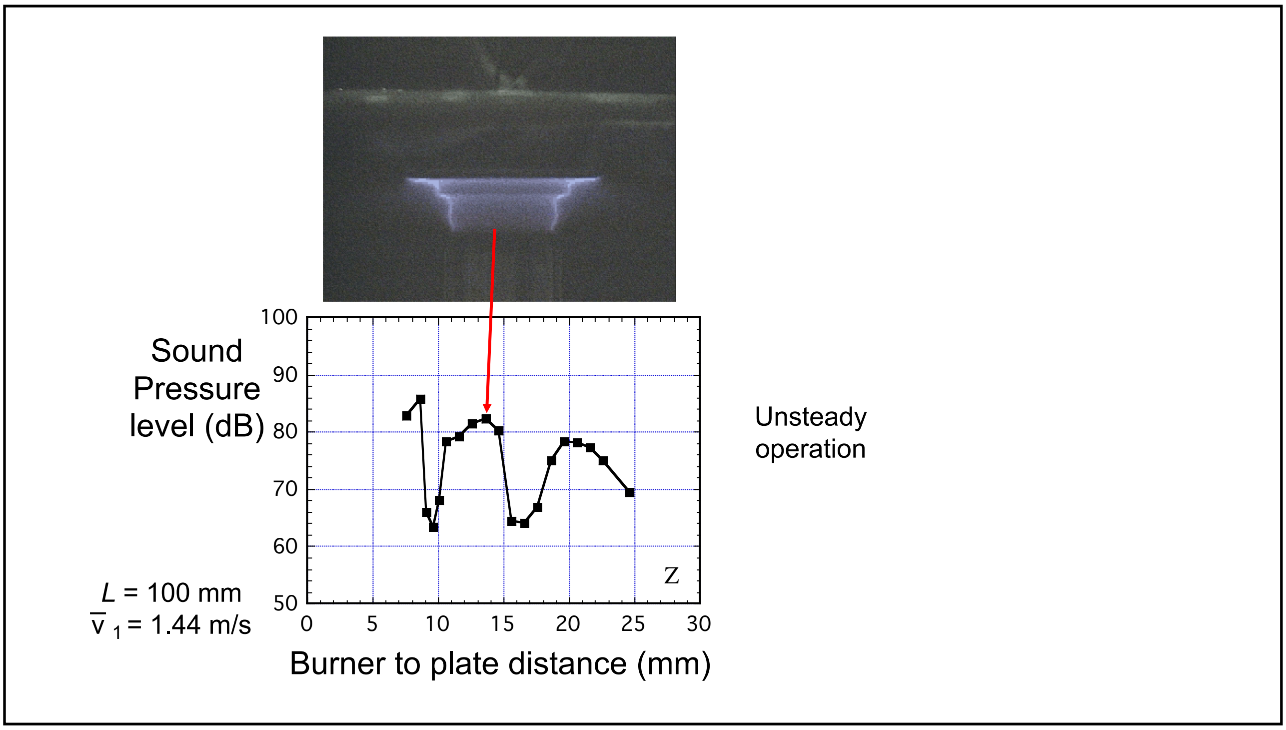
Sound Pressure level (dB)
Unsteady operation
L = 100 mm
$\bar{v}_1$ = 1.44 m/s
Burner to plate distance (mm)
Z

8

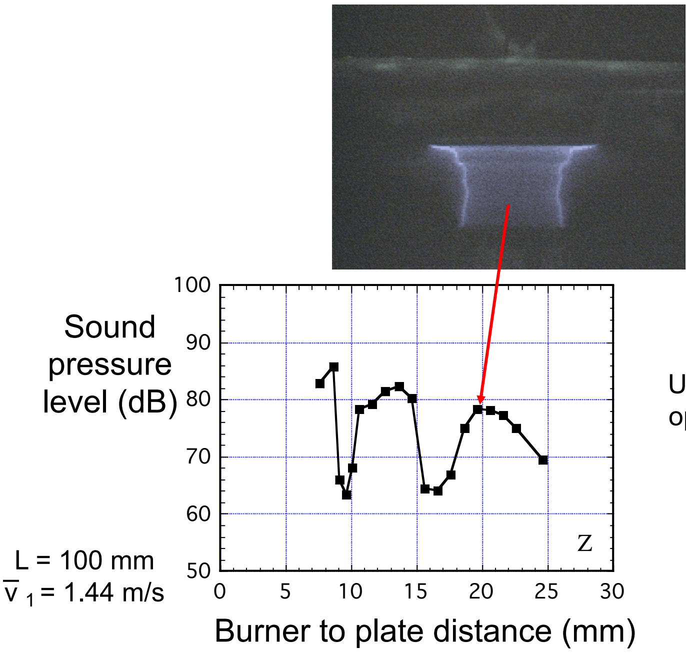

Unsteady operation

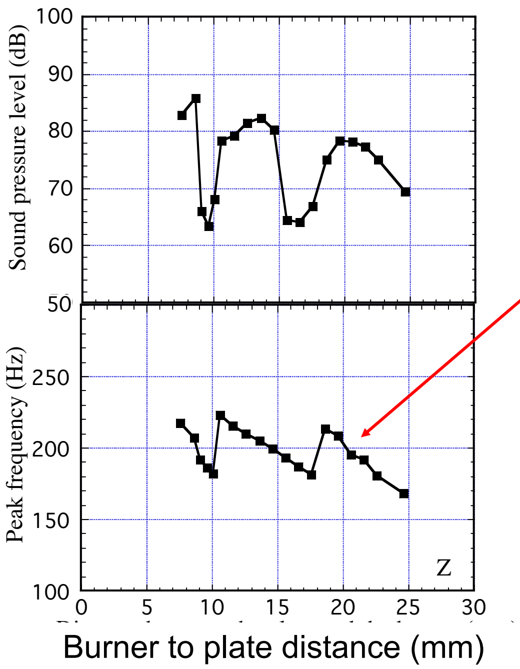

L = 100 mm
$\bar{v}_1$ = 1.44 m/s

Evolution of the fundamental frequency
sawtooth pattern.

In this case, the frequency is around 200Hz when the sound pressure level is highest.

Velocity on the axis, at 1.5 mm above the nozzle exit and heat release detected by the PM.
At *z* = 8.6 mm, the oscillation level is large

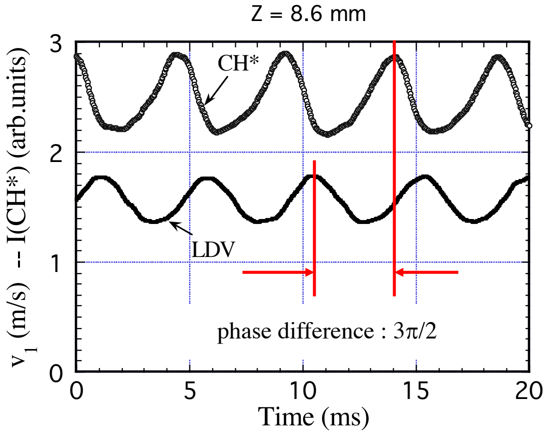

Acoustic response of the burner

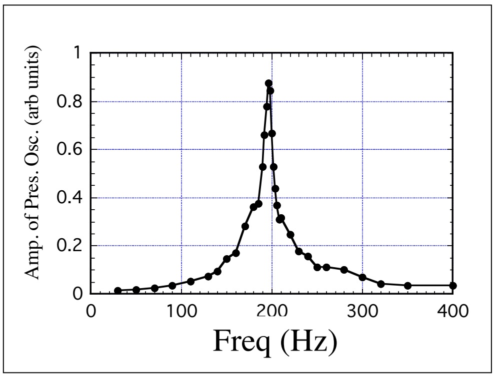

$$\omega_0^2 = (c^2 S_1)/(V L_{eff})$$

$$L_{eff} = \int_{in}^{out} \frac{S_1}{S(z)} dz + \delta_e$$

Helmholtz resonator bulk oscillation inside the burner

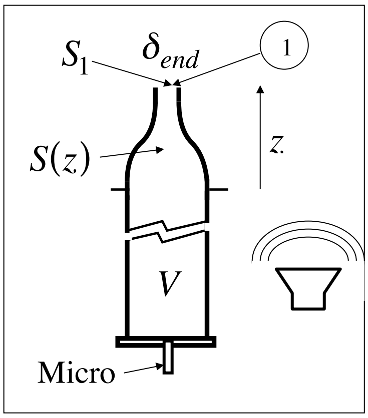

f_o = 202 Hz

Instability model : driven Helmholtz resonator

$$M\frac{d^2v_1'}{dt^2} + R\frac{dv_1'}{dt} + kv_1' = \boxed{-S_1\frac{dp_1'}{dt}}$$

$M = \overline{\rho} S_1 L_{eff}$ Effective mass of air in the pipe

$R = \overline{\rho} S_1 v_1$ System damping

$k = \overline{\rho} c^2 S_1^2 / V$ Gas volume stiffness

The resonator is driven by external pressure fluctuations p_1' at the burner outlet

Instability model : origin of external pressure fluctuations - Model of Price et al. (1969)

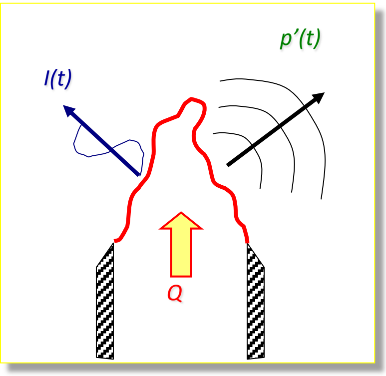

$$p(r,t) = \frac{\rho_0}{4\pi r}\left(\frac{\rho_u}{\rho_b} - 1\right)\left[\frac{d\dot{Q}}{dt}\right]_{t-\tau_a}$$

$$\dot{Q} \propto I \text{ or } A$$

I is the light intensity emitted by free radicals
A is the flame surface area

τ_a time delay between the source and the measurement point

Impinging flame
with acoustic forcing of the flow

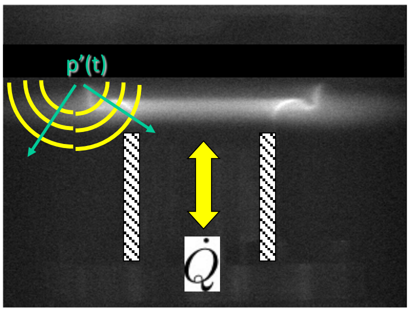

$$p'(r,t) = K(r)\left[\frac{dA'}{dt}\right]_{t-\tau_a}$$

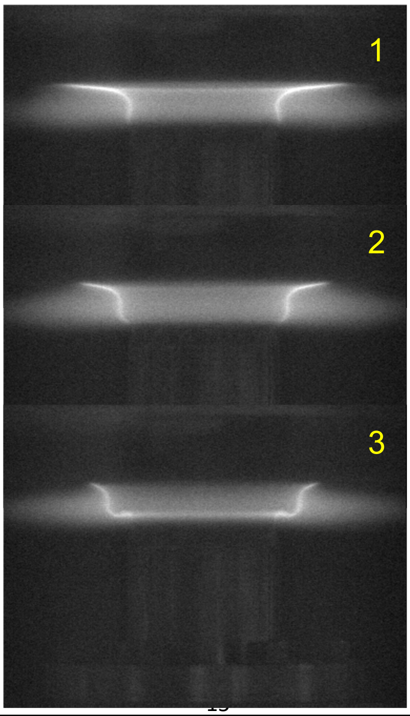

T. Schuller, D. Durox and S. Candel (2002) *Combustion and Flame*, **128**, 88-110. Dynamics of and noise radiated by a perturbed impinging premixed jet flame**.**

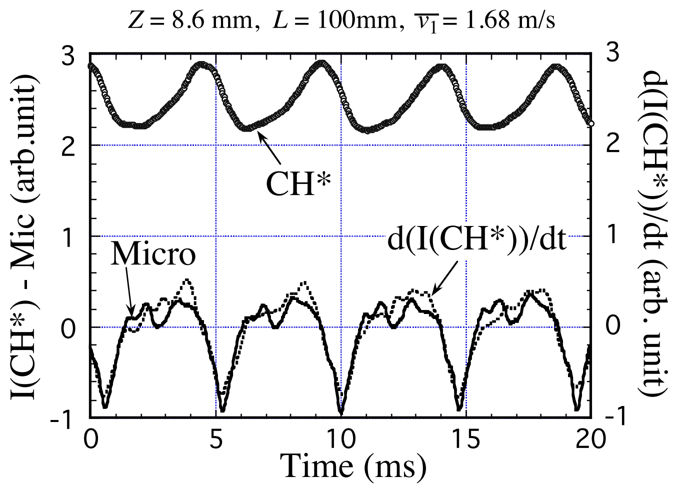

The acoustic pressure and the time derivative of the heat release are similar, confirming that the source is suitably identified

Transfer function

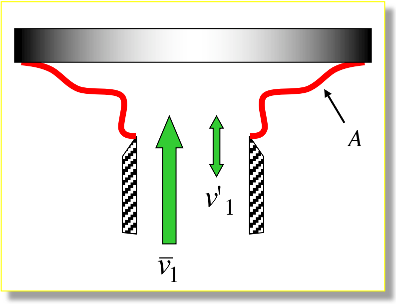

Velocity perturbations are convected by the mean flow along the flame front.

Fluctuations of the flame surface *A(t)* are induced by these velocity perturbations after a convective delay τ_c
τ_c is of the order of z/v_1.

$$A'(t) = n(v'_1)_{t-\tau_c}$$

n characterizes the coupling between the flame surface fluctuation and the velocity perturbation

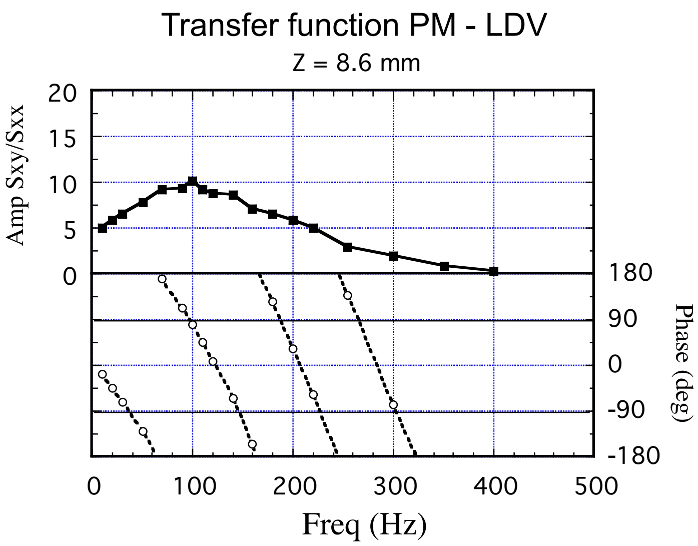

The phase difference between the velocity and the heat release yields a mean convective time which is of the order of z/v_1

$$M\frac{d^2v_1'}{dt^2} + R\frac{dv_1'}{dt} + kv_1' = \boxed{-S_1\frac{dp_1'}{dt}}$$

$$p'(r,t) = K(r)[\frac{dA'}{dt}]_{t-\tau_a}$$

$$A'(t) = n(v_1')_{t-\tau_c}$$

$$\boxed{M\frac{d^2v_1'}{dt^2} + R\frac{dv_1'}{dt} + kv_1' = -S_1K(r_{21})n[\frac{d^2v_1'}{dt^2}]_{t-\tau}}$$

with $\tau = \tau_a + \tau_c$

19

$$\boxed{\frac{d^2v_1'}{dt^2} + 2\delta\omega_0\frac{dv_1'}{dt} + \omega_0^2v_1' = -N[\frac{d^2v_1'}{dt^2}]_{t-\tau}}$$

where $\delta\omega_0 = R/(2M)$ $N = S_1K(r_{21})n/M$

Now $\tau_a << \tau_c$ so that $\tau \simeq \tau_c$

This equation has a solution at the resonant frequency f_0 if :

$\omega_0\tau = (4m-1)\pi/2$ where $m = 1, 2, \ldots$

This imposes a condition on the convective delay:

$$\boxed{\omega_0\tau_c \simeq \omega_0\tau = 3\pi/2 \ \ (\text{modulo } 2\pi)}$$

20

$$\omega_0 \tau_c \simeq \omega_0 \tau = 3\pi/2 \ \ (\text{modulo } 2\pi)$$ so that $$f_0 \tau = 3\pi/4,\ 7\pi/4,\ \ldots$$

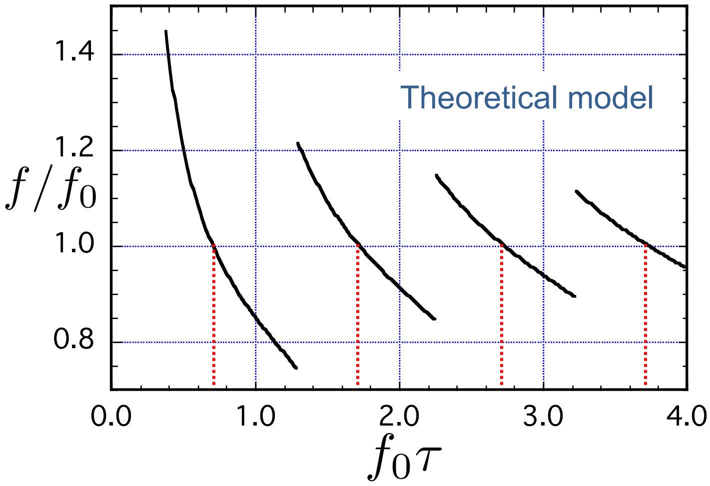

21

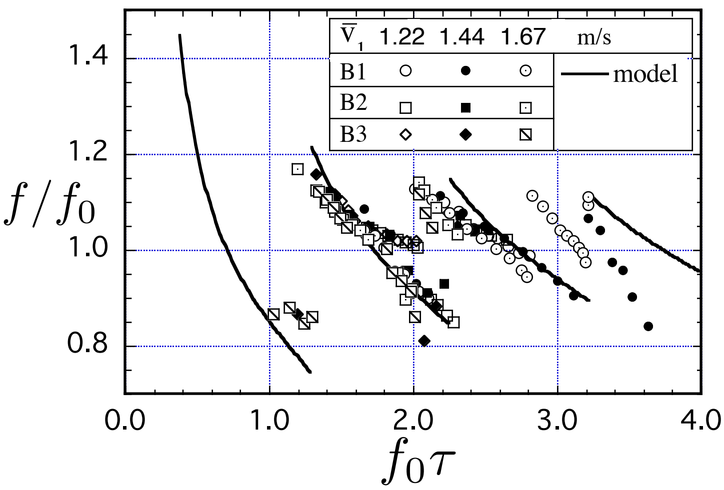

22

Conclusions

- Strong instabilities may be induced when a premixed flame anchored on a burner rim impacts on a plate facing the burner exhaust
- In this study the burner behaves like a Helmholtz resonator
- The frequency of oscillation evolves with the burner to plate separation around the fundamental resonance frequency
- Sudden annihilation of flame surface area produces an intense source of sound
- Flame wall interactions could play a Role in the development of combustion instabilities
- Even without a plate, if flame surface variations are important and fast, and if the sound influences the flow velocity, then an instability can be triggered

23

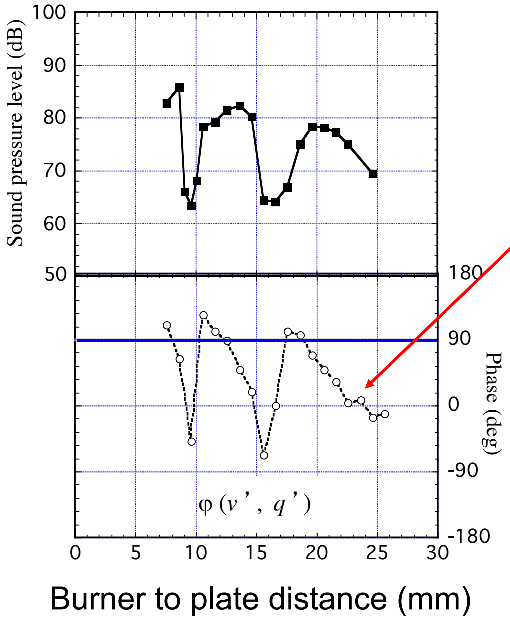

Phase difference between the heat release and the velocity.

When the sound level is the highest, the phase difference is close to $\pi/2$.
Then the heat release lags the velocity with a delay corresponding to $3\pi/2$.

24

Combustion dynamics Lecture 5c

S. Candel, D. Durox , T. Schuller

CentraleSupélec
Université Paris-Saclay, EM2C lab, CNRS

Tsinghua summer school, July 2021

1

Combustion dynamics of inverted conical flames

Confined flames

Unconfined flames

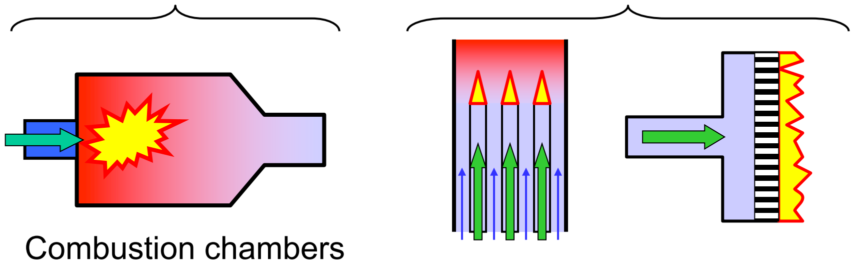

Combustion chambers
Gas turbine
combustors

Domestic
burners

Radiant
burners

In low emission systems operating in premixed lean modes flames are less well stabilized and more susceptible to external perturbations

2

Experimental set-up

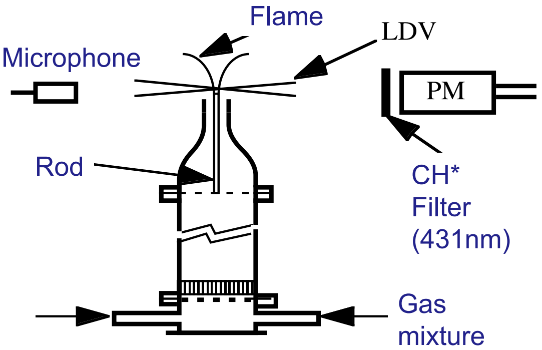

D. Durox, T. Schuller and S. Candel (2005) *Proceedings of the Combustion Institute* **30**, 1717-1724. Combustion dynamics of inverted conical flames.

Inverted conical flame (ICF)

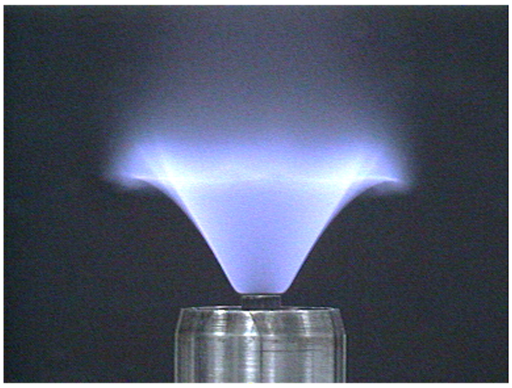

Steady flame

Diameter 22 mm
CH_4 - air
Equivalence Ratio : 0.92
Flow velocity : 2.05 m/s

Self-induced Instability

Certain conditions in terms of equivalence ratio and flow rate give rise to self induced instabilities

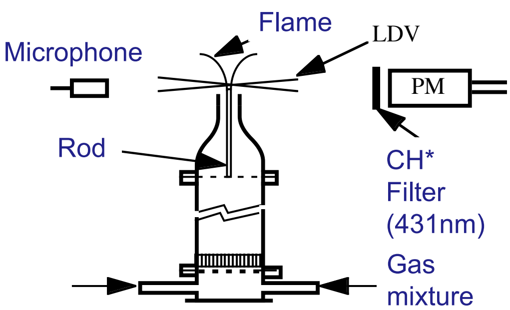

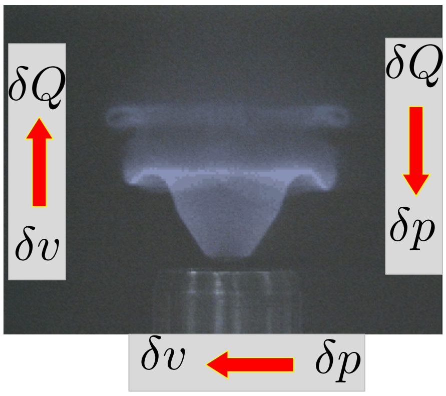

Self-excited flame
at f = 172 Hz
Equivalence ratio : 0.92
Flow velocity : 2.05 m/s
v' = 0.14 m/s

Transfer function

$$\frac{\dot{Q}'}{\overline{\dot{Q}}} = f(\frac{v'}{\overline{v}})$$

$$I \propto \dot{Q}$$

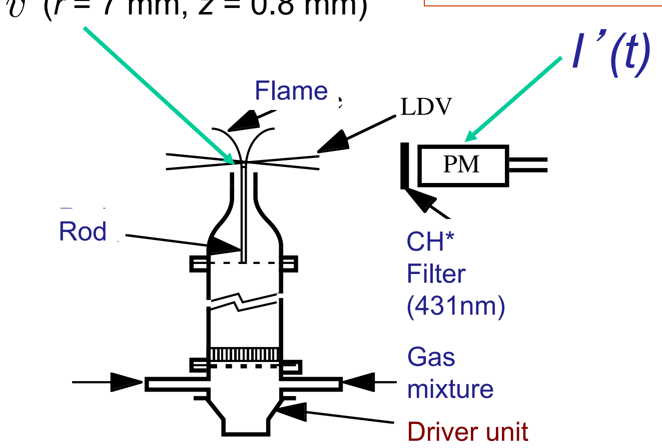

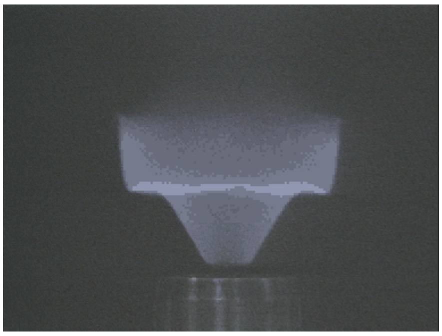

Self-excited flame
at f = 100 Hz
Equivalence ratio : 0.92
Flow velocity : 2.05 m/s
v'_1 = 0.14 m/s

Describing function Φ = 0.92 V_d = 2.05 m/s

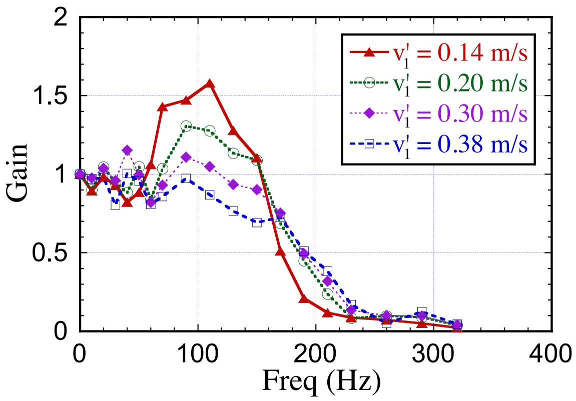

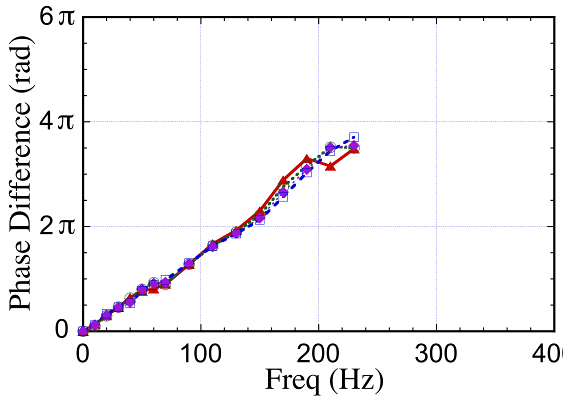

φ is nearly linear
convective lag
τ_c = 8.6 ms

$$I'_{CH*}(t) = G[v'_1]_{t-\tau_c}$$

Flame dynamics

Laser tomography of fresh stream seeded with oil droplets.

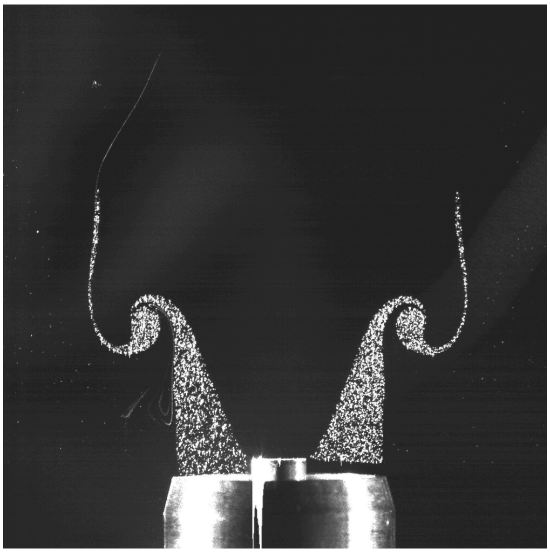

f = 70 Hz

Φ= 0.8
V_d = 1.87 m/s
v'_1= 0.15 m/s

Flame dynamics

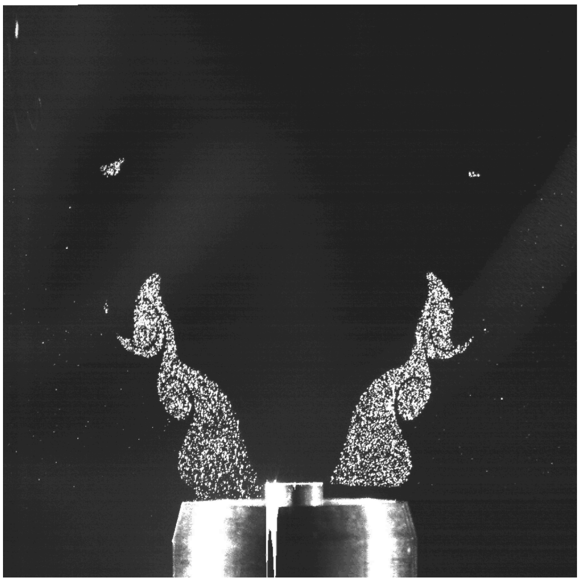

f = 150 Hz

Φ= 0.8
V_d = 1.87 m/s
v'_1= 0.15 m/s

Unsteady vorticity field

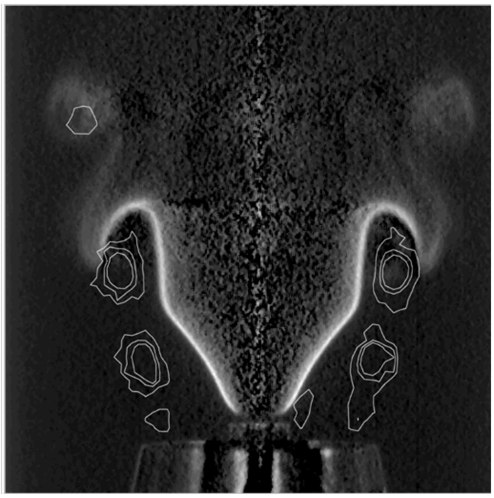

$\Phi = 0.8$

$V_d = 1.87$ m/s, $v'_1 = 0.15$ m/s

$f = 150$ Hz

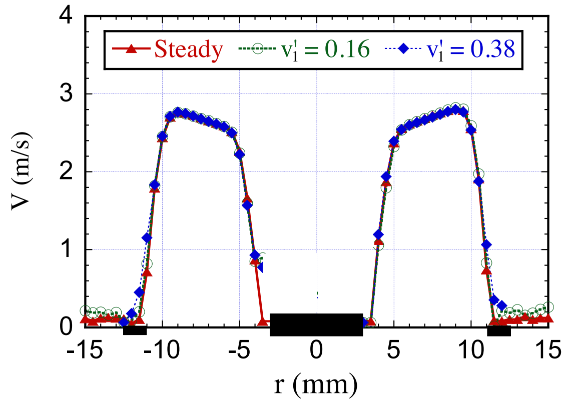

The vortices are convected at a velocity $U_c \simeq 0.5 v_{max}$

Helmholtz resonator

Bulk oscillation inside the burner

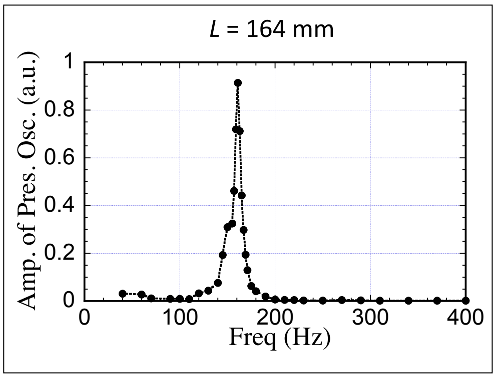

$$\omega_0^2 = (c^2 S_1)/(V L_{eff})$$

$$L_{eff} = \int_{in}^{out} \frac{S_1}{S(z)} dz + \delta_e$$

Mechanism of instability

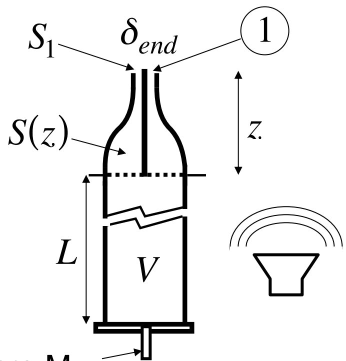

$f_o = 163$ Hz

Mechanism of instability

Helmholtz resonator with driving

$$M\frac{d^2v_1'}{dt^2} + R\frac{dv_1'}{dt} + kv_1' = \boxed{-S_1\frac{dp_1'}{dt}}$$

$M = \overline{\rho} S_1 L_{eff}$ Effective mass of gases

$R = \overline{\rho} S_1 v_1$ System damping

$k = \overline{\rho} c^2 S_1^2 / V$ Stiffness of the gas volume

The resonator is driven by external fluctuations p'_1

Signals measured in self-sustained instability case

$\Phi = 0.92$ $V_d = 2.05$ m/s $v'_1 = 0.14$ m/s $f = 172$ Hz

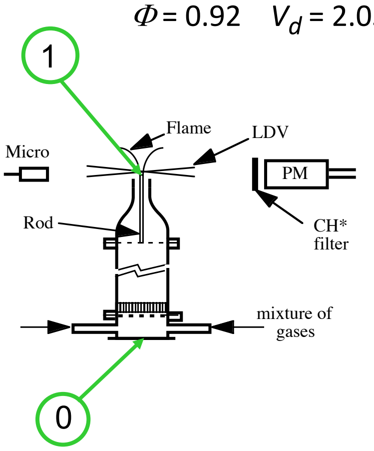

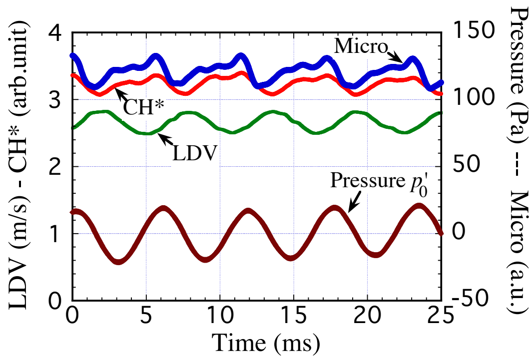

$$p_1'(t) \simeq B\left[I'_{CH*}\right]_{t-\tau_a}$$

Mechanism of instability

$$I'_{CH*}(t) = G[v'_1]_{t-\tau_c}$$

$$p'_1(t) = B[I'_{CH*}]_{t-\tau_a}$$

Time lag model:
the light intensity
fluctuation is
proportional to the
delayed velocity
fluctuation signal

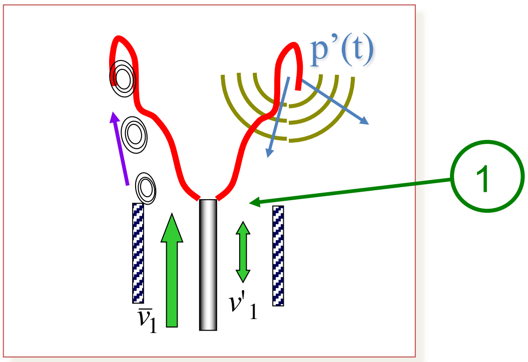

Steady flow streamlines

Average location of the flame front in the absence of perturbation

Averaged image of the flame front positions with a perturbation at 70 Hz

v'_1= 0.15 m/s
f = 70 Hz

Φ= 0.8
V_d = 1.87 m/s

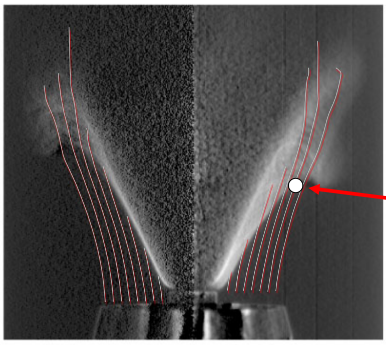

The dot corresponds to

$$h = \tau_c U_c \simeq \tau_c(0.5 v_{max})$$

Mechanism of instability

$$M\frac{d^2v_1'}{dt^2}+R\frac{dv_1'}{dt}+kv_1'=\boxed{-S_1\frac{dp_1'}{dt}}$$

$$\boxed{\begin{aligned}p_1'(t)&=B[I'_{CH*}]_{t-\tau_a}\\ I'_{CH*}(t)&=G[v_1']_{t-\tau_c}\end{aligned}}$$

$$\omega_0^2=\frac{S_1c^2}{VL_e}\qquad 2\delta\omega_0=R/M\qquad \Omega=GBS_1/M$$

Mechanism of instability

$$\boxed{\frac{d^2v_1'}{dt^2}+2\delta\omega_0\frac{dv_1'}{dt}+\omega_0^2v_1'=-\Omega\left[\frac{dv_1'}{dt}\right]_{t-\tau_a-\tau_c}}$$

$$\tau_a<<\tau_c\qquad \tau\simeq\tau_c$$

If δ and Ω are small, a linear analysis indicates that a necessary condition to have an instability is:

$$\boxed{\omega_0\tau \text{ belongs to } [\pi/2,3\pi/2] \text{ modulo } 2\pi}$$

Mechanism of instability

Frequency peak
at the resonance

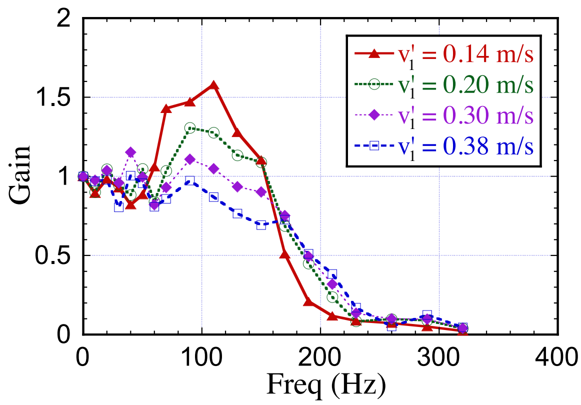

f_o = 163 Hz

Instability
frequency
f = 172 Hz

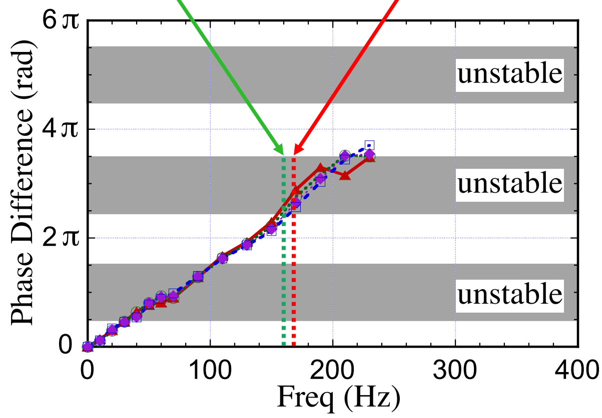

$\Phi = 0.92$ $V_d = 2.05$ m/s

Conclusions

- Inverted conical flames are sensitive to low frequency acoustic excitations.
- They behave like an amplifier in a broad range of frequencies
- The transfer function phase increases linearly : the process involves a convective delay
- The main wrinkling of the flame front is due to vortex structures created in the shear layer
- The strong rolling-up of the flame induces a mutual annihilation of neighboring reactive elements
  - ➡ Rapid variation of flame surface area
  - ➡ Important source of pressure wave.
- With ICF's, at low amplitude modulation, entrainment of air modifies the equivalence ratio near the flame tip and the light emission ceases to be proportional to the heat release.

Combustion dynamics
Lecture 6a

S. Candel, D. Durox , T. Schuller

CentraleSupélec
Université Paris-Saclay, EM2C lab, CNRS

Tsinghua summer school, July 2021

The flame response can be characterized in terms of a transfer function

$$\xrightarrow{u'/\overline{U}} \boxed{\text{Combustion}} \xrightarrow{\dot{Q}'/\overline{\dot{Q}}}$$

$$\mathcal{F}(\omega) = \frac{\dot{Q}'/\overline{\dot{Q}}}{u'/\overline{U}}$$

But the flame transfer function (FTF) only provides the linear growth rate in the analysis of instabilities,

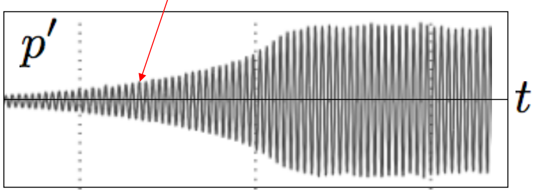

It is more informative to use the flame describing function

$$u'/\overline{U} \longrightarrow \boxed{\text{Combustion}} \longrightarrow \dot{Q}'/\overline{\dot{Q}}$$

$$\mathcal{F}(\omega, u') = \frac{\dot{Q}'/\overline{\dot{Q}}}{u'/\overline{U}}$$

The Flame Describing Function (FDF) extends the transfer function concept to the nonlinear case

In the FDF the flame response depends on the frequency and amplitude of the incident perturbation

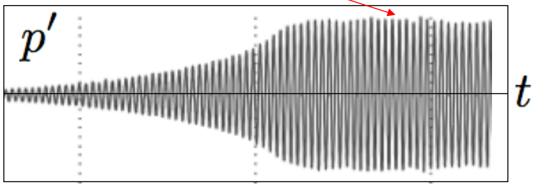

A. Dowling (1999) *Journal of Fluid Mechanics* 394, 51–72. A kinematic model of a ducted flame.

N. Noiray, D. Durox, T. Schuller and S. Candel (2008) *Journal of Fluid Mechanics* **615**, 139-167. A unified framework for nonlinear combustion instability analysis based on the describing function.

F. Boudy, D. Durox, T. Schuller, G. Jomaas and S. Candel (2011) *Journal of Engineering for gas turbine and power.* 33, June. Article 061502. Describing function analysis of limit cycle in a multiple flame combustor.

J. Fluid Mech. (2008), *vol.* 615, *pp.* 139–167. © 2008 Cambridge University Press 139
doi:10.1017/S0022112008003613 Printed in the United Kingdom

A unified framework for nonlinear combustion instability analysis based on the flame describing function

N. NOIRAY, D. DUROX, T. SCHULLER AND S. CANDEL
Ecole Centrale Paris, EM2C Laboratory, CNRS, 92295 Châtenay-Malabry, France

(Received 6 March 2008 and in revised form 8 July 2008)

Analysis of combustion instabilities relies in most cases on linear analysis but most observations of these processes are carried out in the nonlinear regime where the system oscillates at a limit cycle. The objective of this paper is to deal with these two manifestations of combustion instabilities in a unified framework. The flame is recognized as the main nonlinear element in the system and its response to perturbations is characterized in terms of generalized transfer functions which assume that the gain and phase depend on the amplitude level of the input. This 'describing function' framework implies that the fundamental frequency is predominant and that the higher harmonics generated in the nonlinear element are weak because the higher frequencies are filtered out by the other components of the system. Based on this idea, a methodology is proposed to investigate the nonlinear stability of burners by associating the flame describing function with a frequency-domain analysis of the burner acoustics. These elements yield a nonlinear dispersion relation which can be solved, yielding growth rates and eigenfrequencies, which depend on the amplitude level of perturbations impinging on the flame. This method is used to investigate the regimes of oscillation of a well-controlled experiment. The system includes a resonant upstream manifold formed by a duct having a continuously adjustable length and a combustion region comprising a large number of flames stabilized on a multipoint injection system. The growth rates and eigenfrequencies are determined for a wide range of duct lengths. For certain values of this parameter we find a positive growth rate for vanishingly small amplitude levels, indicating that the system is linearly unstable. The growth rate then changes as the amplitude is increased and eventually vanishes for a finite amplitude, indicating the existence of a limit cycle. For other values of the length, the growth rate is initially negative, becomes positive for a finite amplitude and drops to zero for a higher value. This indicates that the system is linearly stable but nonlinearly unstable. Using calculated growth rates it is possible to predict amplitudes of oscillation when the system operates on a limit cycle. Mode switching and instability triggering may also be anticipated by comparing the growth rate curves. Theoretical results are found to be in excellent agreement with measurements, indicating that the flame describing function (FDF) methodology constitutes a suitable framework for nonlinear instability analysis.

It is more informative to use the flame describing function

$$u'/\overline{U} \longrightarrow \boxed{\text{Combustion}} \longrightarrow \dot{Q}'/\overline{\dot{Q}}$$

$$\mathcal{F}(\omega, u') = \frac{\dot{Q}'/\overline{\dot{Q}}}{u'/\overline{U}}$$

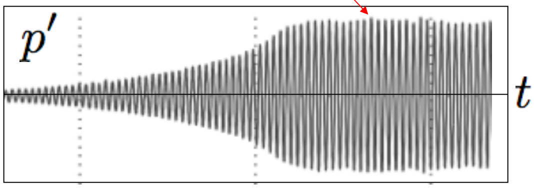

The Flame Describing Function (FDF) extends the transfer function concept to the nonlinear case

In the FDF the flame response depends on the frequency and amplitude of the incident perturbation

$u'/\overline{U}$ → **Combustion** → $\dot{Q}'/\overline{\dot{Q}}$

The flame response may be characterized in terms of a transfer function

$$\mathcal{F}(\omega) = \frac{\dot{Q}'/\overline{\dot{Q}}}{u'/\overline{U}}$$

The flame response may be characterized by a describing function. The transfer functions depend on the input level

$$\mathcal{F}(\omega, u') = \frac{\dot{Q}/\overline{Q}}{u'/\overline{u}}$$

The flame transfer function (FTF) only provides the linear growth rate

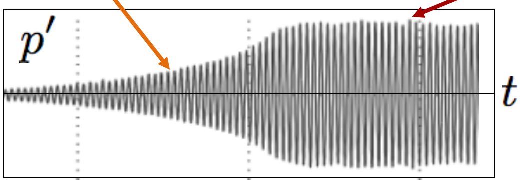

The flame describing function (FDF) gives access to the nonlinear growth rates. It can be used to determine limit cycle amplitudes and nonlinear features like mode switching, triggering and hysteresis

Nonlinear dynamics and flame describing function concepts

A framework for nonlinear instability analysis

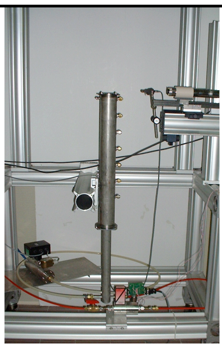

Perforated plate

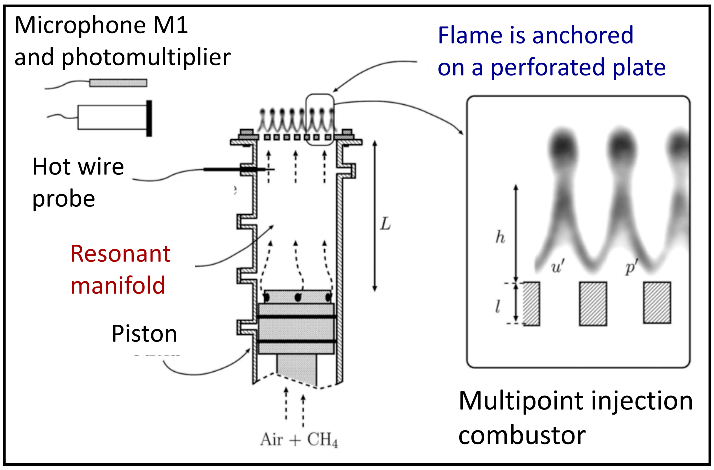

Equivalence ratio : $\Phi = 0.86$
Volumetric flow rate : $\dot{m} = 5.4\,10^{-3}\,\mathrm{kg\ s}^{-1}$
Thermal power : 14.4 kW

- Diameter D : 70 mm
- Depth L easily adjustable : from 90 to 750 mm
- Unconfined reaction layer

7

Combustion regimes

Depending on the burner depth L combustion is either **stable** or **unstable**.

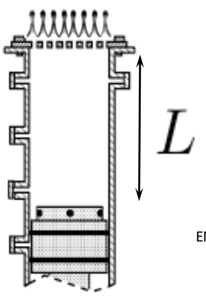

EM2C,CNRS,ECP

N. Noiray, D. Durox, T. Schuller and S. Candel (2008) *Journal of Fluid Mechanics* 615, 139-167. A unified framework for nonlinear combustion instability analysis based on the describing function.

N. Noiray, D. Durox, T. Schuller and S. Candel (2009) *International Journal of Aeroacoustics*. 8, 157-176. A method for estimating the noise level of unstable combustion based on the flame describing function.

8

Flames dynamics

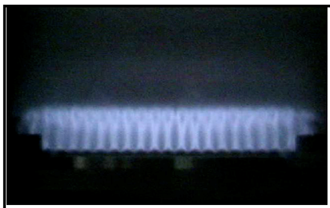

EM2C,CNRS,ECP

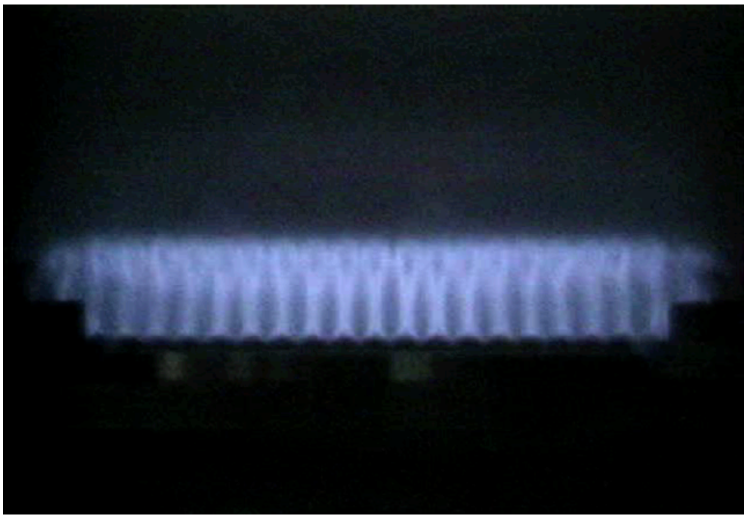

Oscillation cycle (f=530 Hz) in a typical unstable situation (high amplitude sound radiation > 110 dB at 40 cm from the burner)

Typical self-sustained oscillations

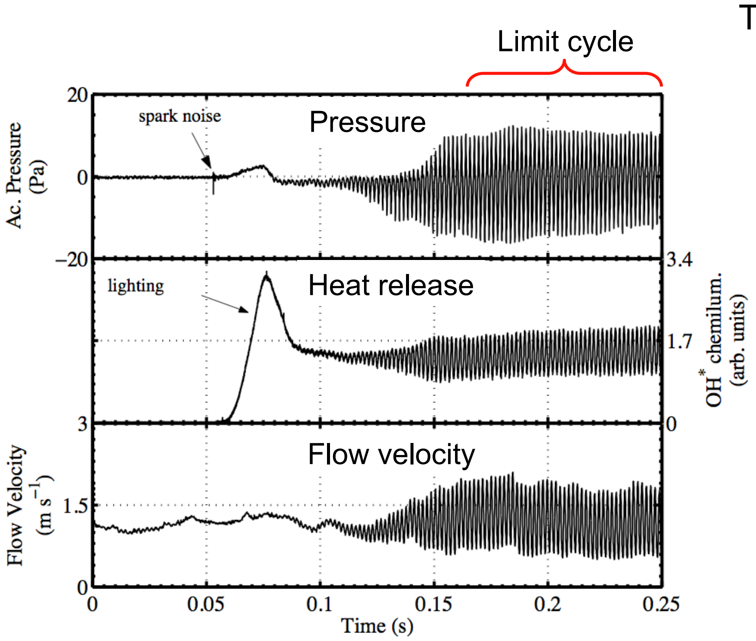

$L = 460\,\mathrm{mm}$

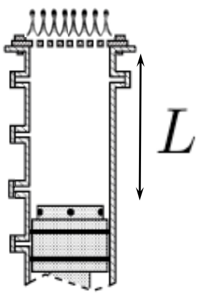

Prediction of limit cycle amplitude constitutes a central challenge

Henri Poincaré

Driving and coupling leading to self-sustained oscillations

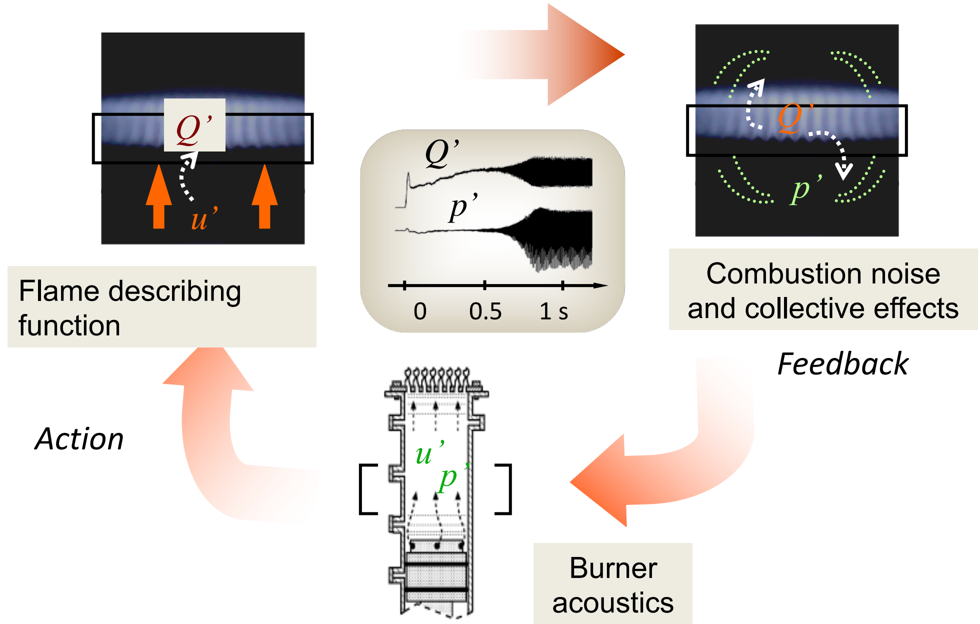

Nonlinear flame response

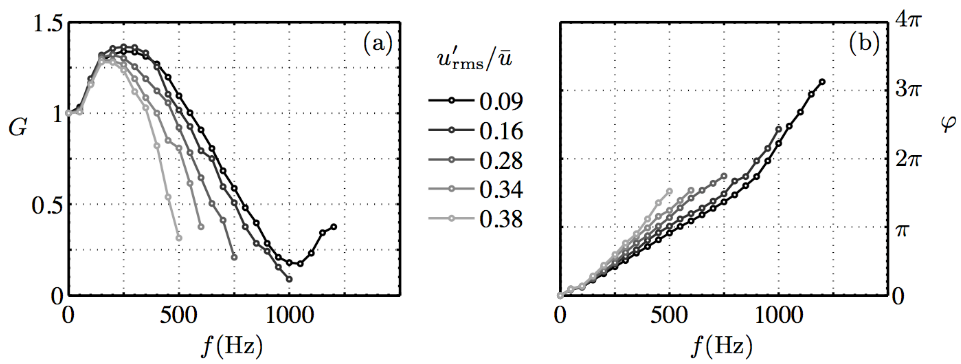

The flame response can be characterized in terms of a describing function

$$\mathcal{F}(\omega, u') = \frac{\dot{Q}/\overline{Q}}{u'/\overline{u}} = \frac{\text{Relative heat release fluctuation}}{\text{Relative velocity fluctuation}}$$

$$\boxed{\mathcal{F}\left(\omega_r, |u'|\right) = G\left(\omega_r, |u'|\right) \mathrm{e}^{i\varphi\left(\omega_r, |u'|\right)}}$$

Flame Describing Function

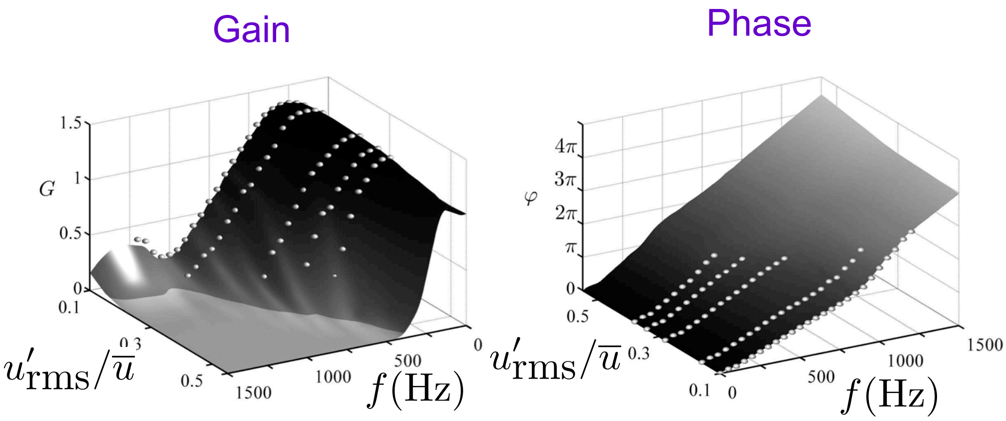

$$\boxed{\mathcal{F}\left(\omega_r, |u'|\right) = G\left(\omega_r, |u'|\right) \mathrm{e}^{i\varphi\left(\omega_r, |u'|\right)}}$$

$$p = p_\omega \exp(-i\omega t)$$
$$\omega = \omega_r + i\omega_i$$
$$p = p_\omega \exp(-i\omega_r t)\exp(\omega_i t)$$

$\omega_r = 2\pi f$ ω_i

Angular frequency Growth rate

The system is unstable if $\boxed{\omega_i > 0}$

The complex roots of the dispersion relation

$$\mathcal{H}(\omega) = 0$$

characterize the stability of the system

$$p = p_\omega \exp(-i\omega t) \quad \omega = \omega_r + i\omega_i$$

System is unstable when $\omega_i > 0$

$$\mathcal{F}(\omega, u') = \frac{\dot{Q}/\overline{Q}}{u'/\overline{u}}$$

FDF: Flame transfer function depends on input level

$$\mathcal{H}(\omega, u') = 0$$

Dispersion relation depends on amplitude

$$\omega_i = \omega_i(u'/\overline{u})$$

Growth rate becomes a function of amplitude

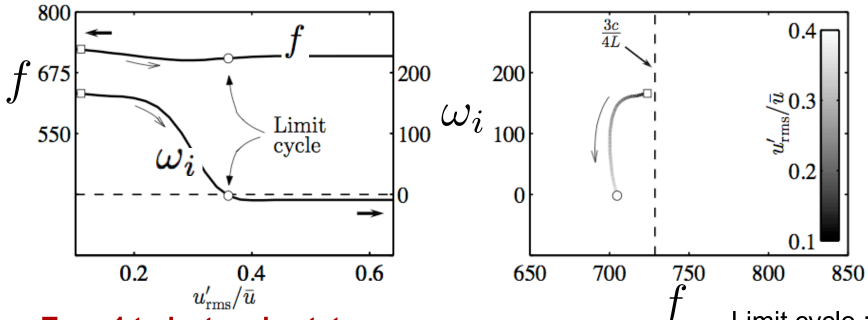

$L = 35$ cm mode 2

3/4 wave

Type 1 trajectory in state space

Limit cycle : $\omega_i = 0$

Positive growth rate indicates that small perturbations are amplified
The limit cycle is obtained when the growth rate vanishes (negligible damping) or when the growth rate equals the damping rate (finite damping)

$$p = p_\omega \exp(-i\omega t) \quad \omega = \omega_r + i\omega_i$$

System is unstable when $\omega_i > 0$

$$\mathcal{F}(\omega, u') = \frac{\dot{Q}/\overline{Q}}{u'/\overline{u}}$$

FDF: Flame transfer function depends on input level

$$\mathcal{H}(\omega, u') = 0$$

Dispersion relation depends on amplitude

$$\omega_i = \omega_i(u'/\overline{u})$$

Growth rate becomes a function of amplitude

Type 2 trajectory in state-space

When the perturbation level exceeds a certain amplitude threshold the growth rate become positive ((perturbations are amplified)

1/4 wave

$L = 20$ cm mode 1

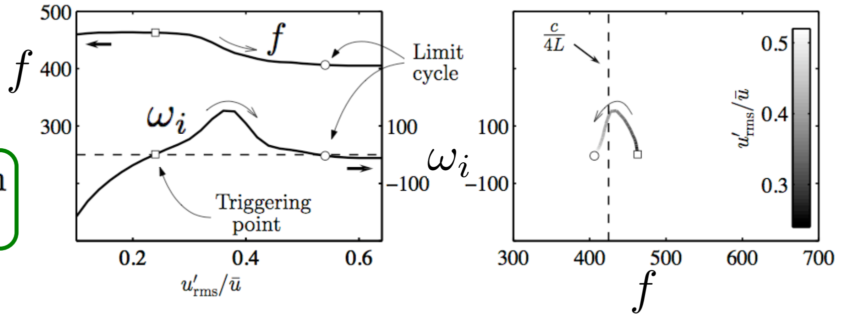

Positive growth rate contours in a « burner depth - velocity fluctuations amplitude » diagram

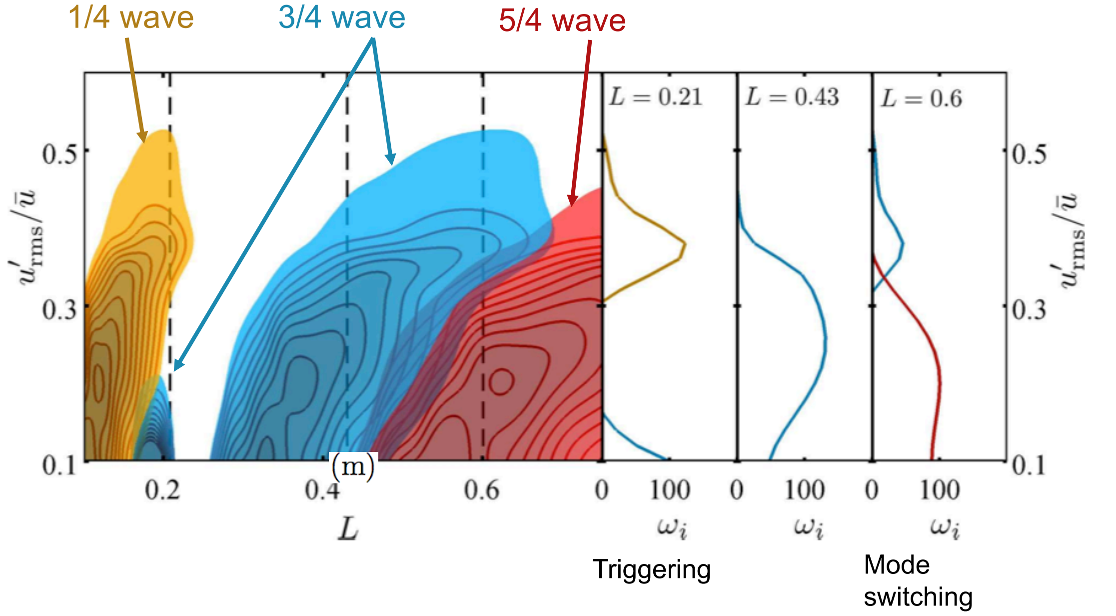

17

Frequency shift during growth of oscillation

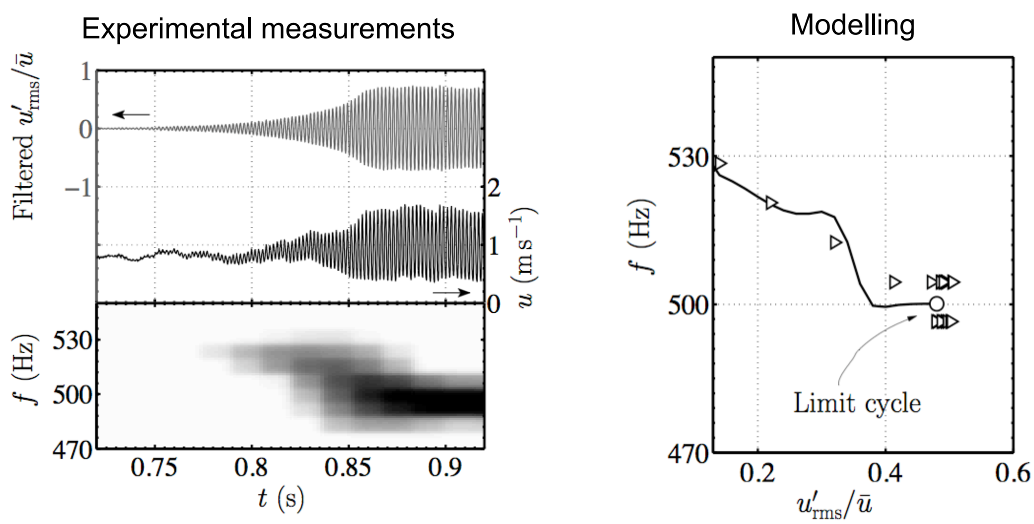

Suitable estimation of the limit cycle amplitude and of the frequency shift during the growth of oscillation

Prediction of the limit cycle amplitudes and of hysteresis

Cavity size L progressively increased

Cavity size L progressively decreased

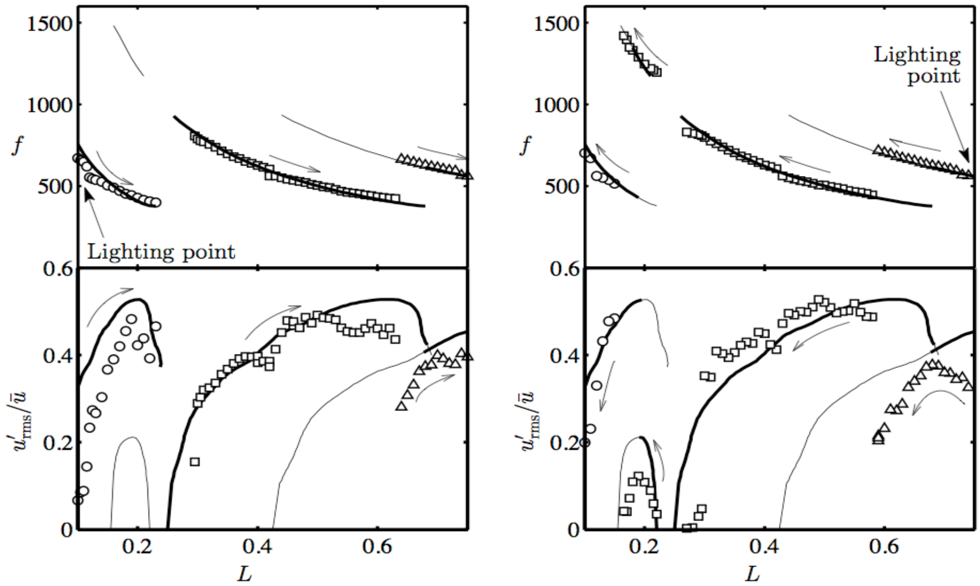

Prediction of mode switching after a large amplitude perturbation

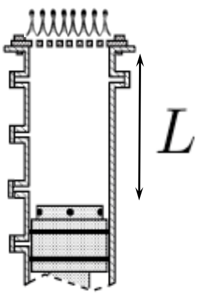

Mode switching takes place when combustion is perturbed by blowing the flame collection with a lateral air blowing

Extension to generic configurations

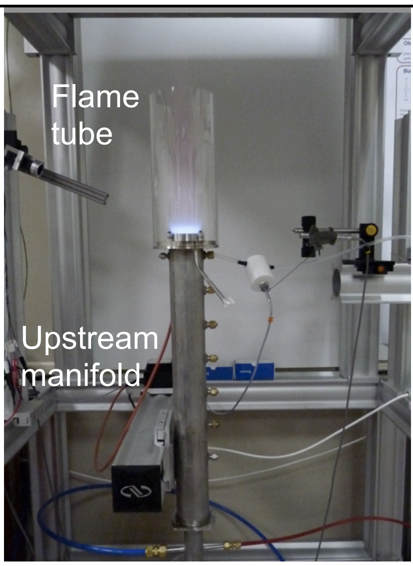

General view of combustion system

Side view of flame collection

F. Boudy, D. Durox, T. Schuller, G. Jomaas and S. Candel (2010) Describing function analysis of limit cycle in a multiple flame combustor. Paper ASME GT2010-22372. *J. of Eng. for gas turbine and power.* 33, June 2011.

F. Boudy, D. Durox, T. Schuller, and S. Candel (2011) *Proceedings of the Combustion Institute* 33. 1121-1128. Nonlinear mode triggering in a multiple flame combustor

21

Combustion dynamics Lecture 6b

S. Candel, D. Durox , T. Schuller

CentraleSupélec
Université Paris-Saclay, EM2C lab, CNRS

Tsinghua summer school, July 2021

Combustion instabilities prediction : recent progress based on Flame Describing Function

Frédéric Boudy, Daniel Durox,
Thierry Schuller and Sébastien Candel

EM2C Laboratory, CNRS and Ecole Centrale Paris,

Feedback resonant loop

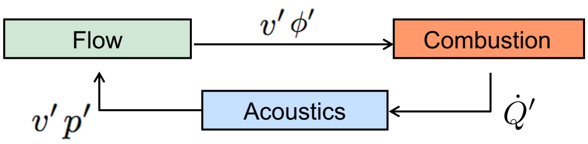

Acoustics

Culick *et al.* (2001) Proceedings RTO/VKI

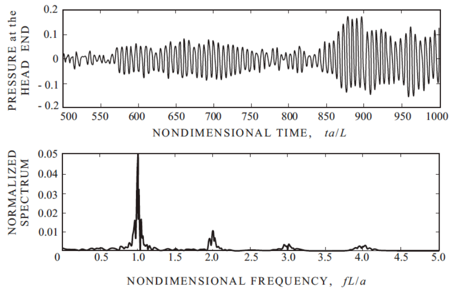

$$p'(x,t) = \bar{p}\sum_{i=1}^{\infty} \eta_n(t)\psi_n(x)$$

Combustion dynamics

Candel *et al.* (1996) In « Unsteady combustion »

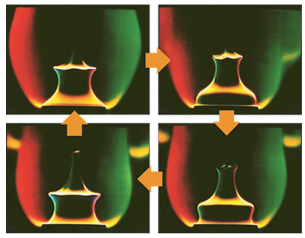

Schlieren images of a conical flame subjected to acoustic modulation

$$\mathcal{F} = \frac{\dot{Q}'/\overline{\dot{Q}}}{u'/\bar{u}} = Ge^{i\omega\tau}$$

3

Many experiments concerning thermoacoustic instabilities indicate that the main nonlinearity results from the flame oscillation

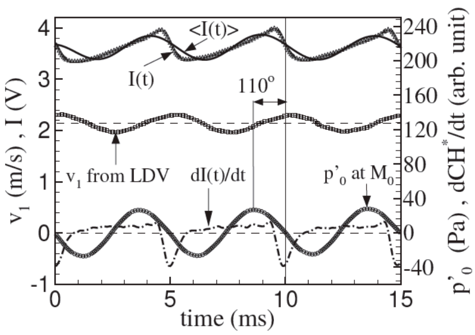

Nonlinear flame

$$\dot{Q}' \big/ \overline{\dot{Q}} \approx \mathcal{O}(1)$$

Linear acoustic

$$p'/p_{mean} \approx \mathcal{O}(0.01)$$

Linear treatment of acoustic with wave equation

$$\nabla^2 p' - \frac{1}{\bar{c}^2}\frac{\partial^2 p'}{\partial t^2} = 0$$

Need of nonlinear treatment of flame / flow interaction

$$\mathcal{F}(\omega, |u'|) = \frac{\dot{Q}' \big/ \overline{\dot{Q}}}{u'/\bar{u}}$$

4

Objectives

(1) Provide modeling elements to assess thermoacoustic instabilities

(2) Develop a nonlinear stability analysis based on the Flame Describing Function, a nonlinear extension of Flame Transfer Function concepts

(3) Show how to anticipate several nonlinear phenomena often observed in combustors

(4) Analyze limitations of the FDF framework

Outline

1. Experimental configuration
2. Linear stability analysis with Flame Transfer Function (FTF)
3. Nonlinear analysis with Flame Describing Function (FDF)
4. Nonlinear modeling results
1. Current issues using FDF framework
2. Conclusions

Experimental setup

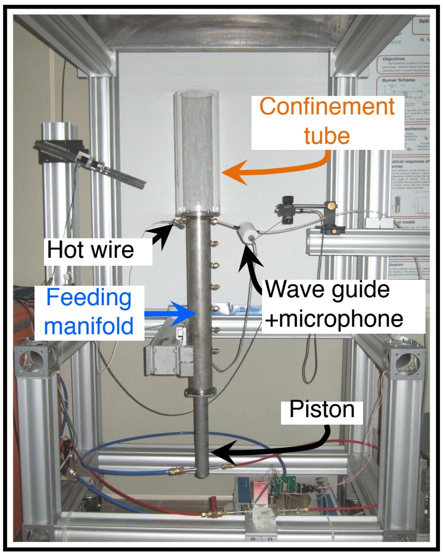

Burner schematic

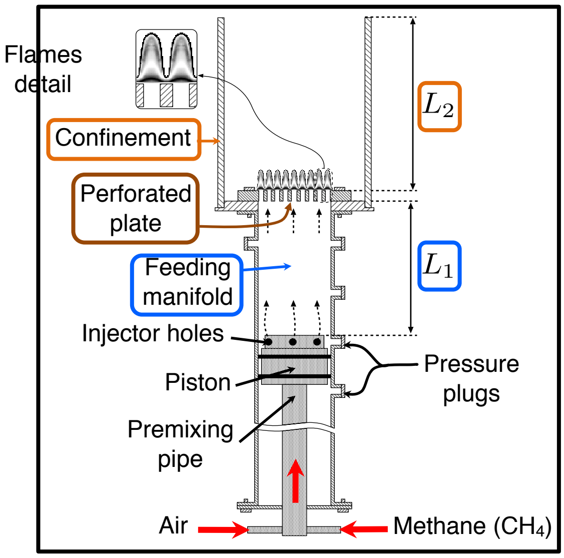

Flexible configuration offering possibilities to analyze combustion instabilities with and without confinement tube

Close-up views of the burner

Piston and feeding manifold

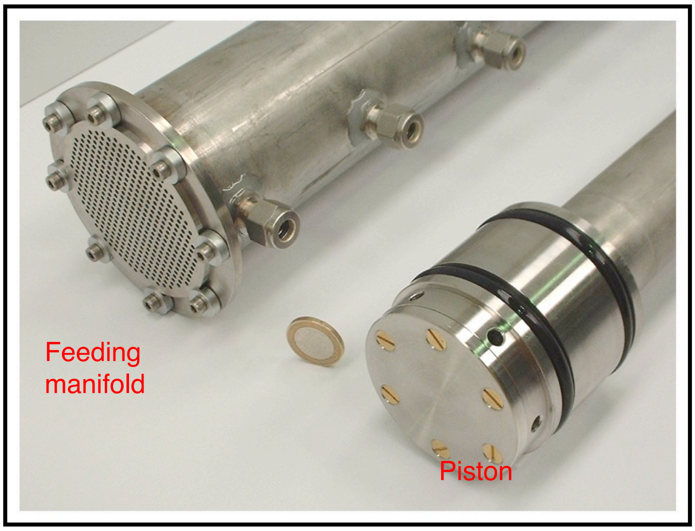

Perforated plate
420 holes of ID 2 mm OR
189 holes of ID 3 mm

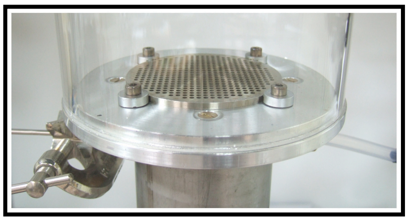

Top view

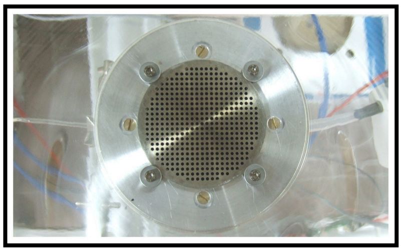

7

Typical transition to self-sustained oscillation

For a given flow operating condition, stability depends on the feeding manifold L_1 and flame confinement L_2 lengths

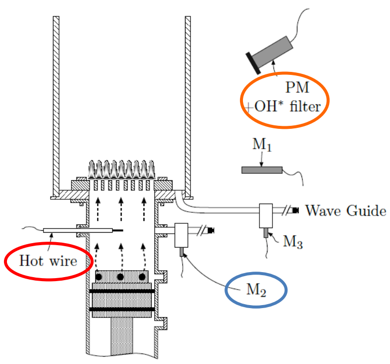

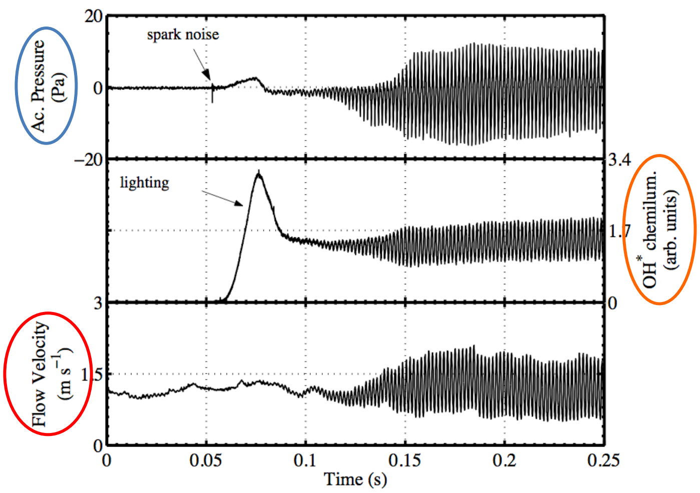

During unstable operation, after ignition and transient growth, oscillations of flow variables reach a limit cycle

8

Typical flame oscillations

Stable regime

Feeding manifold (L_1) 0.25 m
Confinement tube (L_2) 0.1 m

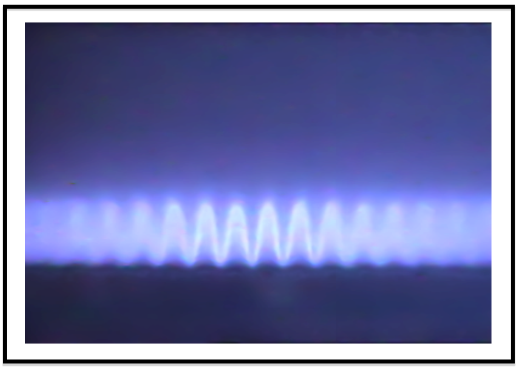

No flame motion SPL = 80 dB

Unstable regime

Feeding manifold (L_1) 0.29 m
Confinement tube (L_2) 0.1 m

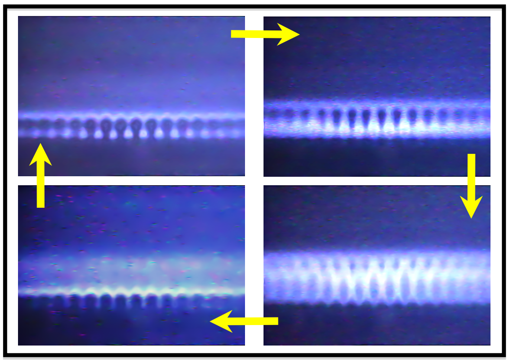

Example of stable and unstable regimes

Exploration as a function of feeding manifold length L_1

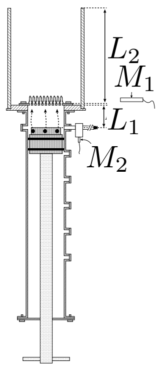

Frequencies and pressure inside the feeding manifold

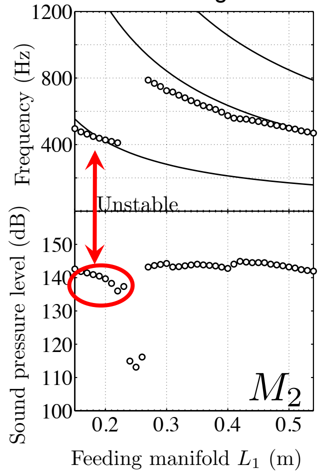

Air-Methane mixture
Confinement 10 cm
ϕ = 1.03

Pressure outside the confinement tube

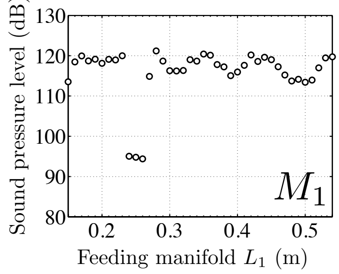

The oscillation frequencies at limit cycles lie close to, but do not always match, the eigenmodes of the combustor

Exploration as a function of feeding manifold length L_1

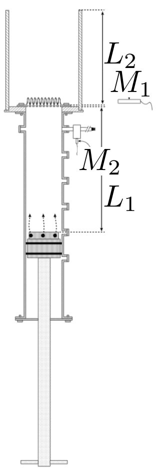

Frequencies and pressure inside the feeding manifold

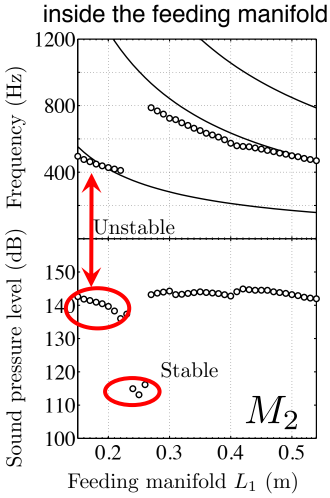

Air-Methane mixture
Confinement 10 cm
ϕ = 1.03

Pressure outside the confinement tube

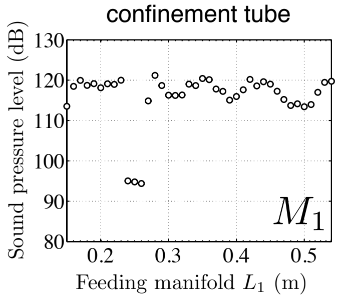

The oscillation frequencies at limit cycles lie close to, but do not always match, the eigenmodes of the combustor

Exploration as a function of feeding manifold length L_1

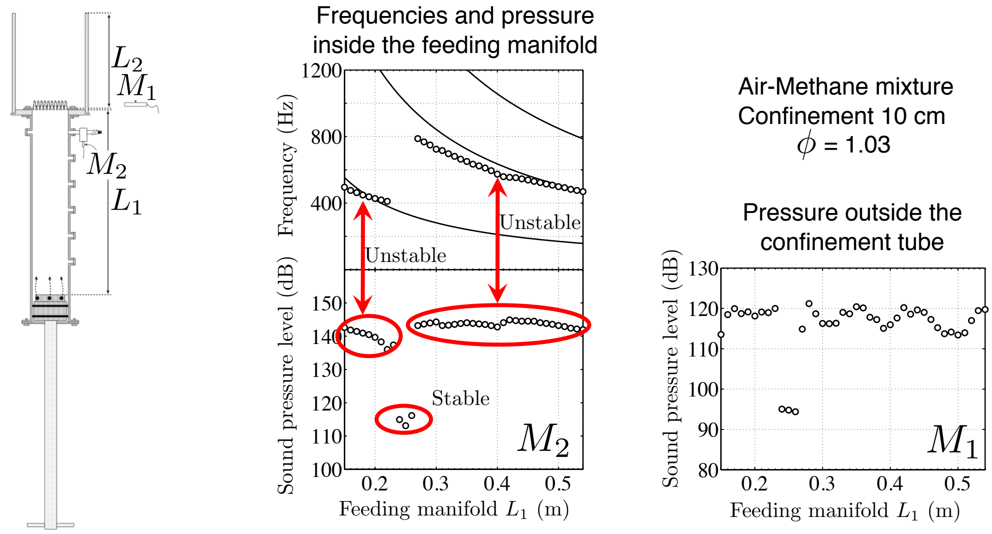

The oscillation frequencies at limit cycles lie close to, but do not always match, the eigenmodes of the combustor

Self-sustained instabilities for different confinement tubes L_2

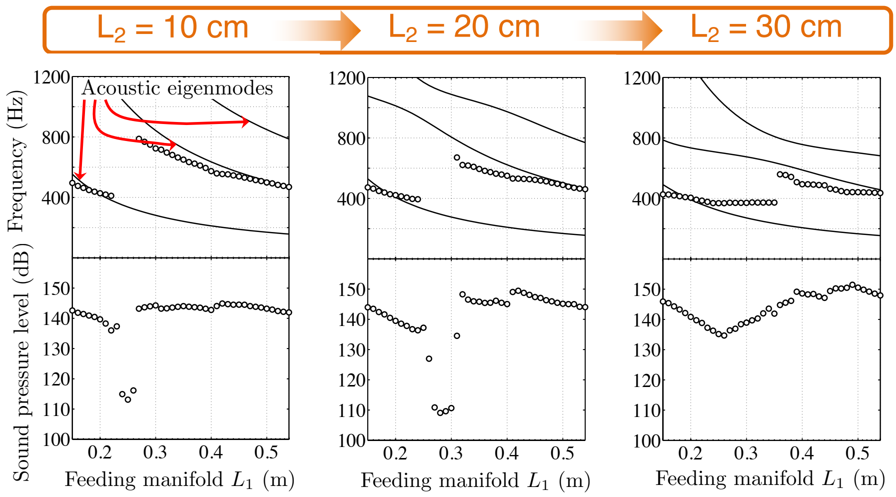

Bands of instabilities also depend on flame confinement. The system with the long confinement tube is always unstable. Larger deviations of limit cycle oscillation frequency from acoustic modes are observed for increased confinement tube lengths

Outline

1. Experimental configuration
2. Linear stability analysis with Flame Transfer Function (FTF)
3. Nonlinear analysis with Flame Describing Function (FDF)
4. Nonlinear modeling results
1. Current issues using FDF framework
2. Conclusions

Different modeling approaches

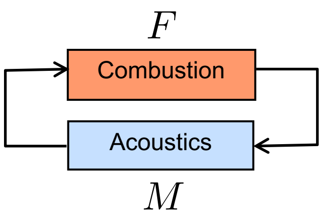

$$M(\omega)X = F$$

A B C

Acoustic Analysis	Linear Stability analysis	Nonlinear stability analysis
No unsteady flame $F = 0$	Flame Transfer Function (FTF) $F = F(\omega)$	Flame Describing Function $F = F(\omega, \lvert u' \rvert)$
Acoustic modes and modal structure	Initial oscillation frequency and exponential growth	Instability frequencies and growth rate evolution
No information on unstable modes	No information at limit cycle, limited to the prediction of linearly unstable modes	Limit cycle amplitude, frequency shift, hysteresis, mode switching, triggering

A – Acoustic analysis : $M(\omega)X = 0$

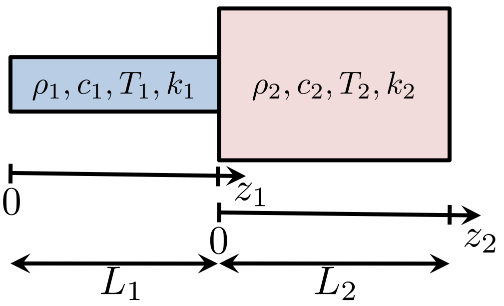

+

Boundary and matching conditions

$$u'_{1,0} = 0$$
$$p'_{2,L_2} = 0$$

$$S_2 u'_{2,0} = S_1 u'_{1,L_1}$$
$$p'_{2,0} = p'_{1,L_1}$$

$$\underbrace{\begin{pmatrix} 1 & -1 & 0 & 0 \\ 0 & 0 & e^{ik_2L_2} & e^{-ik_2L_2} \\ e^{ik_1L_1} & e^{-ik_1L_1} & -1 & -1 \\ \frac{S_1}{\rho_1 c_1} e^{ik_1L_1} & -\frac{S_1}{\rho_1 c_1} e^{-ik_1L_1} & -\frac{S_2}{\rho_2 c_2} & \frac{S_2}{\rho_2 c_2} \end{pmatrix}}_{\text{M}} \underbrace{\begin{pmatrix} A_1^+ \\ A_1^- \\ A_2^+ \\ A_2^- \end{pmatrix}}_{X} = \begin{pmatrix} 0 \\ 0 \\ 0 \\ 0 \end{pmatrix}$$

Solution : $X = X_0 \exp(-i\omega t)$ ω is a real number $\omega = 2\pi f$

Comparison between predictions and measurements

Frequencies measured at limit cycles are compared to the eigenmodes solutions of $det(M) = 0$

Confinement 10 cm ϕ= 1.03

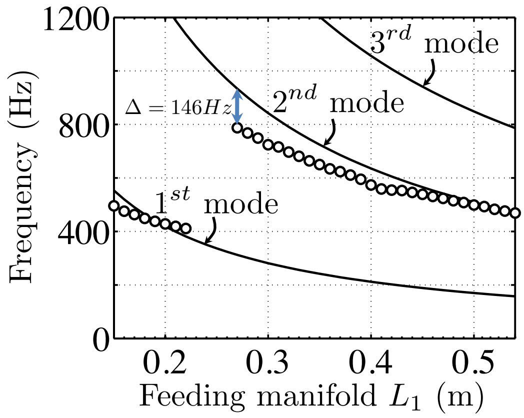

Limit cycle frequencies lie close but are shifted with respect to the acoustic predicted modes

The stable band between L_1=0.23 and 0.26 m is not predicted

Switch between the different acoustic mode remains unexplained

B - Linear stability analysis : $M(\omega)X = F(\omega)$

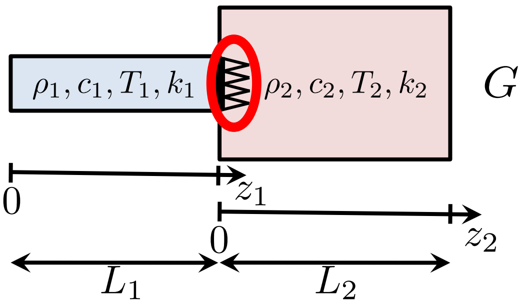

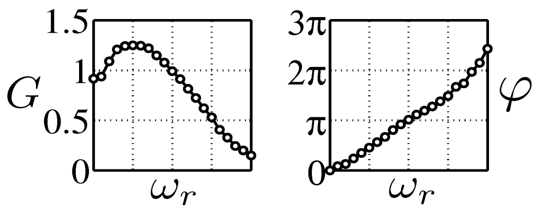

Flame Transfer Function (FTF)

$$\boxed{\mathcal{F}(\omega) = \frac{\dot{Q}'/\bar{\dot{Q}}}{u'/\bar{u}} = G(\omega_r)e^{i\varphi(\omega_r)}}$$

Solution : $X = X_0 \exp(-i\omega t)$

ω is now a complex number

$\omega = \omega_r + i\omega_i$

$\omega_r = 2\pi f$: Angular oscillation frequency

ω_i Growth rate : instability when $\omega_i > 0$

FTF determination

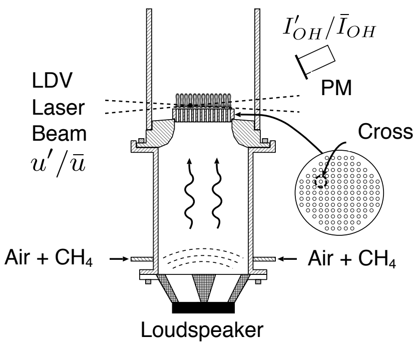

$$\mathcal{F} = \frac{I'_{OH}/\bar{I}_{OH}}{u'/\bar{u}} \simeq \frac{\dot{Q}'/\bar{\dot{Q}}}{u'/\bar{u}}$$

Instability bands are determined by the phase of the FTF $\omega_i > 0$

$\pi < \varphi < 2\pi$ modulo 2π

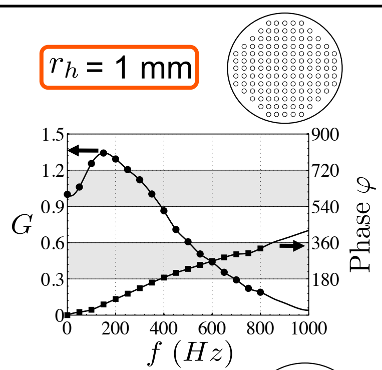

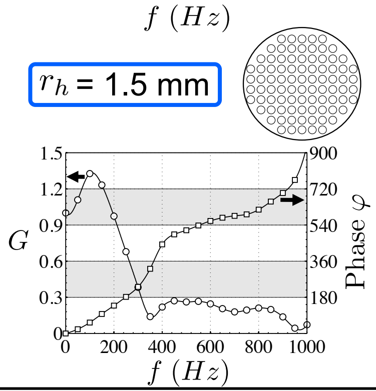

Comparison between predictions with FTF and measurements

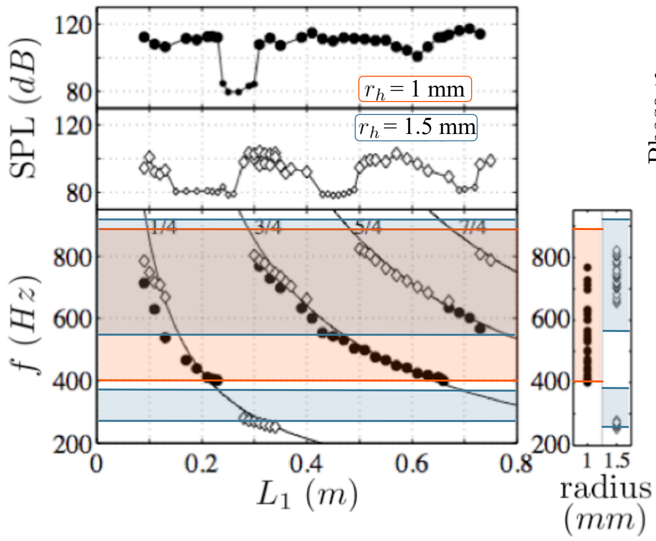

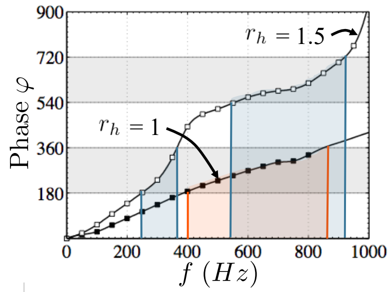

Oscillation frequencies at limit cycle (almost) lie within instability bands

Amplitudes of oscillation remain unknown

Outline

1. Experimental configuration
2. Linear stability analysis with Flame Transfer Function (FTF)
3. Nonlinear analysis with Flame Describing Function (FDF)
4. Nonlinear modeling results
1. Current issues using FDF framework
2. Conclusions

C - Nonlinear stability analysis : $M(\omega)X = F(\omega, |u'|)$

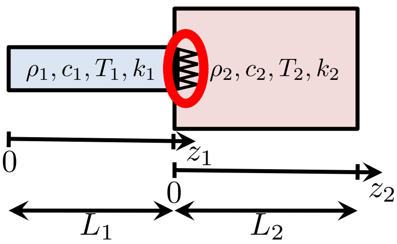

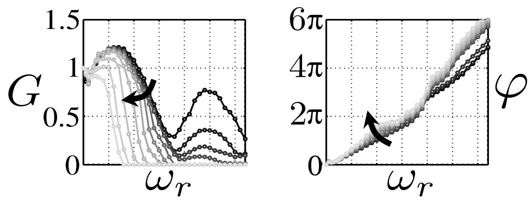

Flame Describing Function (FDF)

$$\mathcal{F}(\omega, |u'|) = \frac{\dot{Q}'/\dot{\bar{Q}}}{u'/\bar{u}} = G(\omega_r, |u'|)e^{i\varphi(\omega_r, |u'|)}$$

Solution : $X = X_0 \exp(-i\omega t)$

$\omega = \omega_r + i\omega_i$

ω is a complex number that depends on the input level

$\omega_r = \omega_r(|u'|)$: Angular oscillation frequency

$\omega_i = \omega_i(|u'|)$: Growth rate : instability when $\omega_i > 0$

23

Nonlinear stability analyses

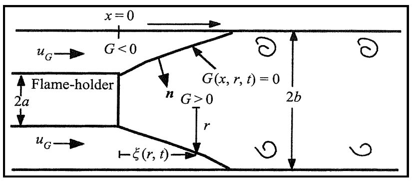

Dowling (1999) JFM 394

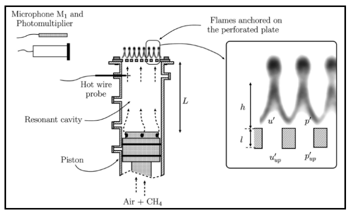

Noiray *et al.* (2008) JFM 615

Describing Function (DF) has been used to account for the nonlinear saturation associated with flashback.

Nonlinear Gain
Linear Phase

Possibility to determine limit cycle levels. The method is limited to linearly unstable modes

The Flame Describing Function has been devised to include the nonlinear dependance of the phase lag

Nonlinear Gain
Nonlinear Phase

Possibility to determine limit cycle levels. The method encompasses linearly unstable modes and nonlinearly unstable modes

24

FDF determination

FTF

$$u' \longrightarrow \boxed{\mathcal{F}(\omega_r)} \longrightarrow \dot{Q}'$$

The FTF is determined for a single input level

FDF

$$u' \longrightarrow \boxed{\mathcal{F}(\omega_r, |u'|)} \longrightarrow \dot{Q}'$$

The FDF is determined by a set of FTF measured for increasing input levels

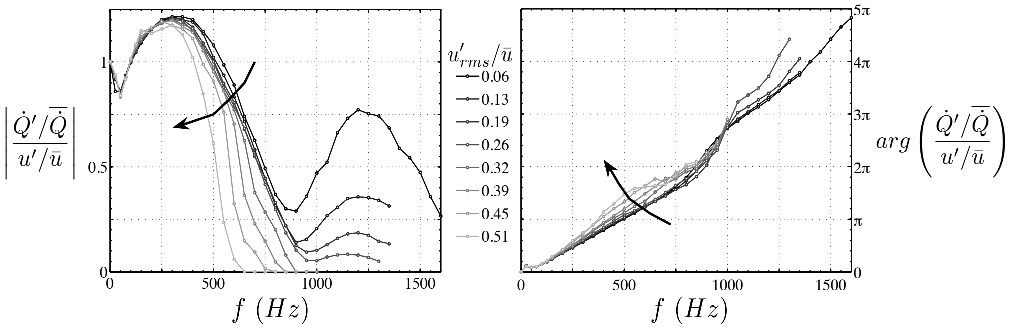

Outline

1. Experimental configuration
2. Linear stability analysis with Flame Transfer Function (FTF)
3. Nonlinear analysis with Flame Describing Function (FDF)
4. Nonlinear modeling results
1. Current issues using FDF framework
2. Conclusions

Use of FDF for stability analysis

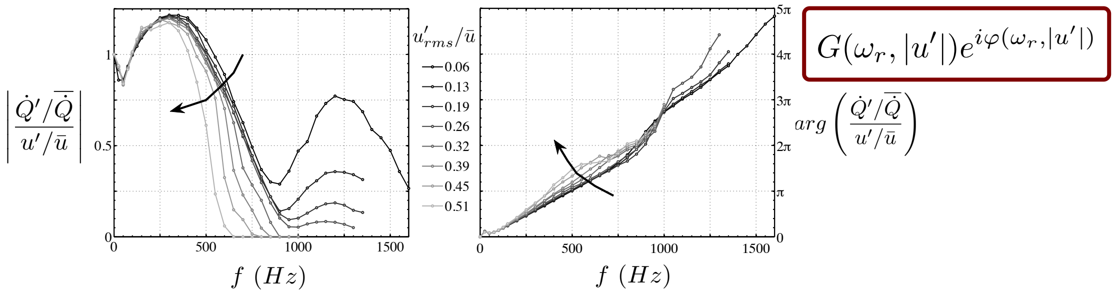

Growth rates are calculated separetly for the 3 modes using the following procedure

$$\underset{F=0}{\boxed{\omega(|u'|=0)}} \rightarrow \underset{F=F(\omega_r,|u'_1|)}{\boxed{\omega(|u'_1|)}} \rightarrow \underset{F=F(\omega_r,|u'_2|)}{\boxed{\omega(|u'_2|)}} \dashrightarrow \underset{F=F(\omega_r,|u'_n|)}{\boxed{\omega(|u'_n|)}}$$

These growth rates and frequencies depend on the fluctuation amplitude :

$$\omega_r = \omega_r(u'/\bar{u})$$
$$\omega_i = \omega_i(u'/\bar{u})$$

This procedure is repeated for each length L_1 of the feeding manifold

27

Stability analysis for mode 1 : Analysis of a linearly unstable mode

Growth rates $\omega_i=\omega_i(|u'|,L_1)$ are calculated for the first eigenmode of the combustor

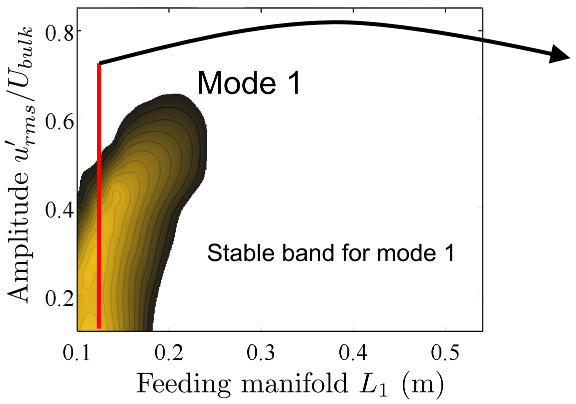

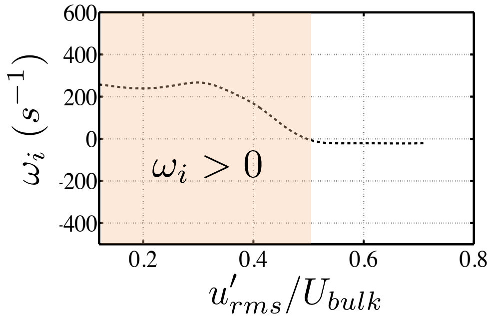

Limit cycle is reached when ω_i equals zero. The method yields the limit cycle oscillation level and oscillation frequency.

Regions where ω_i is negative are linearly stable

Linearly unstable mode : Positive growth rate for infinitesimally small amplitude

28

Stability analysis for mode 1 : Analysis of a nonlinearly unstable mode

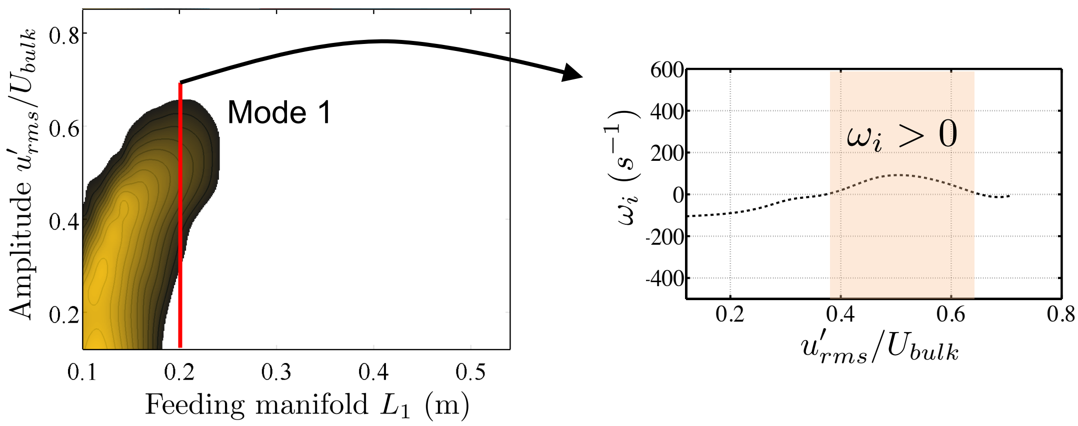

Nonlinearly unstable mode : Negative growth rate for small perturbation amplitudes, but positive values above a certain threshold.
Limit cycle is reached when $\omega_i = 0$

Stability analysis for mode 2 and 3

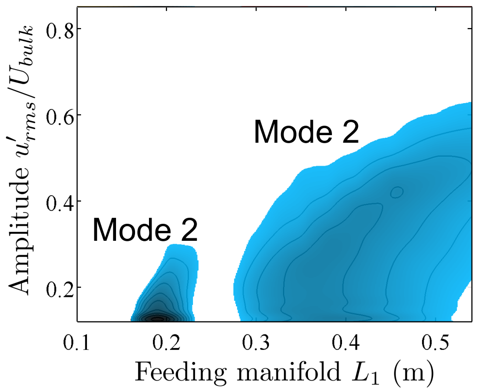

Mode 2 is linearly unstable for most of the feeding manifold lengths

Mode 3 is linearly unstable for most of the feeding manifold lengths

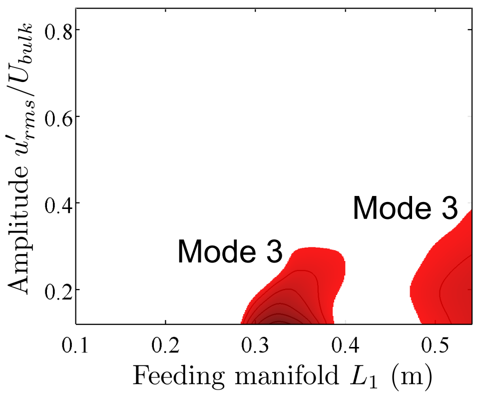

Bifurcation diagram

Obtained by superposition of instability bands calculated for each mode separately

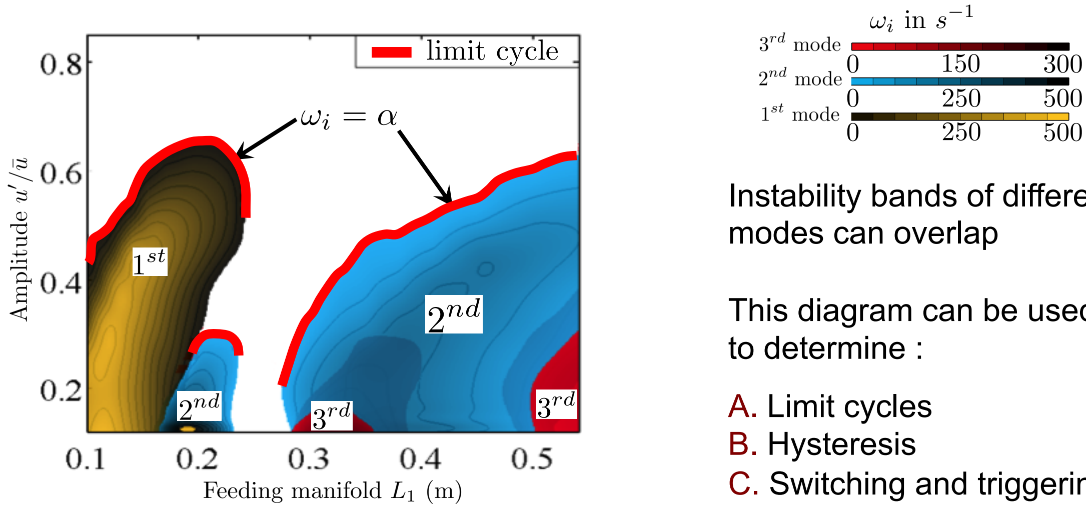

Instability bands of different modes can overlap

This diagram can be used to determine :

A. Limit cycles
B. Hysteresis
C. Switching and triggering

Limit cycle (A) and hysteresis (B) predictions

L_1=0.15 m ⟶ L_1=0.54 m

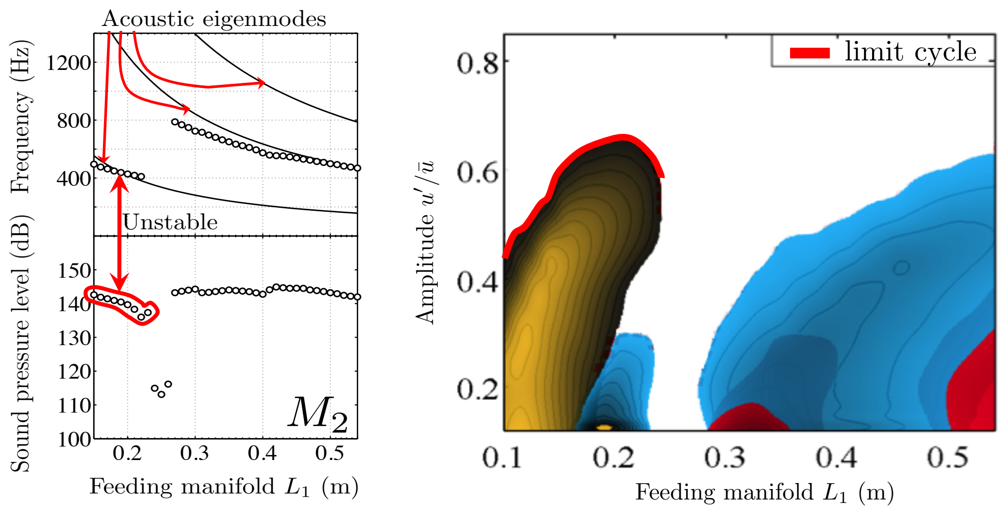

Limit cycle (A) and hysteresis (B) predictions

L_1=0.15 m → L_1=0.54 m

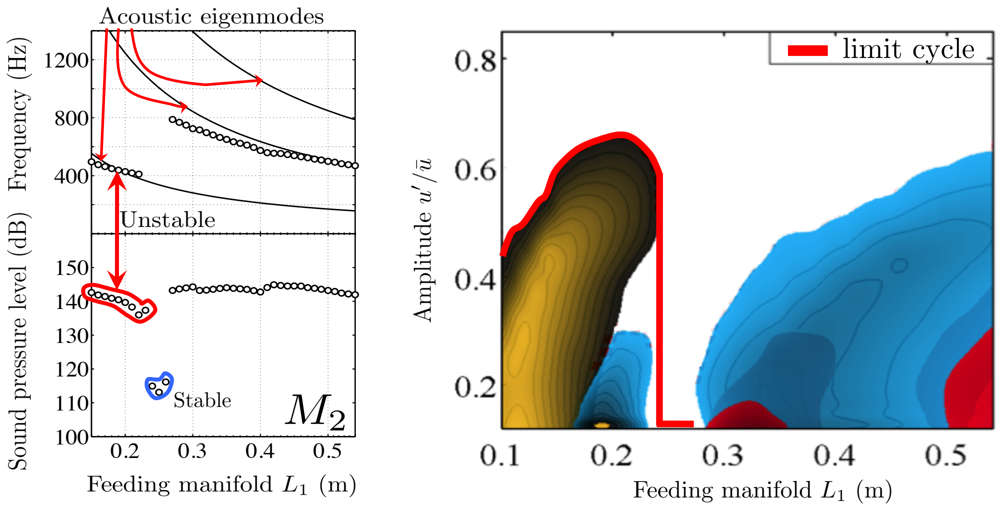

33

Limit cycle (A) and hysteresis (B) predictions

L_1=0.15 m → L_1=0.54 m

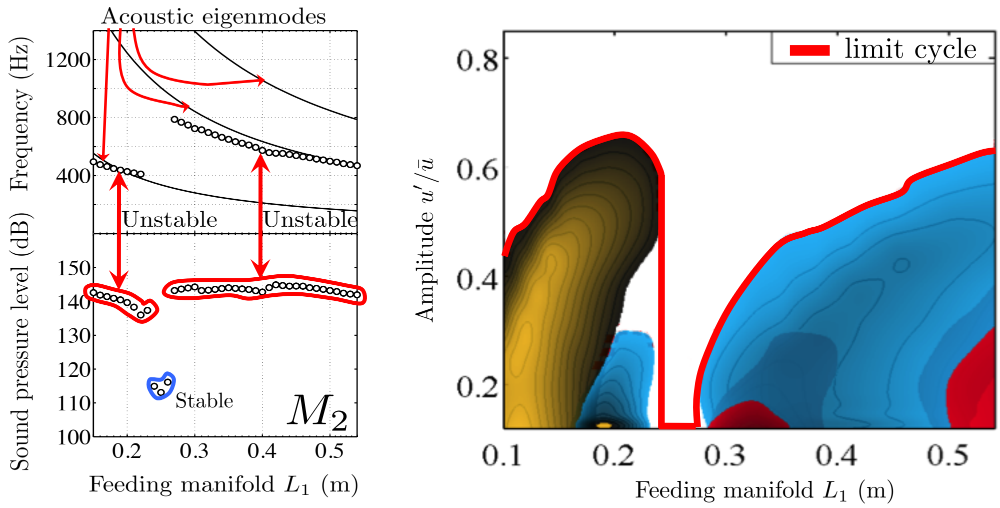

34

Limit cycle (A) and hysteresis (B) predictions

L_1=0.54 m → L_1=0.15 m

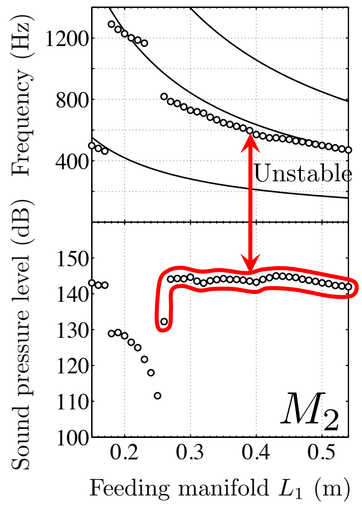

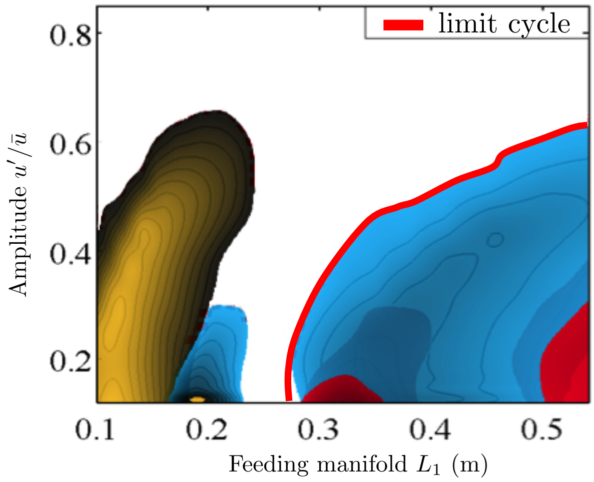

35

Limit cycle (A) and hysteresis (B) predictions

L_1=0.54 m → L_1=0.15 m

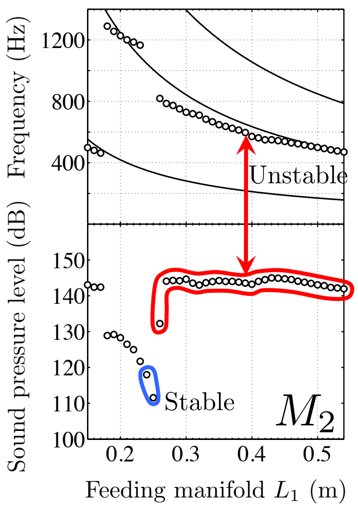

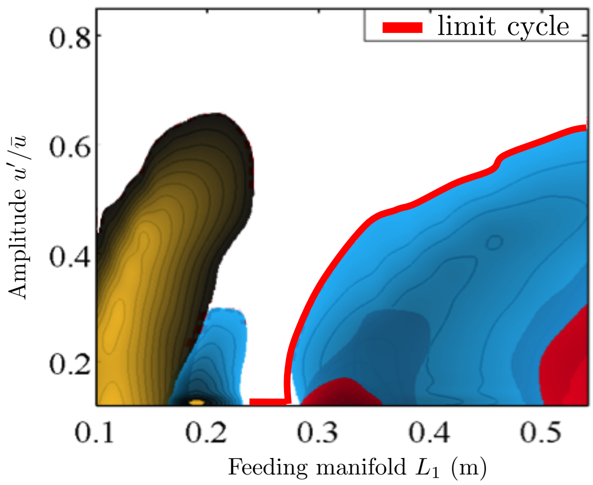

36

Limit cycle (A) and hysteresis (B) predictions

L_1=0.54 m → L_1=0.15 m

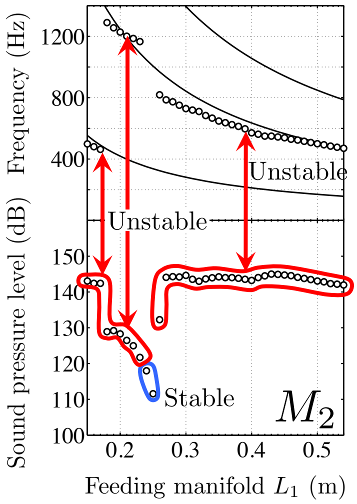

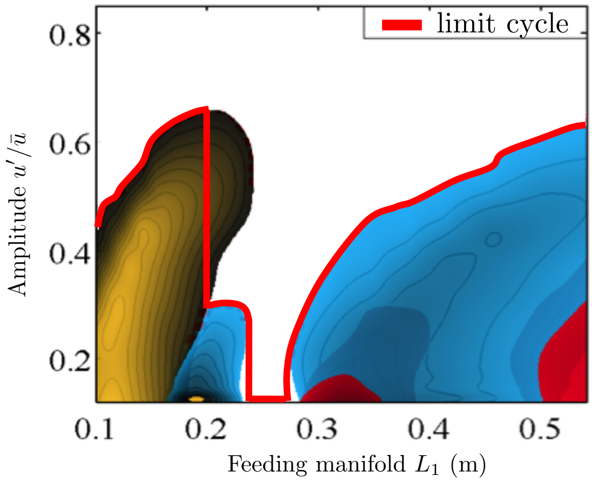

C. Analysis of mode switching and triggering

Mode switching

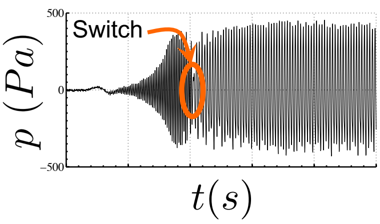

Change of frequency and oscillation level in the absence of external perturbation

Mode triggering

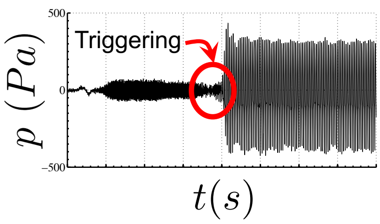

Change of frequency and oscillation level due to an external perturbation of finite amplitude

This problem is often evoked, Wicker et al. (1996), Dowling (1997), Culick (2001), Lieuwen et al. (2002), Lieuwen (2003), Stow et al. (2004).

It is shown here that these phenomena can be explained within the Flame Describing Function (FDF) framework.

Analysis of mode triggering

The system is set where mode 2 is linearly unstable and mode 1 nonlinearly unstable

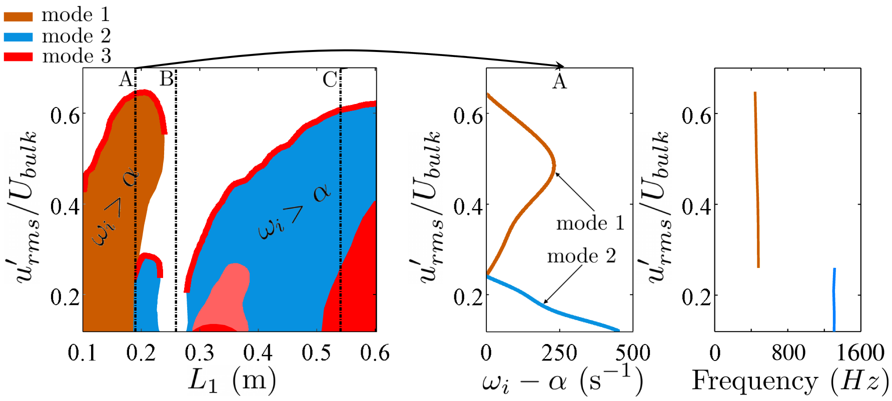

A : Unstable – 2 limit cycles

B : Stable – No limit cycle

C : Unstable – 1 limit cycle

In this case, the limit cycle level reached by mode 2 is close but lower than the threshold level to trigger mode 1 : use of an external perturbation is needed.

Boudy *et al.* (2011) Proc. Comb. Inst. 33

39

Mode triggering

FDF calculation prediction

Switch 2nd (1313 Hz) → 1st (447 Hz)

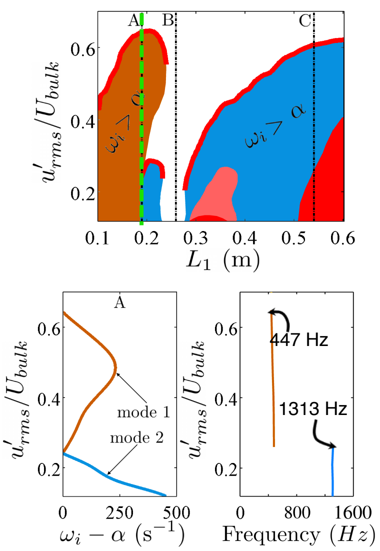

Experiment

Triggering assisted with an external pulse

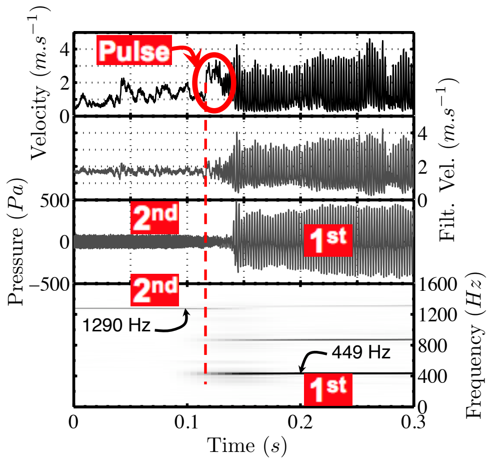

40

Analysis of mode switching

The system is set where mode 3 is linearly unstable and mode 2 nonlinearly unstable

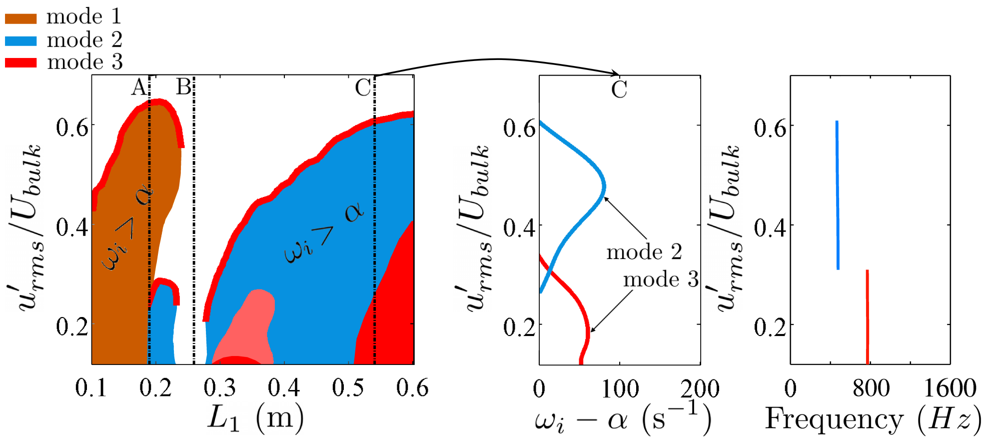

A : Unstable – 2 limit cycles
B : Stable – No limit cycle
C : Unstable – 1 limit cycle

In this case, the limit cycle level reached by mode 3 is close but sligthly higher than the threshold level to trigger mode 2 : the system naturally switches to mode 2.

41

Natural mode switching

FDF calculation prediction

Switch 3rd (769 Hz) → 2nd (465 Hz)

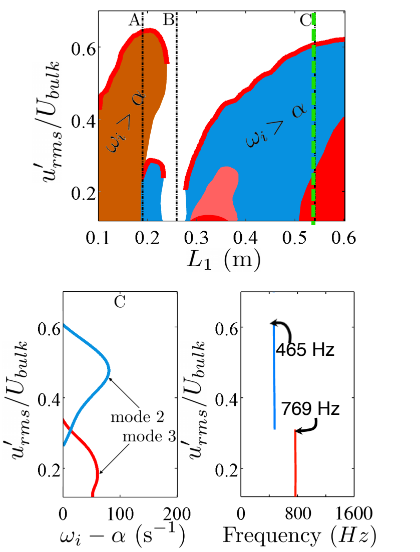

Experiment

Switch naturally to mode 2 during growth

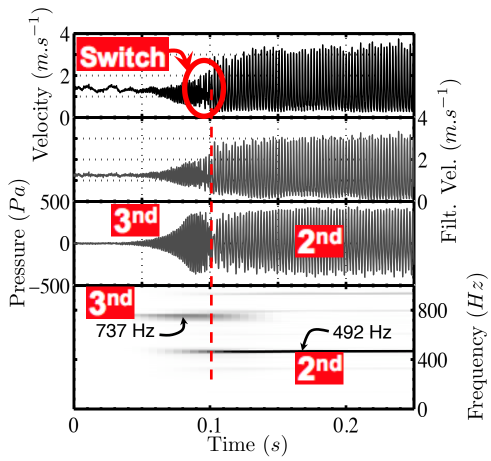

42

Validation of FDF framework

Unconfined laminar flames
Noiray et al. (2008) JFM 615

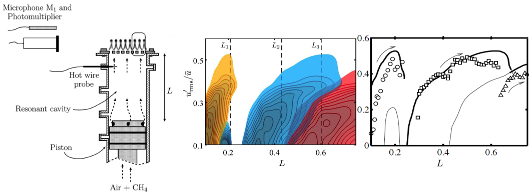

Confined Turbulent swirling flame
Palies et al. (2011) C&F 158

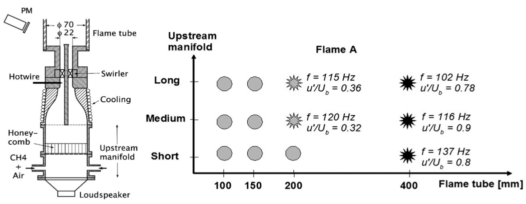

Confined laminar flames
Boudy et al. (2011) JEGTP 133
Boudy et al. (2011) PCI 33

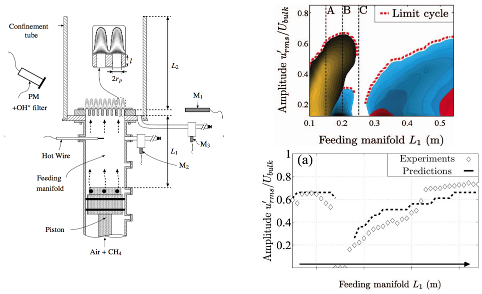

Possibility to anticipate
- Limit cycle amplitudes
- Limit cycle frequencies (including frequency shift)
- Hysteresis
- Triggering
- Mode switching

Outline

1. Experimental configuration
2. Linear stability analysis with Flame Transfer Function (FTF)
3. Nonlinear analysis with Flame Describing Function (FDF)
4. Nonlinear modeling results
1. Current issues using FDF framework
2. Conclusions

Limit cycles with variable amplitude

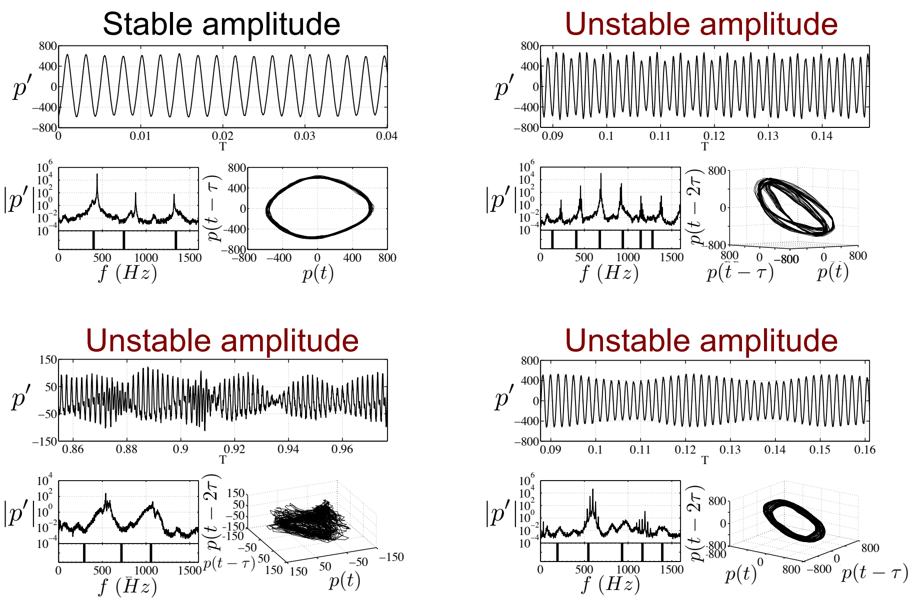

The amplitude and frequency of the limit cycle is not always fixed at a certain value

45

Analysis of cases featuring multiple frequencies

Experiments indicate that multiple unstable modes may coexist for some conditions. One of such example is presented here

Stable limit cycle

Galloping limit cycle

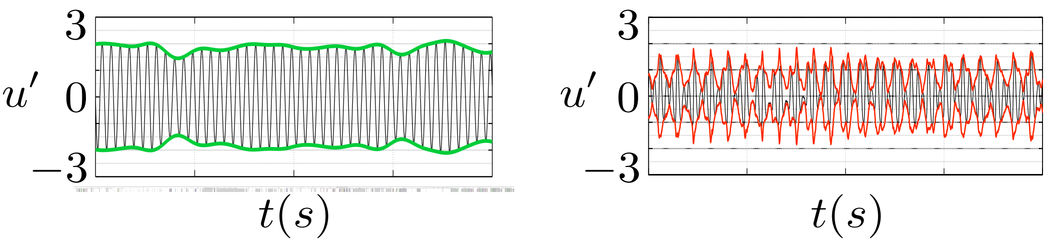

This problem is often evoked, Sterling (1993), Moeck et al. (2010), Lamraoui et al. (2011), Kabiraj et al. (2011)

It is shown here that some of these features can be explained through the nonlinear flame dynamics within the Flame Describing Function (FDF) framework.

46

Analysis of a configuration with two simultaneously unstable modes

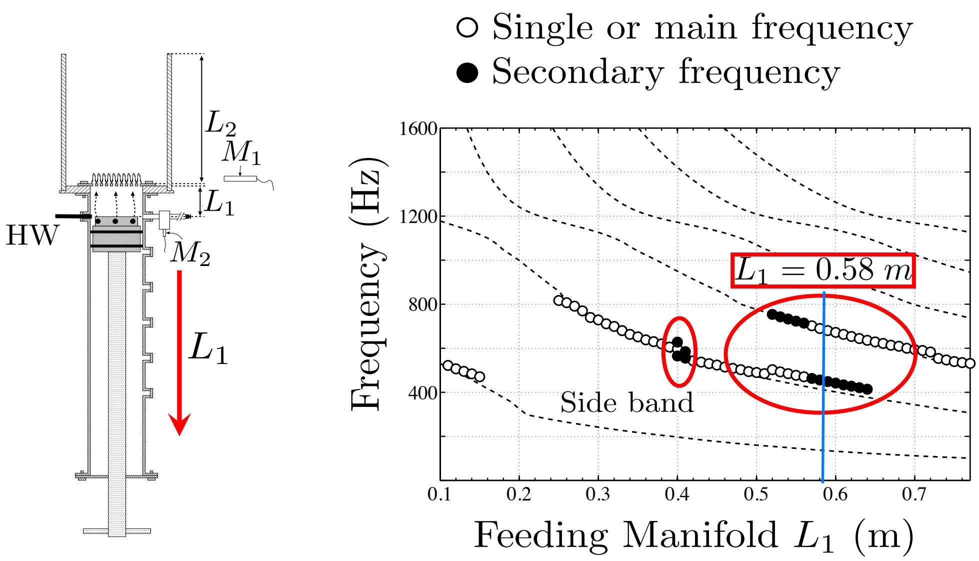

47

Pressure measurements for L_1 = 0.58 m

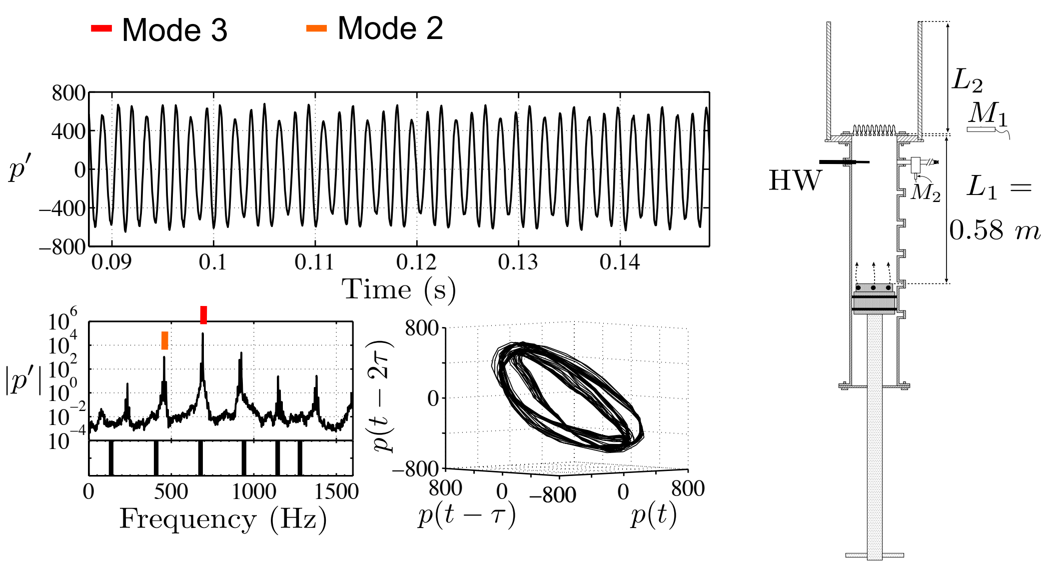

48

Analysis of the bifurcation diagram in the region where two simultaneously unstable modes were observed

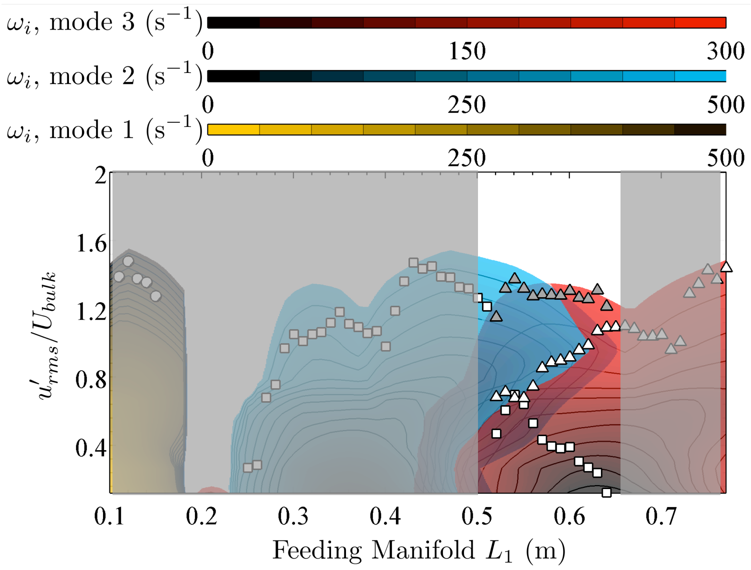

Overlap of mode 3 linearly unstable and mode 2 nonlinearly unstable. The objective is to delineate cases where mode switching (single frequency at limit cycle) or simultaneous modes oscillations (galloping limit cycle with two frequencies) occur.

Growth rate trajectories

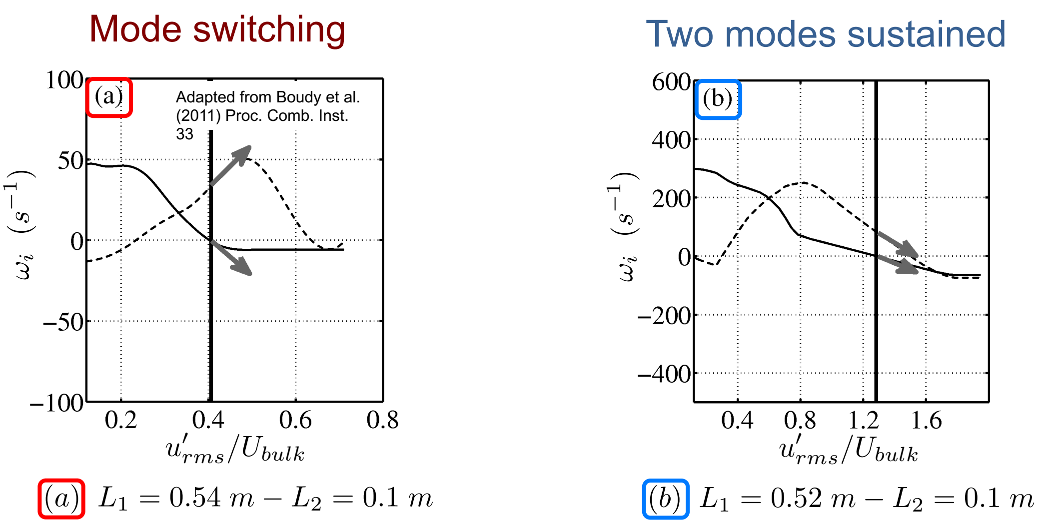

The product of the slopes of the growth rates is negative

The product of the slopes of the growth rates is positive

Conclusions

FDF framework allows predictions of instability frequency and amplitude during thermoacoustic self-sustained oscillations

When modes overlap different nonlinear phenomena can be anticipated leading to hysteresis, triggering and mode switching, which are well retrieved by predictions

Current efforts aim at predicting self-sustained oscillations featuring multiple frequencies. FDF calculations allow to consider situations where one unstable mode takes over or two modes coexist

Generalization of the FDF framework to predict variable amplitude limit cycles is in progress

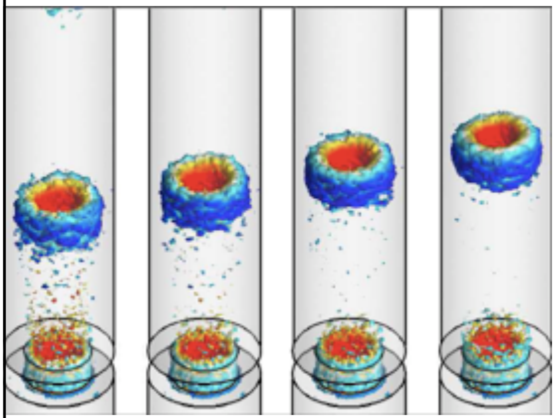

Combustion dynamics
Lecture 7a

S. Candel, D. Durox , T. Schuller

CentraleSupélec
Université Paris-Saclay, EM2C lab, CNRS

Tsinghua summer school, July 2021

Combustion dynamics control concepts

Control techniques

Balance of the acoustic energy within the system

Acoustic response of the combustor

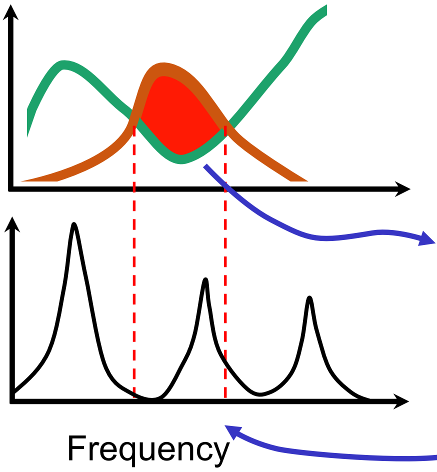

Acoustic losses at the boundaries

Acoustic gain of the combustion process

Acoustic energy balance positive : potential thermoacoustic coupling

Control techniques

Balance of the acoustic energy within the system

Acoustic response of the combustor

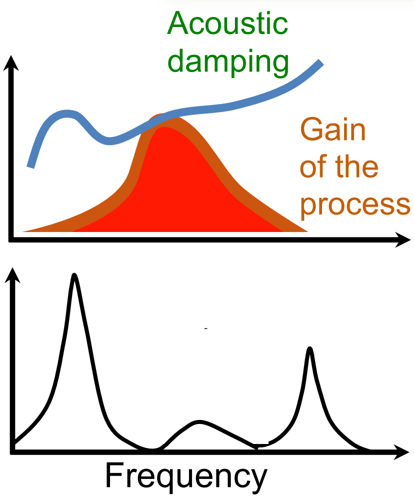

Acoustic losses at the boundaries and in the volume

Acoustic gain of the combustion process

First strategy : increase losses by inserting liners, Helmholtz resonators, quarter wave cavities perforated bias flow systems…

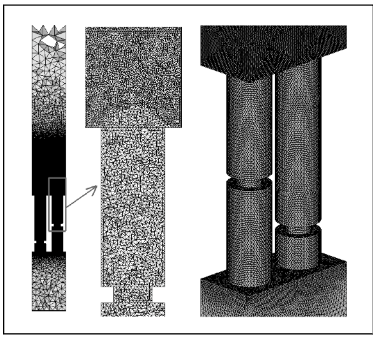

Reactive flow simulation
Compressible flow solver AVBP :

- 4 million cells, 3D calculations
- No flame thickening
- 1 step Arrhenius kinetics
- Modulated velocity inlet
- Non reflecting outlet
- Periodic lateral boundaries
- TTGC scheme

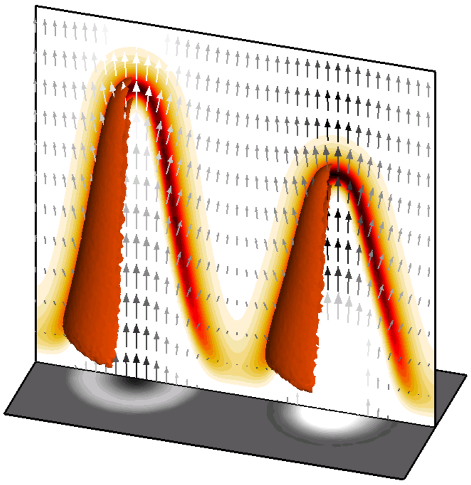

Acoustic excitation
(f = 650Hz)

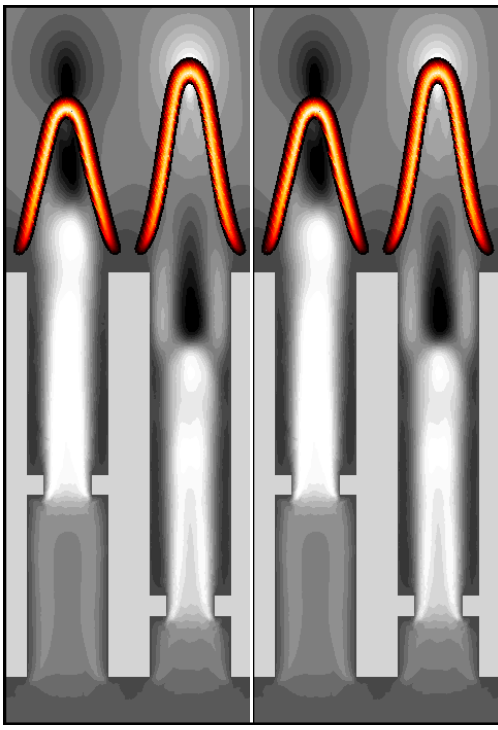

3D simulation
of a system equipped
with a dynamic phase
converter

N. Noiray, D. Durox, T. Schuller and S. Candel (2009) *Proceedings of the Combustion Institute.* 32, 3163-3170. Dynamic phase converter for passive control of combustion instabilities.

Dynamical control of instabilities

- A novel concept developed to control flame dynamics relies on mode conversion
- A Dynamical Phase Converter (DPC) demonstrated experimentally and numerically
- Technology adapted to pratical configurations (patent)

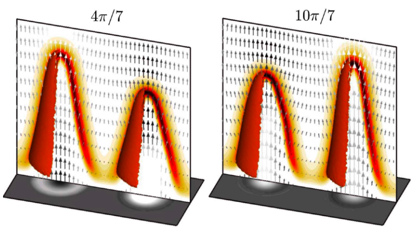

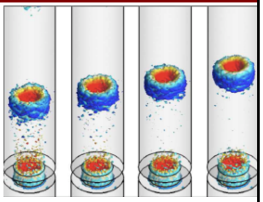

Simulation of mode conversion in a duct

N. Noiray, D. Durox, T. Schuller and S. Candel (2007) *Proceedings of the Combustion Institute*. 31. 1283-1290. Passive control of combustion instabilities involving premixed flames anchored on perforated plates.

N. Noiray, D. Durox, T. Schuller and S. Candel (2008) A novel strategy for passive control of combustion instabilities. ASME 2008 Gas turbine technical congress and exposition, Berlin, Germany, GT2008-51520.

N. Noiray, D. Durox, T. Schuller and S. Candel (2009) *Proceedings of the Combustion Institute*. 32, 3163-3170. Dynamic phase converter for passive control of combustion instabilities.

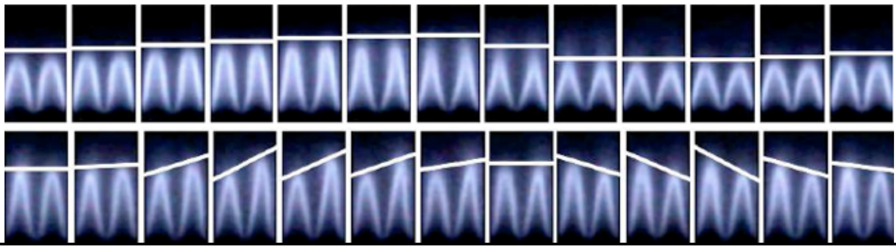

Top : coherent flame response to incoming perturbations. Bottom : response of the system equipped with the DPC

7

Active control concepts

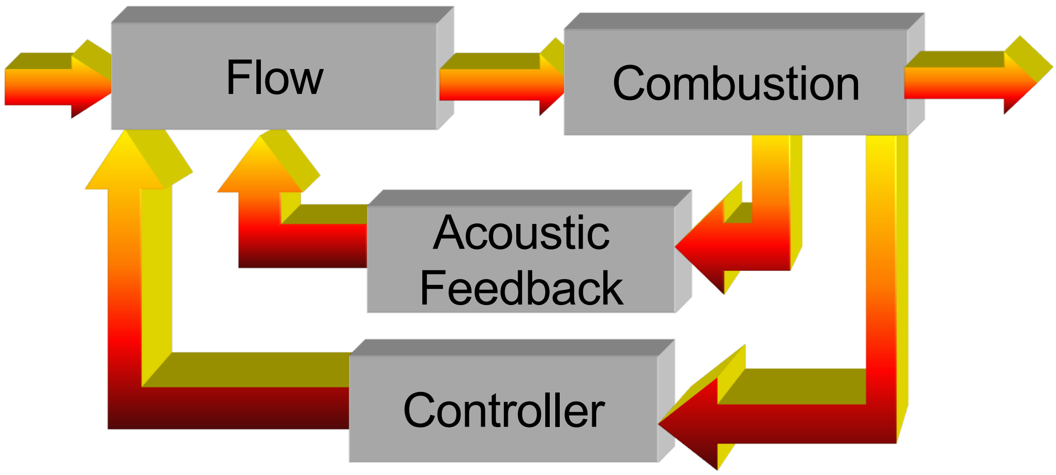

8

Active control

Active methods: theoretical studies during the 50's.

Tsien (1952), Marble (1953), Crocco and Cheng (1956)…Sensitive time lag model was introduced to analyze rocket instabilities and their control.

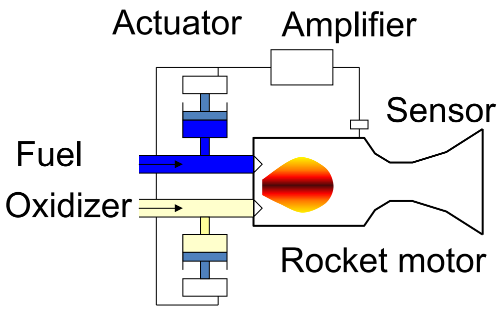

Frank Marble and H.S. Tsien in China

S. Candel (2002) *Proceedings of the Combustion Institute*, **29**. 1-28. Combustion dynamics and control : progress and challenges. (Hottel Lecture).

Practical demonstrations of concept achieved in the 1980's: Dines 1984, Bloxsidge et al. 1987, Poinsot et al. 1987, Billoud et al (1992)...

Further studies in the 1990's : additional demonstrations, actuator developments, low-order modeling of control, control algorithms (self-tuning, state feedback, robust control, adaptive and self-adaptive control…),

More recent work : actuators and sensors for practical applications, scale-up and application in real systems, control modeling, multidimensional simulation

Adaptive control of combustion instabilities

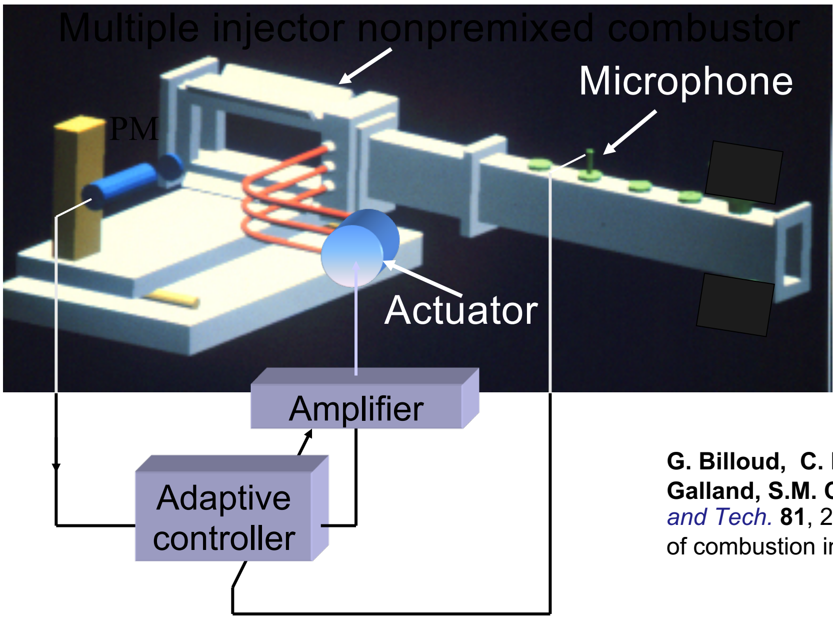

G. Billoud, C. Huynh Huu, M. A. Galland, S.M. Candel (1992) *Comb. Sci. and Tech.* **81**, 257. Adaptive active control of combustion instabilities.

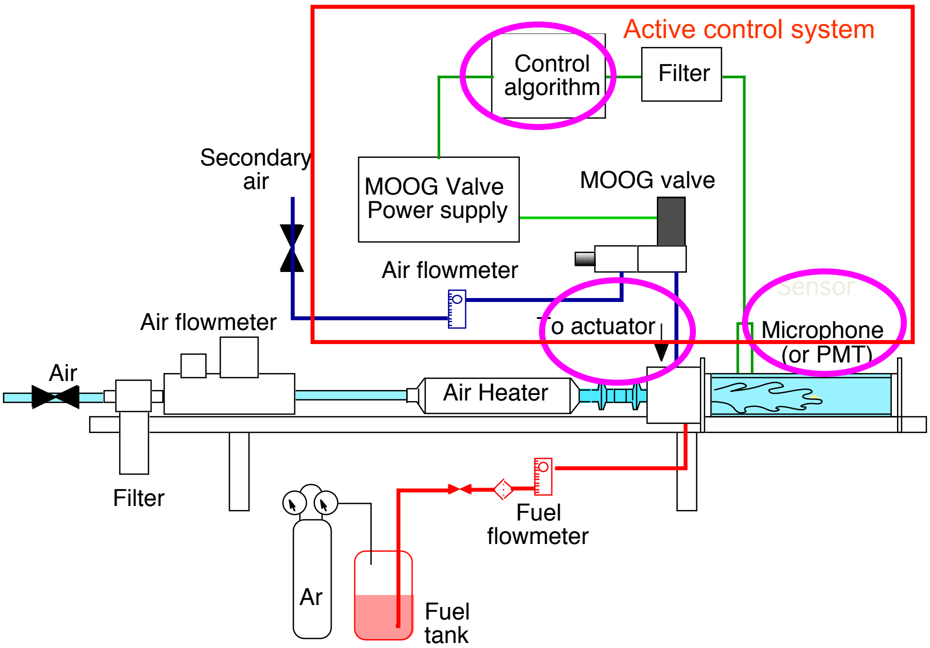

D. Bernier, S. Ducruix, F. Lacas, S. Candel, N. Robart and T. Poinsot (2003) *Combustion Science and Technology* **175**, 993-1013. Transfer function measurements in a model combustor : application to active instability control.

Schematic Active Control of the Siemens model Vx4.3A heavy duty gas turbine

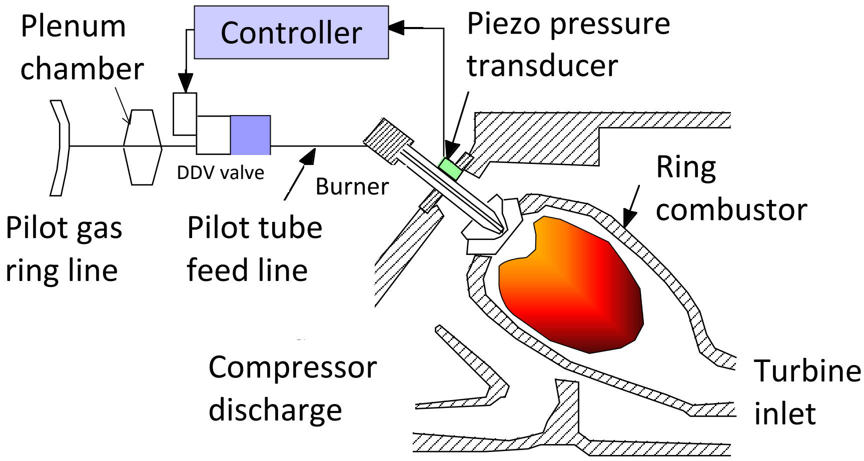

Adapted from Hermann (2001)

Numerical simulation of active control with low order models

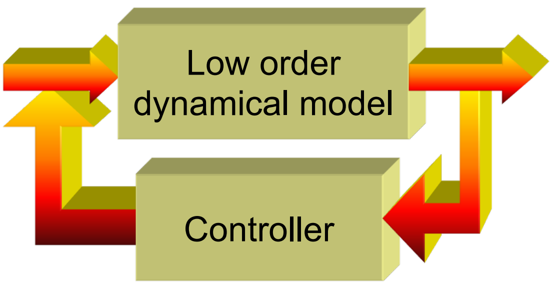

- Difficulty in modeling complex nonlinear dynamics and in describing actuator effects
- Useful as a guide for controller development

Tsien (1952), Marble and Cox (1953), Crocco and Cheng (1955), Bloxsidge (1984), Lang et al (1987), Culick et al (1991), Yang and Fung (1992), McManus et al (1993), Koshigoe et al (1995), Annaswamy et al. (1998), Paschereit (1998) …

Block diagrams representation of active control systems

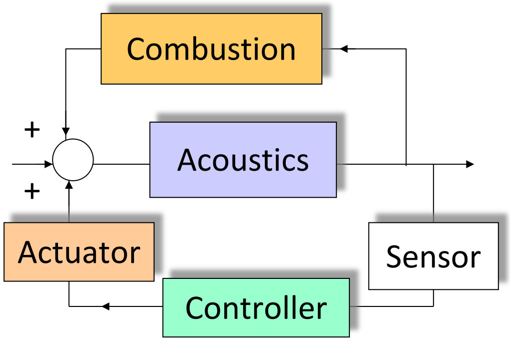

Representation of combustor coupled to an external control loop

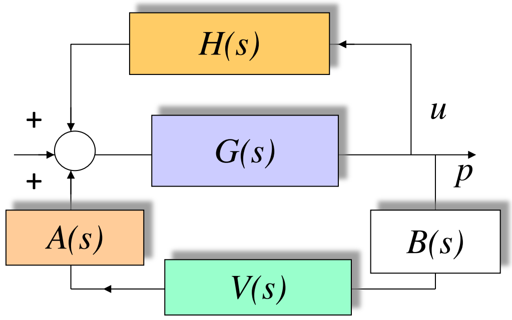

Transfer function description of the system

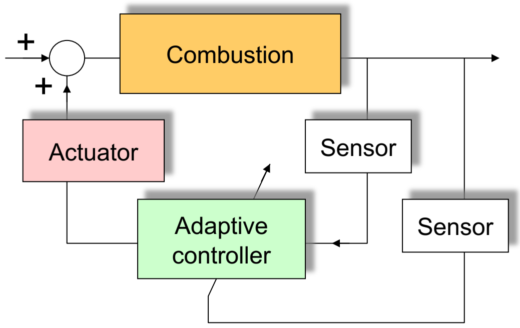

Adaptive control system

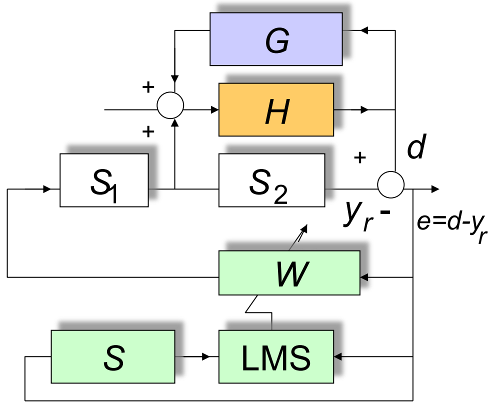

Transfer function representation of adaptive control

H : combustion

G : acoustic feedback

W : LMS filter

S , *S* : actuator transfer function and secondary path between actuator and sensor

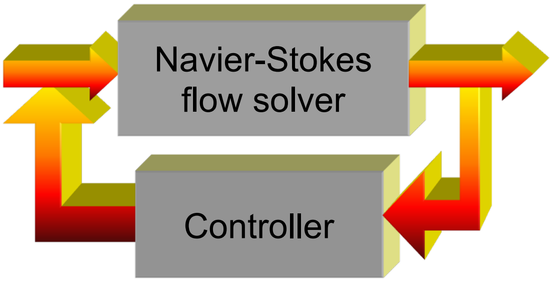

Numerical simulation of active control with CFD software tools

- Less well documented
- Important requirements in terms of computer ressources
- Difficulties in actuator description and in coupling the flow solver to the controller

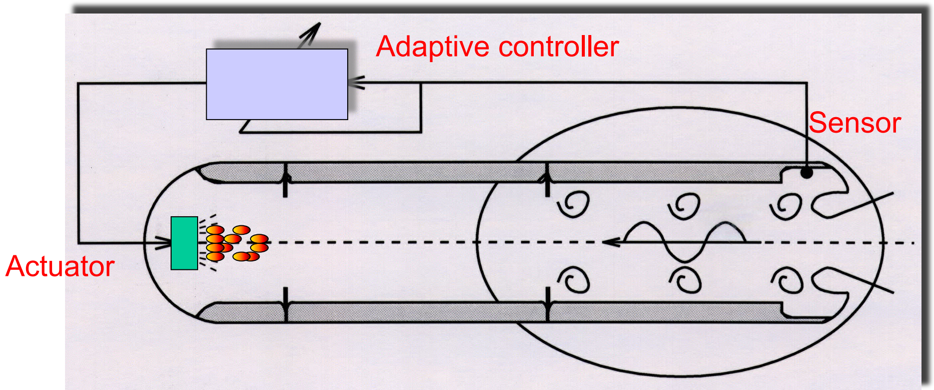

Vortex driven instabilities and conceptual adaptive control system

Objective : Reduce vortex driven instabilities in large solid propellant solid rocket motors.

Diminish the pressure oscillation by injecting a liquid oxidizer through an actuator. This oxidizer reacts with the surrounding hot gases. If properly phased this will reduce the oscillation

M. Mettenleiter, E. Haile and S. Candel (2000) *Journal of Sound and Vibration.* 230, 761-789. Adaptive control of aeroacoustic instabilities.

J. Anthoine, M. Mettenleiter, O. Repellin, J.M. Buchlin and S. Candel (2003) *Journal of Sound and Vibration* 262, (5) 1009-1046. Influence of adaptive control on vortex driven instabilities in a scaled model of solid propellant motors.

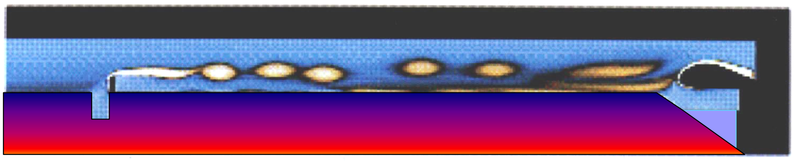

(1)

Vortices shed by baffle

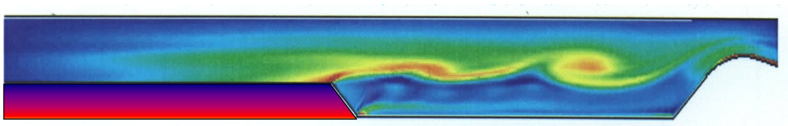

(2)

Vortices shed by propellant edge

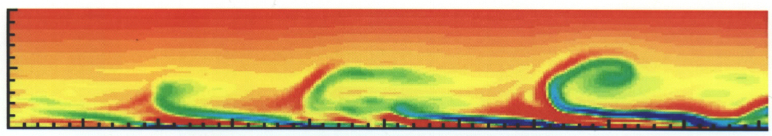

(3)

Vortices shed by turning flow originating from propellant

19

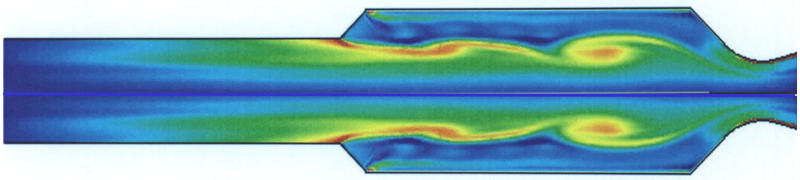

$$mT = \frac{l}{kU} + \frac{l}{c - U} + \Delta t$$

Number of vortices

Acoustic period

Convective time

Acoustic time

Delay of conversion from convective to acoustic mode

$$\Delta t = \alpha T$$

$$\frac{m - \alpha}{f} = \frac{l}{U}\left[\frac{1}{k} + \frac{M}{1 - M}\right] \Rightarrow f = \frac{kU}{l}\frac{m - \alpha}{1 + kM}$$

J. E. Rossiter (1964) Wind-tunnel experiments on the flow over rectangular cavities at subsonic and transonic speeds. *Aero. Res. Counc. R&M*, No. 3438.

20

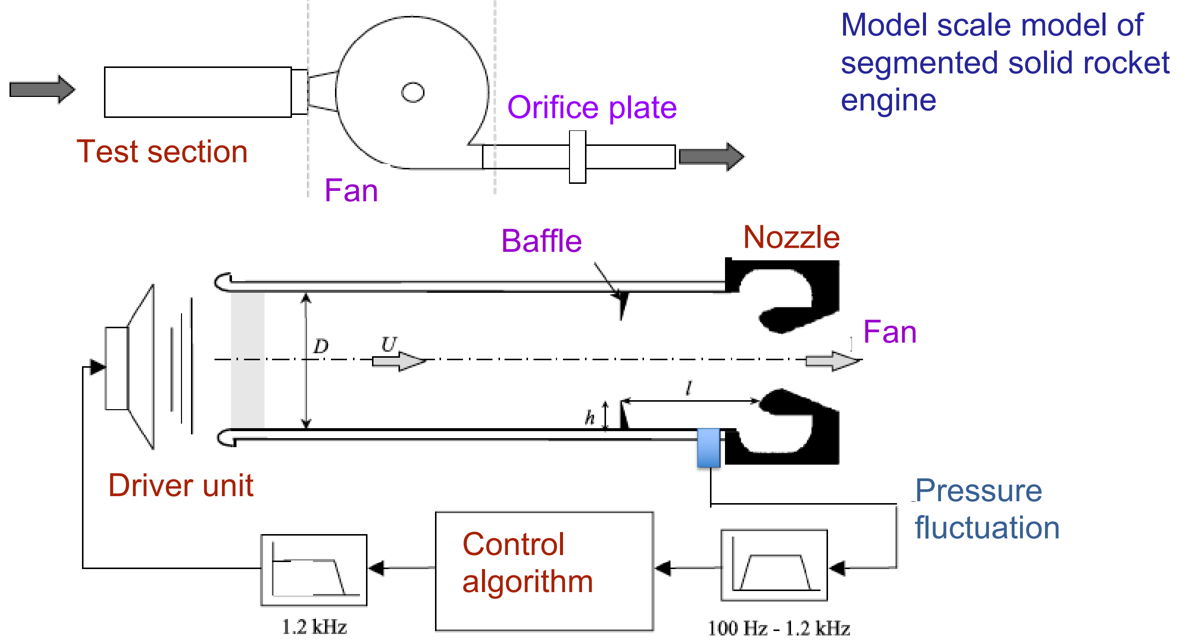

J. Anthoine, M. Mettenleiter, O. Repellin, J.M. Buchlin and S. Candel (2003) *Journal of Sound and Vibration* 262, (5) 1009-1046. Influence of adaptive control on vortex driven instabilities in a scaled model of solid propellant motors.

21

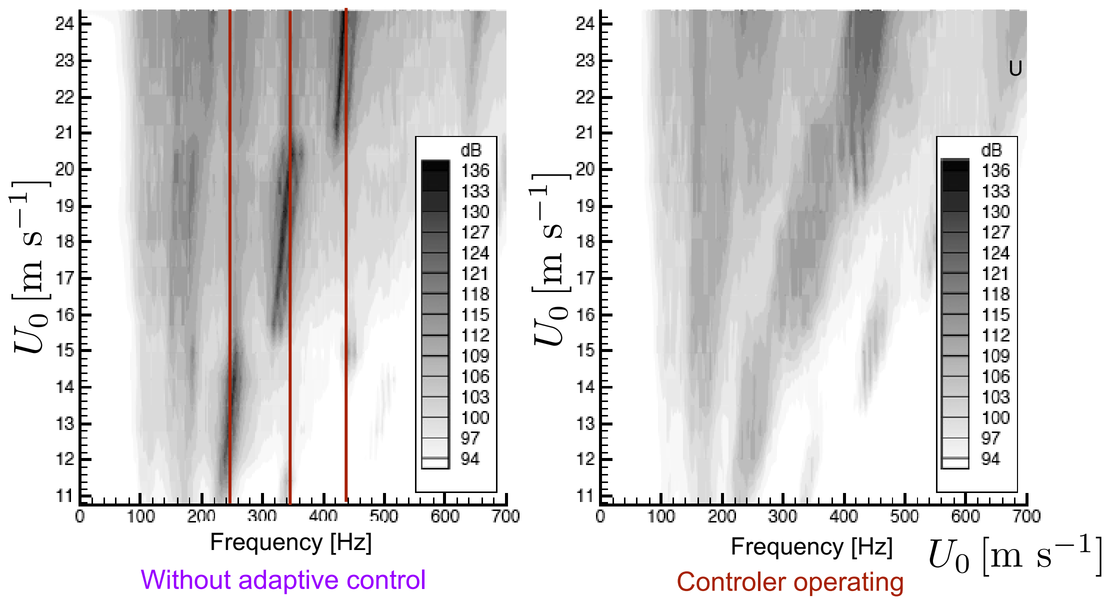

Contours of pressure fluctuations as a function of to frequency and mean flow velocity

22

Multidimensional simulation of active control

Actuator description by distributed source terms

$$
\begin{aligned}
\rho^{n+1} &= \rho^{n+1} + \boxed{\delta t \dot{\omega}_s} \\
(\rho u)^{n+1} &= (\rho u)^{n+1} + (\delta t \dot{\omega}_s) u_s \\
(\rho v)^{n+1} &= (\rho v)^{n+1} + (\delta t \dot{\omega}_s) v_s \\
(\rho E)^{n+1} &= (\rho E)^{n+1} + (\delta t \dot{\omega}_s)(e + U^2)
\end{aligned}
$$

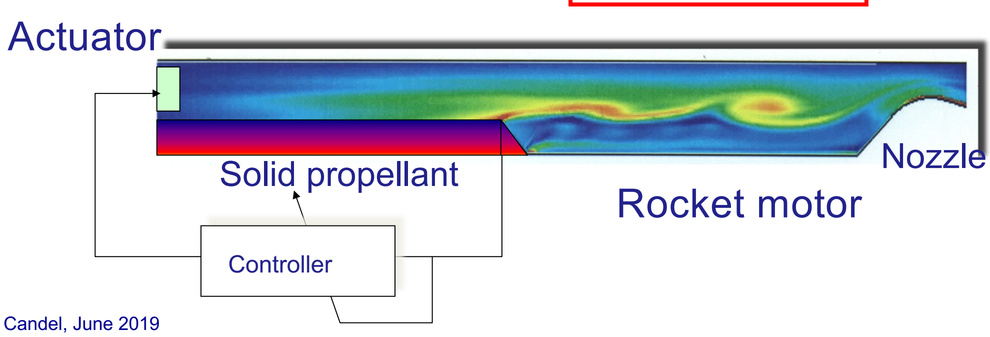

23

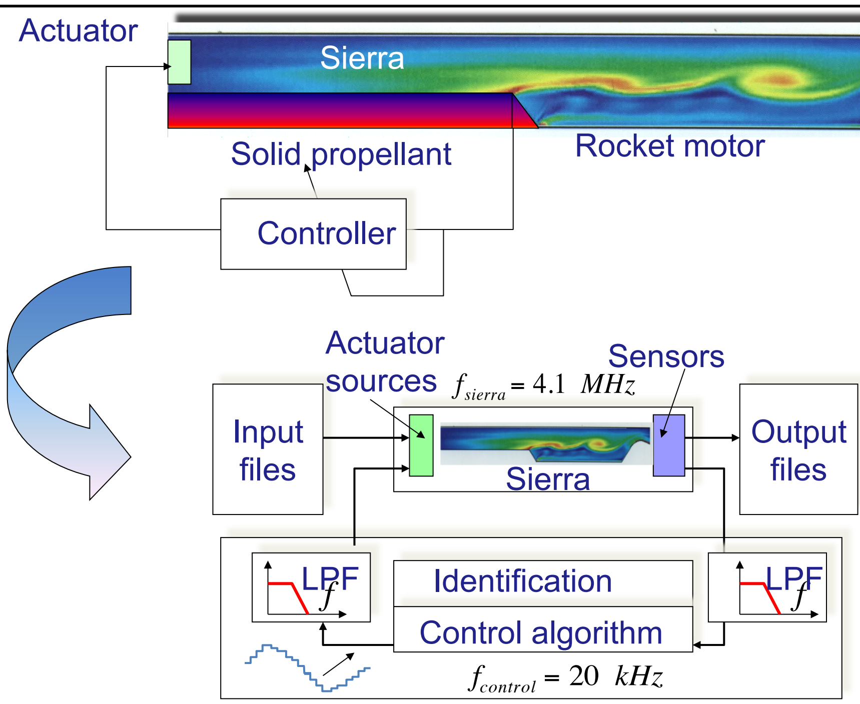

Coupling of flow solver with an adaptive controller

24

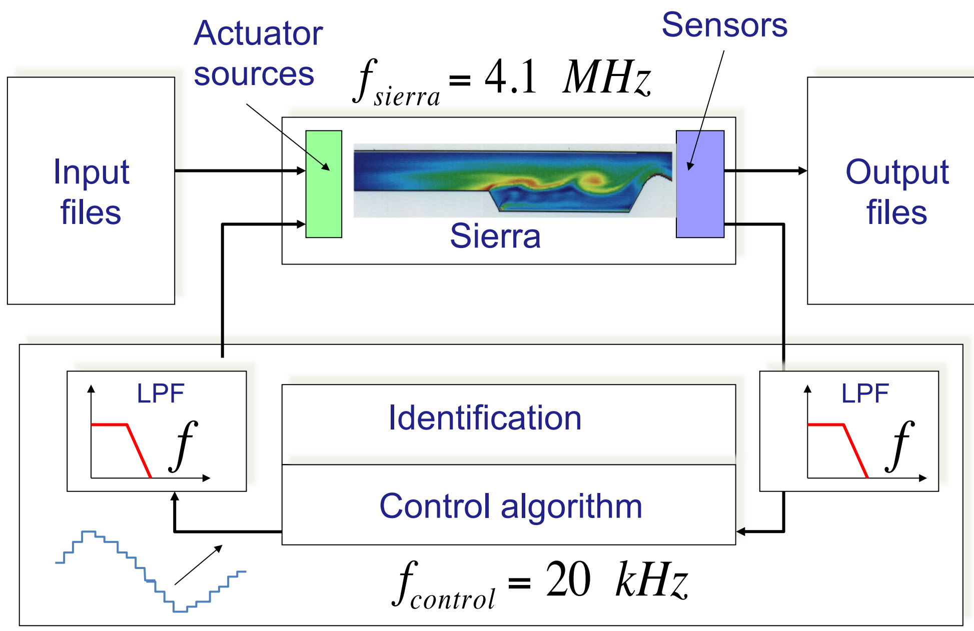

This mismatch rapidly deteriorates the simulation

The problem is suppressed by placing low pass filters at the controller input and output

25

Controller switched on

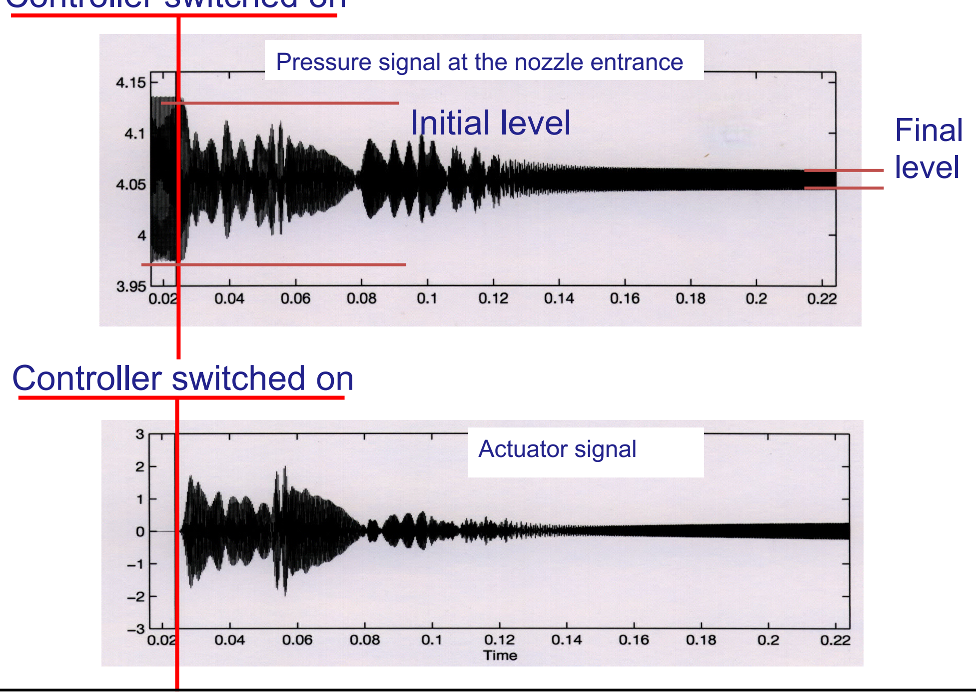

26

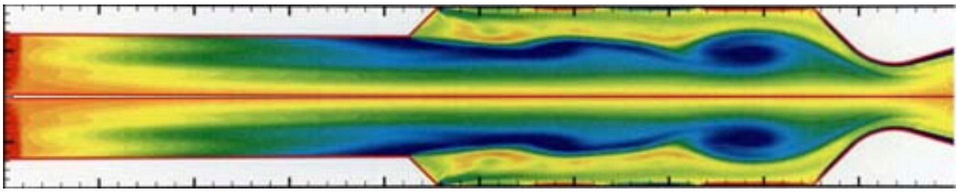

Resonant vortex shedding before control (elevated level of pressure fluctuation)

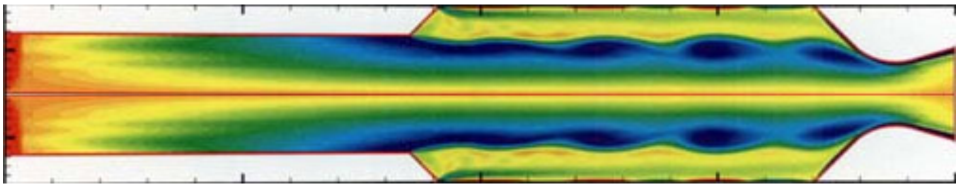

Vortex shedding under controlled operation (pressure fluctuation level is reduced by controller)

M. Mettenleiter, F. Vuillot and S. Candel (2002) *AIAA Journal* **40**, 860-868. Numerical simulation of active control in unstable rocket motors.

Combustion dynamics
Lecture 7b

S. Candel, D. Durox , T. Schuller

CentraleSupélec
Université Paris-Saclay, EM2C lab, CNRS

Tsinghua summer school, July 2021

1

A novel strategy for passive control of combustion instabilities through modification of flame dynamics

Nicolas Noiray, Daniel Durox, Thierry Schuller and Sébastien Candel

EM2C Laboratory, CNRS - Ecole Centrale Paris,
92295 Châtenay-Malabry, FRANCE

2

Background

Thermoacoustic instabilities cause serious problems in a wide range of combustion industrial applications

Causes : Resonant coupling between flames and burner acoustics

Consequences :

- Structural vibration (sometimes destruction)
- Heat fluxes enhancement to the boundaries
- Flame extinction

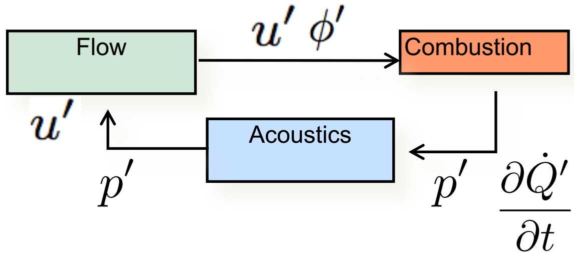

Solutions : Active control
Passive control

Passive control techniques

First strategy : modify the losses
Helmholtz resonators,
perfortated linings,
quarter wave cavities, baffles

Balance of the acoustic energy within the system

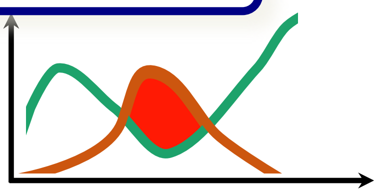

Acoustic losses
boundary conditions

Acoustic gain induced by the flame

Acoustic response of the combustor

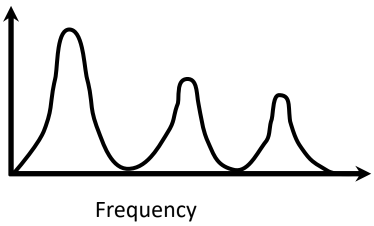

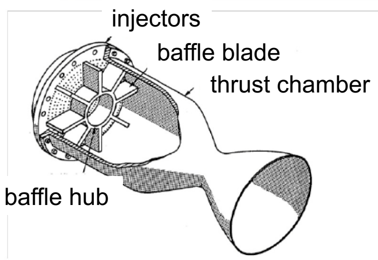

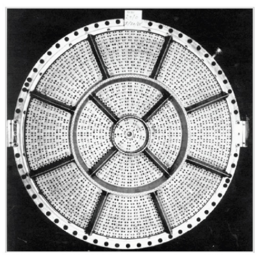

Passive control techniques

Second strategy : modify the gain by acting on the flame dynamics

Acoustic losses : boundary conditions

Acoustic gain induced by the flame

Balance of the acoustic energy within the system

Acoustic response of the combustor

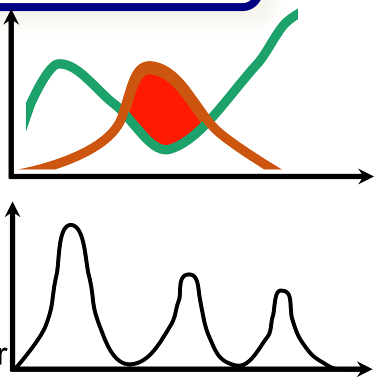

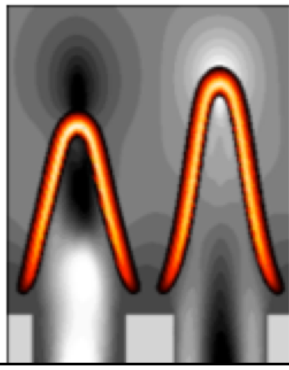

5

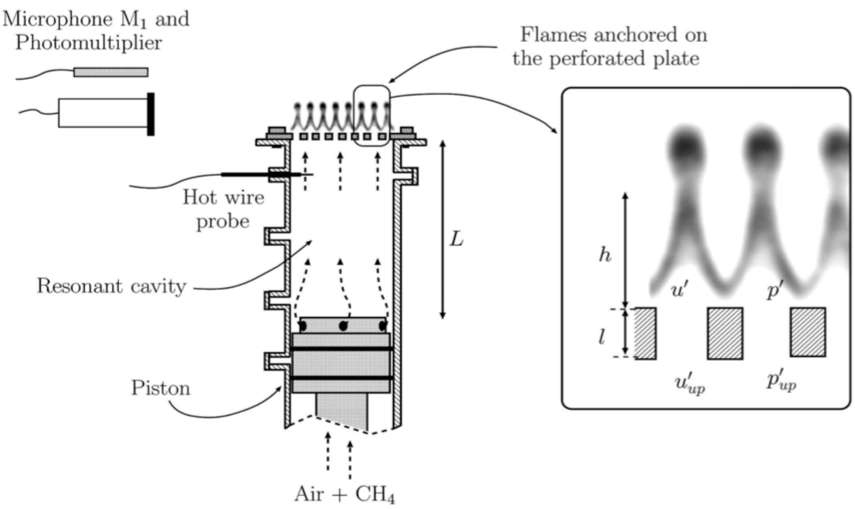

Perforated plate
400 holes
hole radius 1 mm
holes spacing 3 mm

Eq. ratio : $\Phi = 0.86$
Mass flow rate : $\dot{m} = 5.4\,10^{-3}\,\mathrm{kg\ s^{-1}}$
Thermal power : $14.4\ \mathrm{kW}$

Burner diameter D : 70 mm
Adjustable burner depth L from 90 to 750 mm
Unconfined flame configuration

6

7

Combustion regimes

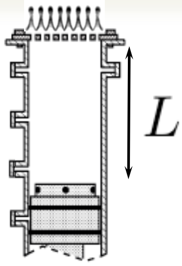

Depending on the burner size L, the combustion regime is either **stable** or **unstable**.

8

Flame dynamics

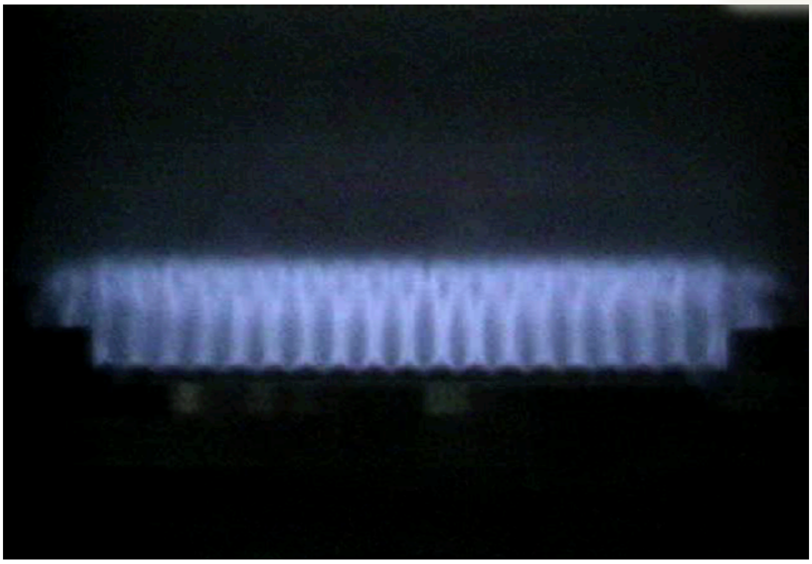

Oscillation cycle (f = 530 Hz) for a typical **unstable combustion regime.**

The SPL exceeds 110 dB, 40 cm away from the flames

Burner size influence

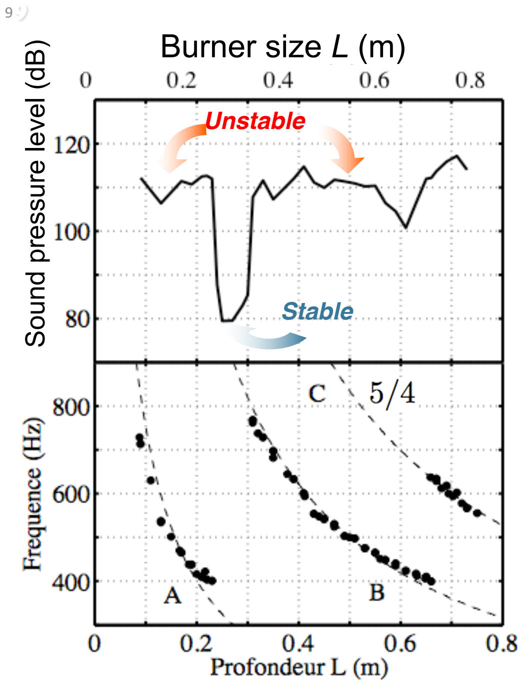

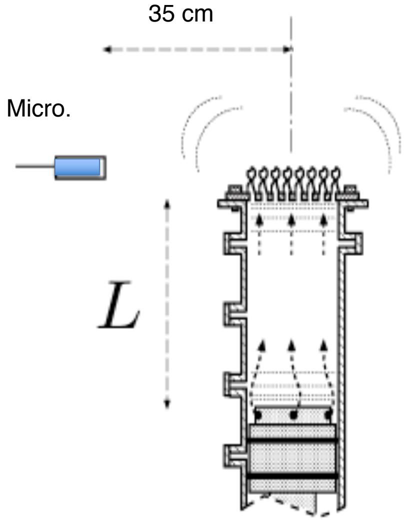

Dynamic Phase Converter (DPC) Principle *(Patent FR 0705344)*

Make use of the **multiple flame configuration** and try to **avoid the coherent response** of the flames to acoustic perturbations

Problem : the ***acoustic wavelengths are much larger than the flame dimensions*** (acoustic perturbations propagate at the sound speed) so it is not possible to decouple the individual flames from each others with an acoustic-based device

Transform the acoustic perturbations which impinge on the flames **to hydrodynamic perturbations** (convective vortices) which travel at the mean velocity (much lower than the sound speed)

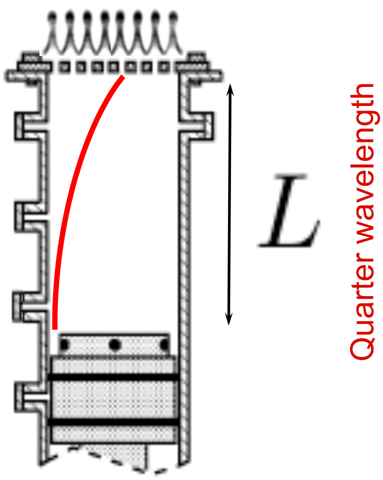

Create a shear layer by adding a constriction, an orifice plate or a sudden expansion in the injectors

The out-of-phase response of the flames to an acoustic perturbation hinders the growth of oscillations

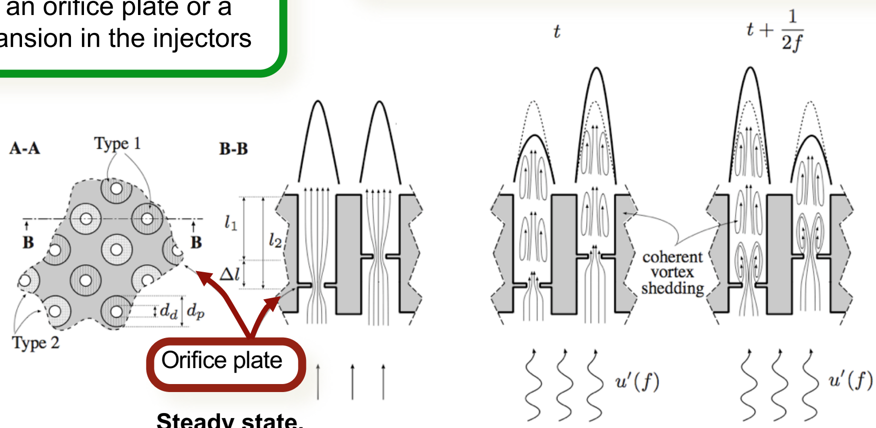

Steady state, identical flames

Acoustic perturbation

Instead of suffering the coherent vortex shedding (possible mechanism yielding thermo-acoustic instability) it is here used to suppress the resonant coupling

The target frequency is fixed f

The phase difference between the two types of flames is

$$\Delta\varphi = 2\pi f \frac{\Delta l}{\mathcal{U}_{cv}}$$

where $\mathcal{U}_{cv}$ is the vortices velocity and Δl is the stagger distance

In order to achieve an opposite motion ($\Delta\varphi = \pi$), Δl has to be defined as

$$\Delta l = \frac{\mathcal{U}_{cv}}{2f}$$

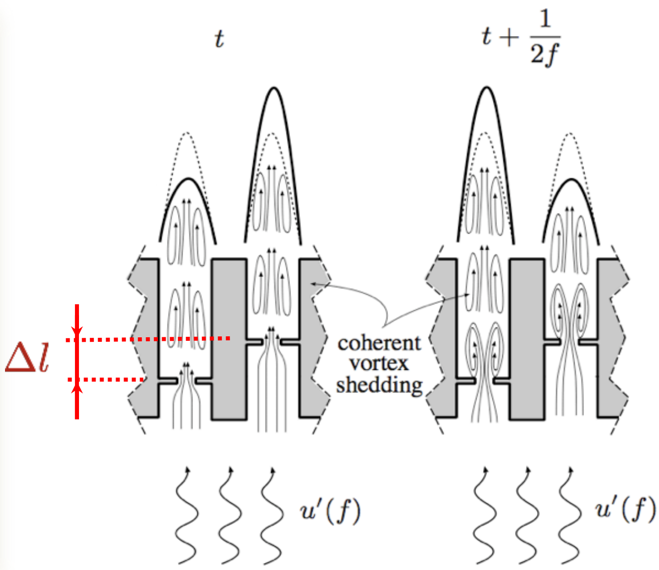

Convection velocity

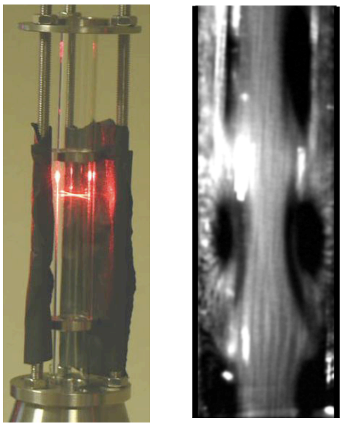

Forced flow experiments :
confined jet - LDV centerline measurements

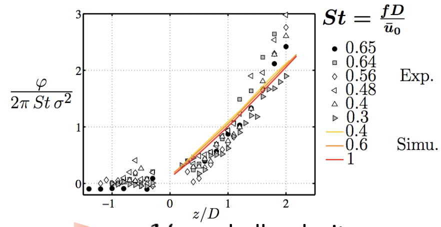

$\mathcal{U}_{cv} \simeq$ bulk velocity

Q-criterion isosurface

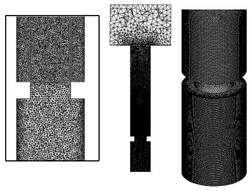

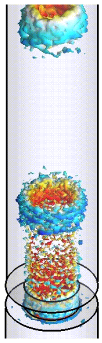

Numerical LES simulations :
code **AVBP** (Cerfacs), 1.7 M cells, compressible flow, 3D, pulsed velocity inlet, non-reflecting outlet boundary, TTGC scheme, f=1000 Hz, channel diameter and bulk velocity : D=2mm, U=2m/s

13

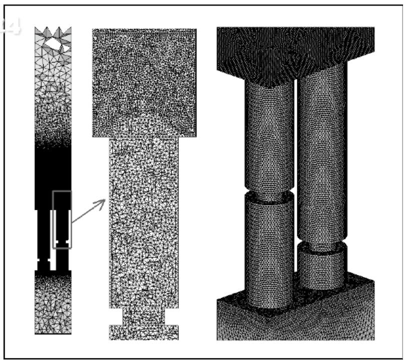

Reactive flow simulation
Compressible LES solver AVBP :

- 4 million of cells, 3D
- Non-thickened flame
- 1 step reaction
- Pulsed velocity inlet
- Non reflecting outlet boundary
- Periodic boundary conditions
- TTGC scheme

Dynamic phase converter forced flow simulations and experiments

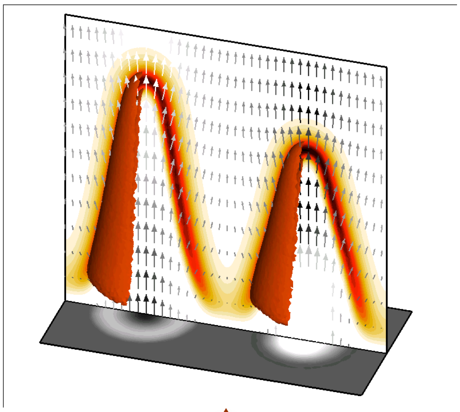

Acoustic excitation
(f = 650Hz)

14

Color contours :
Reaction rate

$\lambda = 52$ cm

Inlet condition :

$\bar{u} = 0.65 \ \mathrm{m\,s^{-1}}$
$f = 650$ Hz
$u' = 0.1\,\bar{u}\,\cos(2\pi f t)$

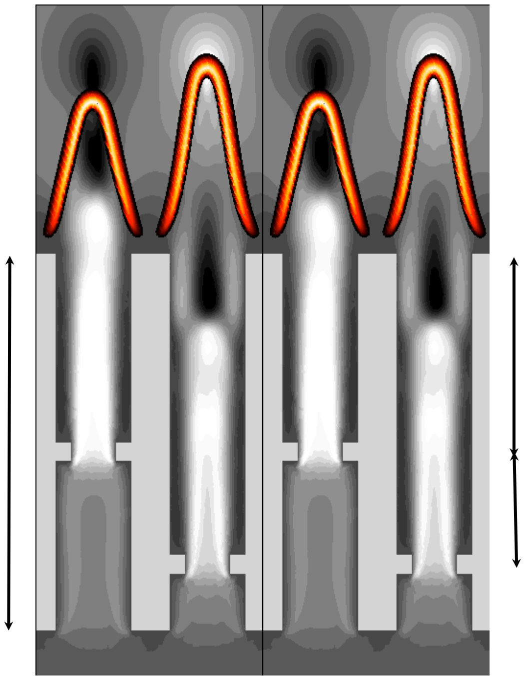

Gray contours :
Axial fluctuating velocity

Velocity measurements

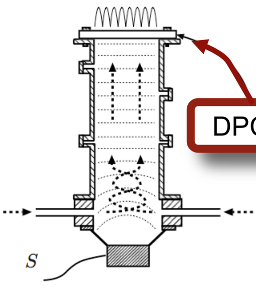

DPC Injector

$\Delta l = 4$ mm
$\mathcal{U}_{cv} = 5.3 \ \mathrm{m\,s^{-1}}$
Nominal frequency
$$f = \frac{\mathcal{U}_{cv}}{2\Delta l} \simeq 660 \text{ Hz}$$

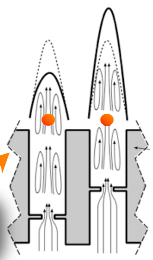

-LDV -
beams cross points

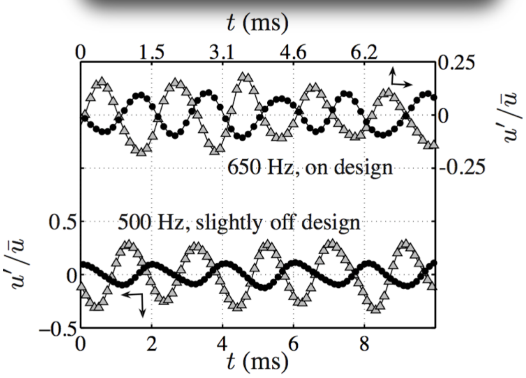

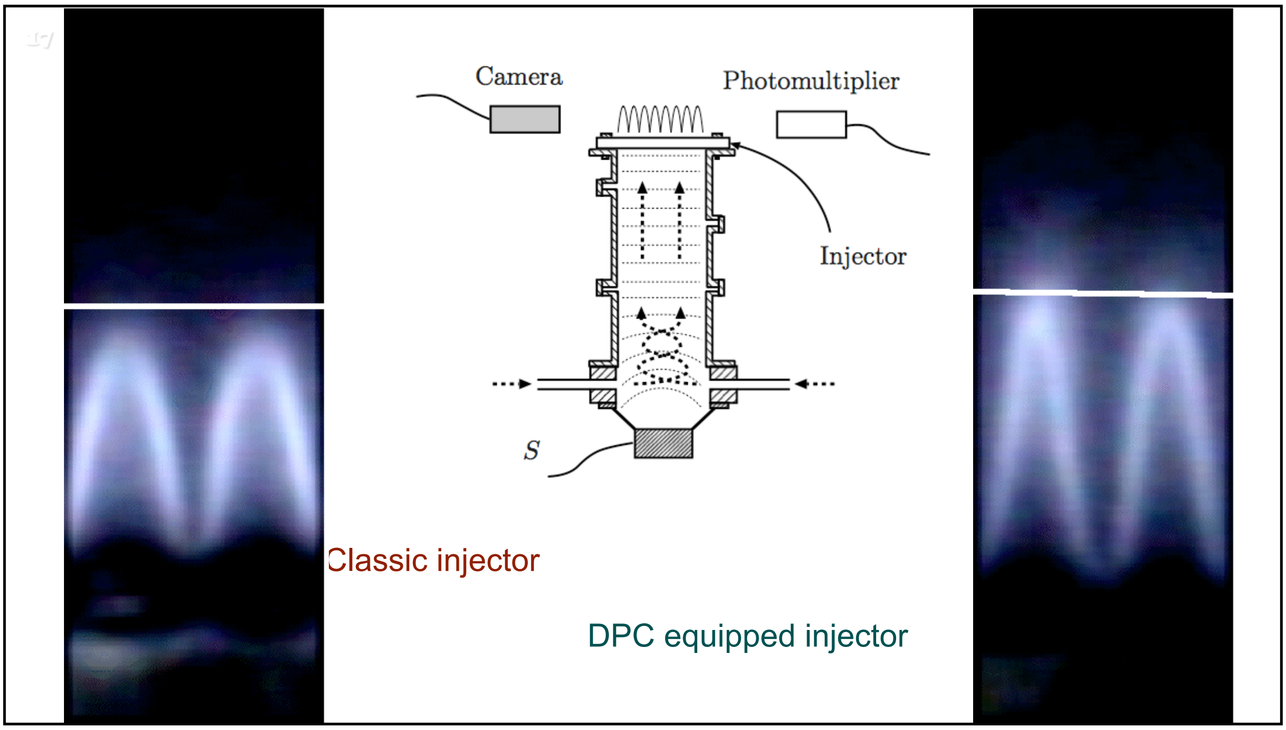
Camera
Photomultiplier
Injector
S
Classic injector
DPC equipped injector

17

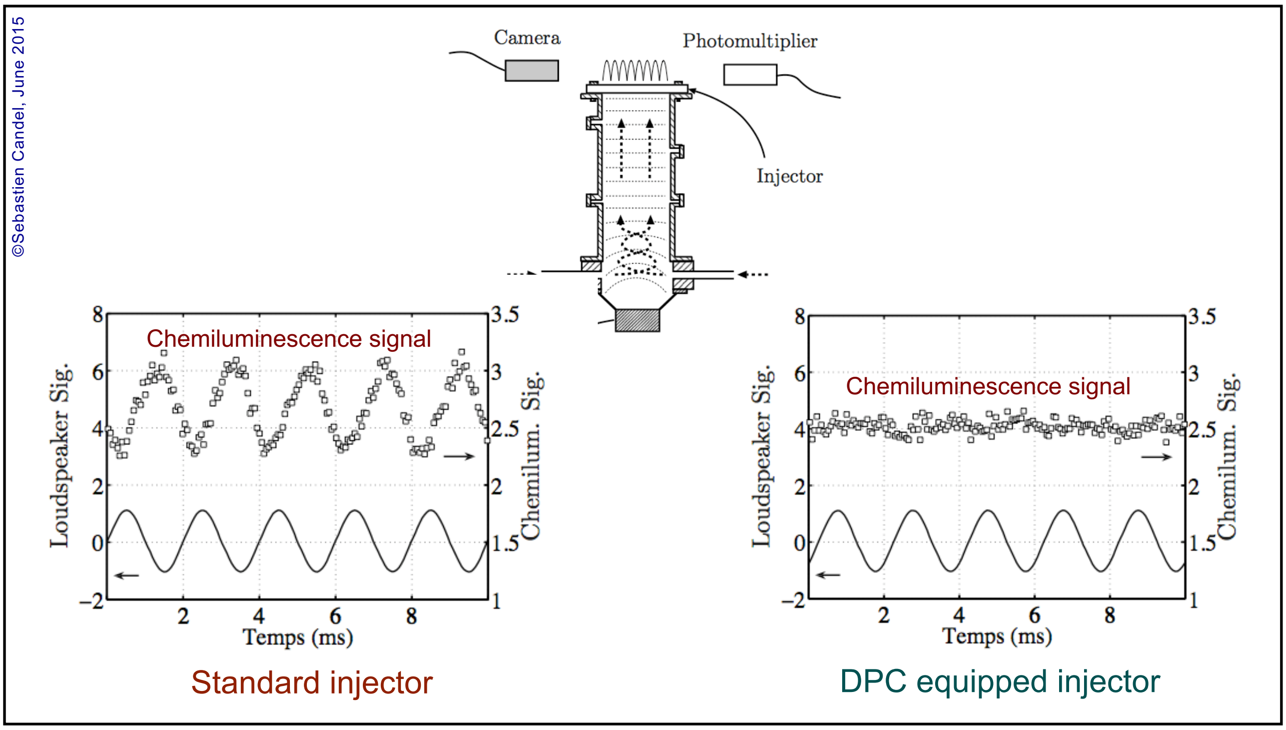
©Sebastien Candel, June 2015
Camera
Photomultiplier
Injector
Chemiluminescence signal
Loudspeaker Sig.
Chemilum. Sig.
Temps (ms)
Standard injector
Chemiluminescence signal
Loudspeaker Sig.
Chemilum. Sig.
Temps (ms)
DPC equipped injector

18

△ Standard injector

□ Injector including constrictions at the same axial level (no staggering)

● Dynamic phase converter (DPC)

Unforced operation

Nominal frequency $f = \frac{\mathcal{U}_{cv}}{2\Delta l} = 1215 \text{ Hz}$

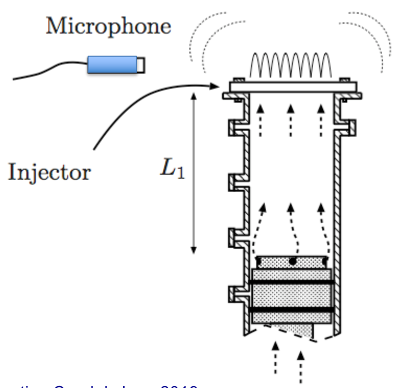

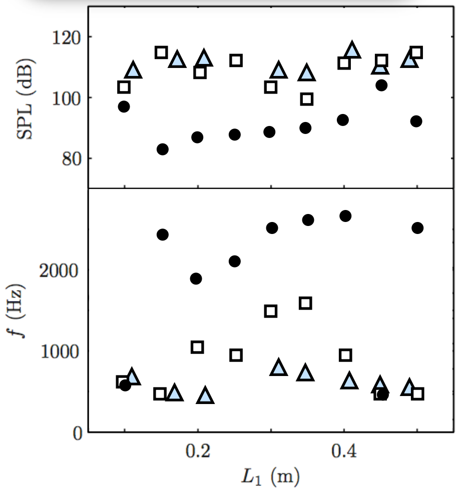

Features of the DPC

Advantages :

- Simple sizing method,
- Low requirement in terms of space and mass,
- Minor modification of the injection geometry,
- Broad band effictiveness,

Drawbacks :

- **A trade-off between additional head loss** (which depends on the constrictions dimensions) **and vortices strength has to be considered** to alter as less as possible the steady state performance
- **Eigenmodes far from the nominal frequency may arise** but could be suppressed with additional damping devices

Conclusions

- A new passive control strategy was developed. A hydrodynamic instability is used to suppress a thermo-acoustic instability.

- The dynamic phase converter was successfully tested numerically and experimentally :
  - under forced flow operation
  - without forcing

- The configuration features small scale laminar flames but the principle could be transferred to larger turbulent flames.

21

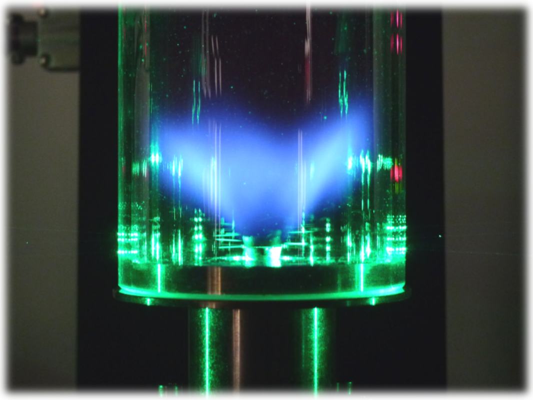

Combustion dynamics
Lecture 8

S. Candel, D. Durox , T. Schuller

CentraleSupélec
Université Paris-Saclay, EM2C lab, CNRS

Tsinghua summer school, July 2021

Swirling flame combustiondynamics

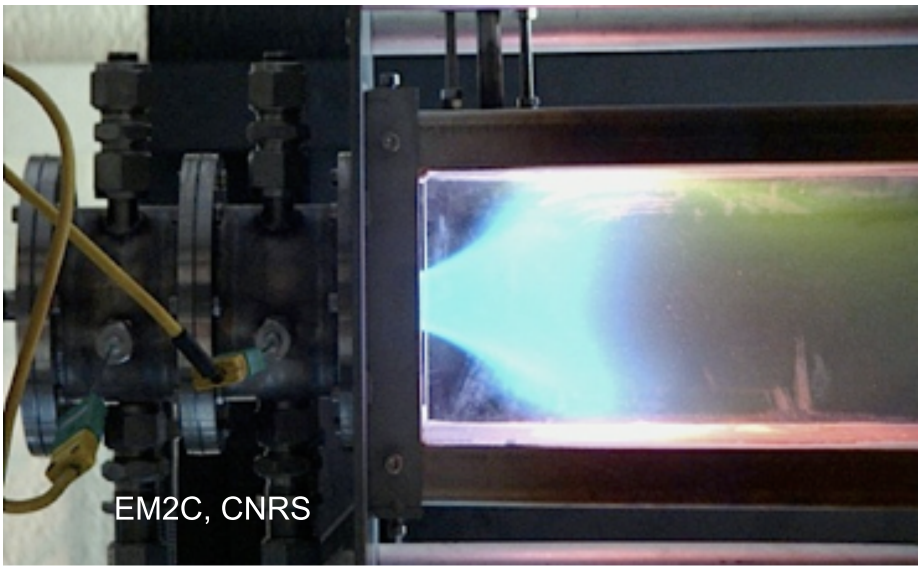

Swirling flame dynamics

- Swirl is used in jet engines systems to stabilize combustion
- It serves to anchor the flame in modern lean premixed gas turbines
- It is exploited in a variety of other combustion processes
- Swirling flame dynamics constitutes a central issue in many applications

Thermal power plant

GE-Snecma CFM56

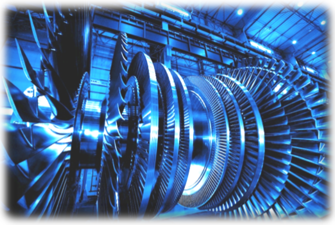

Alstom gas turbine

3

Combustion stabilization and swirl

- Stabilization relies on a central recirculation zone (CRZ) formed by hot combustion products which continuously initiate the reaction process
- Swirling flames are more compact than flames anchored on a bluff body allowing a notable reduction in the chamber size
- However, swirling combustors often develop self-sustained oscillations which have serious consequences
- There are many other dynamical issues which arise in practical systems and deserve fundamental investigations

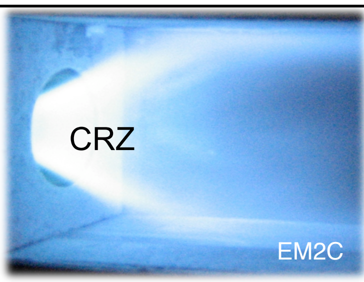

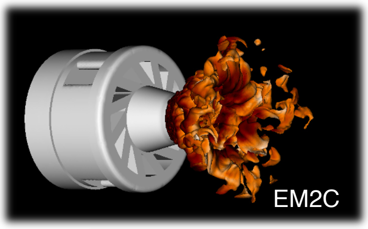

4

Objectives

- Examine the interaction between a swirler and axial acoustic waves
- Determine effects of this interaction and obtain the flame response in terms of a describing function
- Use the describing function in the analysis of a generic system comprising a single injector

S. Candel, D. Durox, T. Schuller, J.F. Bourgouin and J. Moeck (2014) *Annual Review of Fluid Mechanics*. 46, 147-173. Dynamics of swirling flames.

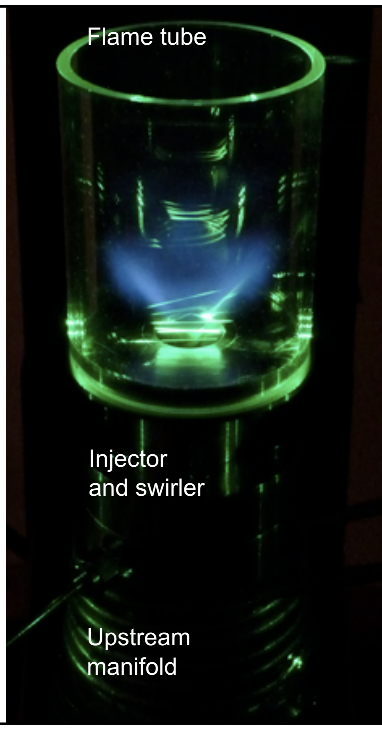

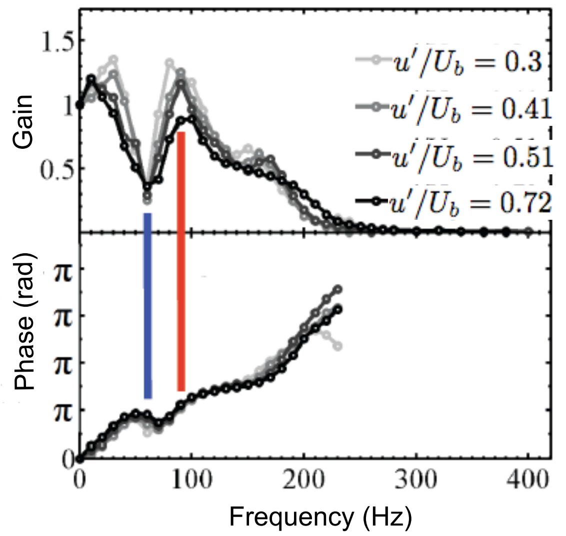

Experimental flame describing function

$$\Phi = 0.7 \quad U_b = 2.67\,\mathrm{m\ s}^{-1}$$

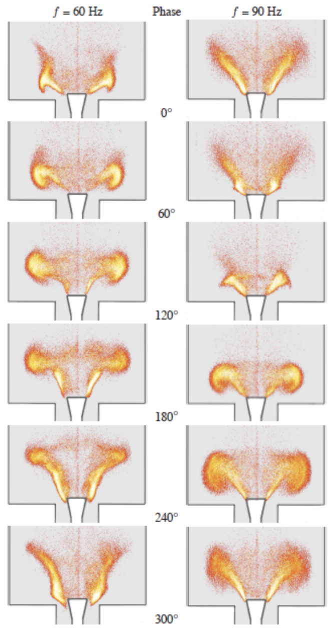

Distributions of phase average volumetric heat release

7

Examine interactions between swirlers and axial acoustic waves

Acoustics in a duct

Acoustics in duct with swirler

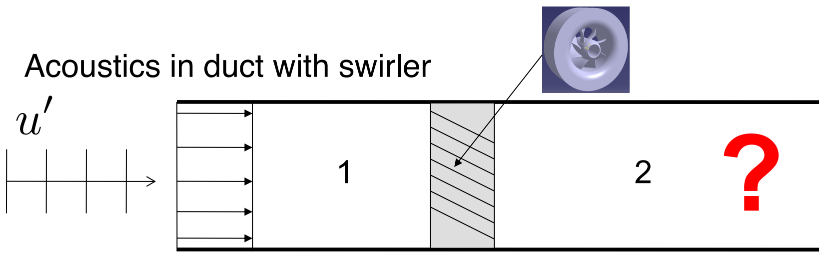

Determine

- Flow field induced on the downstream side of the swirler
- Phase velocities and disturbance amplitudes

8

Nick Cumpsty

Proc. R. Soc. Lond. A. **357**, 323–344 (1977)
Printed in Great Britain

The interaction of entropy fluctuations with turbine blade rows; a mechanism of turbojet engine noise

By N. A. Cumpsty† and F. E. Marble‡
† *Whittle Laboratory, University Engineering Department, Madingley Road, Cambridge CB3 OEL, UK.*
‡ *Division of Engineering and Applied Science, California Institute of Technology, California, U.S.A.*

(*Communicated by Sir William Hawthorne, F.R.S. – Received 23 November 1976*)

Frank Marble

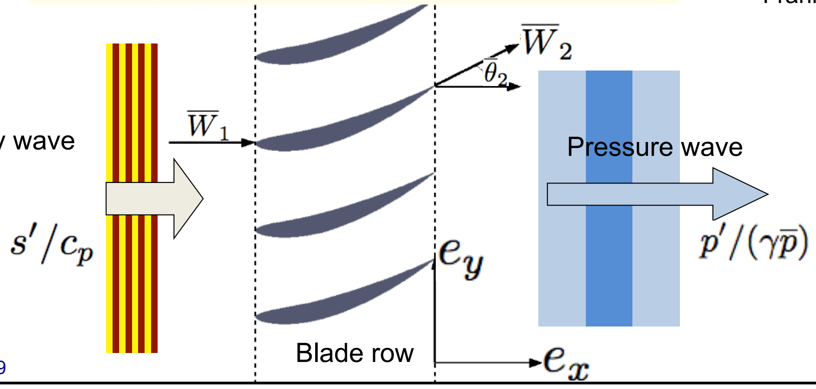

(A) Actuator disk analysis

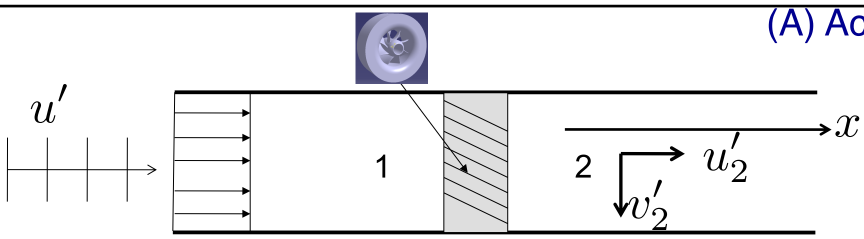

Based on the theory of Marble & Cumpsty (1977) :

$$u_1' = \frac{A}{\rho\, c}\exp i\omega\left(\frac{x}{c} - t\right) + \frac{A\, R}{\rho\, c}\exp i\omega\left(-\frac{x}{c} - t\right)$$

Incident and reflected acoustic wave

$$\boxed{u_2' = \frac{A}{\overline{\rho}\,\overline{c}}\exp i\omega\left(\frac{x}{\overline{c}} - t\right)}$$

Acoustic mode

$$\boxed{v_2' = B\exp i\omega\left(\frac{x}{\overline{u}_2} - t\right)}$$

Convective (vorticity) mode

(B) Filtered velocity signals

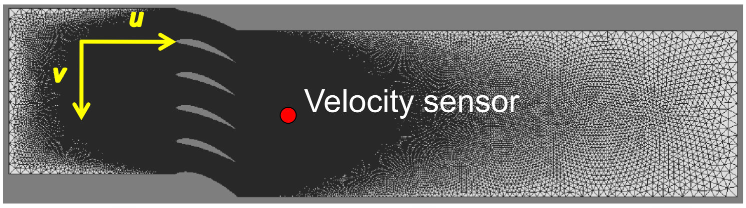

$$v_2' = u_2' \tan \overline{\theta}_2$$
$$\overline{\theta}_2 = 25°$$

$f = 60\,\mathrm{Hz}\quad u'_\infty = 1\,\mathrm{m\,s^{-1}}$ $\qquad f = 100\,\mathrm{Hz}\quad u'_\infty = 1\,\mathrm{m\,s^{-1}}$

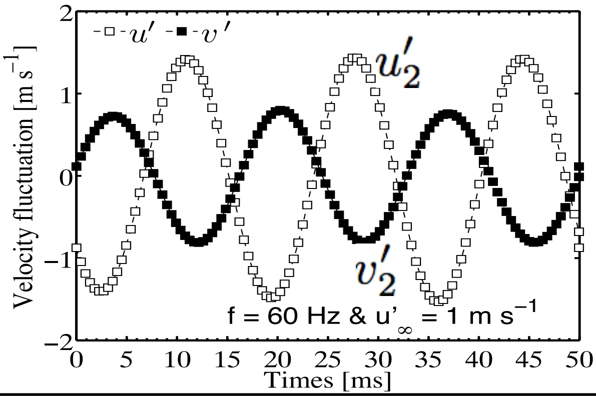

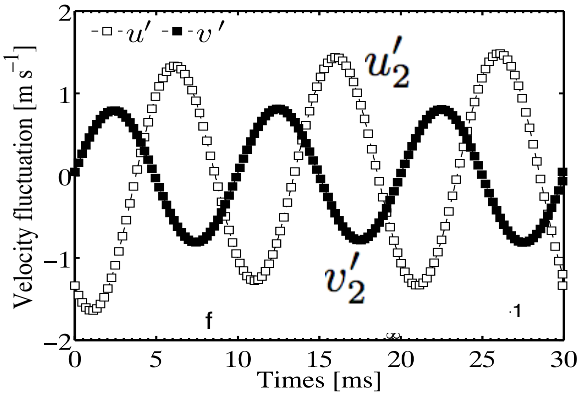

11

(C) Experiments

- Axial and azimuthal velocities are measured with LDV
- Cross-spectral density analysis provides the phase and corresponding velocity

$$\begin{cases} U_b = 2.67\,\mathrm{m\,s^{-1}} \\ f = 60\,\mathrm{Hz} \\ f = 100\,\mathrm{Hz} \\ u'/U_b = 0.5 \end{cases} \qquad \begin{cases} d = 22\,\mathrm{mm} \\ L = 50\,\mathrm{mm} \end{cases}$$

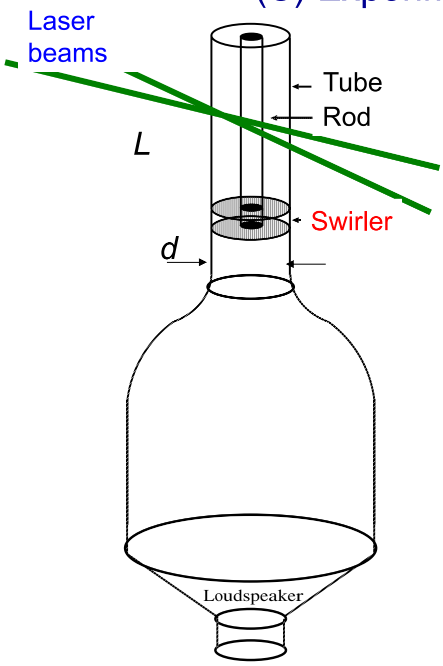

12

(C) Experimental phase data

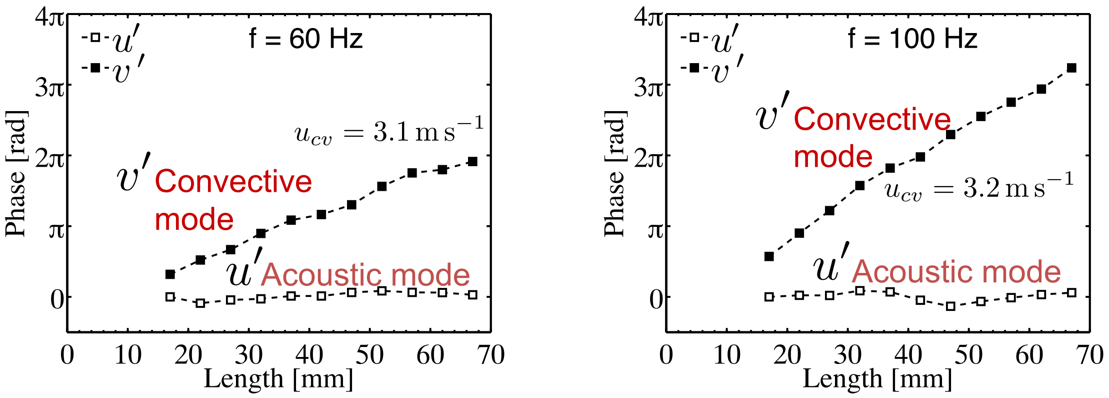

u' Acoustic mode v' Convective mode

P. Palies, D. Durox, T. Schuller and S. Candel (2011) *Journal of Fluid Mechanics.* **672**,545-569. Acoustic-convective mode conversion in an airfoil cascade.

(D) Mode conversion

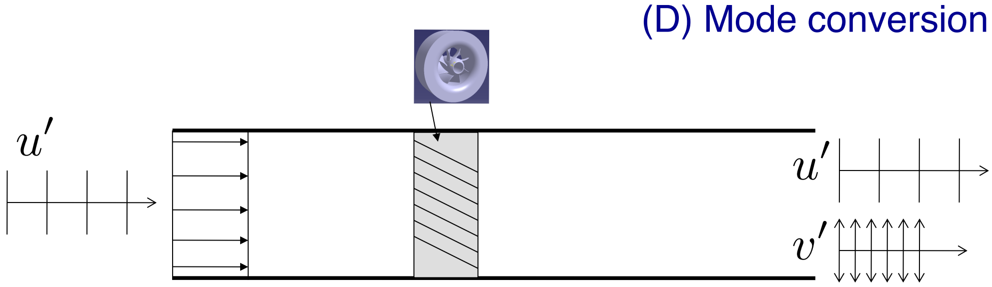

Mode conversion at the swirler generates

- An axial acoustic wave
- An azimuthal velocity fluctuation in the 3D case or a transverse velocity fluctuation in the 2D case.

This corresponds to a convective vorticity mode

There are important consequences on the flame dynamics

This interaction is reflected in the flame describing function

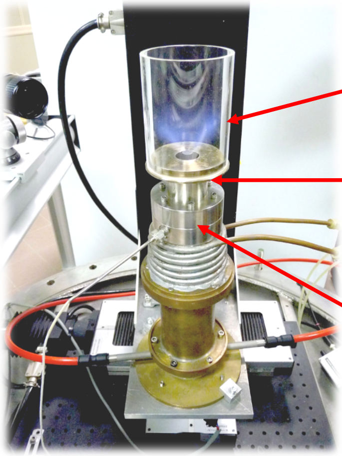

1 - Flame tube

2 - Injector

3 - Swirler

Global view of the experiment

$$
\begin{aligned}
U_b &= 2.67\,\mathrm{m\,s^{-1}}, \quad \text{(Flame A)} \\
U_b &= 4.13\,\mathrm{m\,s^{-1}} \quad \text{(Flame B)} \\
S &= 0.55 \quad \text{(Swirl number)} \\
\phi &= 0.7 \quad \text{(Equivalence ratio)}
\end{aligned}
$$

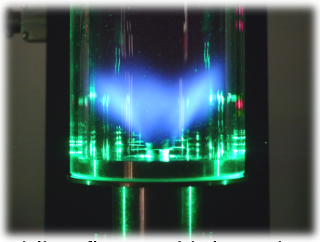

Swirling flame with laser beams

3 - Swirler

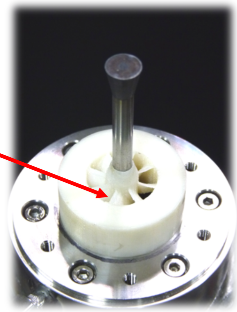

Close-up view of the axial swirler

The flame response can be characterizedin terms of a transfer function

$$
u'/\overline{U} \longrightarrow \boxed{\text{Combustion}} \longrightarrow \dot{Q}'/\overline{\dot{Q}}
$$

$$
\mathcal{F}(\omega) = \frac{\dot{Q}'/\overline{\dot{Q}}}{u'/\overline{U}}
$$

But the flame transfer function(FTF) only provides the linear growth rate in the analysis of instabilities,

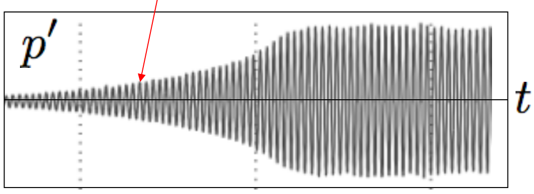

It is more informative to use the flame describing function

$$\xrightarrow{u'/\overline{U}} \boxed{\text{Combustion}} \xrightarrow{\dot{Q}'/\overline{\dot{Q}}}$$

$$\mathcal{F}(\omega, u') = \frac{\dot{Q}'/\overline{\dot{Q}}}{u'/\overline{U}}$$

The Flame Describing Function (FDF) extends the transfer function concept to the nonlinear case

In the FDF the flame response depends on the frequency and amplitude of the incident perturbation

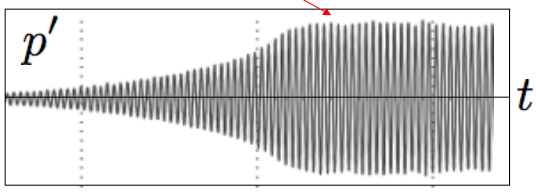

N. Noiray, D. Durox, T. Schuller and S. Candel (2008) *Journal of Fluid Mechanics* **615**, 139-167. A unified framework for nonlinear combustion instability analysis based on the describing function.

Nonlinear analysis

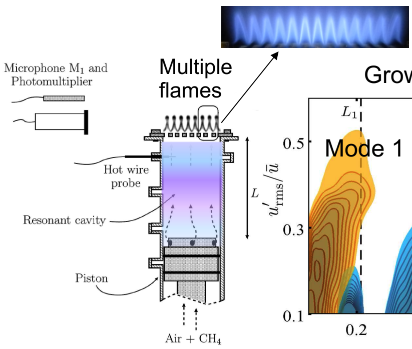

Growth rate contours

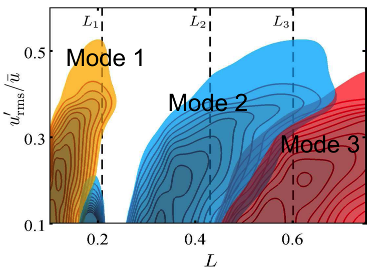

Comparison between limit cycle amplitudes predicted and measured

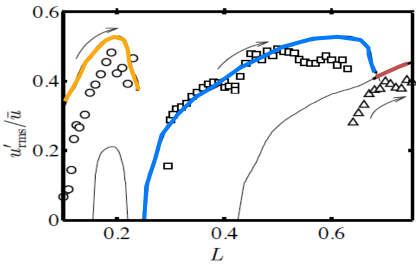

L is the size of the upstream manifold

The FDF can be used to predict
- Limit cycle amplitudes and frequencies (including frequency shift)
- Nonlinear triggering and mode switching

F. Boudy, D. Durox, T. Schuller, and S. Candel (2011) *Proceedings of the Combustion Institute* 33. 1121-1128. Nonlinear mode triggering in a multiple flame combustor.

F. Boudy, D. Durox, T. Schuller, G. Jomaas and S. Candel (2011) *Journal of Engineering for gas turbine and power.* 33, June. Article 061502. Describing function analysis of limit cycle in a multiple flame combustor.

Linear analysis

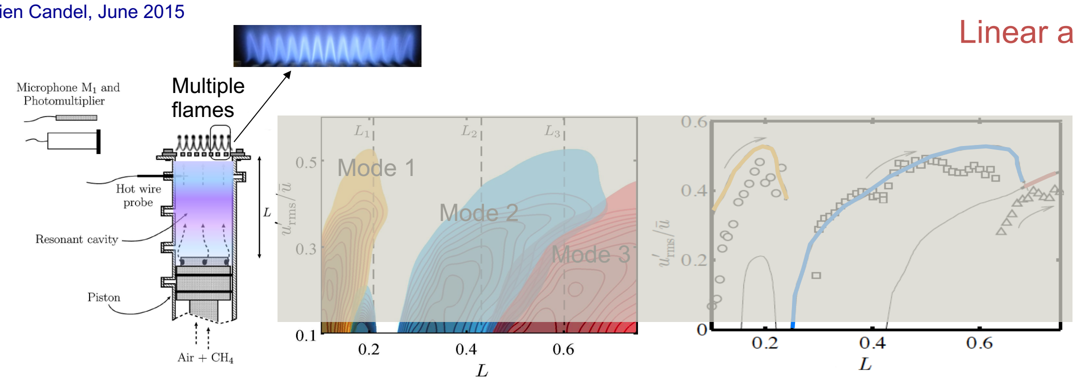

L is the size of the upstream manifold

Linear analysis provides an indication on growth rates but yields no information on limit cycle amplitudes and frequency shifting during instability growth

Linear analysis also gives no indication on nonlinear triggering and mode switching and misses many of the complexities observed in practice

Experimental determination of the Flame Describing Function

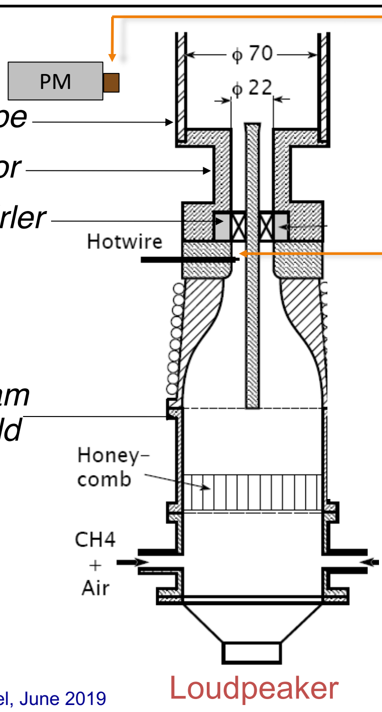

$$\mathcal{F}(\omega, u') = \frac{\dot{Q}'/\overline{\dot{Q}}}{u'/\overline{U}}$$

Hotwire is located on the upstream side of the swirler

A loudspeaker is at the base of the burner

Flame Describing Function

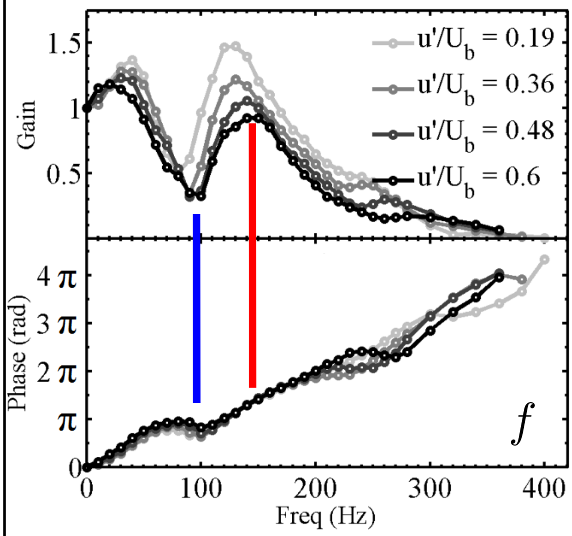

Operating Point B : U_b = 4.16 m/s

The characteristic frequencies of the gain response scale with a Strouhal number based on the bulk velocity

It is interesting to examine the maximum and minimum responses of the flame

P. Paliès, D. Durox, T. Schuller and S. Candel (2010) *Combustion and Flame.* 157(9) 1698-1717. The combined dynamics of swirler and turbulent swirling flames.

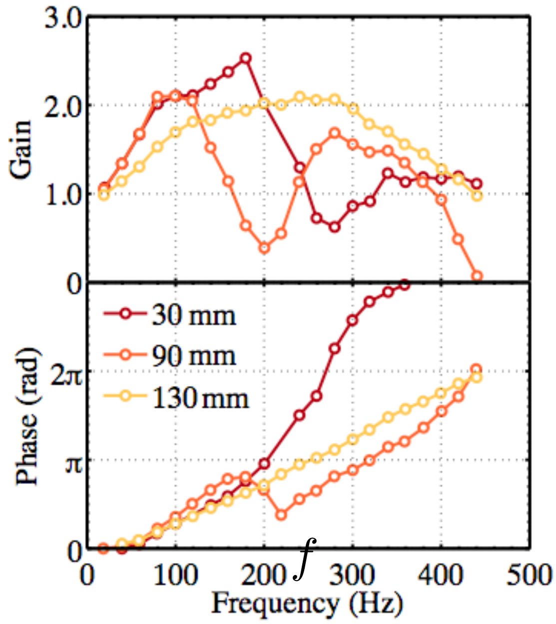

T. Komarek , W. Polifke (2010) *Journal of Engineering for Gas Turbine and Power*, 132:061503, Impact of swirl fluctuations on the flame response of a perfectly premixed swirl burner.

Effect of mode conversion process on flame dynamics

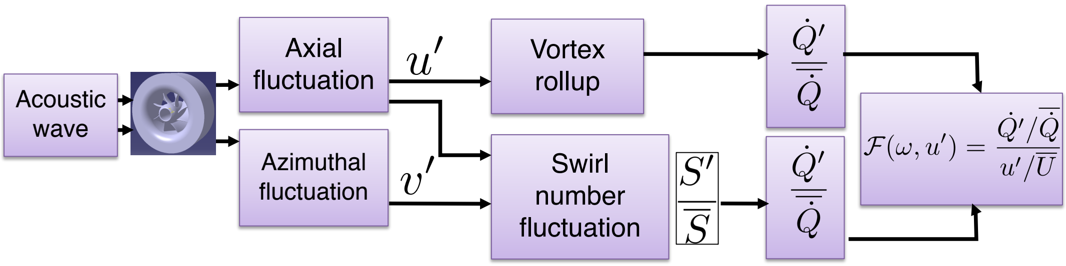

$$\frac{v'}{\overline{v}} = \frac{u'}{\overline{u}}\exp(i\phi) \qquad \frac{S'}{\overline{S}} = \frac{v_2'}{\overline{v}_2} - \frac{u_2'}{\overline{u}_2}$$

Two mechanisms combine to define the flame response to incident perturbations :

- Swirl number fluctuations
- Vortex rollup of the flame sheet

23

Velocity components at the injector exhaust and swirl number fluctuations

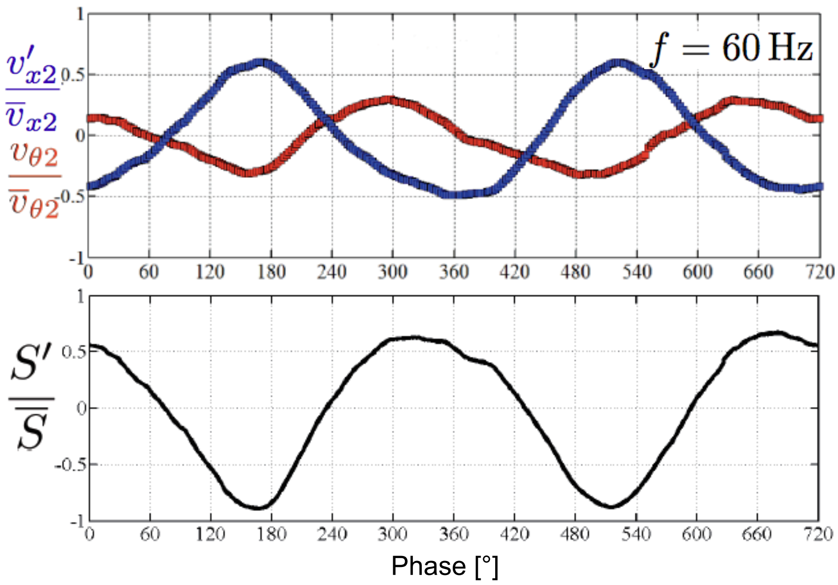

P. Paliès, D. Durox, T. Schuller, and S. Candel (2011) *Combustion and Flame.* 157 1698-1717. The combined dynamics of swirler and turbulent swirling flames.

24

Velocity components at the injector exhaust and swirl number fluctuations

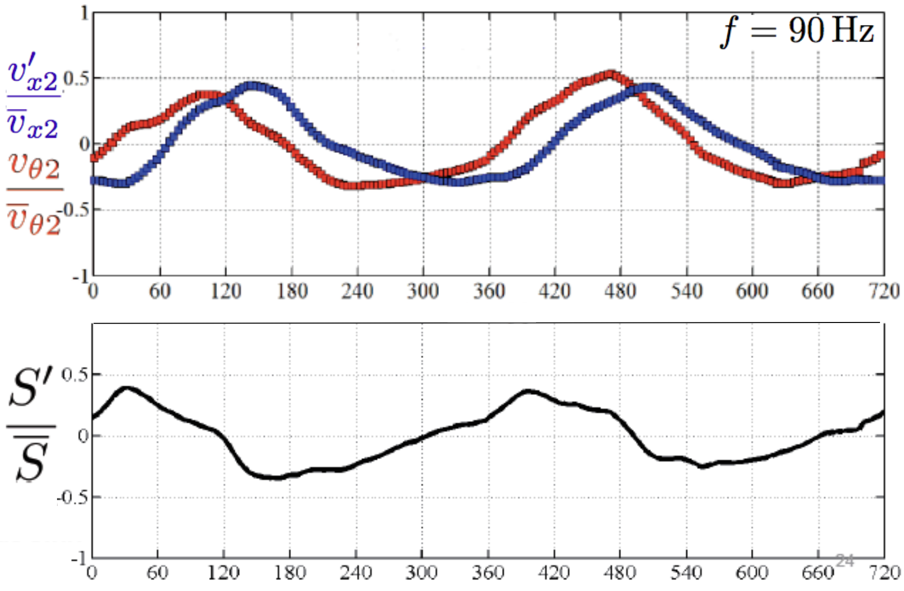

P. Paliès, D. Durox, T. Schuller, and S. Candel (2011) *Combustion and Flame.* 157 1698-1717. The combined dynamics of swirler and turbulent swirling flames.

Swirling flames dynamics

Swirl number fluctuations *act at the base of the flame and influence the flame angle*

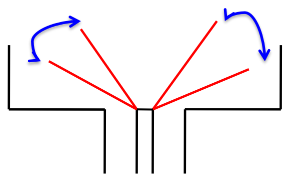

Vortex rollup
acts at the extremity of the flame

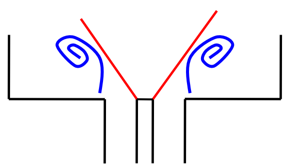

Depending on the frequency, these mechanisms interfer constructively or destructively to determine the transfer function gain

f = 60 Hz f = 90 Hz **Flame A**

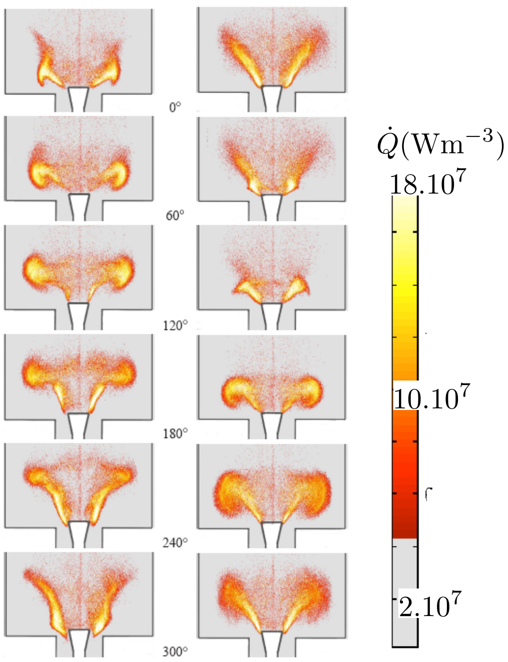

Flame dynamics can also be investigated with Large Eddy Simulations

Mesh : 6 millions cells

AVBP LES flow solver

Time step : $1.25 \times 10^{-7}\mathrm{s}$

Subgrid model : WALE

Thickened Flame Model
(thickening factor *F*=3.3)

Phase locked averaging
over 9 periods of
modulation

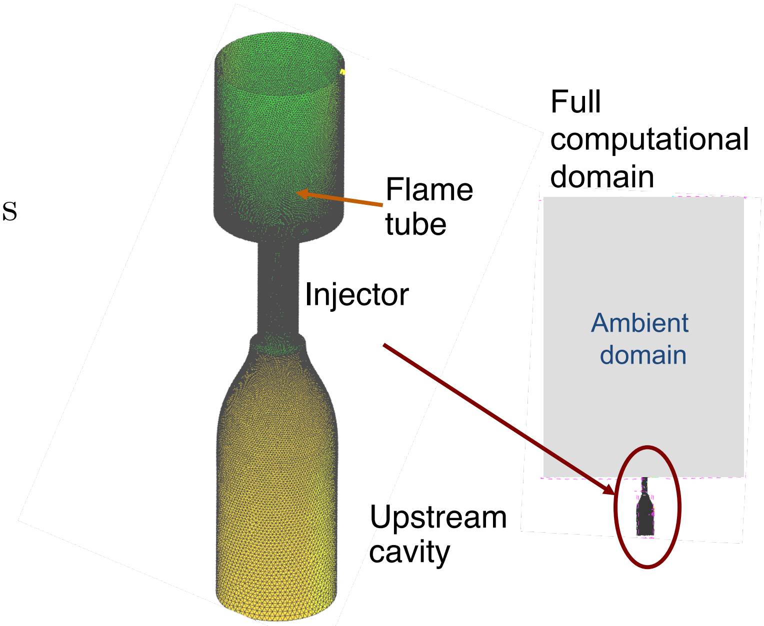

27

Experimental and simulated flame dynamics

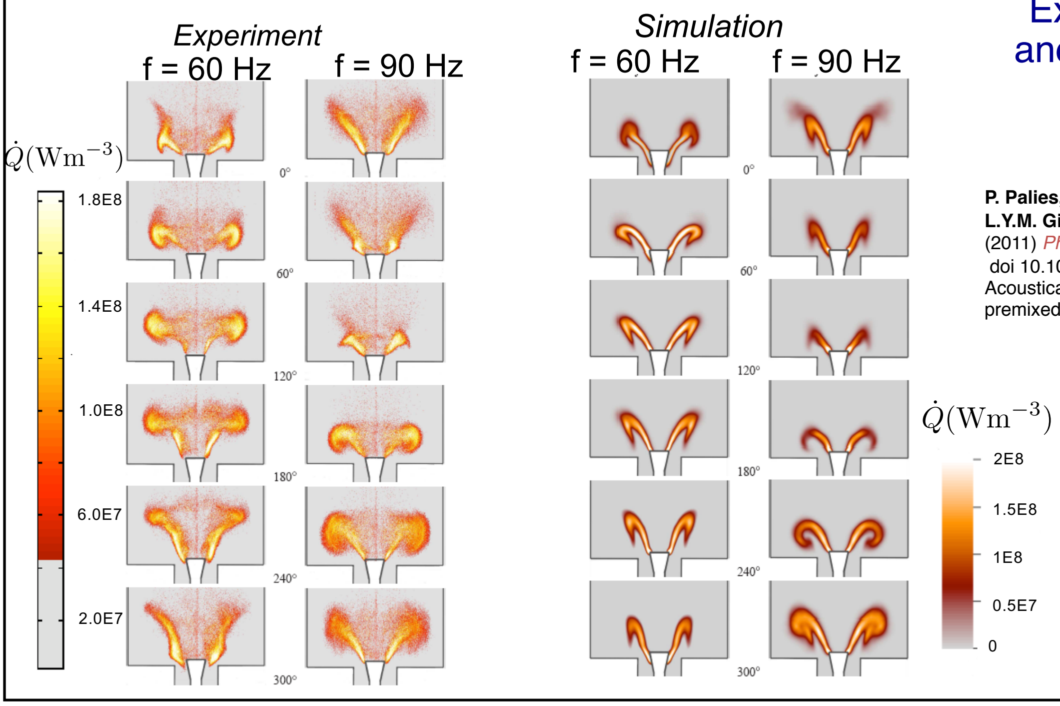

P. Palies, D. Durox, T. Schuller, L.Y.M. Gicquel and S. Candel (2011) *Physics of Fluids*, 23. doi 10.1063/1.3553276. Acoustically perturbed turbulent premixed swirling flame.

28

Flame transfer function modeling

The flame transfer function can be deduced from a perturbed level set equation

$$\frac{\partial G_1}{\partial t} + (\mathbf{v}_0 + S_D \mathbf{n}) \cdot \nabla G_1 = \underbrace{-\mathbf{v}_1 \cdot \nabla G_0}_{(1)}$$

Kinematic equation for a perturbed swirling flame :

$$\frac{\partial G_1}{\partial t} + (\mathbf{v}_0 + S_{T_0} \mathbf{n}) \cdot \nabla G_1 = \underbrace{-\mathbf{v}_1 \cdot \nabla G_0}_{(1)} + \underbrace{S_{T_1} |\nabla G_0|}_{(2)}$$

The flame motion is controlled by :
(1) Velocity fluctuations $\boldsymbol{v}_1$ (described by Schuller *et al.* 2003)
(2) Fluctuations in turbulent burning velocity S_{T1} (2)

29

Swirling flame transfer function

Kinematic equation for a perturbed swirling V-flame:

$$\frac{\partial G_1}{\partial t} + (\mathbf{v}_0 + S_{T_0} \mathbf{n}) \cdot \nabla G_1 = -\mathbf{v}_1 \cdot \nabla G_0 + S_{T_1} |\nabla G_0|$$

(1) FTF of a laminar V-flame submitted to convective disturbances

Effects of turbulent burning velocity

$$\mathcal{F}^s_{th}(\omega) = \mathcal{F}^V_{th} \times \left[1 - \frac{S_{T1}/S_{T0}}{v'_x/\bar{v}_x}\right]$$

(2) Fluctuations of the turbulent burning velocity S_{T1}/S_{T0} result from swirl number oscillations modeled in terms of the incident perturbations *v'_x and v'_θ*

$$\frac{S_{T_1}}{S_{T_0}} = \chi \frac{v'_\theta}{\bar{v}_\theta} + \zeta \frac{v'_x}{\bar{v}_x}$$

(3) Azimuthal disturbances convected by the mean flow downstream the swirler feature a phase lag at the burner outlet with respect to axial perturbations, which is a function of the distance to the swirler outlet

$$\frac{v'_\theta}{\bar{v}_\theta} = \frac{v'_x}{\bar{v}_x} \exp(i\phi)$$

30

Transfer function of swirling flames

$$\frac{v_{\theta 2}}{\overline{v}_{\theta 2}} = \frac{v_{z2}}{\overline{v}_{z2}} \exp(i\phi)$$

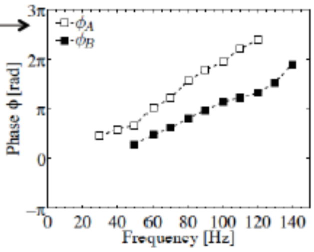

$$\mathcal{F}^s_{th}(\omega) = \underbrace{\mathcal{F}^v_{th}(\omega)}_{\text{FTF of a V flame}}\left[1 - \underbrace{(\zeta + \chi \exp(i\phi))}_{\text{Swirl number fluctuations}}\right]$$

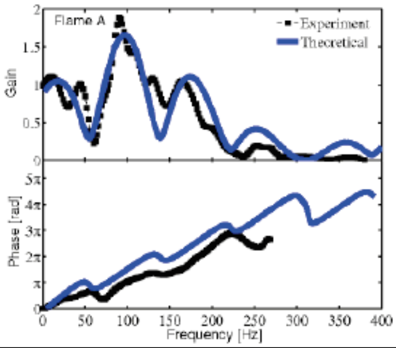

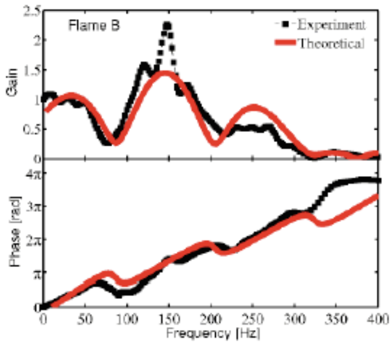

31

Flame transfer function modeling

Flame A, $U_b = 2.67\ m/s$

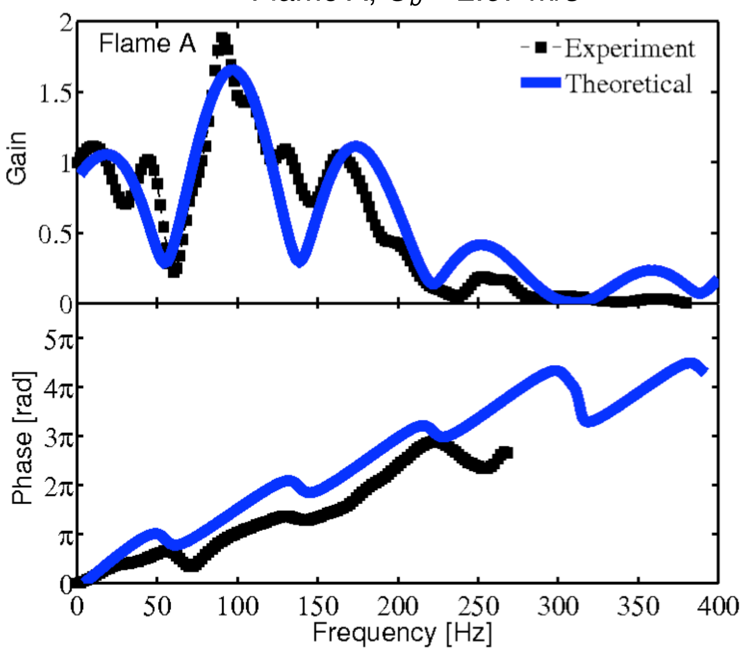

Good agreement between theory and experiment

Minimum and maximum locations are well retrieved

The phase is slightly overestimated in the model

32

Use the describing function to analyze a generic system comprising a single injector

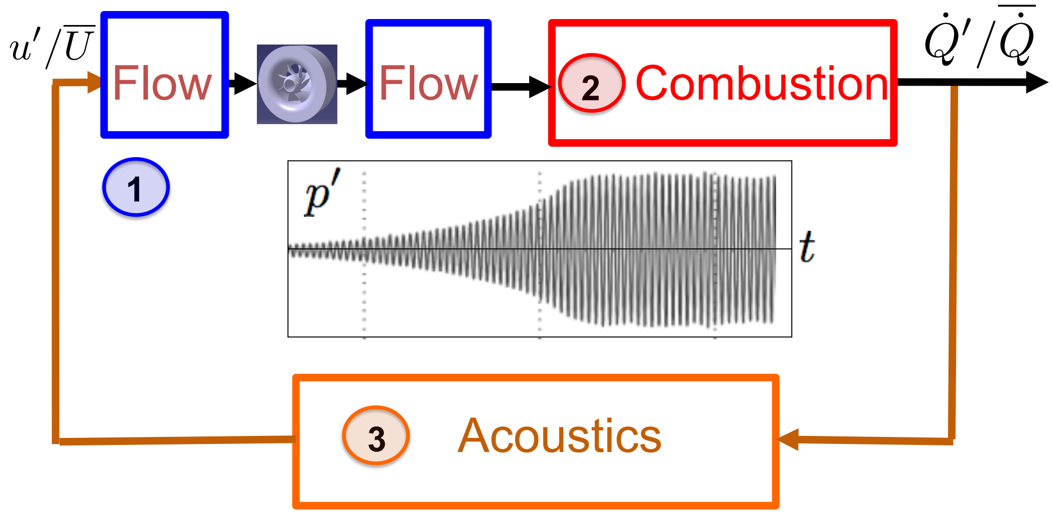

Predict combustion system instabilities
Determine amplitudes and frequencies at limit cycles.
Anticipate mode switching, triggering, hysteresis…

33

Prediction of instabilities

Four flame tube lengths l_3

l_3 = 100 mm
l_3 = 150 mm
l_3 = 200 mm
l_3 = 400 mm

Three upstream manifold lengths l_1

short : l_1 = 117 mm
medium : l_1 = 181 mm
long : l_1 = 245 mm

Two operating points

A : U_b = 2.67 m/s
B : U_b = 4.13 m/s

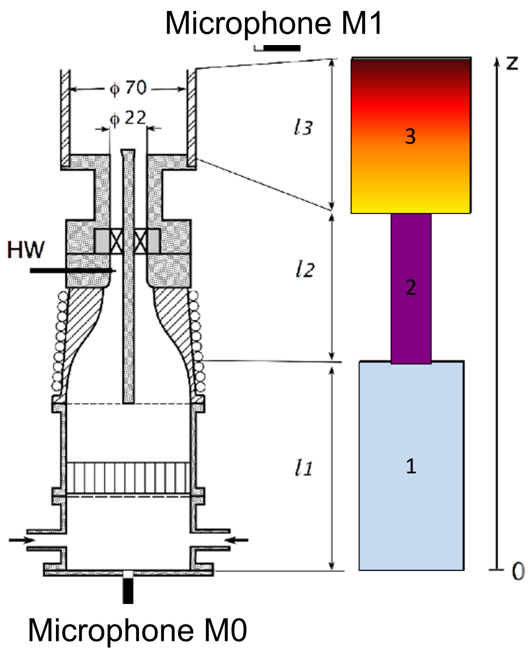

Physical system Model

34

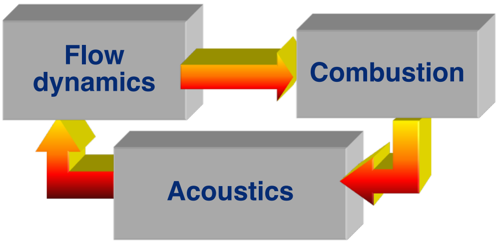

The flame response is represented by the flame describing function

$$\mathcal{F}(\omega, u') = \frac{\dot{Q}'/\overline{\dot{Q}}}{u'/\overline{U}}$$

- When this is combined with a network description of the system acoustics one obtains a nonlinear dispersion relation

$$\mathcal{D}(\omega, u') = 0$$

- The complex roots of this relation depend on the amplitude level

$$\omega = \omega_r(u') + i\omega_i(u')$$

- When the growth rate is greater than the damping rate the perturbation grows

$\omega_i(u') > \alpha$ The limit cycle is obtained when $\omega_i(u') = \alpha$

35

Combining the balance of mass and the balance of energy

$$\frac{1}{\gamma}\frac{\mathrm{d}\ln p}{\mathrm{d}t} + \nabla \cdot \mathbf{u} = \frac{1}{\rho c_p T}\dot{q}$$

Linearizing around the mean state assuming a low Mach number and isobaric combustion region

$$\frac{1}{\rho_0 c_0^2}\frac{\partial p'}{\partial t} + \nabla \cdot \mathbf{u}' = \frac{\gamma - 1}{\rho_0 c_0^2}\dot{q}'$$

Integrating over a control volume V with no pressure jump across the flame

$$\int_V \left[\frac{1}{\rho_0 c_0^2}\frac{\partial p'}{\partial t} + \nabla \cdot \mathbf{u}'\right]\mathrm{dV} = \int_V \left[\frac{\gamma - 1}{\rho_0 c_0^2}\dot{q}'\right]\mathrm{dV}$$

Assuming that the flame is compact with respect to the wavelength

$$\int_S \mathbf{u}' \cdot \mathbf{n}\,\mathrm{dS} = \frac{\gamma - 1}{\rho_0 c_0^2}\int_V \dot{q}'\,\mathrm{dV}$$

The difference between the volumetric flow rates is determined by fluctuations in heat release rate :

$$\boxed{S_3 u_3'} - \boxed{S_2 u_2'} = \frac{\gamma - 1}{\rho_0\, c_0^2}\dot{Q}'$$

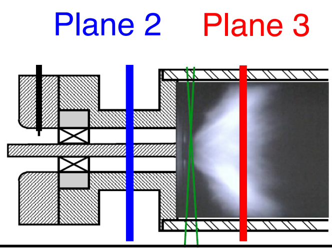

36

Theoretical modeling

Combining an acoustic analysis with the jump condition expressed previously one obtains the following system :

$$\underbrace{\begin{bmatrix} e^{ik_1l_1} & e^{-ik_1l_1} & -1 & -1 & 0 & 0 \\ 1 & -1 & 0 & 0 & 0 & 0 \\ \frac{S_1}{\rho_1c_1}e^{ik_1l_1} & \frac{-S_1}{\rho_1c_1}e^{-ik_1l_1} & \frac{-S_2}{\rho_2c_2} & \frac{S_2}{\rho_2c_2} & 0 & 0 \\ 0 & 0 & \frac{KS_2}{\rho_2c_2}e^{ik_2l_2} & \frac{KS_2}{\rho_2c_2}e^{-ik_2l_2} & \frac{-S_3}{\rho_3c_3} & \frac{S_3}{\rho_3c_3} \\ 0 & 0 & 0 & 0 & e^{ik_3l_3} & e^{-ik_3l_3} \\ 0 & 0 & e^{ik_2l_2} & e^{-ik_2l_2} & -1 & -1 \end{bmatrix}}_{M} \begin{bmatrix} A_1 \\ B_1 \\ A_2 \\ B_2 \\ A_3 \\ B_3 \end{bmatrix} = \begin{bmatrix} 0 \\ 0 \\ 0 \\ 0 \\ 0 \\ 0 \end{bmatrix}$$

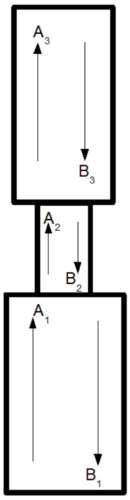

The determinant of this matrix must vanish *D(ω,u') = Det[M] = 0*
Roots of this dispersion relation *D(ω,u')* depend on the geometrical characteristics and on the flame response.

$$K = K(\omega, u')$$

Convention $a' = \tilde{a}e^{-i\omega t}$ $\quad \omega = \omega_r + i\omega_i \quad \omega_r = 2\pi f$

Results of instability analysis

Time traces of pressure and heat release rate for flame A with the short upstream manifold

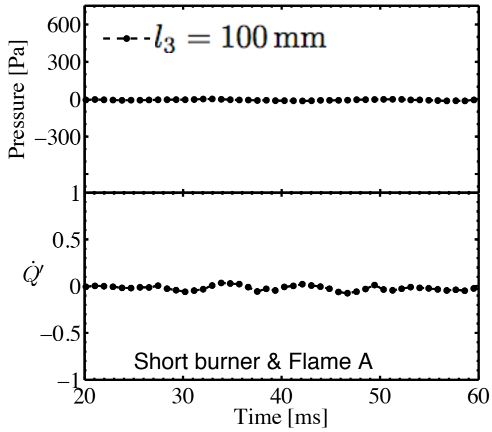

Stable case

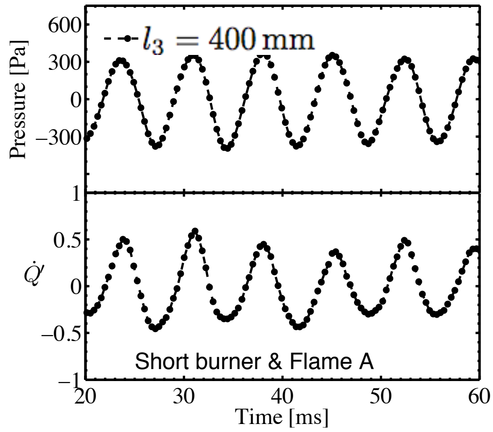

Unstable case

Results : flame A

Frequency - Growth rate trajectories for stable and *unstable* cases

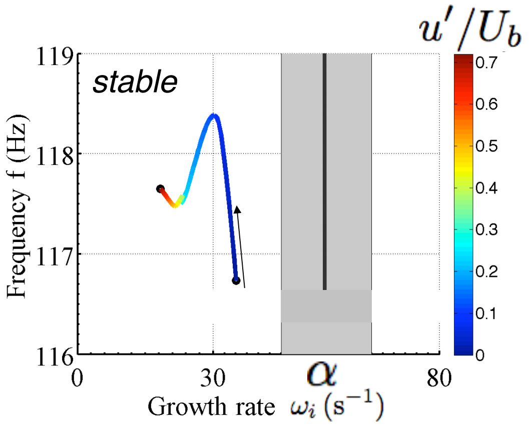

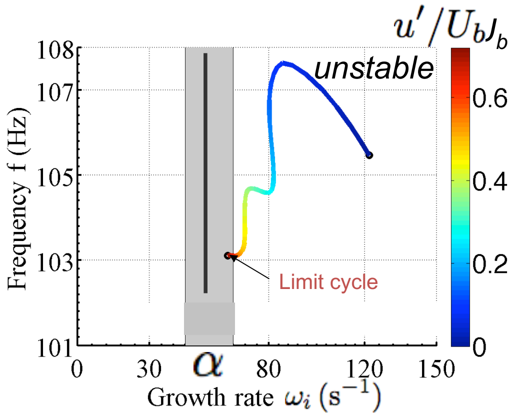

Medium upstream manifold – Flame tube l_3 = 100 mm

Trajectory is on the left of the gray zone indicating that the system is stable as observed during experiments for this configuration

Long upstream manifold – Flame tube l_3 = 400 mm

Trajectory is on the right of the gray zone indicating that the system is unstable as observed during experiments for this configuration. Limit cycle : f = 102 Hz – u'/U_b = 0.78

P. Palies, D. Durox, T. Schuller and S. Candel (2011) *Combustion and Flame*, 158, 1980-1991. Swirling flame instability analysis based on the flame describing function methodology.

C.F. Silva, F. Nicoud, T. Schuller, D. Durox, and S. Candel (2013) *Combustion and Flame.* 160, 1743-1754. Combining a Helmholtz solver with the Flame Describing Function to assess combustion instability in a swirled combustor.

39

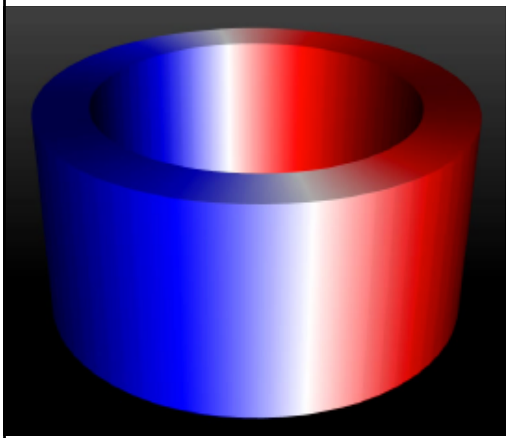

Combustion dynamics Lecture 9

S. Candel, D. Durox , T. Schuller

CentraleSupélec
Université Paris-Saclay, EM2C lab, CNRS

Tsinghua summer school, July 2021

1

Modal analysis of chamber acoustics

Rectangular cavities
Cylindrical cavities
Annular cavities

2

It is now useful to examine the modal response of cavities. We will successively consider rectangular and cylindrical enclosures. For simplicity one assumes rigid wall or pressure release boundary conditions. More general situations may also be handled with modal concepts but they are not considered in this study.

A rectangular chamber with rigid walls

We first consider a rectangular chamber bounded by rigid walls

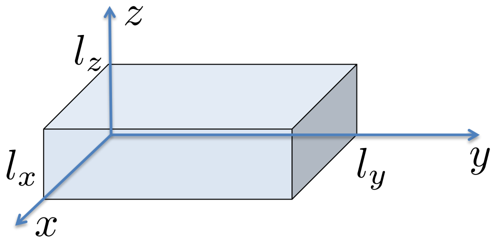

- Harmonic disturbances in the cavity may be written in the form

$$p(\boldsymbol{x},t) = \Psi(\boldsymbol{x})e^{-i\omega t}$$

$\Psi(\boldsymbol{x})$ satisfies the Helmholtz equation and rigid wall boundary conditions

$$\nabla^2\Psi + k^2\Psi = 0$$
$$\partial\Psi/\partial n = 0 \quad \text{on} \quad S$$

- The eigenfunctions which satisfy this boundary value problem and the corresponding eigenvalues form an infinite set of solutions.

  For a rectangular cavity one may search the eigenfunctions by making use of a factored form

$$\Psi_n(\boldsymbol{x}) = X(x)Y(y)Z(z)$$

When this expression is substituted in the Helmholtz equation one obtains

$$\frac{X''}{X} + \frac{Y''}{Y} + \frac{Z''}{Z} + k^2 = 0$$

- The method of separation of variables indicates at once that each of the three terms which appear on the left side of this equation must be constant. It is convenient to write these constants as

$$-k_x^2, \ -k_y^2, \ -k_z^2$$

respectively so that

$$X'' + k_x^2 X = 0, \ Y'' + k_y^2 Y = 0, \ Z'' + k_z^2 Z = 0$$

The constants appearing in these equations are related by

$$k^2 = k_x^2 + k_y^2 + k_z^2$$

- Consider now the boundary conditions for the function $X(x)$

These conditions are obtained by specifying that

$$\partial\Psi/\partial n = 0 \quad \text{on } x = 0 \text{ and on } x = l_x$$

which yield

$$\big(dX/dx\big)_{x=0} = 0, \quad \big(dX/dx\big)_{x=l_x} = 0$$

The solution of $X'' + k_x^2 X = 0$

which satisfies the boundary condition at *x*=0 has the form

$$X(x) = a \cos k_x x$$

The other boundary condition is satisfied if

$$\sin k_x l_x = 0$$

This requires that $k_x = n_x \pi / l_x$

Similar considerations finally yield

$$\Psi_{n_x n_y n_z}(\boldsymbol{x}) = A \cos \frac{n_x \pi x}{l_x} \cos \frac{n_y \pi y}{l_y} \cos \frac{n_z \pi z}{l_z}$$

and the corresponding eigenvalues takes the form

$$k^2_{n_x n_y n_z} = \pi^2 \left[\left(\frac{n_x}{l_x} \right)^2 + \left(\frac{n_y}{l_y} \right)^2 + \left(\frac{n_z}{l_z} \right)^2 \right]$$

Each mode is specified by a set of three integer indices.
The corresponding eigenfrequencies are of the form

$$\omega^2_{n_x n_y n_z} = c^2 \pi^2 \left[\left(\frac{n_x}{l_x} \right)^2 + \left(\frac{n_y}{l_y} \right)^2 + \left(\frac{n_z}{l_z} \right)^2 \right]$$

and the resonance frequencies of the cavity are given by

$$f_{n_x n_y n_z} = \frac{c}{2} \left[\left(\frac{n_x}{l_x} \right)^2 + \left(\frac{n_y}{l_y} \right)^2 + \left(\frac{n_z}{l_z} \right)^2 \right]^{1/2}$$

Application

A rectangular chamber is filled with hot gases at a temperature *T*=2000 K

$$l_x = l_y = 0.10\,\mathrm{m},\ l_z = 0.20\,\mathrm{m}$$

The mixture is characterized by a specific heat ratio
$\gamma = 1.4$ and a gas constant $r = \mathcal{R}/W = 287\,\mathrm{J/kg\,K}$

Calculate the eigenfrequencies corresponding to the first few modes
(1,0,0), (0,1,0), (0,0,1), (1,1,0), (1,0,1), (0,1,1) and (1,1,1).

The speed of sound in the cavity is:

$$c = \left[(1.4)(287)(2000)\right]^{1/2} = 896.4\,\mathrm{m/s}$$

The eigenfrequencies are given by

$$f_{n_x n_y n_z} = \frac{c}{2}\left[\left(\frac{n_x}{l_x}\right)^2 + \left(\frac{n_y}{l_y}\right)^2 + \left(\frac{n_z}{l_z}\right)^2\right]^{1/2}$$

$$\begin{aligned}
f_{0,0,1} &= c/2l_z = 2241\,\mathrm{Hz}\\
f_{1,0,0} &= f_{0,1,0} = c/2l_x = 4480\,\mathrm{Hz}\\
f_{1,0,1} &= f_{0,1,1} = (c/2l_z)(5)^{1/2} = 5011\,\mathrm{Hz}\\
f_{1,1,0} &= (c/2l_x)(2)^{1/2} = 6338\,\mathrm{Hz}\\
f_{1,1,1} &= (c/2l_z)(9)^{1/2} = 6723\,\mathrm{Hz}
\end{aligned}$$

A cylindrical cavity with rigid walls

- The chamber has a radius *a* and a length *L*

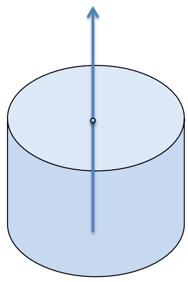

$$\Psi(r,\theta,z) = R(r)\Theta(\theta)Z(z)$$

Substituting this expression

$$\frac{R''}{R} + \frac{1}{r}\frac{R'}{R} + \frac{1}{r^2}\frac{\Theta''}{\Theta} + \frac{Z''}{Z} + k^2 = 0$$

- Applying the method of separation of variables one finds that

$$Z'' + k_z^2 Z = 0, \quad \Theta'' + n^2\Theta = 0$$

$$R'' + \frac{1}{r}R' + (k^2 - k_z^2 - \frac{n^2}{r^2})R = 0$$

$$k_\perp^2 = k^2 - k_z^2$$

- With this definition the radial equation becomes

$$R'' + \frac{1}{r}R' + (k_\perp^2 - \frac{n^2}{r^2})R = 0$$

- The solution of this set of problems now proceeds as follows. First consider the longitudinal equation and the relevant boundary conditions

$$Z'' + k_z^2 Z = 0$$

$$\big(dZ/dz\big)_{z=0} = 0, \quad \big(dZ/dz\big)_{z=L} = 0$$

The function *Z* which satisfies this problem is of form

$$Z(z) = \cos k_z z, \quad k_z = q\pi/L$$

Next let us examine the azimuthal equation

$$\Theta'' + n^2\Theta = 0$$

- The solution of this equation must be periodic with respect to the azimuthal angle

$$\Theta(\theta) = \Theta(\theta + 2\pi)$$

The general solution of this problem takes the form

$$\Theta(\theta) = Ce^{in\theta} + De^{-in\theta}$$

Finally consider the radial problem

$$R'' + \frac{1}{r}R' + (k_\perp^2 - \frac{n^2}{r^2})R = 0, \quad \big(dR/dr\big)_{r=a} = 0$$

The general solution of the radial differential equation may be written in terms of Bessel functions

$$R(r) = AJ_n(k_\perp r) + BY_n(k_\perp r)$$

- Since the Bessel function Y_n is singular as r=0 one deduces that the coefficient B vanishes

The boundary condition on the rigid cylinder yields

$$J'_n(k_\perp a) = 0$$

Consider the roots of the following equation

$$J'_n(\alpha_{mn}) = 0$$

- The radial wave numbers corresponding to these roots are of the form

$$k_{\perp mn} = \alpha_{mn}/a$$

It is sometimes more convenient to express the radial wavenumbers in terms of the roots of the following characteristic equation

$$J'_n(\pi\beta_{mn}) = 0$$

The wavenumbers then take the form

$$k_{\perp mn} = \pi\beta_{mn}/a$$

The modes of the closed cylindrical cavity take the following general form

$$\Psi_{mnq}(r,\theta,z) = J_n(k_{\perp mn} r)\cos\frac{q\pi z}{L}(ae^{in\theta} + be^{in\theta})$$

and the corresponding eigenfrequencies are given by

$$(\frac{\omega_{mnq}}{c})^2 = k_{\perp mn}^2 + k_z^2$$

or more explicitely

$$\omega_{mnq} = c\Big[\Big(\frac{\pi\beta_{mn}}{a}\Big)^2 + \Big(\frac{q\pi}{L}\Big)^2\Big]^{1/2}$$

- The frequencies associated with the cavity modes may be cast in the simple form

$$f_{mnq} = \frac{c}{2}\Big[\Big(\frac{\beta_{mn}}{a}\Big)^2 + \Big(\frac{q}{L}\Big)^2\Big]^{1/2}$$

A liquid rocket engine has a length *L*=1 m and a radius *a*=0.3 m. The gas temperature inside the chamber is *T*=3000 K and the gases have the following properties $\gamma = 1.3,\ r = 460\, J/kg\, K$
Determine the first few eigenfrequencies by considering that the rocket chamber behaves like a rigid enclosure.

The sound velocity in the chamber is

$$c = [(1.3)(460)(3000)]^{1/2} = 1339.4\,\mathrm{m/s}$$

The eigenfrequencies are given by

$$f_{mnq} = \frac{c}{2}\Big[\Big(\frac{\beta_{mn}}{a}\Big)^2 + \Big(\frac{q}{L}\Big)^2\Big]^{1/2}$$

Consider first the purely longitudinal modes characterized by m=0 and n=0.
Calculate the various frequencies as a home work problem

Modal analysis in annular configurations

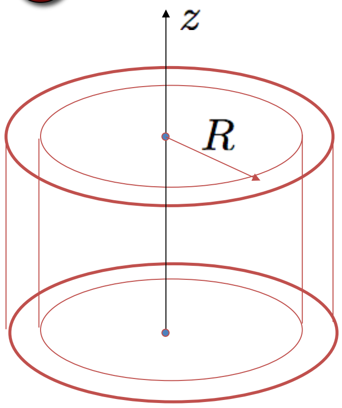

$$\frac{\partial^2 p}{\partial t^2} - \frac{c^2}{R^2}\frac{\partial^2 p}{\partial \theta^2} - c^2\frac{\partial^2 p}{\partial z^2} = 0$$

Harmonic modes are governed by a Helmholtz equation

$$\frac{c^2}{R^2}\frac{\partial^2 p}{\partial \theta^2} + c^2\frac{\partial^2 p}{\partial z^2} + \omega^2 p = 0$$

Purely azimuthal modes

$$p_n = a\exp(in\theta - i\omega_n t) + b\exp(-in\theta - i\omega_n t)$$

$$\omega_n = \frac{nc}{R} \qquad f_n = n\frac{c}{\mathcal{P}}$$

A standing mode in an annular chamber

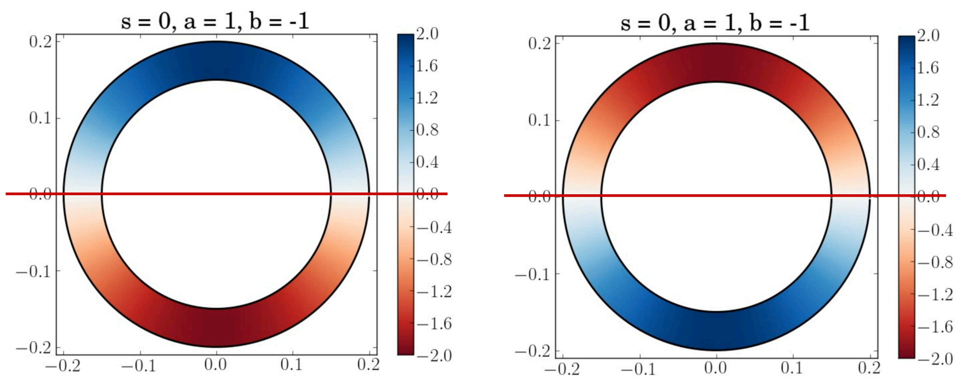

The nodal line is horizontal

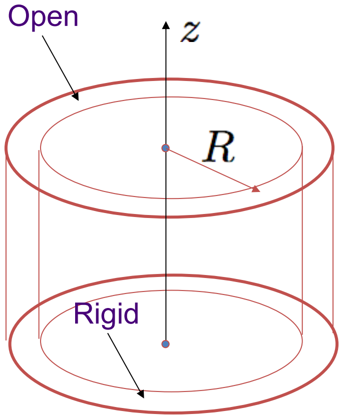

Purely longitudinal modes

$$p_m = \psi_m(z)\exp(-i\omega_m t)$$

$$\psi_m(z) = \cos(k_m z)$$

$$k_m l = (m - \frac{1}{2})\pi$$

$$f_m = (2m-1)(\frac{c}{4l})$$

Mixed mode

$$f_{mn} = [n^2(\frac{c}{\mathcal{P}})^2 + (2m-1)^2(\frac{c}{4l})^2]^{1/2}$$

$$f_{11} = [(\frac{c}{\mathcal{P}})^2 + (\frac{c}{4l})^2]^{1/2} \qquad f_{10} = \frac{c}{4l}$$

19

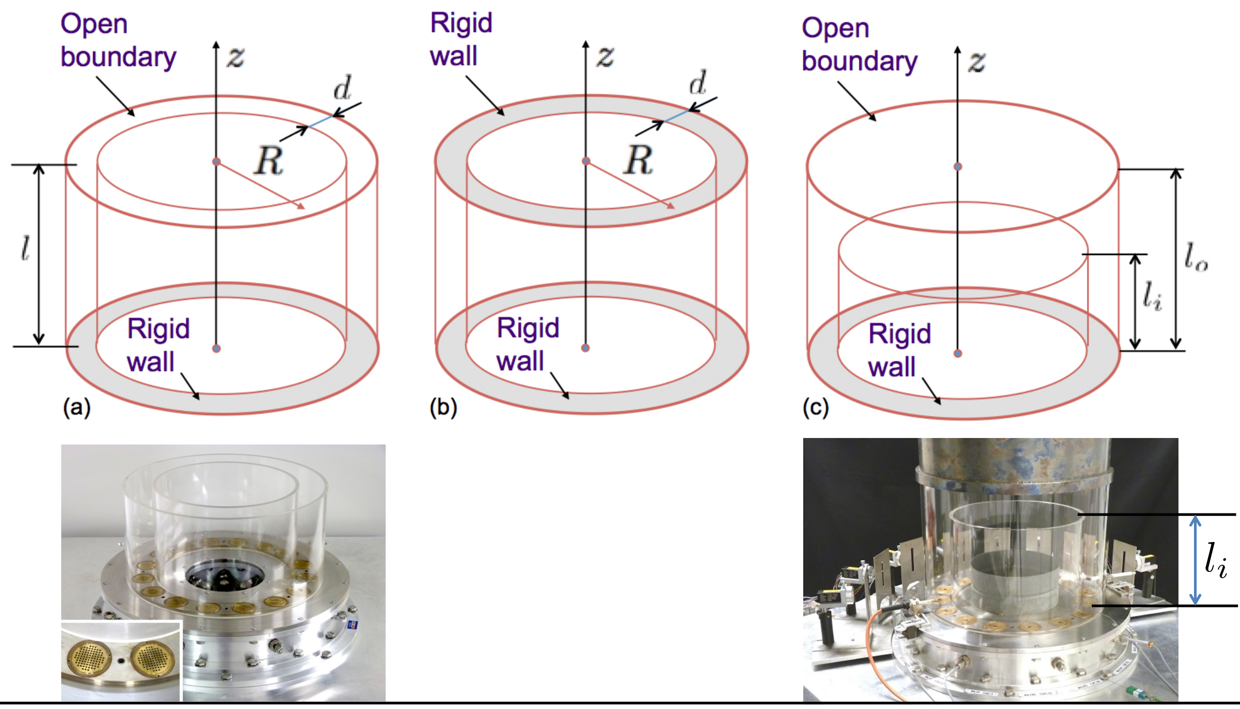

20

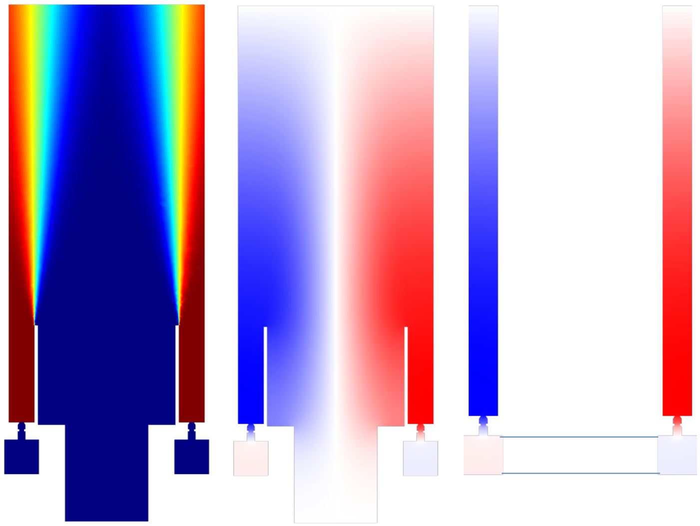

Temperature distribution in a geometry with unequal lateral walls

Pressure distribution corresponding to the 1A1L mode in the geometry with unequal lateral walls

Pressure distribution corresponding to the 1A1L mode in the geometry with equal lateral walls

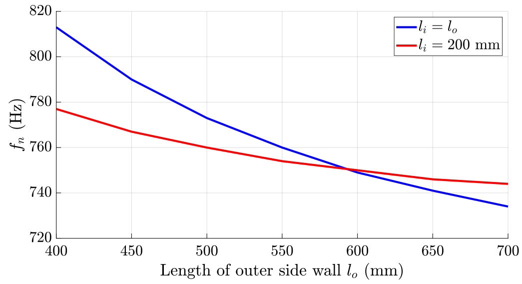

Blue : eigenfrequency evolution as a function of the lateral wall length (equal lengths)
Red : eigenfrequency evolution in the unequal length case

G. Vignat (2020) PhD Thesis, CentraleSupélec, University Paris-Saclay

21

Combustion dynamics
Lecture 10a

S. Candel, D. Durox , T. Schuller

CentraleSupélec
Université Paris-Saclay, EM2C lab, CNRS

Tsinghua summer school, July 2021

Annular combustor dynamics

- Annular combustors are used in many practical systems like jet engines and gas turbines
- In these devices combustion oscillations may be coupled by azimuthal modes
- Because the diameter is the largest dimension, these modes occur in the lower frequency range where the flames established in the chamber are most susceptible to perturbations
- Azimuthal modes are usually less well damped than the longitudinal modes
- Azimuthal coupling raises scientific and technical issues

Annular combustor dynamics constitutes a central issue in many current applications

Overview of swirling flame dynamics research

Single injector systems 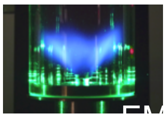	Annular systems with multiple injectors	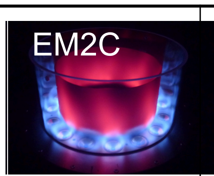	
Theory Simulations Experiments	Theory	Simulations	Experiments
Very large number of investigations	Relatively large number	A few recent simulations	Very few model scale experiments

G. Vignat, D. Durox, T. Schuller and S. Candel (2020) *Combustion Science and Technology.* Combustion dynamics of annular systems. doi.org/10.1080/00102202.2020.1734583

L. Gicquel, G. Staffelbach, T. Poinsot, *Progress in Energy and Combustion Science* 38 (6)(2012) 782–817. Large Eddy Simulations of gaseous flames in gas turbine combustion chambers.

Y. Huang, V. Yang, *Progress in Energy and Combustion Science* 35 (4) (2009) 293–364. Dynamics and stability of lean-premixed swirl-stabilized combustion.

T. C. Lieuwen, V. Yang (eds.), Combustion instabilities in gas turbines, Vol. 210 of Progress in Astronautics and Aeronautics, American Institute of Aeronautics and Astronautics, Inc., 2005.

3

Real systems and laboratory scale annular combustors

CFM 56 turbofan

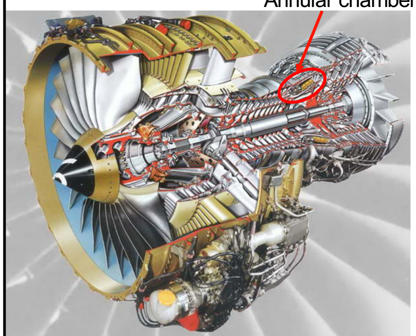

- Annular geometry
- Multiple swirled injectors
- Liquid phase injection (kerosene /air)
- High pressure

Annular combustor MICCA2

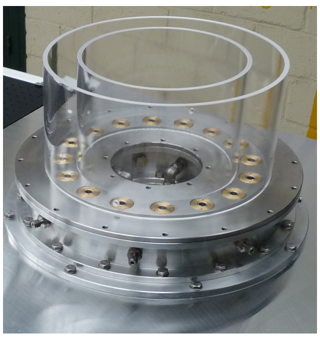

- Annular geometry
- Multiple swirled injectors
- Premixed (propane/air)
- Atmospheric pressure

Annular combustor MICCA-Spray

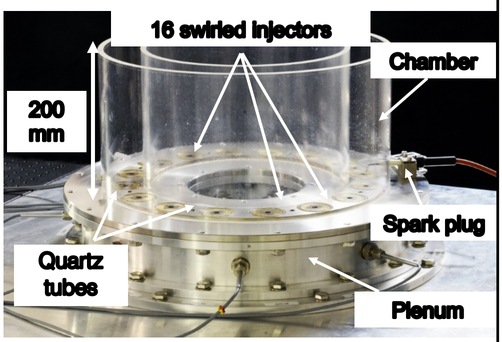

- Annular geometry
- Multiple swirled injectors
- Liquid injection (heptane/air)
- Atmospheric pressure

4

MICCA: Premixed C_3H_8/Air

Bourgouin, JF, Durox, D, Schuller, T, Beaunier, J, Candel, S (2013) *Ignition dynamics of an annular combustor equipped with multiple swirling injectors, Combust Flame* **160**, pp. 1398-1413.

N. A. Worth and J.R. Dawson (2013) *Proc. of the Combust. Inst.* 34, 3127-3134. Self-excited circumferential instabilities in a model annular gas turbine combustor: global flame dynamics.

Two driver units modulate the flow
Hot wire records the velocity fluctuation u'
Photomultiplier records the heat release rate fluctuation $\dot{Q}'$

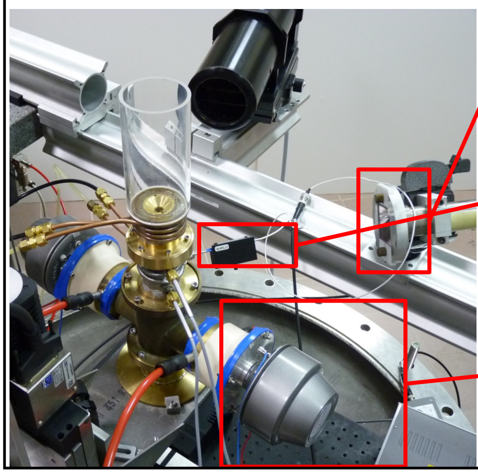

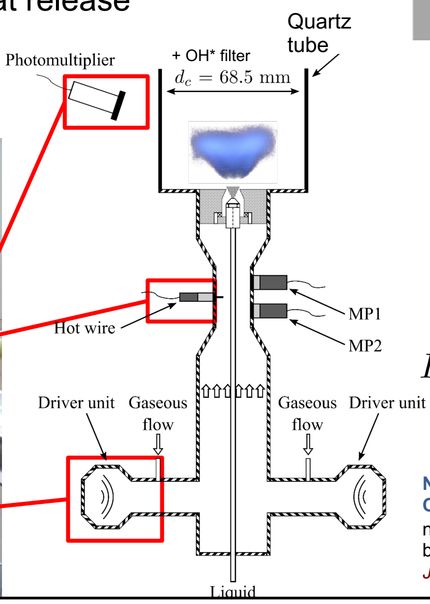

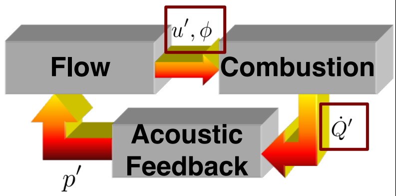

FDF measurements

$$F(\omega, u') = \frac{\dot{Q}'(\omega, u')/\overline{\dot{Q}}}{u'(\omega)/u}$$

Noiray, N., Durox, D., Schuller, T., & Candel, S. (2008). A unified framework for nonlinear combustion instability analysis based on the flame describing function. *Journal of Fluid Mechanics*. **615**, 139-167.

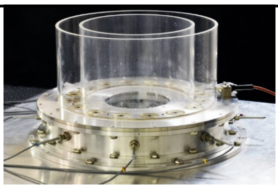

Experimental methodology

MICCA-Spray

Experimental observations Instability data

Single burner: flame dynamics

Changes in the flame shape induce modifications of the flame response

Theoretical framework

Geometrical modifications of the injector

Transfer function tayloring

FDF measurements

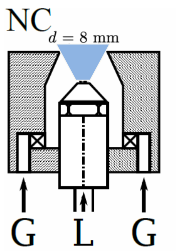

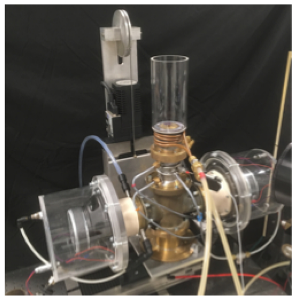

SICCA-Spray set up

7

MICCA annular combustor fed by premixed air and propane

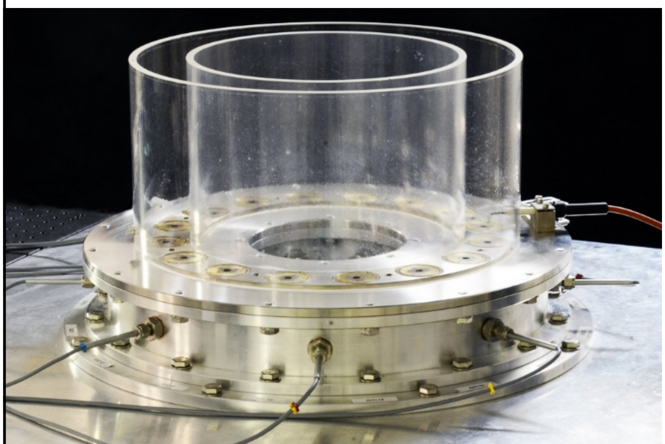

The MICCA annular combustor

Injectors feature in this case an exhaust cup and the flames spread in the lateral direction

8

Five microphones Pr1 to Pr5
An intensified high speed CCD camera

Experimental setup

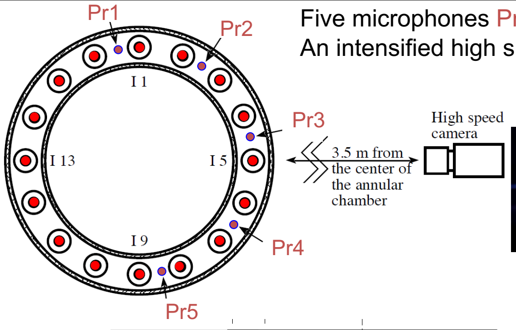

Detailed view of a swirler

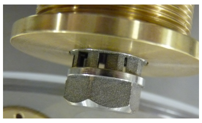

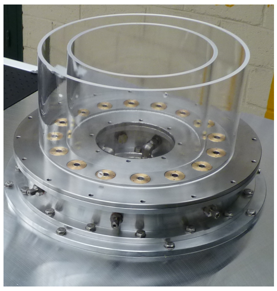

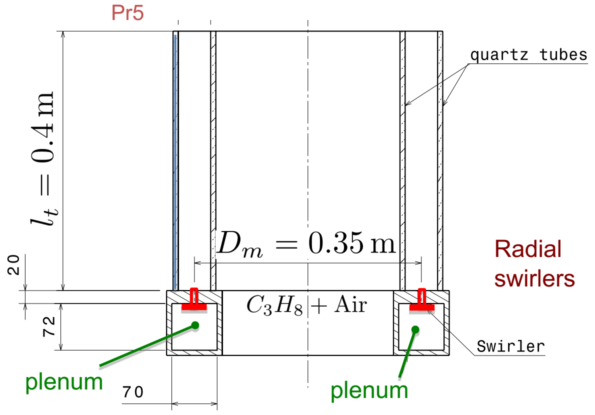

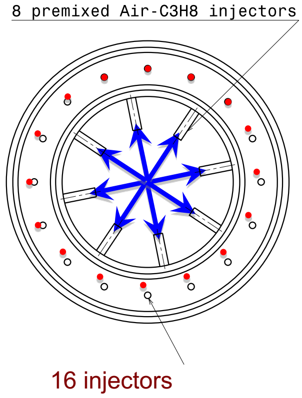

Five microphones Pr1 to Pr5
An intensified high speed CCD camera

Experimental setup

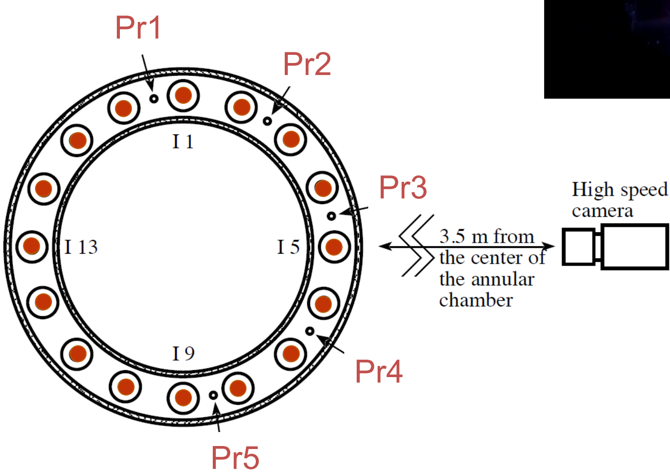

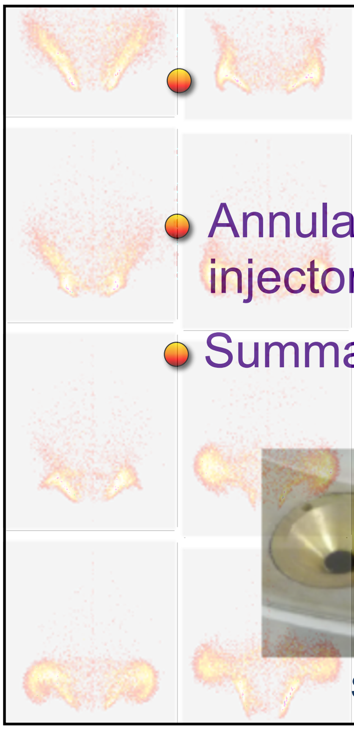

- Annular systems with multiple matrix injectors (MICCA 3)
- Summary points

MICCA 2

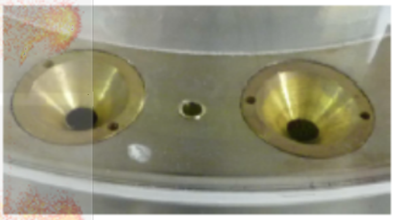

Swirling injectors

MICCA 3

Matrix injectors

11

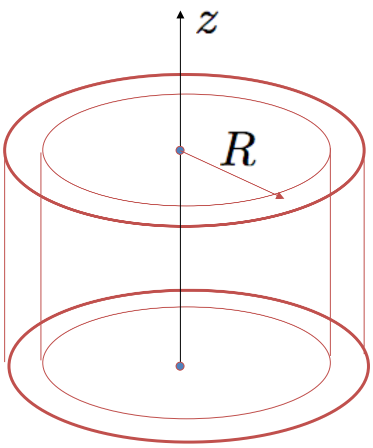

Purely azimuthal modes

Modal structures in annular systems

$$\frac{\partial^2 p}{\partial t^2} - \frac{c^2}{R^2}\frac{\partial^2 p}{\partial \theta^2} - c^2\frac{\partial^2 p}{\partial z^2} = 0$$

Harmonic modes are governed by a Helmholtz equation

$$\frac{c^2}{R^2}\frac{\partial^2 p}{\partial \theta^2} + c^2\frac{\partial^2 p}{\partial z^2} + \omega^2 p = 0$$

$$p_n = a\exp(in\theta - i\omega_n t) + b\exp(-in\theta - i\omega_n t)$$

$$\omega_n = \frac{nc}{R} \qquad f_n = n\frac{c}{\mathcal{P}}$$

12

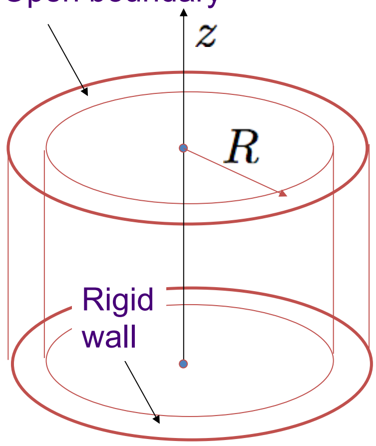

Purely longitudinal modes

$$p_m = \psi_m(z)\exp(-i\omega_m t)$$

$$\psi_m(z) = \cos(k_m z)$$

$$k_m l = (m - \frac{1}{2})\pi$$

$$f_m = (2m-1)(\frac{c}{4l})$$

Mixed modes

$$f_{mn} = [n^2(\frac{c}{\mathcal{P}})^2 + (2m-1)^2(\frac{c}{4l})^2]^{1/2}$$

$$f_{11} = [(\frac{c}{\mathcal{P}})^2 + (\frac{c}{4l})^2]^{1/2} \qquad f_{10} = \frac{c}{4l}$$

13

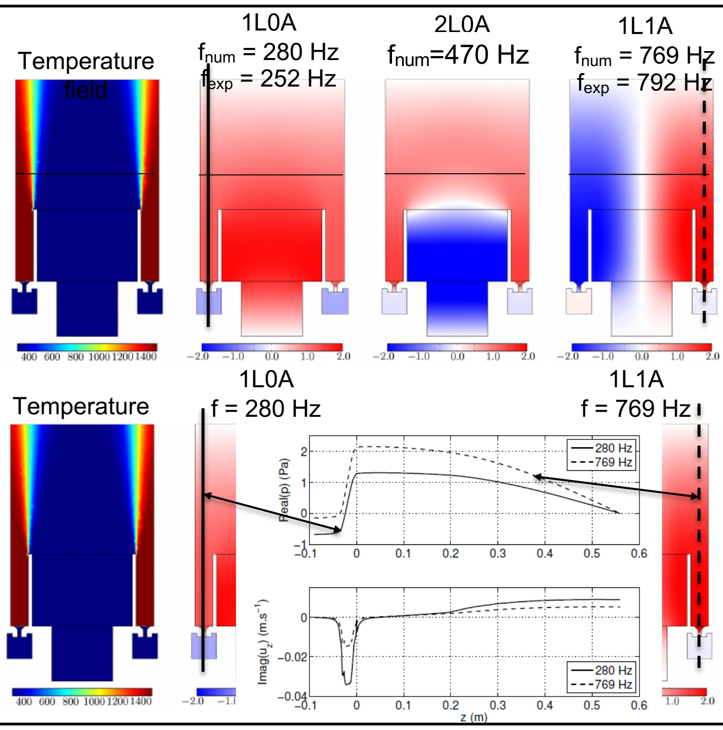

Modal identification

The mode 1L0A approximately corresponds to *m=1, n=0*

The mode 1L1A approximately corresponds to *m=1,n=1*

14

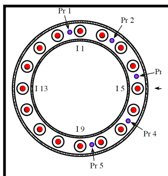

Longitudinal mode 1L0A
(f=252 Hz)

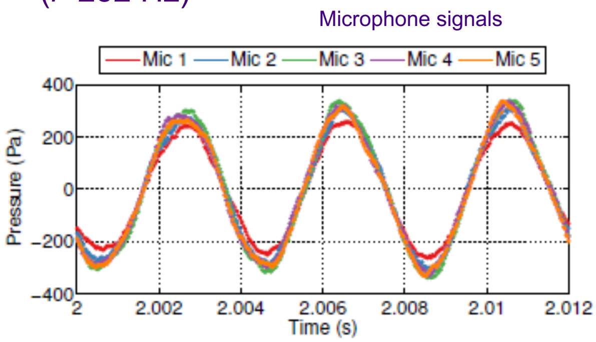

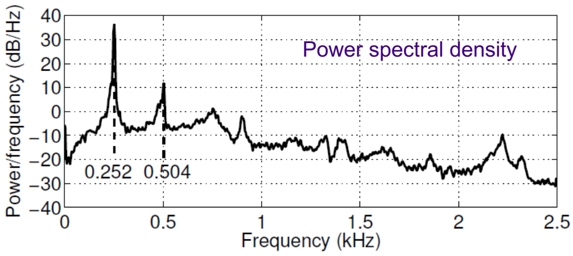

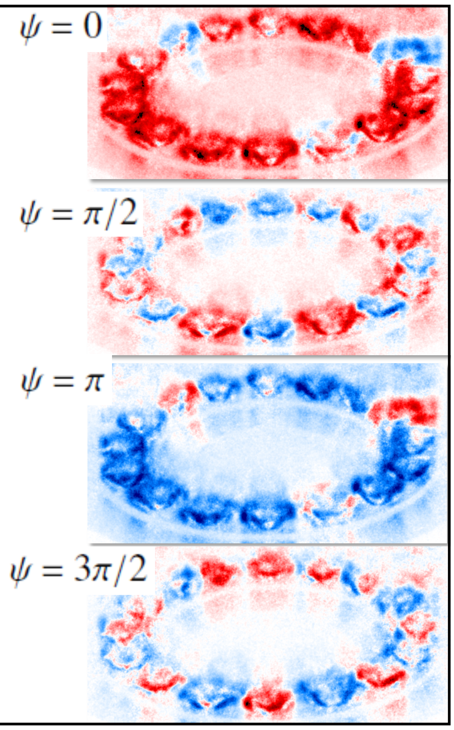

First azimuthal mode (1A)

The pressure field is a sum of two waves rotating in the counterclockwise and clockwise directions

$$p(\theta, t) = a\exp(i\theta - i\omega t) + b\exp(-i\theta - i\omega t)$$

$$s = \frac{|a| - |b|}{|a| + |b|}$$

s = -1: rotating mode in the clockwise direction
s = 0: standing mode
s = 1: rotating mode in the counterclockwise direction

This spin ratio differs from that introduced by Evesque et al.(203)

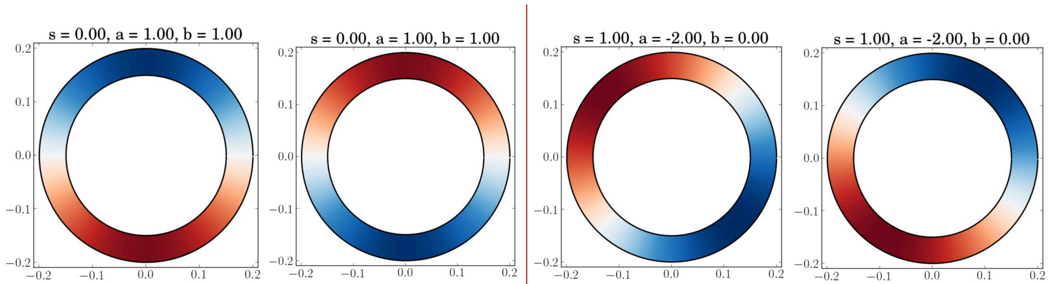

Standing (s=0) Spinning (s=1)

S. Evesque, W. Polifke and C. Pankiewitz (2003) Spinning and azimuthally standing acoustic modes in annular combustors. AIAA Paper 2003-3182.

Pressure signal reconstruction and spin ratio determination

$$p(\theta,t) = a\exp(i\theta - i\omega t) + b\exp(-i\theta - i\omega t)$$

The wave amplitudes a and b can be determined from microphone data

$$\underbrace{\begin{pmatrix} p_1 \\ p_2 \\ \vdots \\ p_n \end{pmatrix}}_{P} = \underbrace{\begin{pmatrix} \exp(i\theta_1) & \exp(-i\theta_1) \\ \exp(i\theta_2) & \exp(-i\theta_2) \\ \vdots & \vdots \\ \exp(i\theta_n) & \exp(-i\theta_n) \end{pmatrix}}_{M} \times \begin{pmatrix} a\exp(-i\omega t) \\ b\exp(-i\omega t) \end{pmatrix} \Rightarrow \begin{pmatrix} a\exp(-i\omega t) \\ b\exp(-i\omega t) \end{pmatrix} = (M^* M)^{-1} M^* P \Rightarrow s = \frac{|a|-|b|}{|a|+|b|}$$

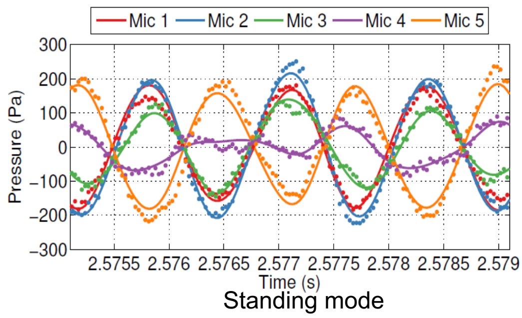

Standing mode

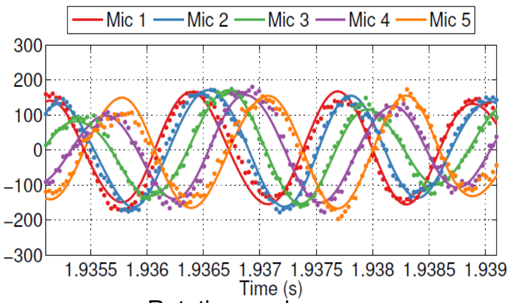

Rotating mode

Symbols : experimental data, Continuous lines : reconstructed signals

17

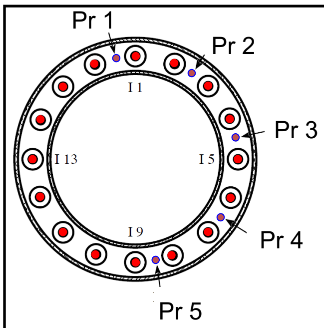

Standing mode

The spin ratio is close to zero. This corresponds to a standing mode

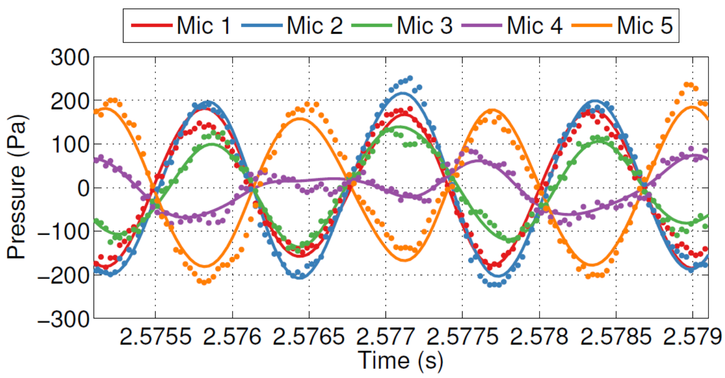

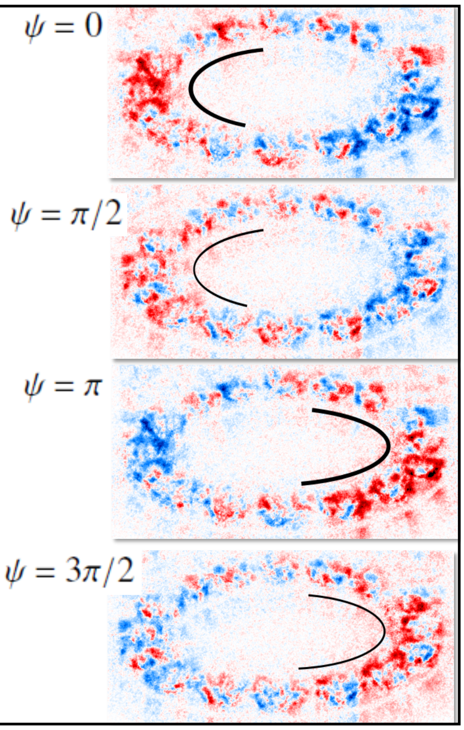

18

Standing mode

Flame dynamics coupled by the 1A1L mode at a frequency *f*=792 Hz

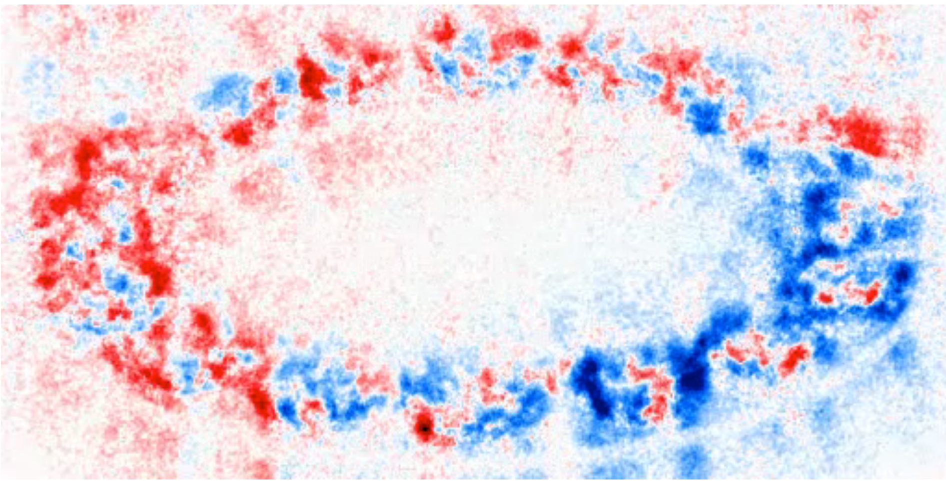

J.F. Bourgouin, D. Durox, T. Schuller, J. Moeck and S. Candel (2013) ASME Paper GT 2013-95010. Self-sustained Instabilities in an Annular Combustor Coupled by Azimuthal and Longitudinal Acoustic Modes.

19

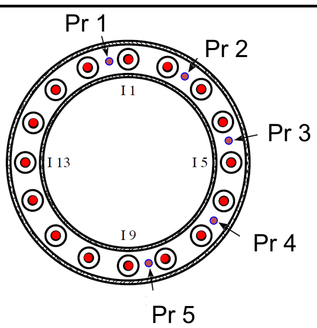

Instability coupled by a rotating mode 1A1L at a frequency of *f*=792 Hz

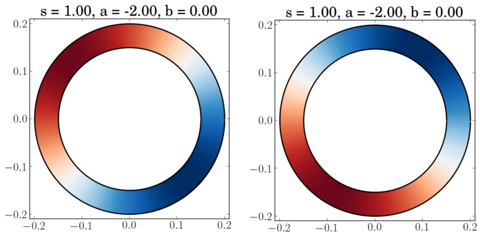

The spin ratio is close to one. The mode rotates in the counterclockwise direction

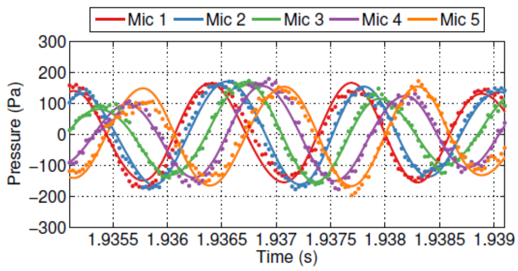

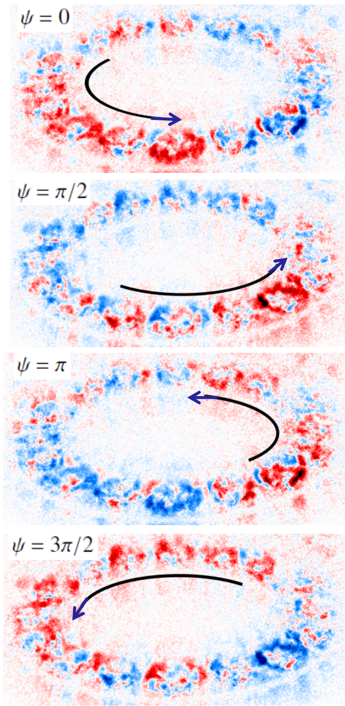

20

Continuous switching from a quasi-spinning mode to a standinging mode

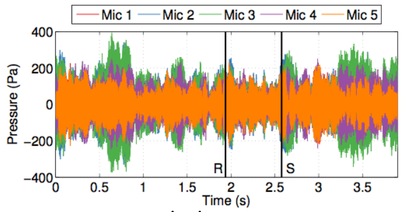

spinning standing

$$p(\theta,t) = a\exp(i\theta - i\omega t) + b\exp(-i\theta - i\omega t)$$

$$s = \frac{|a|-|b|}{|a|+|b|}$$

s = + 1 or -1: spinning

s = 0: standing

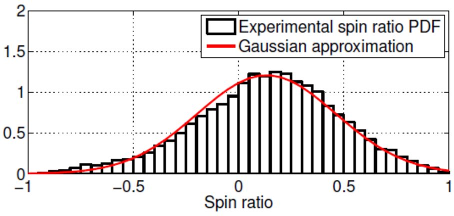

(spinning)

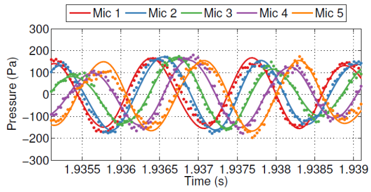

(standing)

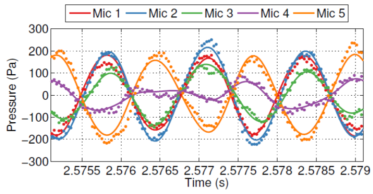

J.F. Bourgouin, D. Durox, T. Schuller, J. Moeck and S. Candel (2013) ASME Paper GT 2013-95010. Self-sustained Instabilities in an Annular Combustor Coupled by Azimuthal and Longitudinal Acoustic Modes.

21

A calculated rotating mode in a gas turbine combustor

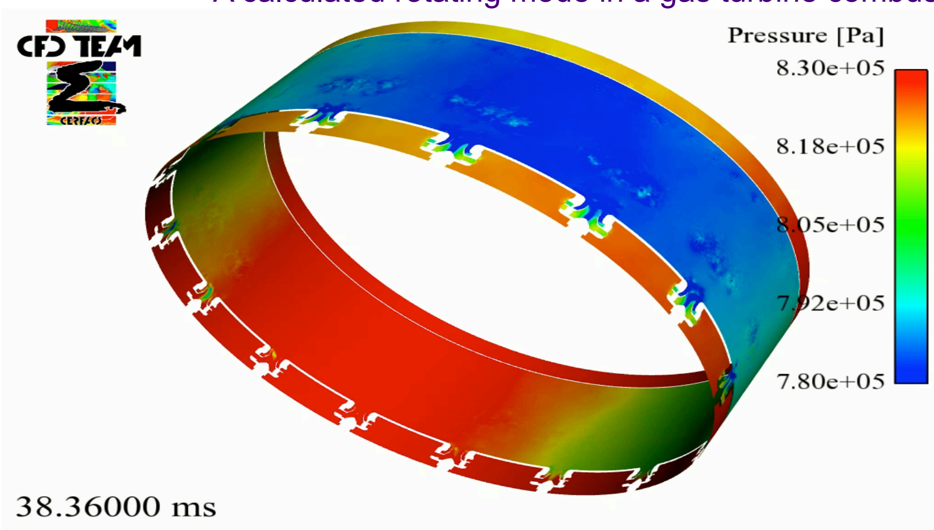

G. Staffelbach, L.Y.M. Gicquel, G. Boudier and T. Poinsot (2009) *Proc. Combust. Inst.* 32, 2909-2916. Large Eddy Simulation of self-excited azimuthal modes in annular combustors.

P. Wolf, G. Staffelbach, L.Y.M. Gicquel, J.D Muller and T. Poinsot (2012) *Combust. Flame* 159, 3398-3413. Acoustic and large eddy simulation of azimuthal modes in annular combustion chambers.

22

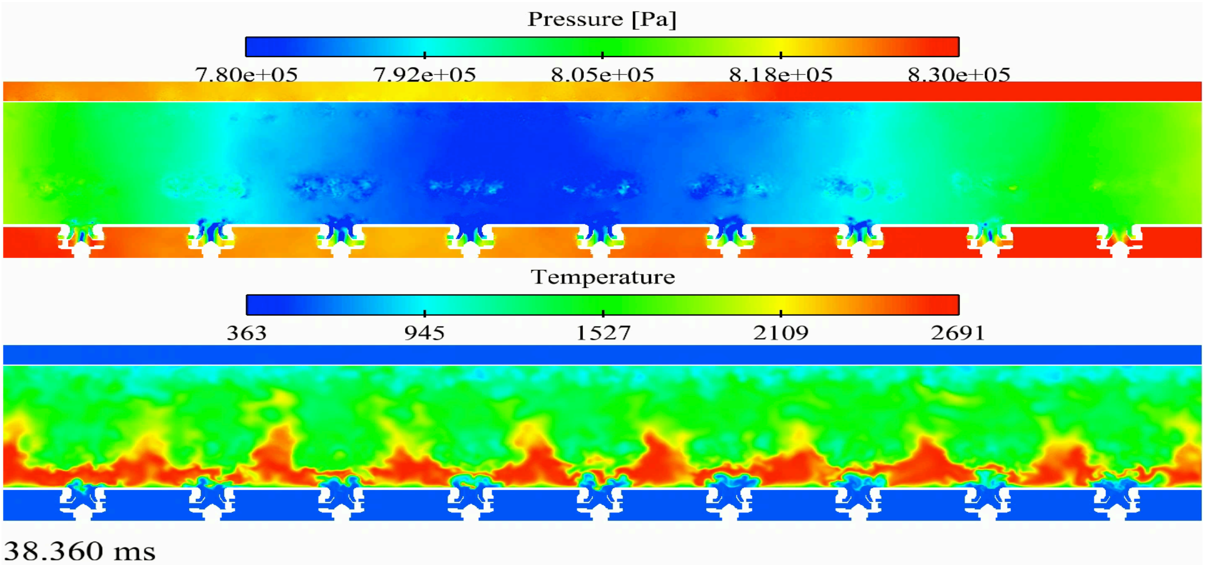

P. Wolf, G. Staffelbach, A. Roux, L. Gicquel, T. Poinsot and and V. Moureau (2009) *C.R. Meca.* 337, 385-394. Massively parallel LES of azimuthal thermo-acoustic instabilities in annular combustors.

P. Wolf, G. Staffelbach, L.Y.M. Gicquel, J.D Muller and T. Poinsot (2012) *Combust. Flame* 159, 3398-3413. Acoustic and large eddy simulation of azimuthal modes in annular combustion chambers.

23

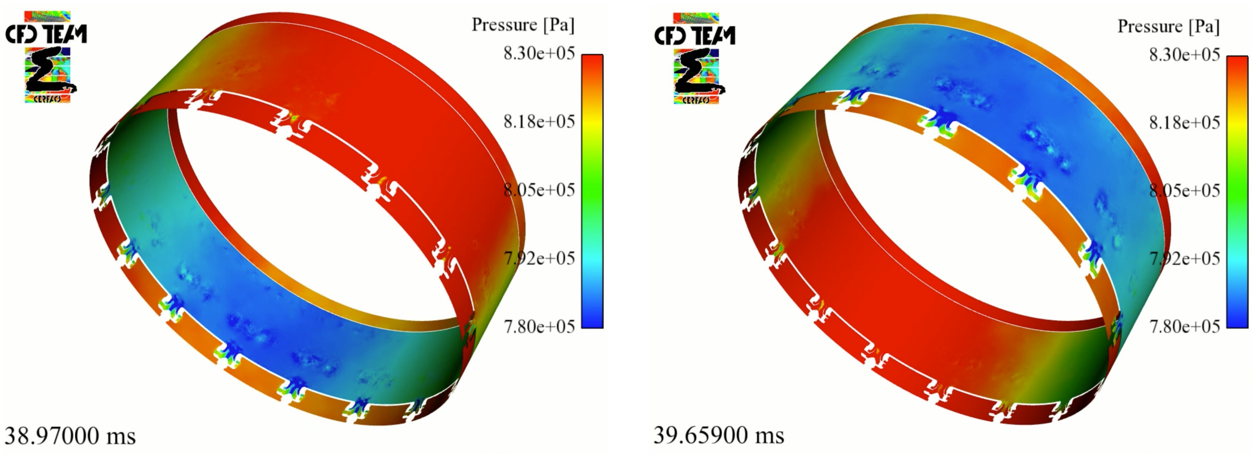

f=725 Hz

24

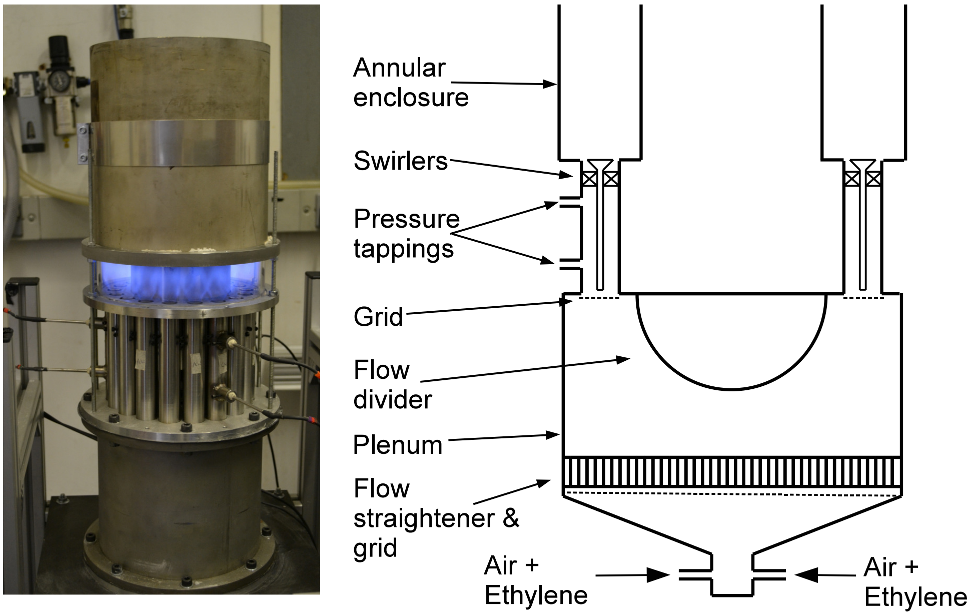

N. A. Worth and J.R. Dawson (2013) *Proc. of the Combust. Inst.* 34, 3127-3134. Self-excited circumferential instabilities in a model annular gas turbine combustor: global flame dynamics.

25

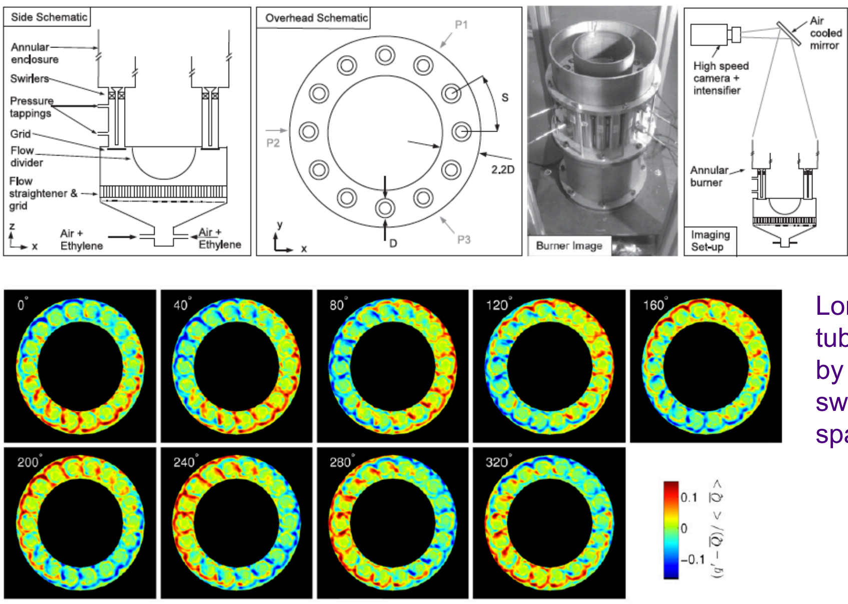

Long injection tubes, stabilization by a bluff body, low swirl. Variable spacing

N. A. Worth and J.R. Dawson (2013) *Proc. of the Combust. Inst.* 34, 3127-3134. Self-excited circumferential instabilities in a model annular gas turbine combustor: global flame dynamics.

26

Heat release rate fluctuations (standing azimuthal mode)

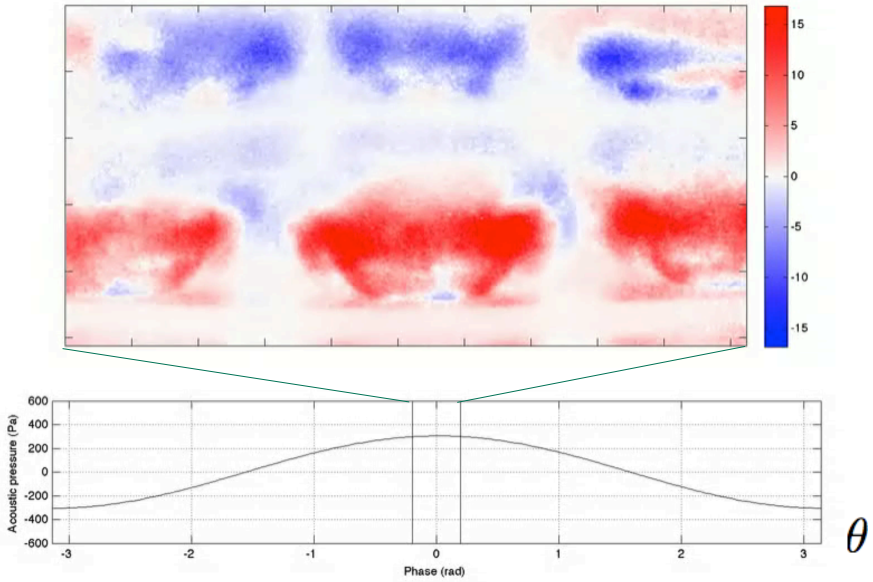

Pressure fluctuation distribution in the chamber

27

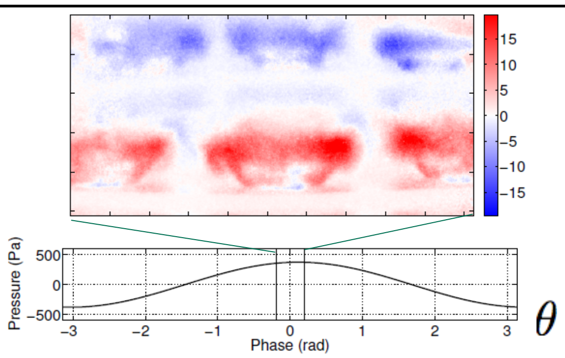

Heat release rate fluctuations (standing azimuthal mode)

Pressure fluctuation distribution in the chamber

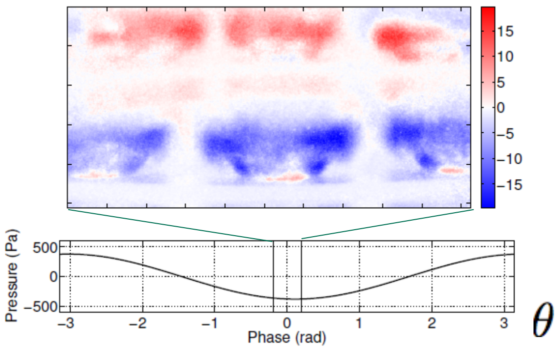

Heat release rate fluctuations (standing azimuthal mode)

Pressure fluctuation distribution in the chamber

28

MICCA3 Experimental setup

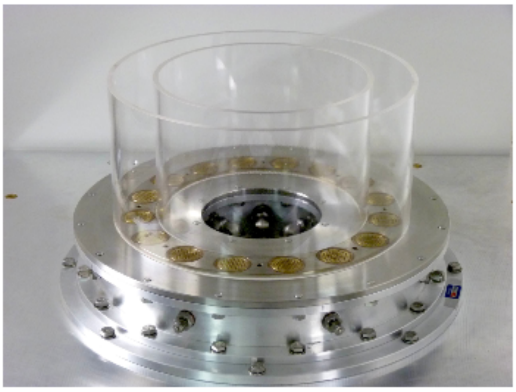

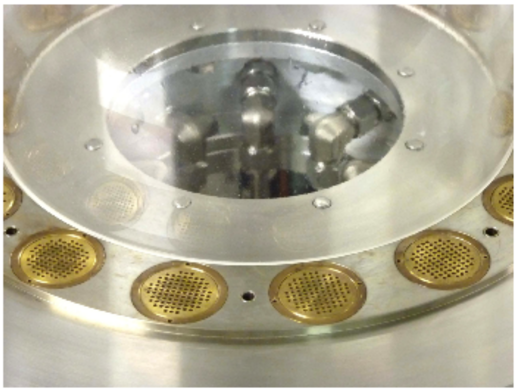

To better understand what determines the structure of the azimuthal modes, it is interesting to work on an annular chamber operating with flames that are simpler than turbulent flames.This is done here by making use of matrix injectors formed by perforated plates

29

MICCA3 with laminar matrix injectors

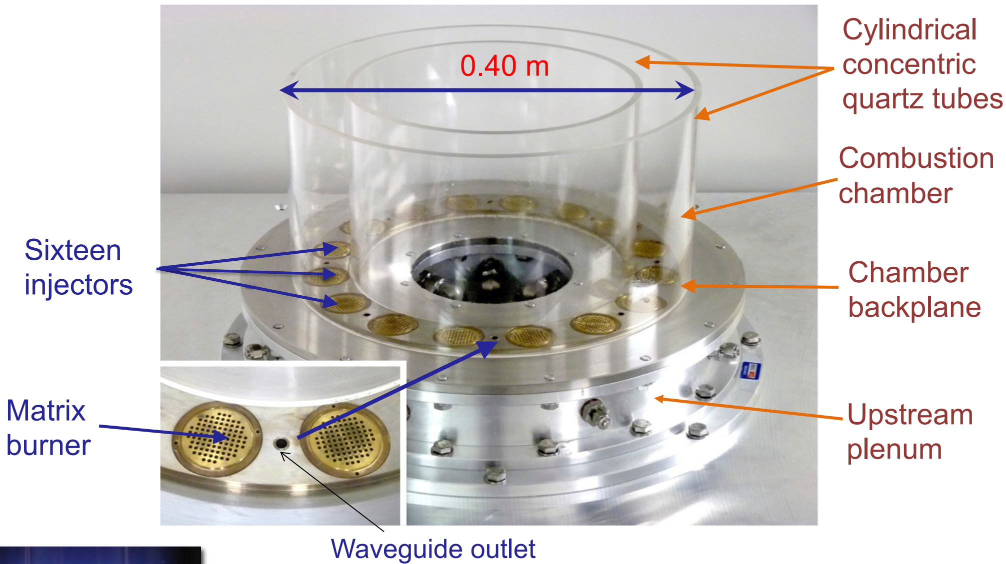

Laminar conical flames stabilised on a single matrix burner

30

Experimental setup

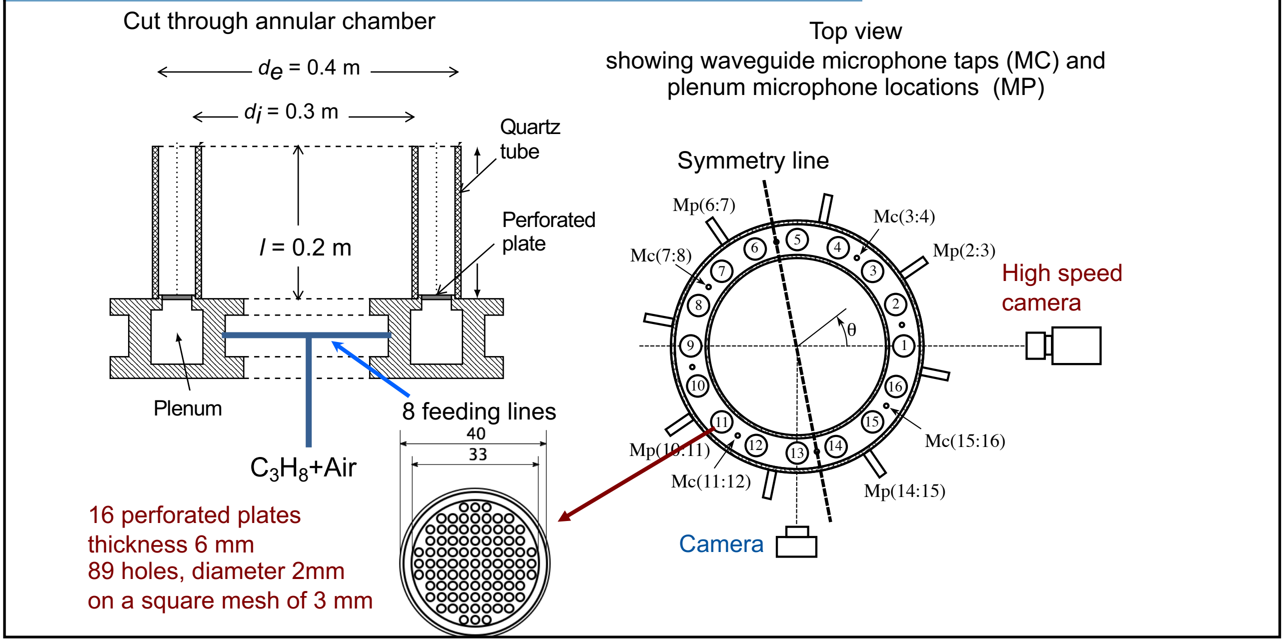

31

Azimuthal coupling modes

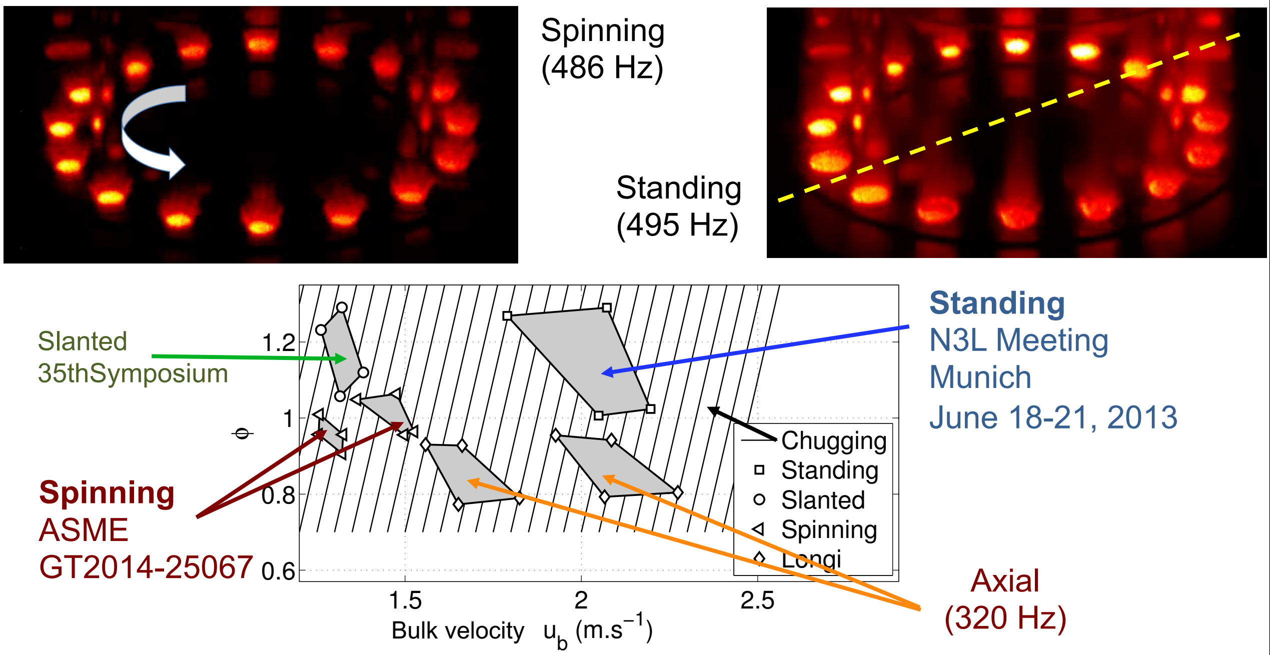

32

Experiments in MICCA 2 annular combustor with matrix Injectors (spinning, standing, slanted modes)

33

Standing mode

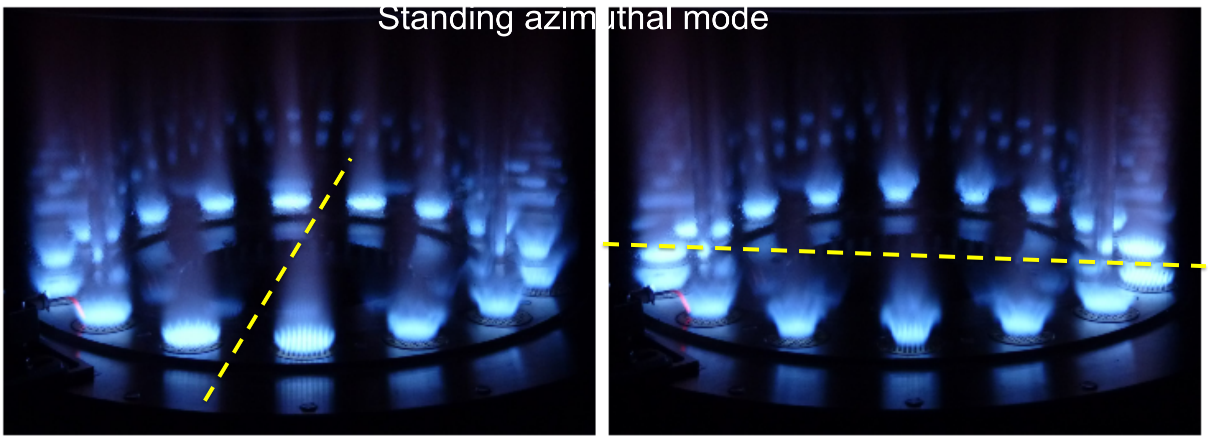

$v_0 = 2.12\,\mathrm{m\ s}^{-1} \phi = 1.11$

- Close to the nodal line, the flames move with a small amplitude of vibration. At 90° from this line, the flames oscillate vigorously, and they are blown-off on their periphery.

34

Standing azimuthal mode

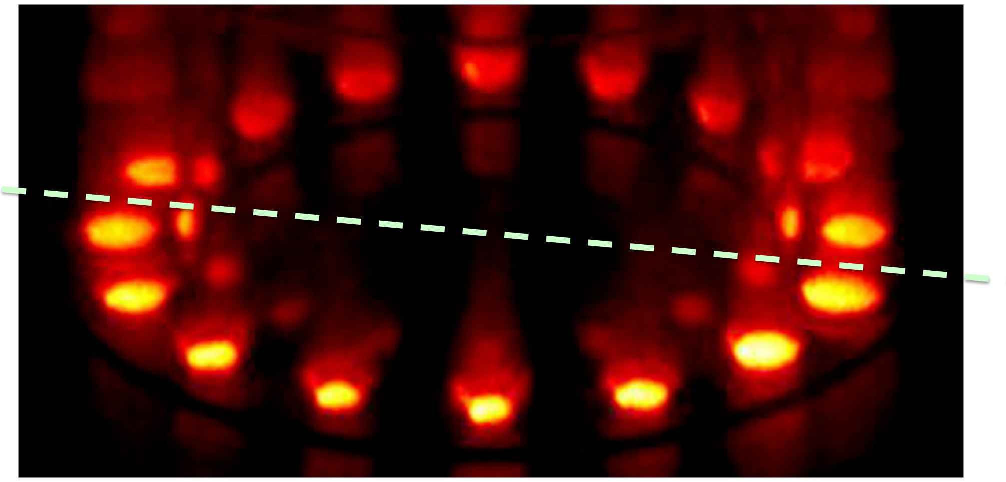

$$v_0 = 2.12\,\mathrm{m\ s}^{-1}\phi = 1.11$$

- Phase average of the oscillation, from the images recorded by the intensified high speed camera at 12500 fr/s. Images are plotted in false color

35

Standing azimuthal mode

High speed film : 12500 frames/s

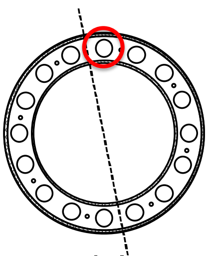

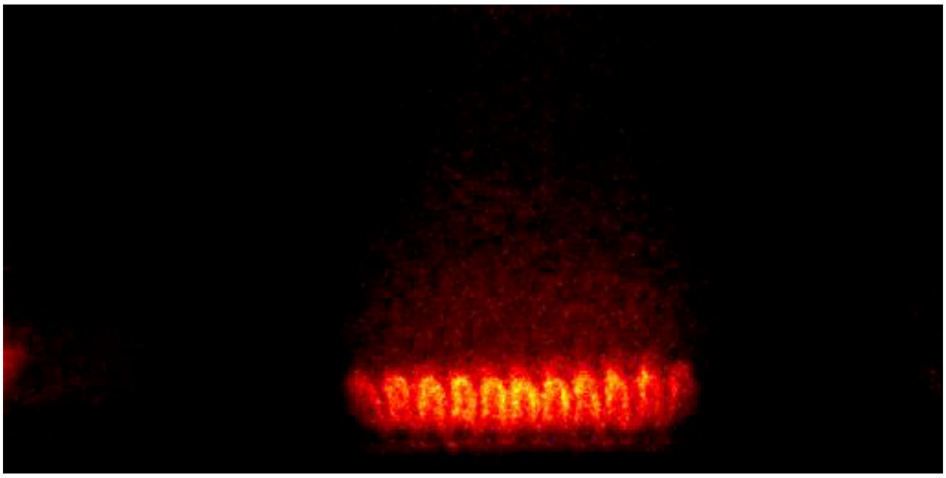

Injector close to the nodal line

36

Standing azimuthal mode

High speed film : 12500 frames/s

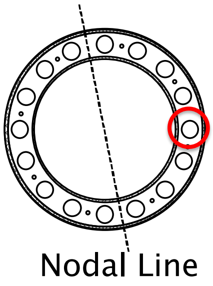

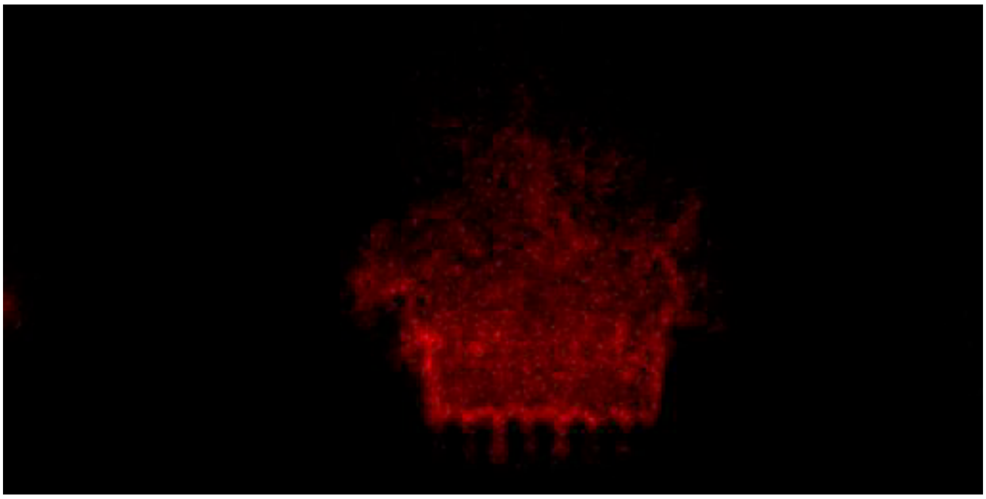

Injector at 90° from the nodal line

Standing azimuthal mode

High speed movie : 12500 frames/s

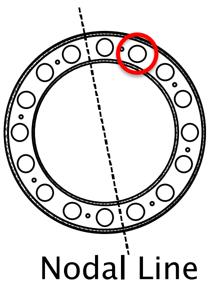

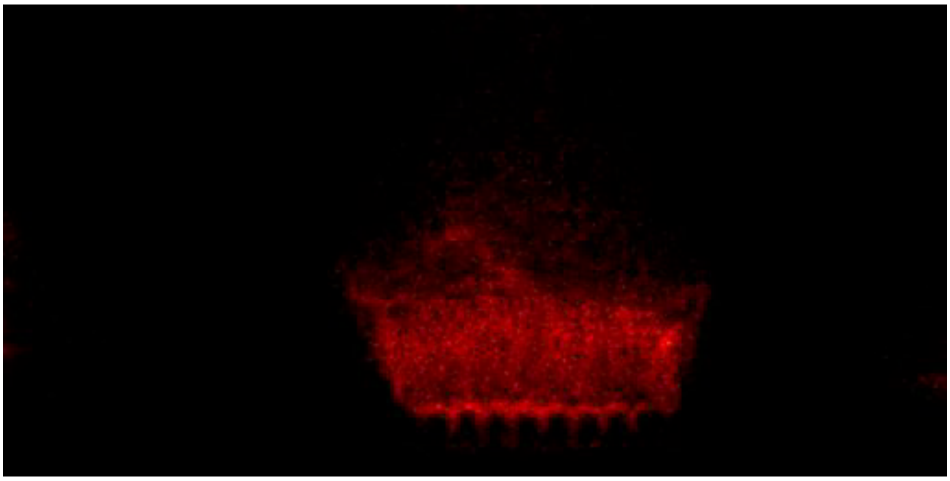

Injector between the nodal line and the orthogonal location

In the combustion chamber

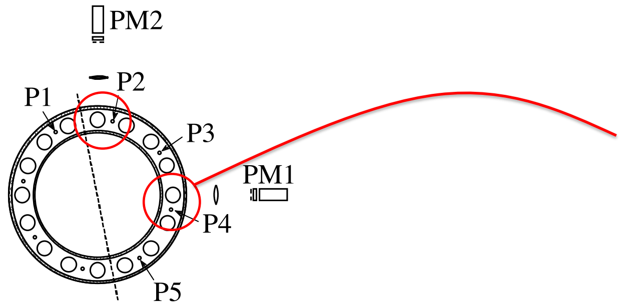

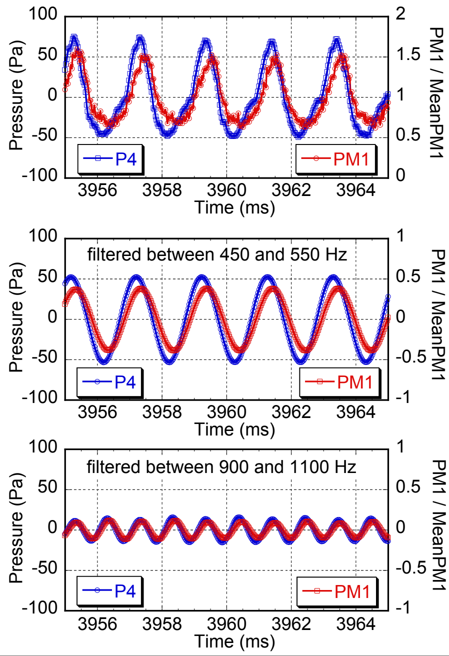

39

Spinning mode

$\phi = 0.96$ and $u_b = 1.49$ m s^{-1}

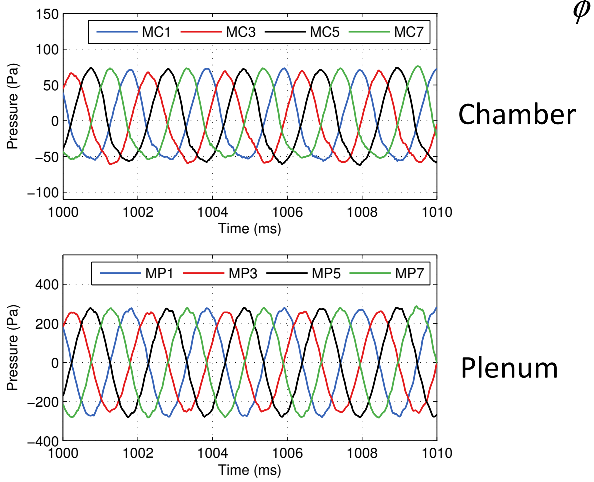

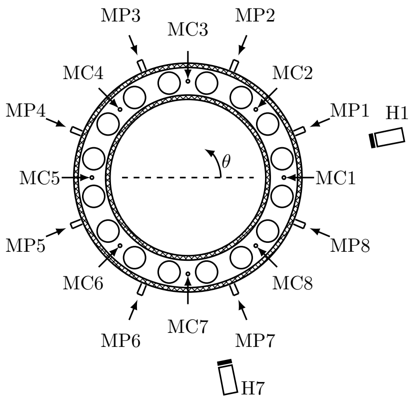

Pressure signals recorded by microphones in the chamber (top) and in the plenum (bottom) for the spinning mode

ASME TurboExpo, June,16-20, 2014, Düsseldorf, Germany.

40

Direct imaging of unstable regime

Standard video (25 frames/s) of the combustor
under spinning mode oscillation

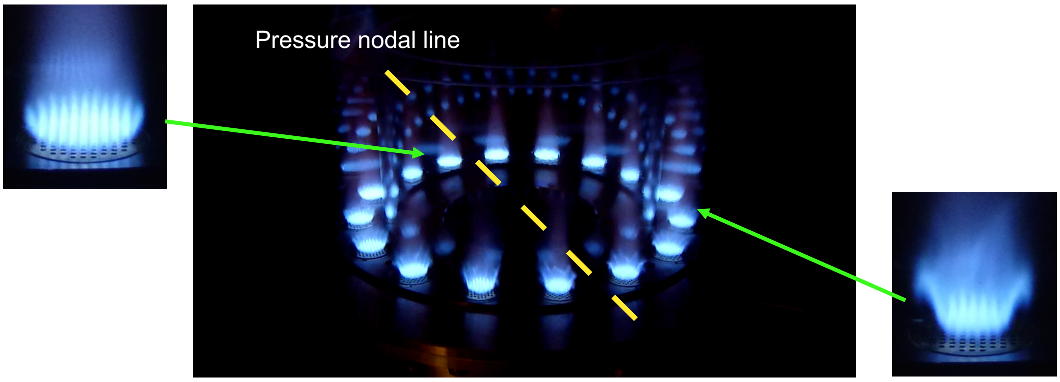

Propane - Air f= 450 Hz

$$\phi = 1.14 \text{ and } u_b = 1.33 m.s^{-1}$$

41

Spinning mode

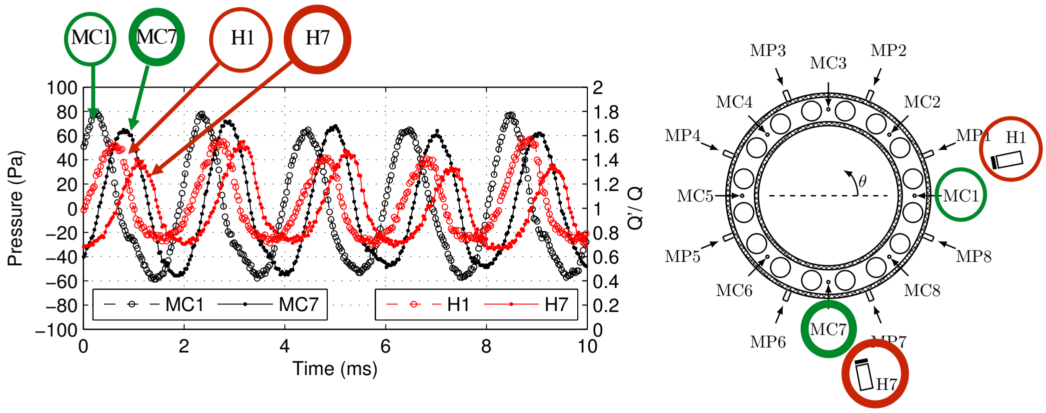

Pressure and photomultiplier signals corresponding to a spinning mode for a bulk velocity u_b = 1.49 m.s^{-1} and an equivalence ratio φ = 0.96.

In black: microphone signals MC1 and MC7 in the chamber.
In red: photomultipliers signals H1 and H7.

42

Spinning mode

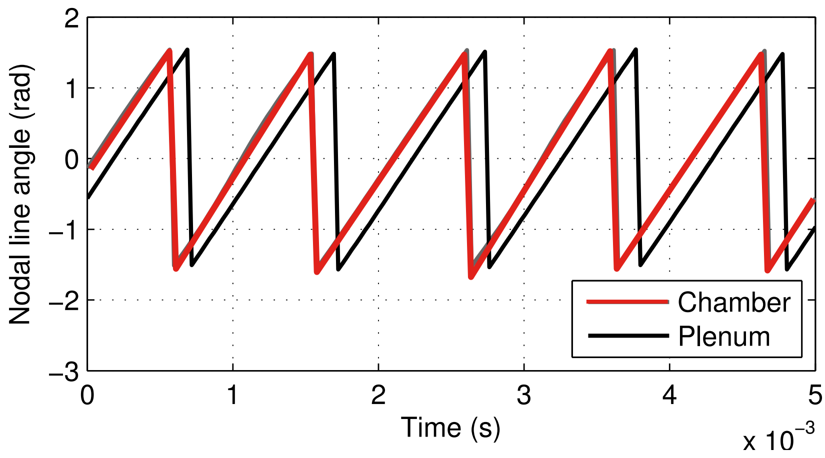

The nodal lines feature an angular shift which can be explained (see lecture tomorrow morning)

43

The slanted mode

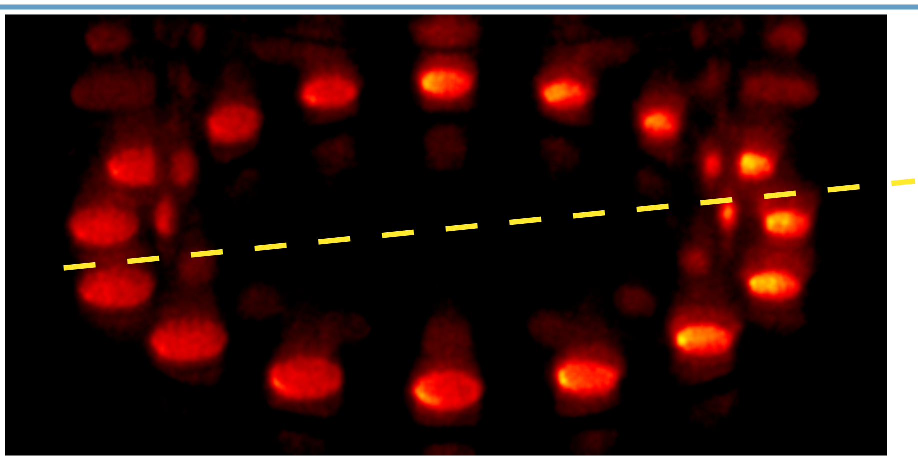

- Images are recorded by an Intensified CMOS camera at a frame rate set at 12500 Hz.
- Each phase of the sequence is averaged over 1000 instantaneous images.
- Some reflections on the transparent walls are visible in the neighborhood of the two sides of the image

44

The slanted mode

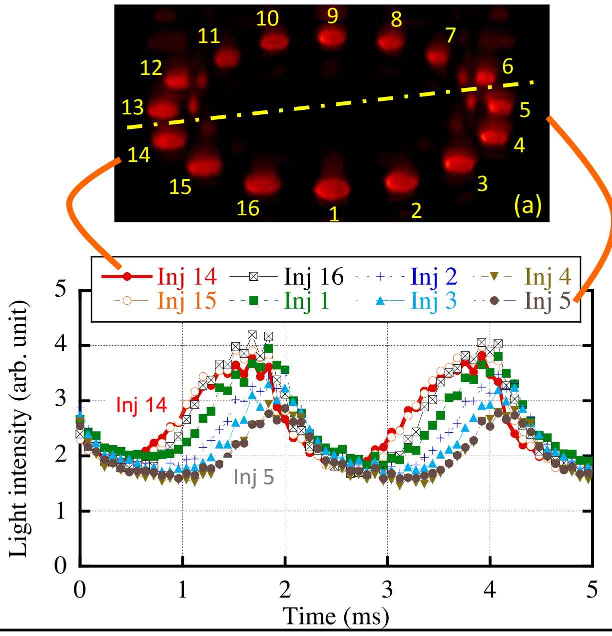

Time evolution of the light intensity for the 8 injectors located on the same side with respect to the line of symmetry, from injector 14 up to injector 5

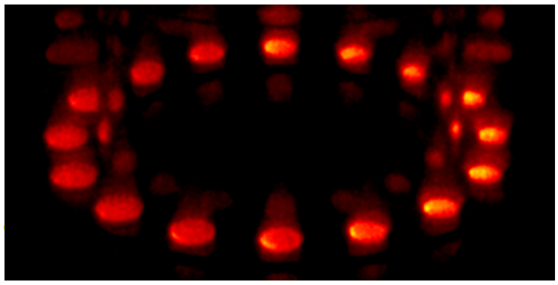

While the pressure signals are in phase in the plenum, the light intensity signals are out of phase

35th International Symposium on Combustion, Aug. 3-8, 2014

45

The slanted mode

Flame Describing Function (FDF) at the frequency of oscillation

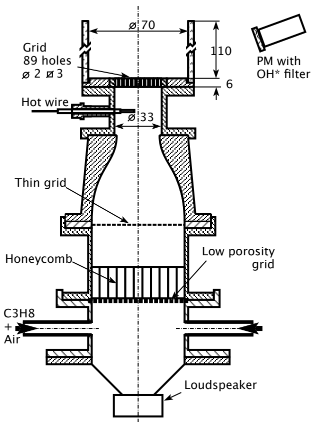

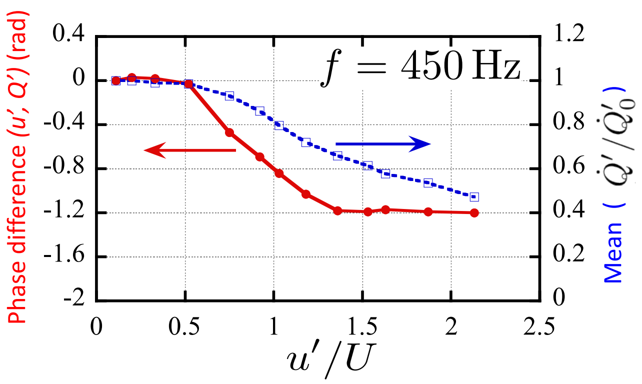

The flame describing function is determined in a single injector configuration that is modulated externally by a driver unit.

Flame response on a single matrix burner versus the relative amplitude of an axial perturbation at the frequency of 450 Hz.

35th International Symposium on Combustion, San Francisco Aug. 3-8, 2014

46

The slanted mode

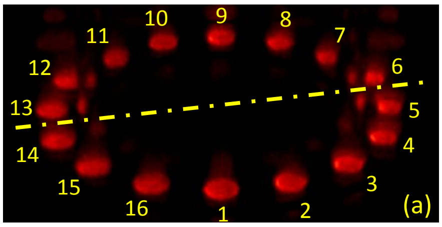

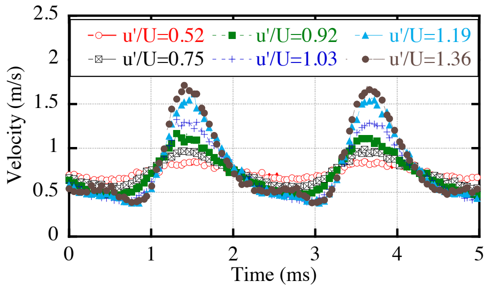

One assumes that the injector velocity signals are in phase

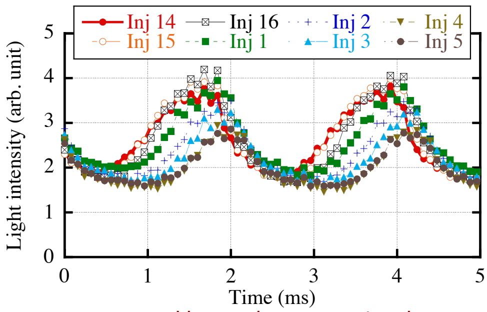

Measured heat release rate signals

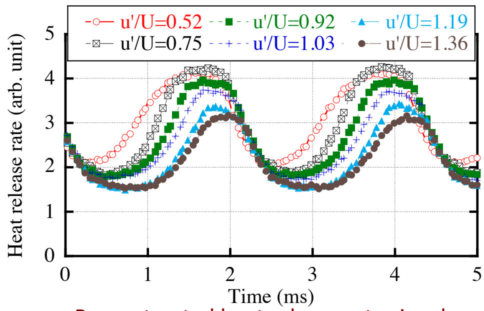

Reconstructed heat release rate signals

35th International Symposium on Combustion, San Francisco Aug. 3-8, 2014

47

Summary points

- The annular system with swirling injectors features various types of thermo-acoustic oscillations
- Analysis of pressure signals indicates a continuous switching between standing and spinning modes. The greatest probability corresponds to the standing mode
- A well established spinning mode is observed in the annular burner equipped with matrix injectors
- The nodal lines in the plenum and chamber feature an angular shift

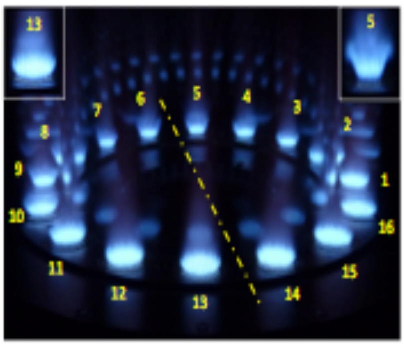

48

Summary points

- In the slanted pattern case the acoustic field comprises an axial mode and a standing azimuthal mode which have coinciding frequencies
- This combination produces a pressure pattern with a maximum amplitude of oscillation on one side of the annulus while the amplitude is minimal on the other side

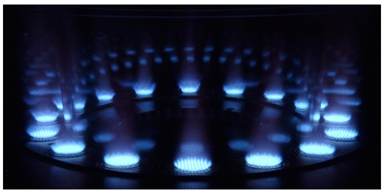

- Using the flame describing function one can explain the time shift in the flame motions at the various injectors which takes the form of a wave sweeping the different injectors
- It is shown that the phase shift evolution in the light intensity of the different injectors is a direct result of the nonlinear response of these elements when they are subjected to large velocity oscillations

35th International Symposium on Combustion, San Francisco Aug. 3-8, 2014

49

MICCA-Spray (liquid spray injection of n-heptane or dodecane

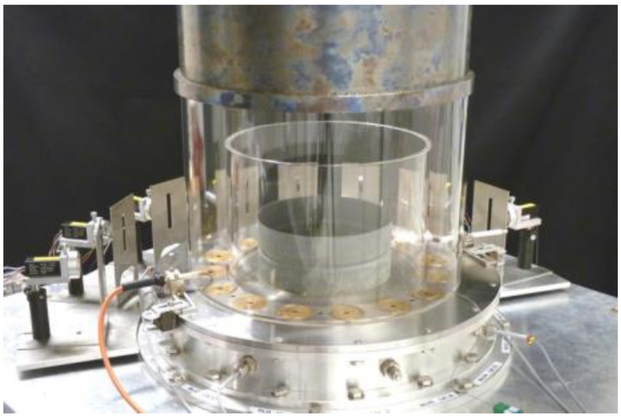

Side view of MICCA Spray

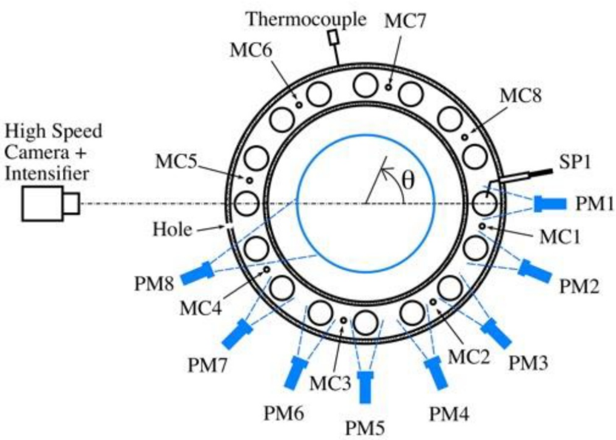

Schematic top view showing locations of the photomultiplier and chamber microphone arrays

50

Large amplitude azimuthal instabilities in MICCA-Spray leading to partial blow-off

n-Heptane (liquid) / air

Equivalence ratio : 0.87

Bulk velocity : 46 m/s

Power : 115 kW

Kevin Prieur

First Clean Sky prize 2018

K. Prieur, D. Durox, T. Schuller and S. Candel (2017) *J. Eng. Gas Turbines Power*. 140, 031503. Strong azimuthal instabilities in a spray annular chamber with intermittent partial blow-off.

51

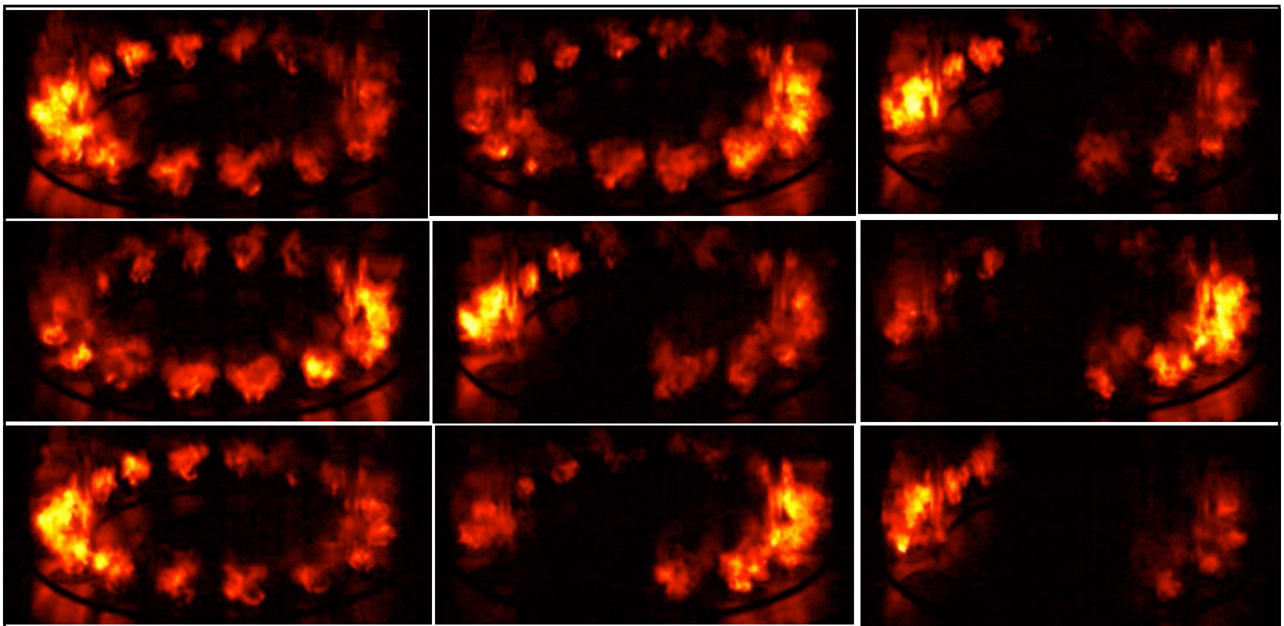

Partial flame blow off in MICCA-Spray in the presence of an azimuthal standing mode of high amplitude (4000 Pa peak)

52

Extinction des flammes situées au voisinage de la ligne nodale

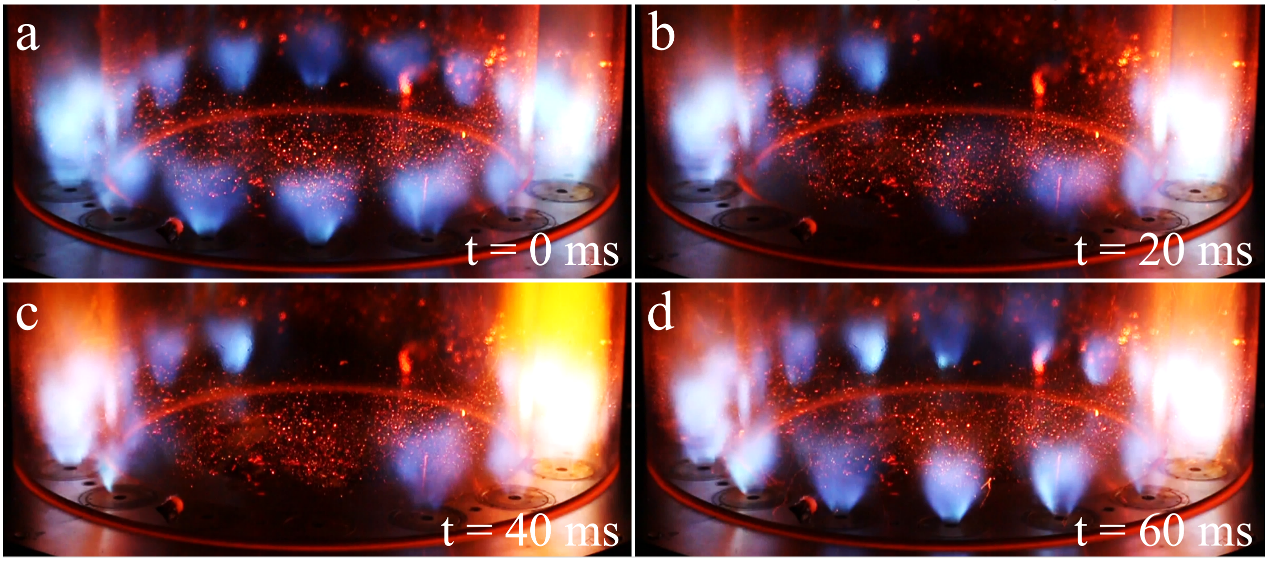

Flames located near the nodal line of the azimuthal mode are blown-off during a period of 20 ms when the level of fluctuation exceeds 4000 Pa

53

Annular combustion dynamics modeling

T. Schuller, T. Poinsot and S. Candel (2020) *Journal of Fluid Mechanics.* Vol. 894, P1-1-P1-95. Dynamics and control of premixed combustion systems based on the flame transfer and describing functions. doi:10.1017/jfm.2020.239

54

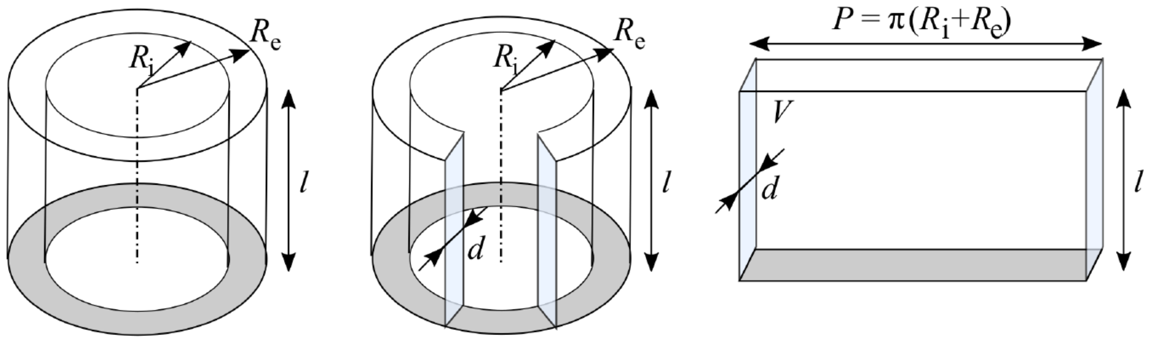

(a) Annular combustor (b) Unwrapping (c) Equivalent rectangular combustor

FIGURE 21. (a) Annular combustor system. The distance between the inner and outer cylinders forming the side walls is small compared to the mean radius $d << (R_i + R_e)/2$. (b) The annular combustor is unwrapped by cutting the geometry by an axial plane. (c) The equivalent rectangular combustor has a width $\mathcal{P} = \pi(R_i + R_e)$, its length is equal to that of the initial annular system. The depth is equal to the distance between the inner and outer cylinders $d = R_e - R_i$.

55

Compact Flame Dynamical Model (CFDM)

Discrete Flame Source Model (DFSM)

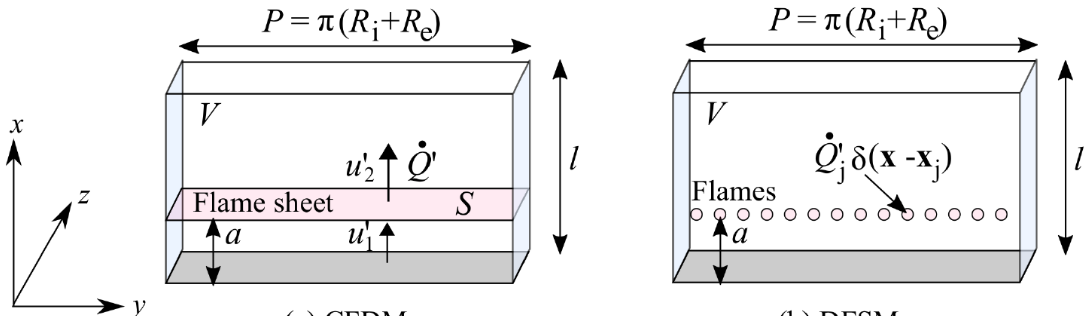

(a) CFDM (b) DFSM

FIGURE 22. (a) Compact Flame Dynamical Model (CFDM). The combustion region is thin compared to the wavelength and it is treated as a discontinuity separating an upstream region 1 from a downstream region 2. (b) Discrete Flame Source Model (DFSM). Combustion takes place in a set of N discrete flames acting like point sources. The point sources are separated by a distance Δx such that $N\Delta x = \mathcal{P}$.

56

$$\tilde{p}_j = \left(A_j^+ e^{ik_{jx}x} + A_j^- e^{-ik_{jx}x}\right) e^{ik_{jy}y}$$

where $(k_{jx})^2 + (k_{jy})^2 = k_j^2 = (\omega/c_j)^2 \quad j = 1, 2$

$$A_j^+ \text{ and } A_j^-$$

This pressure field needs to comply with the acoustic boundary conditions of the system in the transverse and axial directions

Due to the periodicity of the pressure field in the transverse direction

$$\exp(ik_{jy}\mathcal{P}) = \exp(ik_{jy}0) = 1, \quad \text{i.e.} \quad k_{jy}^m \mathcal{P} = 2\pi(m+1)$$
$$m = 0, 1, 2, \ldots$$

57

In these expressions, $\mathcal{P} = \pi(R_i + R_e) = \pi D$ is the mean perimeter

$y = \theta(D/2) \qquad k_{jy}^m y = (m+1)\theta$

$$\psi_j(y) = \cos(k_{jy}^m y) \qquad \psi_j(y) = \sin(k_{jy}^m y)$$

$$\tilde{p}_1 = \left(Ae^{ik_{1x}x} + Be^{-ik_{1x}x}\right)\psi_1(y),$$
$$\tilde{p}_2 = \left(Ce^{ik_{2x}x} + De^{-ik_{2x}x}\right)\psi_2(y).$$

For the axial velocity components, one gets

$$\overline{\rho}_1 c_1 \tilde{u}_1 = \frac{k_{1x}}{k_1}\left(Ae^{ik_{1x}x} - Be^{-ik_{1x}x}\right)\psi_1(y),$$
$$\overline{\rho}_2 c_2 \tilde{u}_2 = \frac{k_{2x}}{k_2}\left(Ce^{ik_{2x}x} - De^{-ik_{2x}x}\right)\psi_2(y)$$

58

For the transverse acoustic velocity components, one has

$$\overline{\rho}_1 c_1 \tilde{v}_1 = -i\frac{k_{1y}^m}{k_1}\left(Ae^{ik_{1x}x} + Be^{-ik_{1x}x}\right)\psi_1'(y)$$

$$\overline{\rho}_2 c_2 \tilde{v}_2 = -i\frac{k_{2y}^m}{k_2}\left(Ce^{ik_{2x}x} + De^{-ik_{2x}x}\right)\psi_2'(y)$$

where $\psi_j'(y) = -\sin(k_{jy}^m y)$ if $\psi_j(y) = \cos(k_{jy}^m y)$

and $\psi_j'(y) = \cos(k_{jy}^m y)$ if $\psi_j(y) = \sin(k_{jy}^m y)$

The acoustic field also needs to comply with the jump conditions for the axial flow components across the flame sheet

Assuming that they can be represented by their specific admittances

$$\beta_1 = \overline{\rho}_1 c_1 \tilde{u}_1/\tilde{p}_1 \text{ and } \beta_2 = \overline{\rho}_2 c_2 \tilde{u}_2/\tilde{p}_2$$

59

One is left with the same dispersion relation as for pure axial modes

$$\frac{\beta_2}{\Gamma} - \beta_1\left(1 + \Theta\,\mathcal{F}\right) = 0$$

This general expression sets the wave numbers k_{1x} and k_{2x} and thus fully defines the angular frequencies ω

$$\frac{\omega_m}{c_j} = \left[\left(\frac{2\pi(m+1)}{\mathcal{P}}\right)^2 + (k_{jx})^2\right]^{1/2} \quad \text{where } j = 1 \text{ or } 2$$

To fully characterize the axial acoustic field, one needs to specify the upstream β_1 and downstream β_2 admittances

60

Configuration	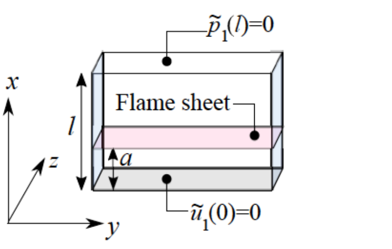	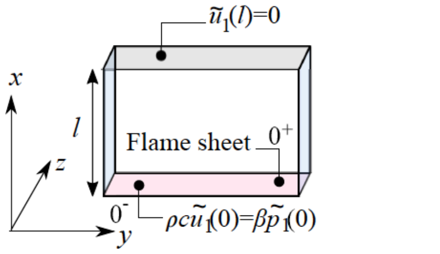
$\beta_1 = \frac{\overline{\rho}_1 c_1 \tilde{v}_1}{\tilde{p}_1}$	$i\frac{k_{1x}}{k_1}\tan(k_{1x}a)$	$\beta(\omega)$
$\beta_2 = \frac{\overline{\rho}_2 c_2 \tilde{v}_2}{\tilde{p}_2}$	$i\frac{k_{2x}}{k_2}\text{cotan}(k_{2x}(l-a))$	$-i\frac{k_{2x}}{k_2}\tan(k_{2x}l)$
Dispersion relation	$\cos(k_x l) - \sin(k_x a)\sin(k_x(l-a))\theta\mathcal{F} = 0$	$\beta\cos(k_x l) + i\frac{k_x}{k}\sin(k_x l) + \cos(k_x l)\beta\theta\mathcal{F} = 0$

61

Recent publications

N. Noiray, D. Durox, T. Schuller and S. Candel (2008) *Journal of Fluid Mechanics* **615**, 139-167. A unified framework for nonlinear combustion instability analysis based on the describing function.

P. Palies, D. Durox, T. Schuller, P. Morenton and S. Candel (2009) *Comptes Rendus Mecanique.* **337**, 395-405. Dynamics of premixed confined swirling flames.

P. Palies, D. Durox, T. Schuller and S. Candel (2010) *Combustion and Flame.* 157(9) 1698-1717. The combined dynamics of swirler and turbulent swirling flames.

P. Palies, D. Durox, T. Schuller, and S. Candel (2011) *Proceedings of the Combustion Institute* **33**. 2967-2974. Modeling of premixed swirling flames transfer functions.

P. Palies, D. Durox, T. Schuller and S. Candel (2011) *Journal of Fluid Mechanics.* **672**,545-569. Acoustic-convective mode conversion in an airfoil cascade.

P. Palies, D. Durox, T. Schuller and S. Candel (2011) *Combustion Science and Technology.* **183**, 704-717. Experimental study on effects of swirler geometry and swirl number on flame describing functions.

P. Palies, D. Durox, T. Schuller, L.Y.M. Gicquel and S. Candel (2011) *Physics of Fluids.* **23**. doi 10.1063/1.3553276. Acoustically perturbed turbulent premixed swirling flame.

P. Palies, D. Durox, T. Schuller and S. Candel (2011) *Combustion and Flame,* **158**, 1980-1991. Swirling flame instability analysis based on the flame describing function methodology.

62

Recent publications

J.P. Moeck, J.F. Bourgouin, D. Durox, T. Schuller and S. Candel (2012) *Combustion and Flame,* 159, 2650-2668. Nonlinear interaction between a precessing vortex core and acoustic oscillations in a turbulent swirling flame.

S. Candel, D. Durox, T. Schuller, P. Paliès, J.F. Bourgouin and J. Moeck (2012*) Comptes Rendus Mecanique*, 340, 758-768. Progress and challenges in swirling flame dynamics.

D. Durox, J.P. Moeck, J.F. Bourgouin, P. Morenton, M. Viallon, T. Schuller and S. Candel (2013) *Combustion and Flame*, 160, 1729-1742. Dynamics of swirling flames generated by a radial swirler equipped with adjustable blades angle.

J.F. Bourgouin, D. Durox, T. Schuller, J. Beaunier and S. Candel (2013) *Combustion and Flame*, 160, 1398-1413. Ignition dynamics of an annular combustor equipped with multiple swirling injectors.

C.F. Silva, F. Nicoud, T. Schuller, D. Durox, and S. Candel (2013*) Combustion and Flame.* 160, 1743-1754. Combining a Helmholtz solver with the Flame Describing Function to assess combustion instability in a swirled combustor.

J.F. Bourgouin, J. Moeck, D. Durox, T. Schuller, and S. Candel (2013*) Comptes Rendus Mecanique*, 341, 211-219. Sensitivity of swirling flows to small changes in the swirler geometry.

F. Boudy, T. Schuller, D. Durox and S. Candel (2013) *Comptes Rendus Mecanique*, 341, 181-190. Analysis of limit cycles sustained by two modes in the Flame Describing Function framework.

63

Recent publications

J. Moeck, J.F. Bourgouin, D. Durox, T. Schuller, and S. Candel (2013) *Experiments in Fluids.* 54. Article 1498. Tomographic reconstruction of heat release rate perturbations induced by helical modes in turbulent swirl flames.

S. Candel, D. Durox, T. Schuller, J.F. Bourgouin and J. Moeck (2014*) Annual Review of Fluid Mechanics.* 46, 147-173. Dynamics of swirling flames.

J.F. Bourgouin, D. Durox, J.P. Moeck, T. Schuller and S. Candel (2015) *Proceedings of the Combustion Institute.* 35 (3) 3237-3244. A new pattern of instability in an annular combustor : the slanted mode.

A. Urbano, L. Selle, G. Staffelbach, B. Cuenot, T. Schmitt, S. Ducruix and S. Candel (2016*) Combustion and Flame.* 169, 129-140. Exploration of combustion instability triggering using Large Eddy Simulation of a multiple injector Liquid Rocket Engine.

K. Prieur, D. Durox, J. Beaunier, T. Schuller and S. Candel (2016) *Combustion and Flame.* A hysteresis phenomenon leading to spinning or standing azimuthal instabilities in an annular combustor.

D. Durox, K. Prieur, T. Schuller and S. Candel (2016) *Journal of Engineering for Gas Turbines and Power.* 138(10)101504, 8 pages. doi: 10.1115/1.4033330. Different flame patterns linked with swirling injector interactions in an annular combustor.

64

Recent publications

D. Laera, K. Prieur, D. Durox, T. Schuller, S. M. Camporeale, S. Candel (2016) Impact of heat release distribution on the spinning modes of an annular combustor with multiple matrix burners. ASME GT2016-56309, Turbo Expo, Seoul, Korea.

K. Prieur, D. Durox, T. Schuller and S. Candel (2016) Influence of the cup angle on the flame describing function of a swirled injector with liquid fuel. International Symposium on Thermoacoustic Instabilities in Gas Turbines and Rocket Engines: Industry meets Academia.

K. Prieur, D. Durox, J. Beaunier, T. Schuller and S. Candel (2017) *Combustion and Flame*. 175, 283-291. A hysteresis phenomenon leading to spinning or standing azimuthal instabilities in an annular combustor.

A. Urbano, Q. Douasbin, L. Selle, G. Staffelbach, B. Cuenot, T. Schmitt, S. Ducruix and S. Candel (2017) *Proceedings of the Combustion Institute.* 36, 2633-2639. Study of flame response to transverse acoustic modes from the LES of a 42-injector rocket engine.

K. Prieur, D. Durox, J. Beaunier, T. Schuller and S. Candel (2017) *Proceedings of the Combustion Institute.* 36, 3717-3724. Ignition dynamics in an annular combustor for liquid spray and premixed gaseous injection.

D. Laera, K. Prieur, D. Durox, T. Schuller, S. Camporeale and S. Candel (2017). *J. Eng. Gas Turbines Power.* 2017, 139(5): 051505-051505-10. doi:10.1115/1.4035207. Impact of heat release distribution on the spinning modes of an annular combustor with multiple matrix burners.

D. Laera, K. Prieur, D. Durox, T. Schuller, S. Camporeale and S. Candel (2017). *Combustion and Flame*. 184, 136-152. Flame describing function analysis of spinning and standing modes in an annular combustor and comparison with experiments.

Recent publications

K. Prieur, D. Durox, G. Vignat, T. Schuller and S. Candel (2018). *J. Eng. Gas Turbines Power* 140(3), 031503 (Oct 17, 2017) (10 pages). Strong Azimuthal Combustion Instabilities in a Spray Annular Chamber With Intermittent Partial Blow-Off.

T. Lancien, D. Durox, K. Prieur, S. Candel and R. Vicquelin (2018) *J. Eng. Gas Turbines Power* 140(2), 021504 (Oct 10, 2017) (10 pages). doi: 10.1115/1.4037827. Large Eddy Simulation of Light-Round in an Annular Combustor With Liquid Spray Injection and Comparison With Experiments

T. Lancien, D. Durox, K. Prieur, S. Candel and R. Vicquelin (2019) *Proceedings of the Combustion Institute*, 37, 5021-5029. Leading point behavior during the ignition of an annular combustor with liquid n-heptane injectors.

J.P. Moeck, D. Durox, T. Schuller and S. Candel (2019) *Proceedings of the Combustion Institute,* 37, 5343-5350. Nonlinear themoacoustic mode synchronization in annular combustors.

G. Vignat, D. Durox, K. Prieur and S. Candel (2019) *Proceedings of the Combustion Institute,* 37, 5205-5213. An experimental study into the effect of injector pressure-loss on self sustained combustion instabilitiesin a swirled burner

Recent publications

K. Prieur, G. Vignat, D. Durox, T. Schuller and S. Candel (2019) *Journal of Engineering for Gas Turbines and Power* Vol. 141 / 061007-11. Flame and spray dynamics during the light-round process in an annular system equipped with multiple swirl spray injectors.

G. Vignat, D. Durox, A. Renaud and S. Candel (2020) *Journal of Engineering for Gas Turbines and Power Vol. 142 (1) 011016.* High amplitude combustion instabilities in an annular combustor inducing pressure field deformation and flame blow-off. doi.org/10.1115/1.4045515

S. Puggelli, T. Lancien, K. Prieur, D. Durox, S. Candel and R. Vicquelin (2020) *Journal of Engineering for Gas Turbines and Power* Vol. 142 (1) 011018. Impact of wall temperature in Large Eddy Simulation of light round in an annular liquid fueled combustor and assessment of wall models. doi.org/10.1115/1.4045341

G. Vignat, D. Durox, T. Schuller and S. Candel (2020) *Combustion Science and Technology.* Combustion dynamics of annular systems. doi.org/10.1080/00102202.2020.1734583

T. Schuller, T. Poinsot and S. Candel (2020) *Journal of Fluid Mechanics.* Dynamics and control of premixed combustion systems based on the flame transfer and describing functions. doi:10.1017/jfm.2020.239

Recent publications

G. Vignat, P. Ranjendram Soundarajan, D. Durox, A. Vié, A. Renaud and S. Candel (2020) A joint experimental and LES characterization of the liquid fuel spray in a swirl injector. *ASME Turbo-Expo*, London, UK, ASME Paper GT2020-14935.

K. Topperwien, F.Collin-Bastiani, E. Riber, B. Cuenot, G. Vignat, K. Prieur, D. Durox, S. Candel and R. Vicquelin (2020) Large eddy simulation of flame dynamics during the ignition of a swirling injector unit and comparison with experiments. *ASME Turbo-Expo*, London, UK, ASME Paper GT2020-16197.

P. Rajendram Soundarajan, G. Vignat, D. Durox, A. Renaud and S. Candel (2020) Effect of different fuels on combustion instabilities in an annular combustor. *ASME Turbo-Expo*, London, UK, ASME Paper GT2020-15123.

G. Vignat, D. Durox, A. Renaud, T. Lancien, R. Vicquelin and S. Candel (2021) *Combustion and Flame,* 225, 305-319. Investigation of transient PVC dynamics in a strongly swirled spray flame using high speed planar laser imaging of SnO2 microparticles.

G. Vignat, N. Minesi, P. Rajendram Soundararajan, D. Durox, A. Renaud, V. Blanchard, C.O. Laux and S. Candel (2021) *Proceedings of the Combustion Institute* 38, Online. Improvement of lean blow out performance of spray and premixed swirled flames using nanosecond repetitively pulsed discharges.

G. Vignat, E. Lo Schiavo, D. Laera, A. Renaud, L. Gicquel, D. Durox and S.Candel (2021) *Proceedings of the Combustion Institute* 38, Online. Dynamics of spray and swirling flame under acoustic oscillations : a joint experimental and LES investigation.

G. Vignat, P. Ranjendram Soundarajan, D. Durox, A. Vié, A. Renaud and S. Candel (2021) *Journal of Engineering for Gas Turbines and Power*. Online, doi:10.1115/1.4049771. GTP-20-1635. A joint experimental and LES characterization of the liquid fuel spray in a swirl injector.

P. Rajendram Soundarajan, G. Vignat, D. Durox, A. Renaud and S. Candel (2021) *Journal of Engineering for Gas Turbines and Power*. Online, doi:10.1115/1.4049702. GTP-20-1585. Effect of different fuels on combustion instabilities in an annular combustor.

69

Nonlinear interaction between the precessing vortex core and acoustic oscillations

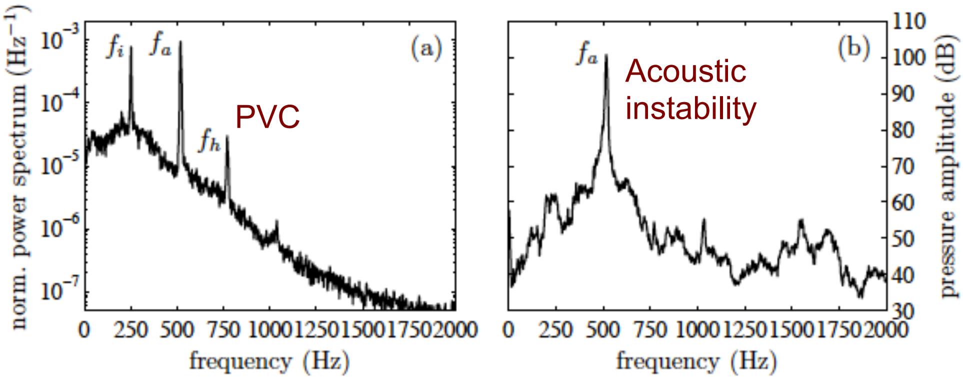

Figure 15: Spectral distributions of photomultiplier (a) and microphone (b) signals, $\phi = 0.69$, $u_b = 9.9\,\mathrm{m.s}^{-1}$. One vertical half of the photomultipliers field of view is masked, and the signal has been normalized by the mean value. The microphone is located outside of the flame tube. f_i, f_a, and f_h denote interaction, acoustic and helical-mode frequency, respectively.

$$f_i = f_h - f_a$$

J.P. Moeck, J.F. Bourgouin, D. Durox, T. Schuller and S. Candel (2012) *Combustion and Flame,* 159, 2650-2668. Nonlinear interaction between a precessing vortex core and acoustic oscillations in a turbulent swirling flame.

70

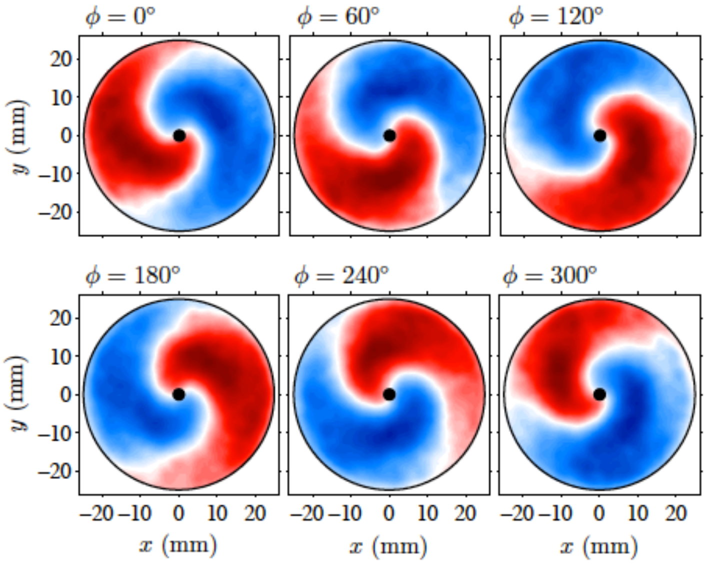

Figure 19: Phase-averaged images of the light intensity deviation from the mean distribution in the burner gathered from a top view at the interaction frequency (254 Hz).

J.P. Moeck, J.F. Bourgouin, D. Durox, T. Schuller and S. Candel (2012) *Combustion and Flame,* 159, 2650-2668.
Nonlinear interaction between a precessing vortex core and acoustic oscillations in a turbulent swirling flame.

71

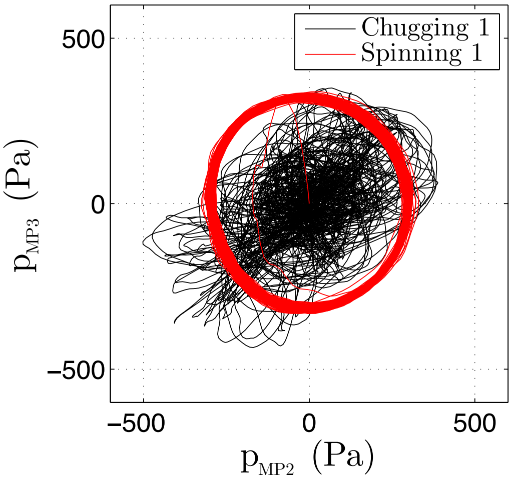

Combustion dynamics
Lecture 10b

S. Candel, D. Durox , T. Schuller

CentraleSupélec
Université Paris-Saclay, EM2C lab, CNRS

Tsinguha summer school, July 2021

1

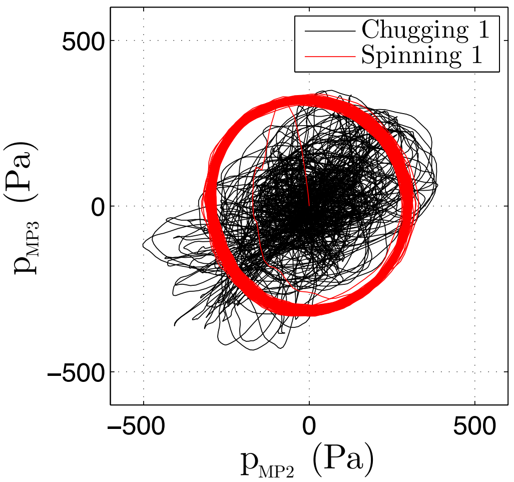

A hysteresis phenomenon leading to spinning or standing azimuthal instabilities in an annular combustor

Kevin Prieur, Daniel Durox,
Thierry Schuller et Sébastien Candel

K. Prieur, D. Durox, J. Beaunier, T. Schuller and S. Candel (2017) *Combustion and Flame.* 175, 283-291.
A hysteresis phenomenon leading to spinning or standing azimuthal instabilities in an annular combustor.

2

MICCA2 configuration

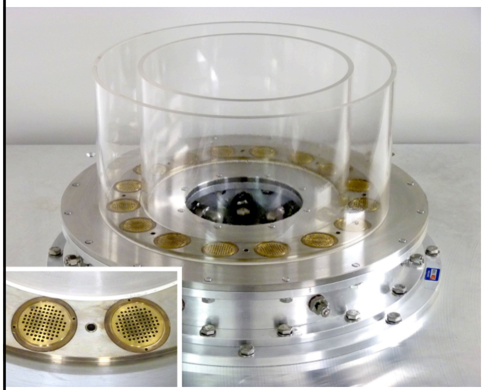

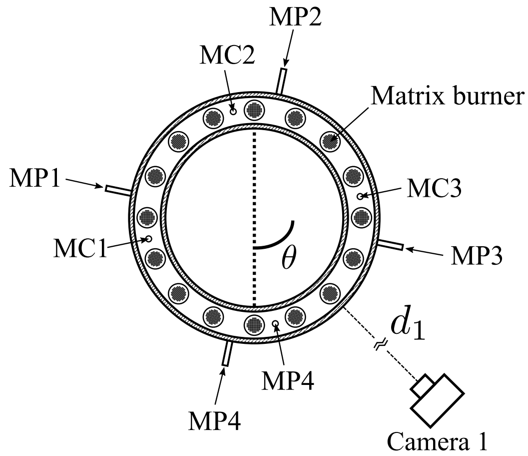

MICCA 2 is equipped with
16 matrix injectors

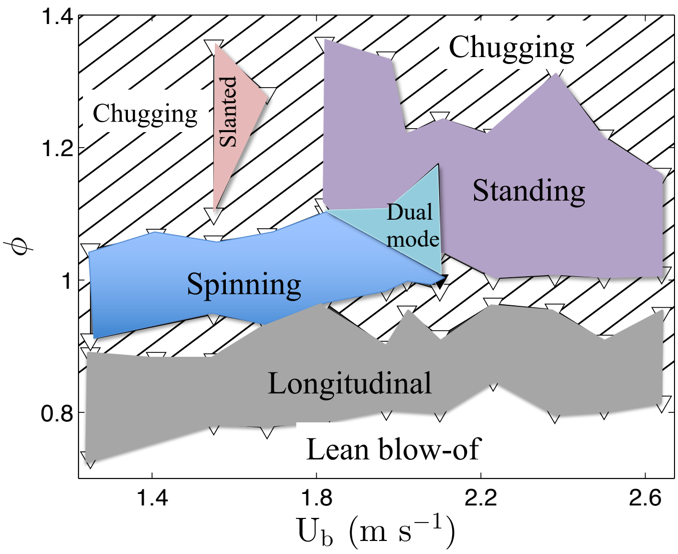

The dual mode region is where the spinning and standing regions overlap. The hatched area is where the chugging mode is manifested. The blank area corresponds to the lean extinction limits of the chamber

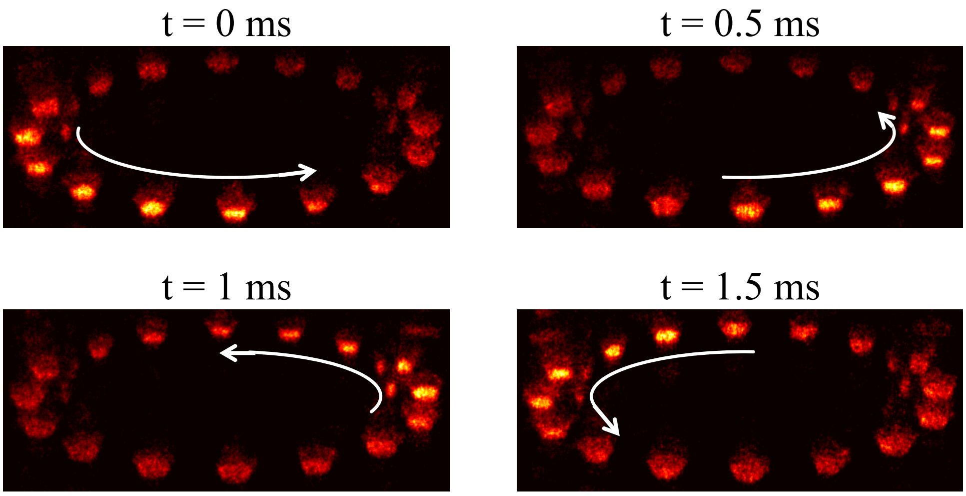

High-speed snapshots of the full annular combustion chamber during a spinning mode cycle (T = 2 ms). The mode is rotating in a counter-clockwise direction and the maximum luminosity reached by each flame during the cycle is the same for all burners.

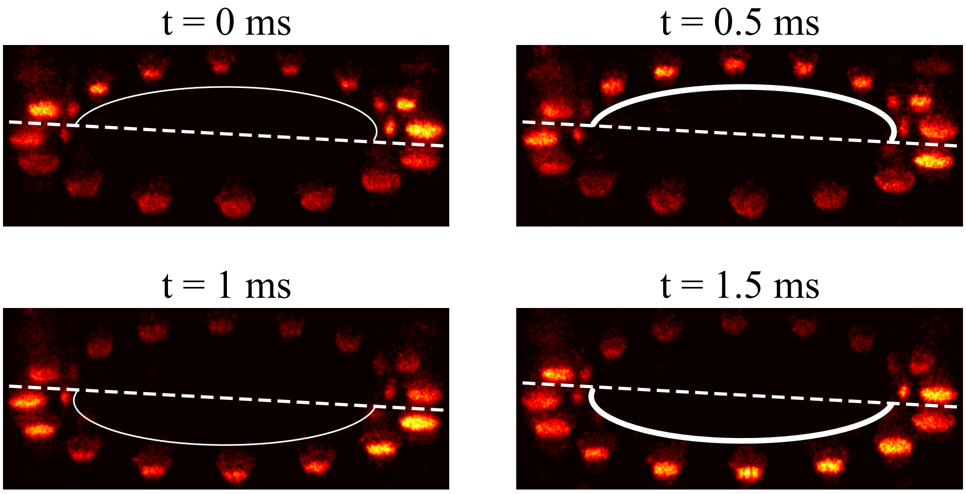

High-speed images of the full annular combustion chamber during a standing mode cycle (T = 2 ms). The nodal line (dashed line) is fixed between two burners. The thickness of the curved line gives an indication on the oscillation level. The flames next to the nodal line have a lower amplitude of oscillation than those situated near the anti-nodal region

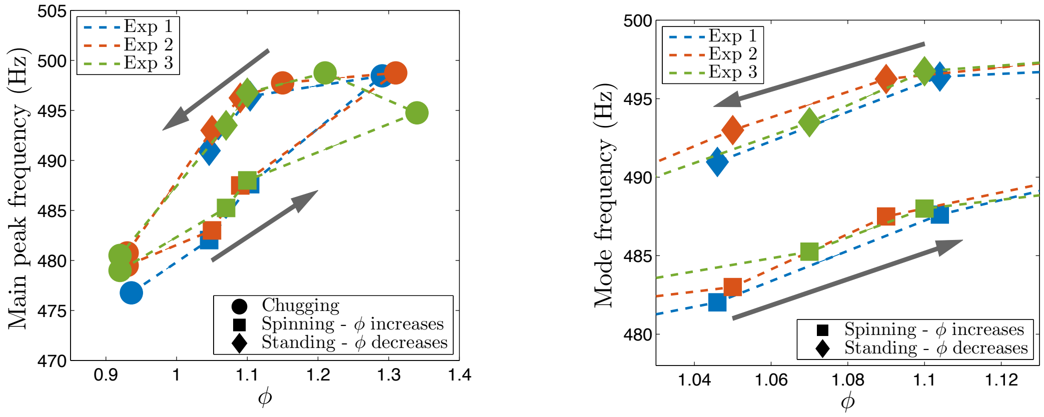

Left: hysteresis cycles for operating conditions indicated in. Arrows indicate the path followed during the experiment. When ϕ increases from 0.9 to 1.1 a spinning mode arises. When ϕ is diminished from 1.2 to 1.1 a standing mode prevails. Right: zoom on the loop for ranging between 1.03 and 1.13.

7

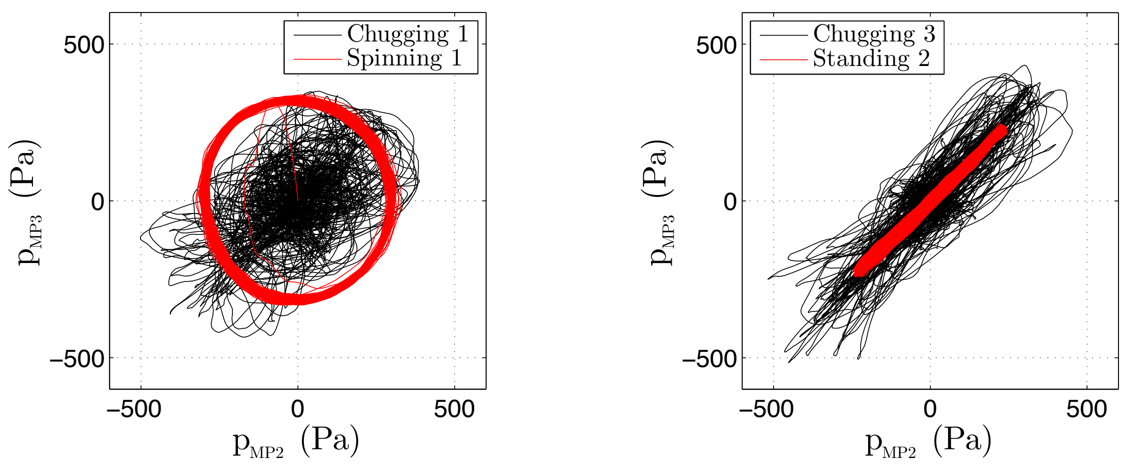

State space maps of the pressure signals ($t_{max} = 0.4\,\mathrm{s}$) recorded by microphones MP2 and MP3 in the plenum separated by a 90° angular shift

8

Conclusion

- Multiple longitudinal and azimuthal modes are observed in the annular configuration in regions which in general do not overlap
- Spinning and standing modes with stable limit cycles are observed for the same flow operating conditions in a limited « Dual mode » domain
- The oscillation arising in this « Dual mode » region depends on the path taken to reach the operating point. If ϕ is increased, with the same air mass flow rate, from lean conditions to the target value, a spinning mode is obtained. If ϕ is decreased from rich conditions, a standing mode is manifested at the target conditions
- The spinning and standing modes do not switch from one to the other but instead when a mode arises, it is locked on.
- The chugging oscillation observed just outside the region of azimuthal instability contains information that can be used to predict the azimuthal mode structure that will be established in the « Dual mode » domain.

- It would be interesting to see if these observations can be explained by recent theoretical analysis like (Ghirardo et al., 2015) which allow the coexistence of both spinning and standing modes for the same operating conditions. This is however not straightforward since the theory relies on a nonlinear time invariant relationship between heat release rate and pressure fluctuation in the chamber

K. Prieur, D. Durox, J. Beaunier, T. Schuller and S. Candel (2017) *Combustion and Flame.* 175, 283-291.
A hysteresis phenomenon leading to spinning or standing azimuthal instabilities in an annular combustor.

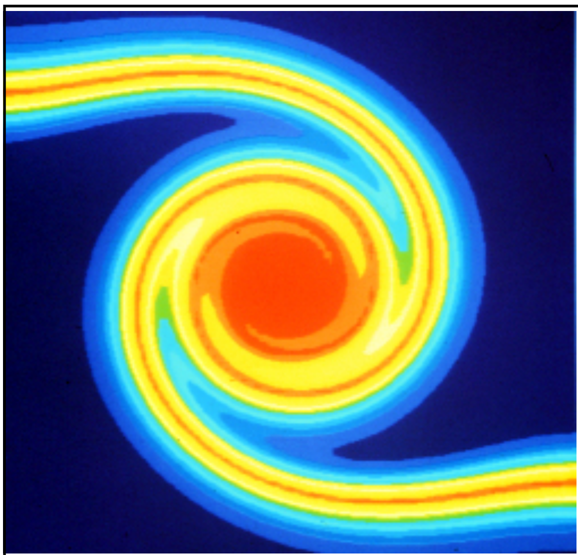

Combustion dynamics
Lecture 10c

S. Candel, D. Durox , T. Schuller

CentraleSupélec
Université Paris-Saclay, EM2C lab, CNRS

Tsinguha summer school, July 2021

1

Computational Flame Dynamics

Historical perspective (RANS, DNS, LES)
Laminar flame dynamics
Large eddy simulation of turbulent flames
Ignition of annular combustors
Annular systems azimuthal instabilities

2

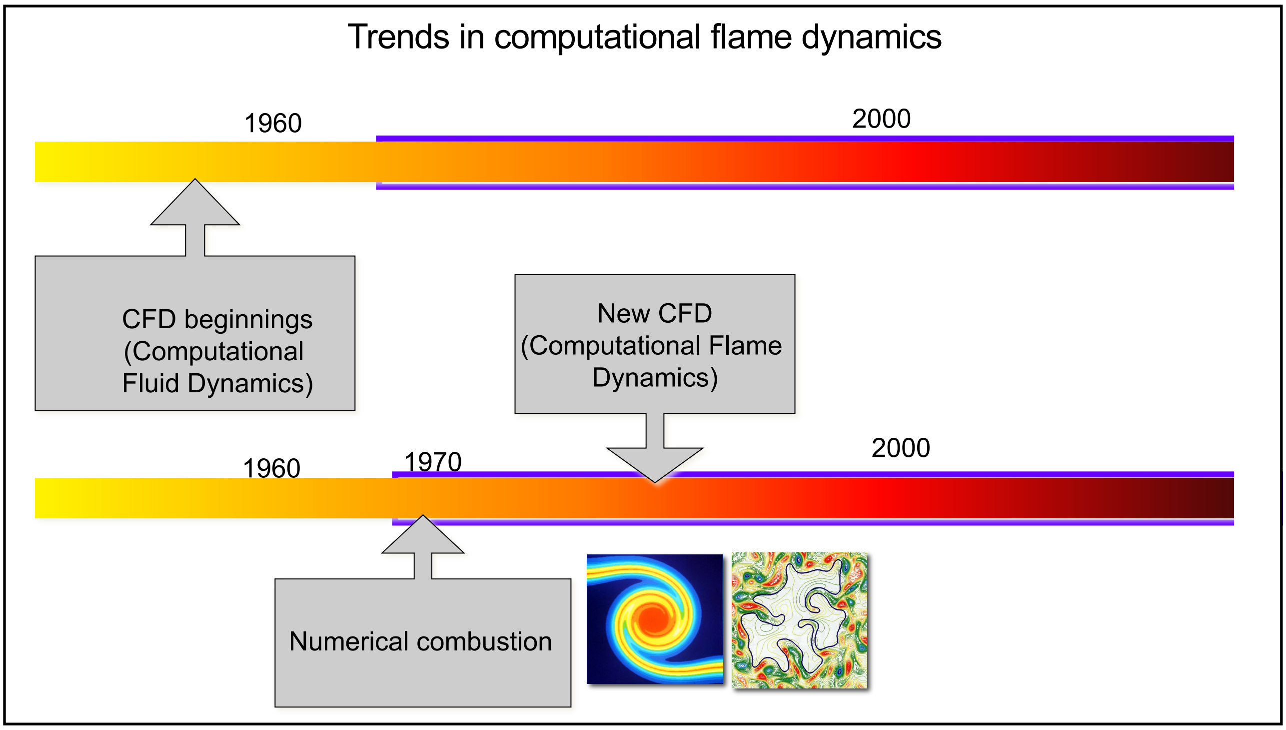

3

Simulation is crucial to the development of advanced combustion concepts

Direct simulation	Large eddy simulation	Reynolds average Navier-Stokes equations
All temporal and spatial scales are calculated	Large scales are calculated, small scales are represented by subgrid scale models	Equations are averaged and Reynolds stresses and turbulent fluxes are modeled

Laboratory → Applications

4

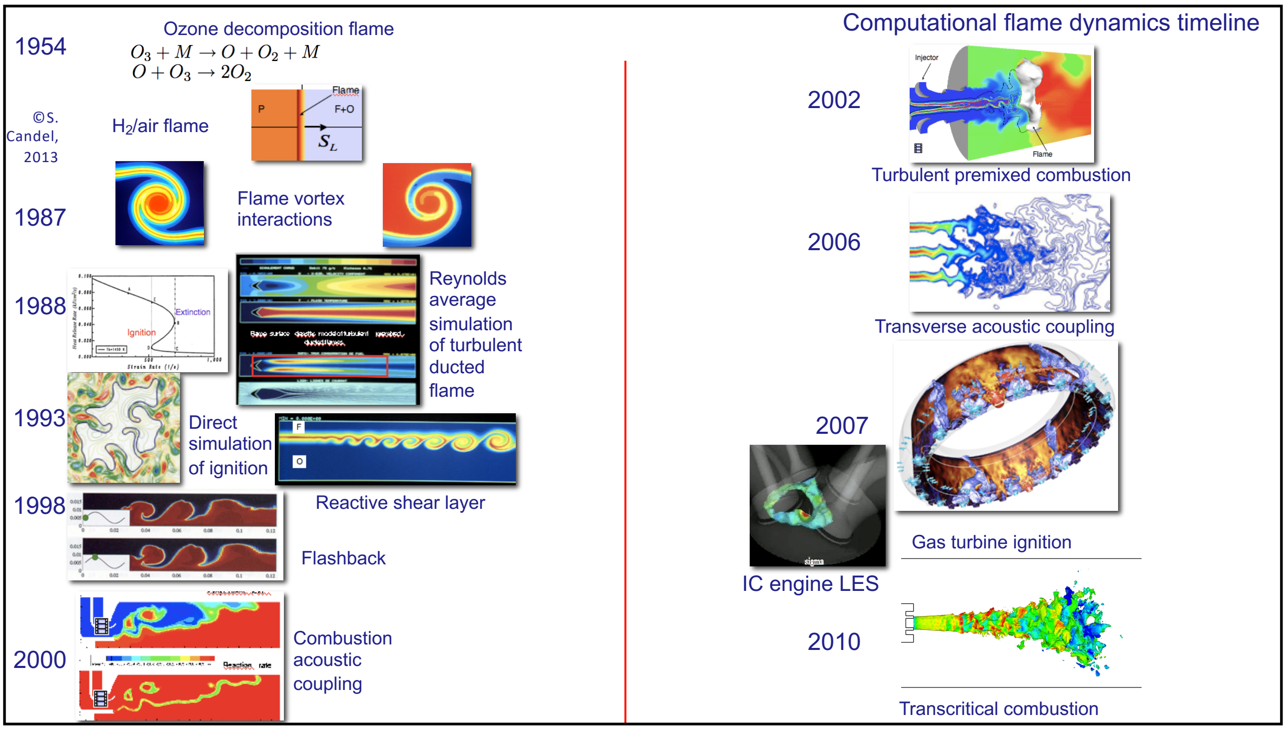
Computational flame dynamics timeline
1954
Ozone decomposition flame
$O_3 + M \rightarrow O + O_2 + M$
$O + O_3 \rightarrow 2O_2$
©S. Candel, 2013
H_2/air flame
Flame
P
F+O
S_L
1987
Flame vortex interactions
1988
Extinction
Ignition
Reynolds average simulation of turbulent ducted flame
1993
Direct simulation of ignition
Reactive shear layer
1998
Flashback
2000
Combustion acoustic coupling
2002
Injector
Flame
Turbulent premixed combustion
2006
Transverse acoustic coupling
2007
IC engine LES
Gas turbine ignition
2010
Transcritical combustion

5

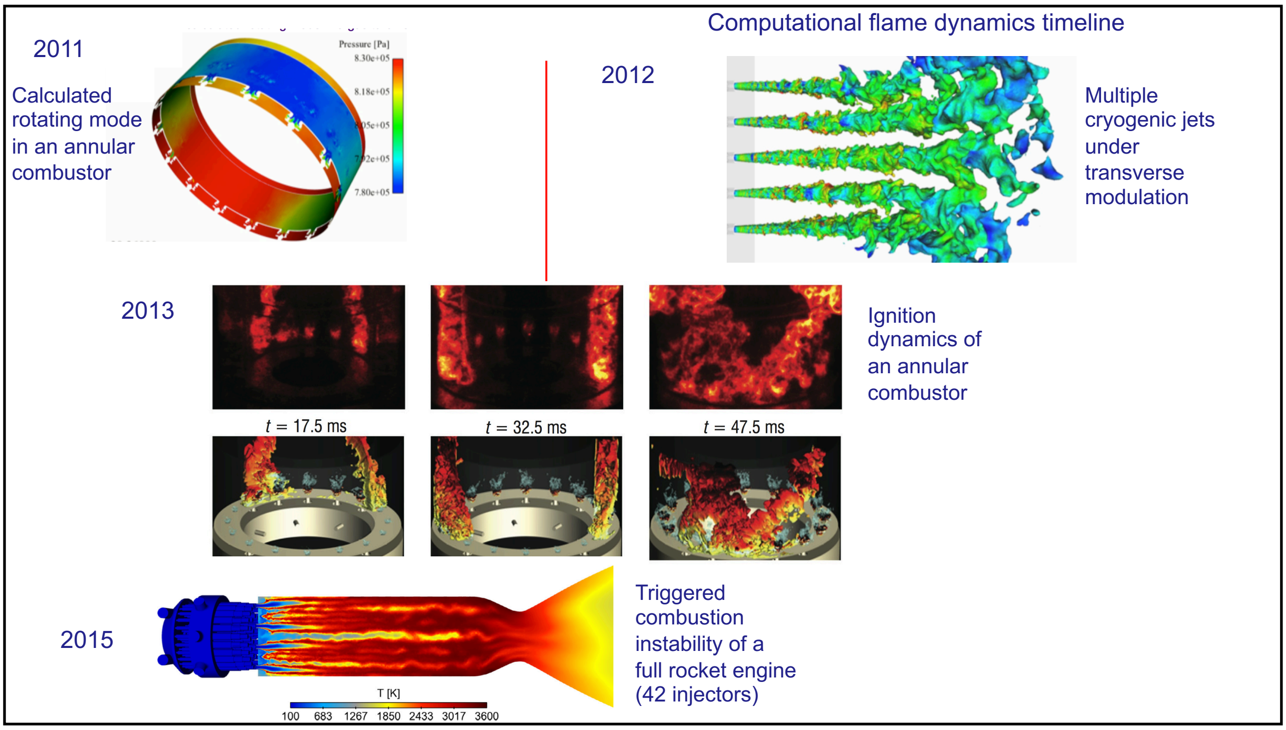
Computational flame dynamics timeline
2011
Calculated rotating mode in an annular combustor
Pressure [Pa]
8.30e+05
8.18e+05
7.80e+05
2012
Multiple cryogenic jets under transverse modulation
2013
t = 17.5 ms
t = 32.5 ms
t = 47.5 ms
Ignition dynamics of an annular combustor
2015
T [K]
100 683 1267 1850 2433 3017 3600
Triggered combustion instability of a full rocket engine (42 injectors)

6

Large Eddy Simulations in fluid mechanics
(observed in the Web of Science)

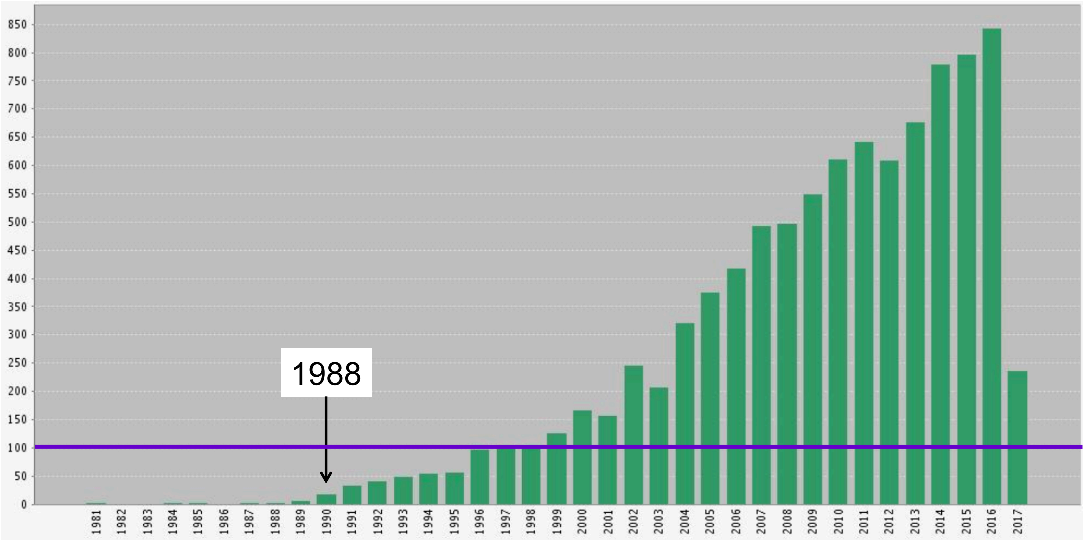

Large eddy simulations appear in the late 1980th

7

(1) Much of the current modeling effort in combustion is carried out in the LES framework

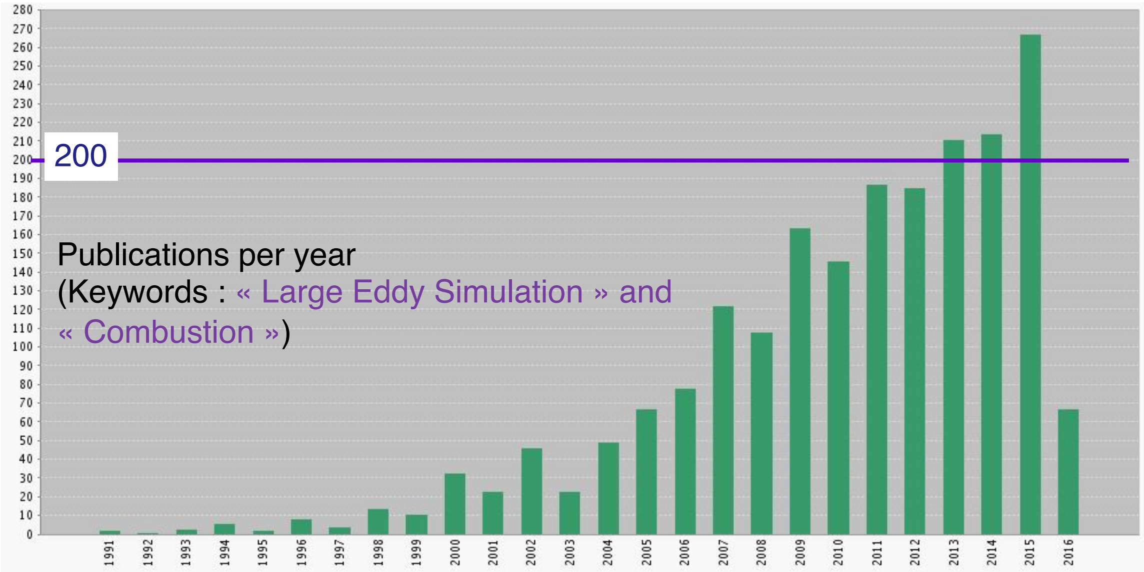

Over two hundred publications per year featuring these two keywords

8

Direct simulation of premixed flames is feasible if…

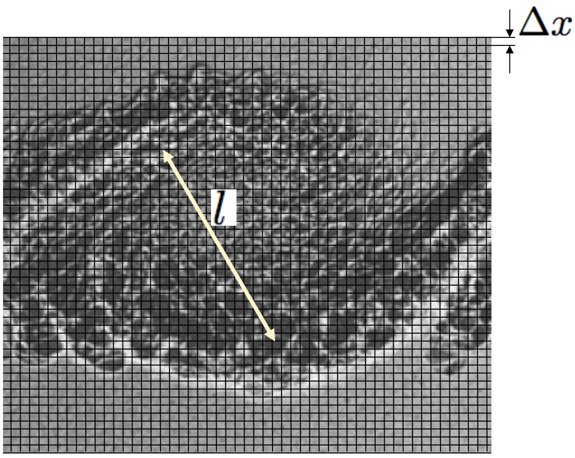

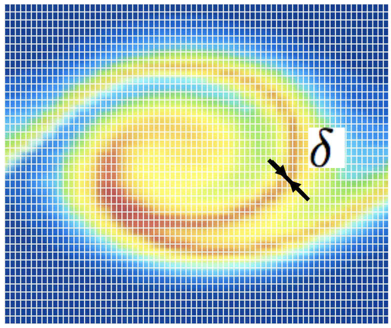

A minimum of n points
is used to discretize the flame

$$N\Delta x > l$$
$$\Delta x = l_k$$

$$\delta = n\Delta x$$
$$\frac{N}{n} > \frac{l}{\delta}$$

$$N > (\mathrm{Re}_l)^{3/4} \qquad (N/n)^2 > \mathrm{Re}_l \mathrm{Da}$$

This limits direct simulation to low Reynolds and Damköhler numbers

$$N = 1000 \qquad N^3 = 10^9$$

$n = 20$ to resolve the flame

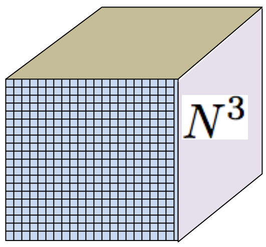

$$\mathrm{Re}_l < N^{4/3} = 10^4$$
$$\mathrm{Re}_l \mathrm{Da} < (N/n)^2 = 2500$$

If one chooses $\mathrm{Re}_l = 250$

then $\mathrm{Da} < 10$

In simulations of turbulent flames at Damköhler numbers greater than unity (typical of combustion conditions where the chemical time is short compared to the mechanical time) the Reynolds number can only take moderate values

This restricts the domain accessible to direct simulation

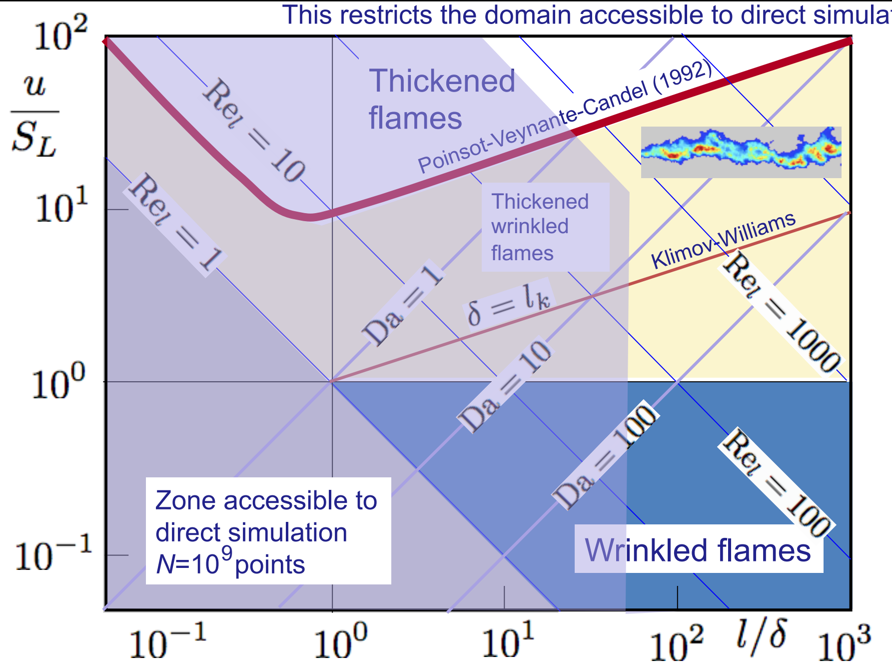

T. Poinsot, S. Candel and A. Trouvé (1996) *Progress in Energy and Combustion Science.* **21**, 531-576.
Direct numerical simulation of premixed turbulent combustion.

11

Combustion dynamics of flames interacting with equivalence ratio perturbations

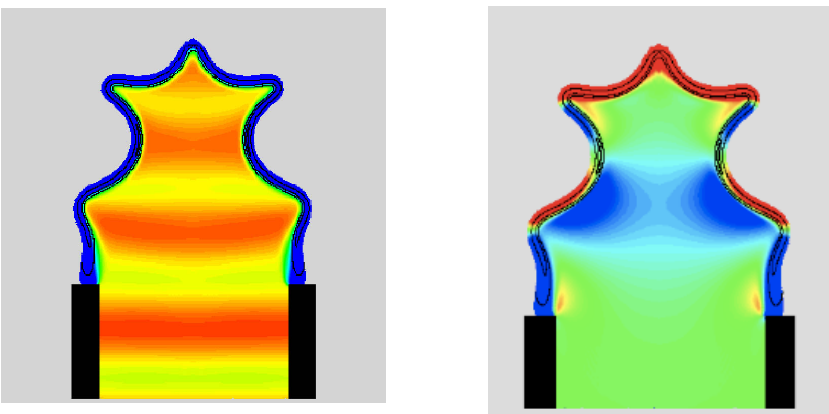

Conical flame perturbed by equivalence ratio modulations

Inverted flame perturbed by equivalence ratio modulations

A.L. Birbaud, S. Ducruix, D . Durox and S. Candel (2008) *Combustion and Flame.* 154, 356-367. The nonlinear response of inverted « V »-flames submitted to equivalence ratio nonuniformities.

12

Combustion dynamics of flames interacting with equivalence ratio perturbations

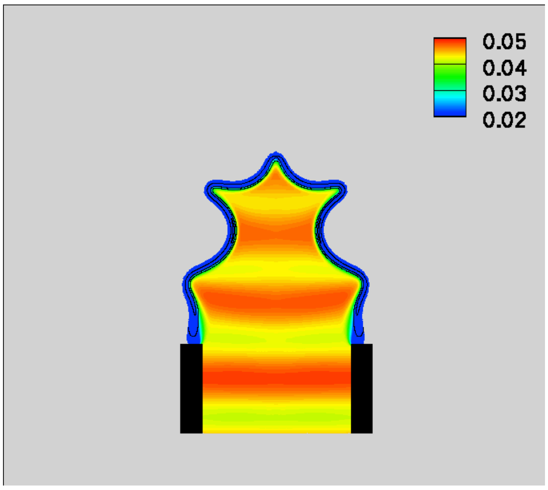

Conical flame perturbed by equivalence ratio modulations

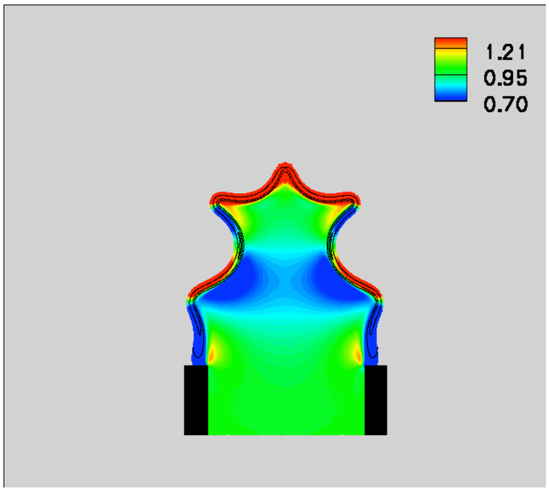

Velocity field perturbed by equivalence ratio modulations

A.L. Birbaud, S. Ducruix, D . Durox and S. Candel (2008) *Combustion and Flame.* 154, 356-367. The nonlinear response of inverted « V »-flames submitted to equivalence ratio nonuniformities.

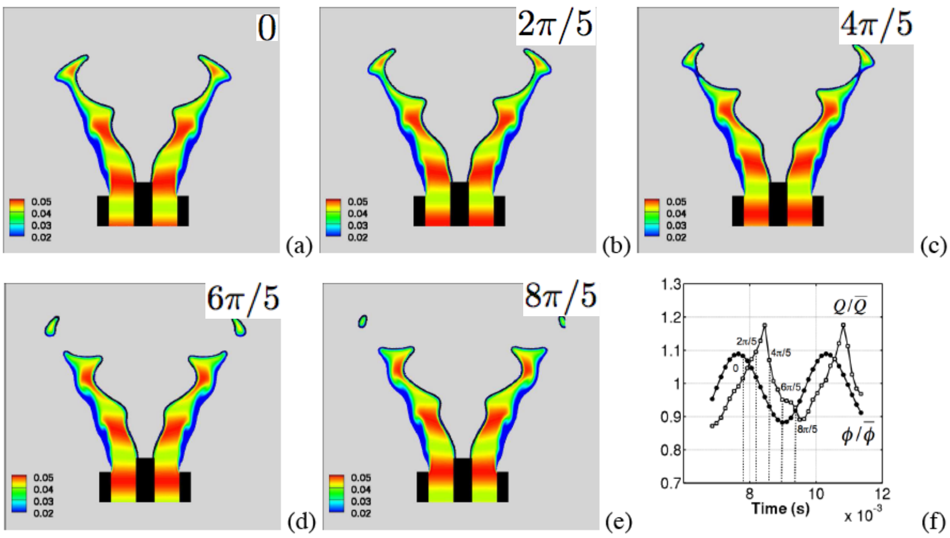

(a-e) Methane mass fraction distributions during a cycle. $\phi(t) = \phi_0 + \phi_1 \sin \omega t$

(f) Relative heat release and equivalence ratio perturbation

$$f = 375\,\text{Hz},\ \phi'/\overline{\phi} = 0.1,\ \phi = 0.8$$

(2) It is hoped that LES will allow to analyze practical applications

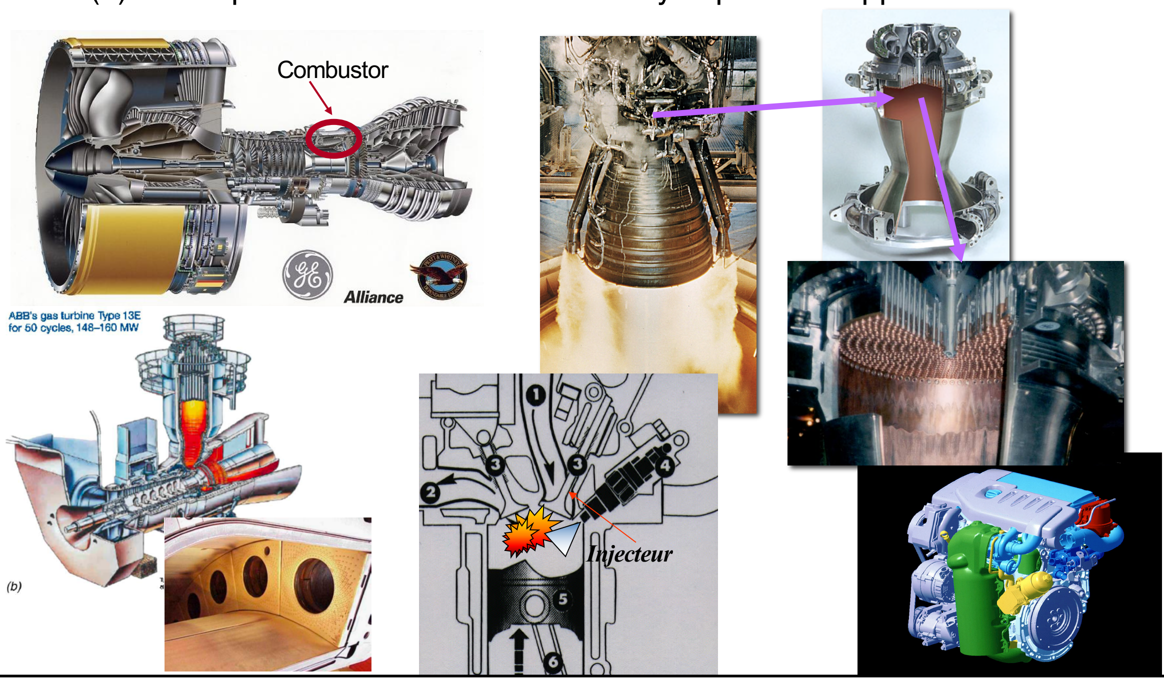

The future clearly lies in Large Eddy Simulations

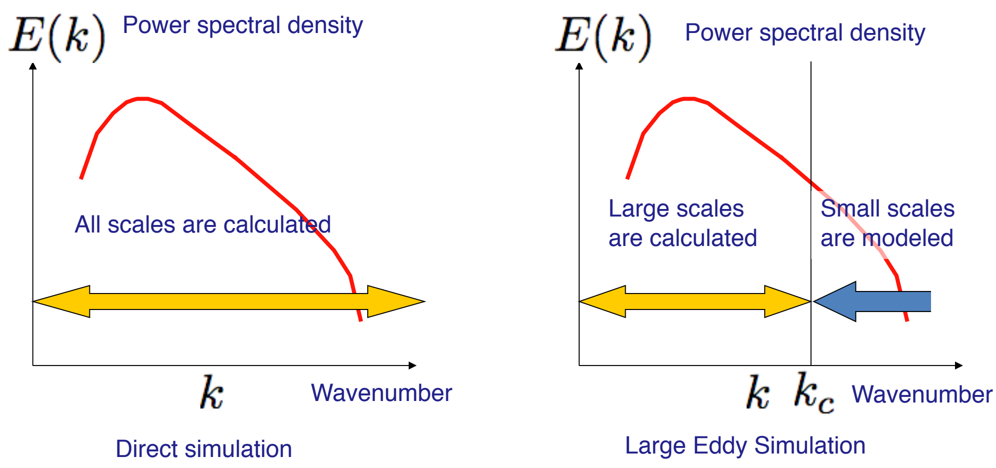

$$k_c \simeq 1/\Delta$$

DNS

LES

Large eddy simulation of turbulent combustion

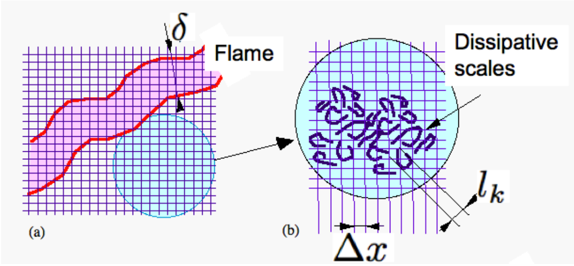

In direct simulation, dissipative scales and flame must be resolved on the grid

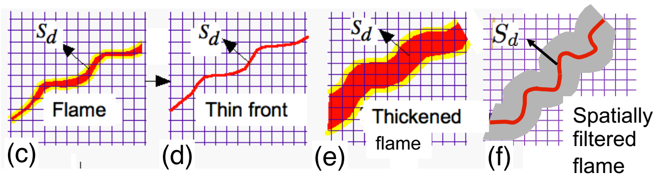

In large eddy simulations the small scales are modeled but the grid is too rough to resolve the flame :

- The flame is replaced by a thin front (d)
- The flame is artificially thickened (e)
- The flame is spatially filtered (f)

The thickened flame method

LES methods are now widely used to examine combustion dynamics and instabilities. LES naturally describes the flame motion induced by the large scales

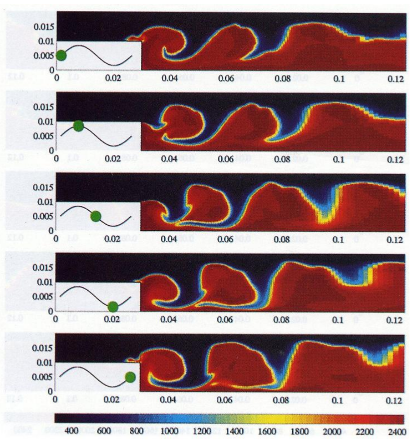

One effective model in premixed combustion relies on the artificial thickening of the flame so that it can be calculated on a relatively coarse grid.

This method, originally proposed by Bracco and O'Rourke in a different context, was later explored by Thibaut and Candel (1998) in a simulation of oscillations in a dump configuration.

D. Thibaut and S. Candel (1998) *Combustion and Flame*, **113**, 51-65. Numerical study of unsteady turbulent premixed combustion. Application to flashback simulation.

Combined with a subgrid scale efficiency function the flame thickening method (FTM) has been extensively exploited to investigate combustion dynamics in premixed gas turbine combustors

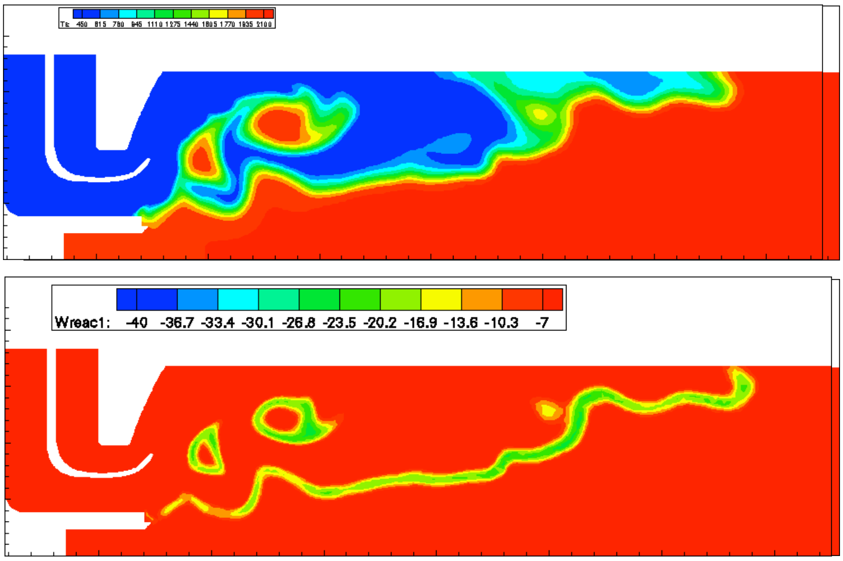

Temperature distribution

Heat release rate distribution

S. Ducruix, T. Poinsot and S. Candel (2002) Large eddy simulation of combustion instabilities in a swirled combustor. In *Turbulent mixing and combustion,* A. Pollard and S. Candel, eds. Kluwer, Dodrecht, Chapter 31, pp. 357-366.

19

Swirling flame calculations with LES and complex chemistry give access to practical applications

Tabulated Thermochemistry for Compressible flows formalism (FTACLES)

Air
623 K

CH4
388 K

Air
623 K

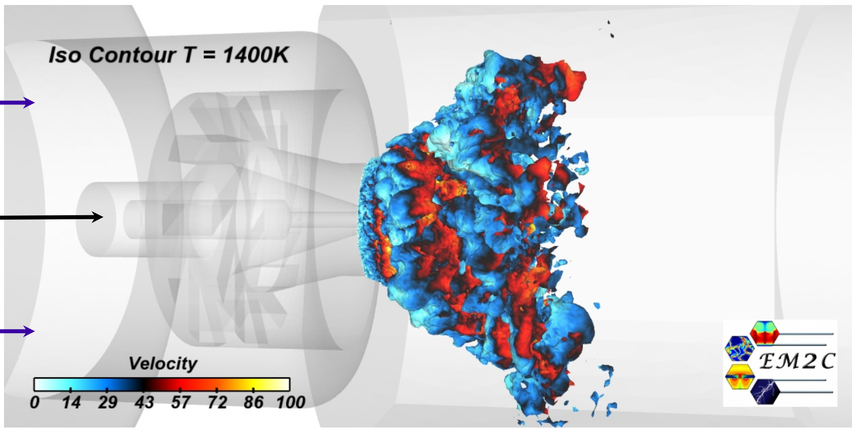

AVBP

8.1 million nodes,
40.2 million cells,
$(\Delta x)_{min}$ = 0.08 mm
180 000 CPU hours
(With 2000 cores the restitution time is about 1 week)

$\Phi = 0.8$

R. Vicquelin, B. Fiorina, S. Payet, N. Darabiha& O. Gicquel 2011 Coupling tabulated chemistry with compressible CFD solvers. *Proceedings of the Combustion Institute* 33 (1), 1481–1488.

P. Auzillon, O. Gicquel, N. Darabiha, D. Veynante, B. Fiorina (2012) A Filtered Tabulated Chemistry model for LES of stratified flames. *Combustion and Flame*, 159 (8), pp.2704-2717.

20

Ignition of an annular combustor

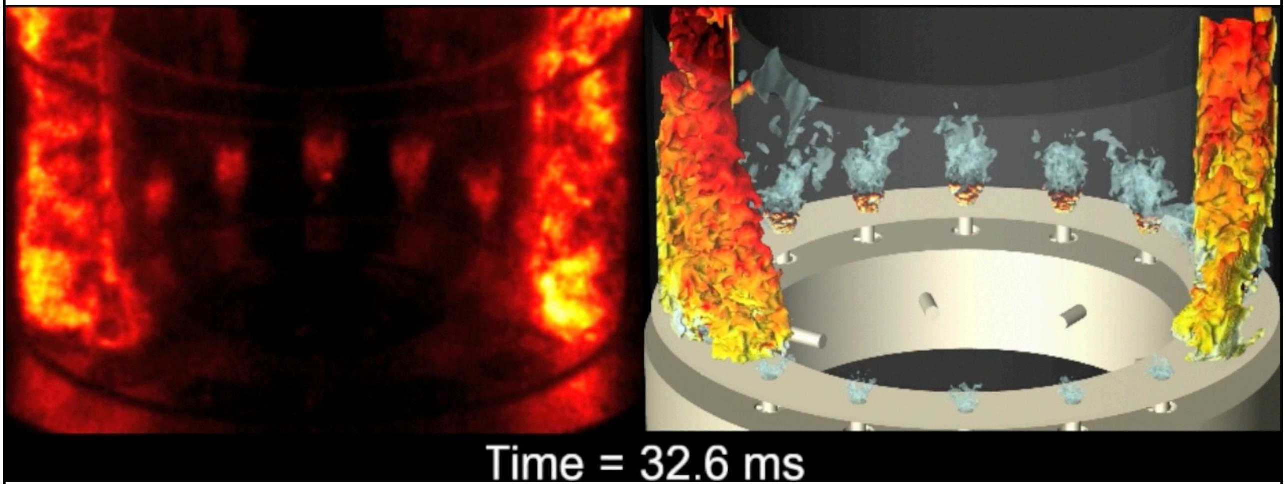

Experiment Simulation

M. Philip, M. Boileau, R. Vicquelin, T. Schmitt, D. Durox, J.F. Bourgouin and S. Candel (2014) *Physics of fluids*, 26, 091106. doi: 10.1063/1.4893452. Ignition sequence in a multi-injector combustor**.**

M. Philip, M. Boileau, R. Vicquelin, T. Schmitt, D. Durox, J.F. Bourgouin, S. Candel (2015). *Journal of Eng. Gas Turbines Power (ASME)* 137(3), 031501 GTP14-1375 doi: 10.1115/1.4028265. Simulation of the ignition process in an annular multiple-injector combustor and comparison with experiments.

21

Light round ignition of the MICCA combustor. Experiment and simulation. $U_b = 24\,\mathrm{m\ s^{-1}}$

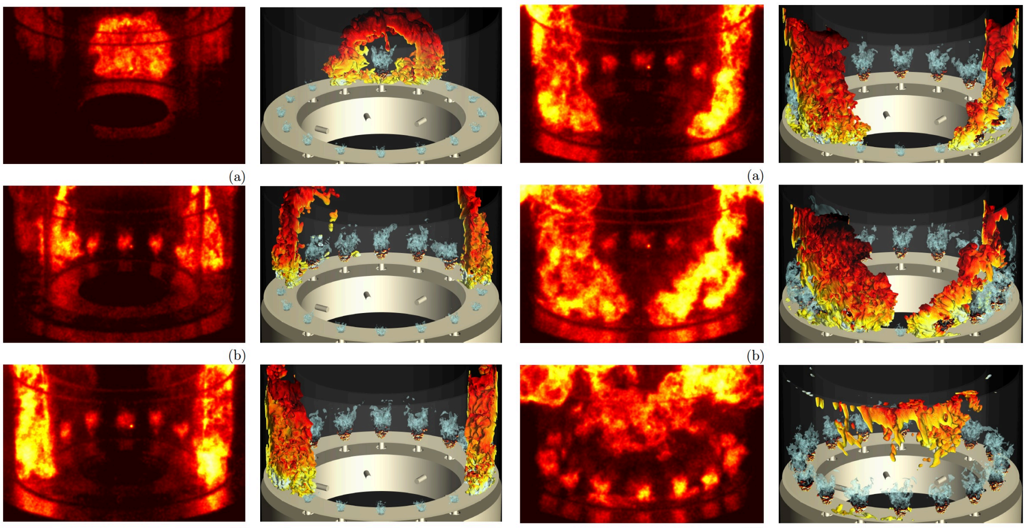

Experiment Simulation Experiment Simulation

M. Philip, M. Boileau, R. Vicquelin, T. Schmitt, D. Durox, J.F. Bourgouin, S. Candel (2015*) Journal of Engineering for Gas Turbine and Power (ASME)* 137(3), 031501 Simulation of the ignition process in an annular multiple-injector combustor and comparison with experiments.

PARTNERSHIP FOR ADVANCED COMPUTING IN EUROPE

22

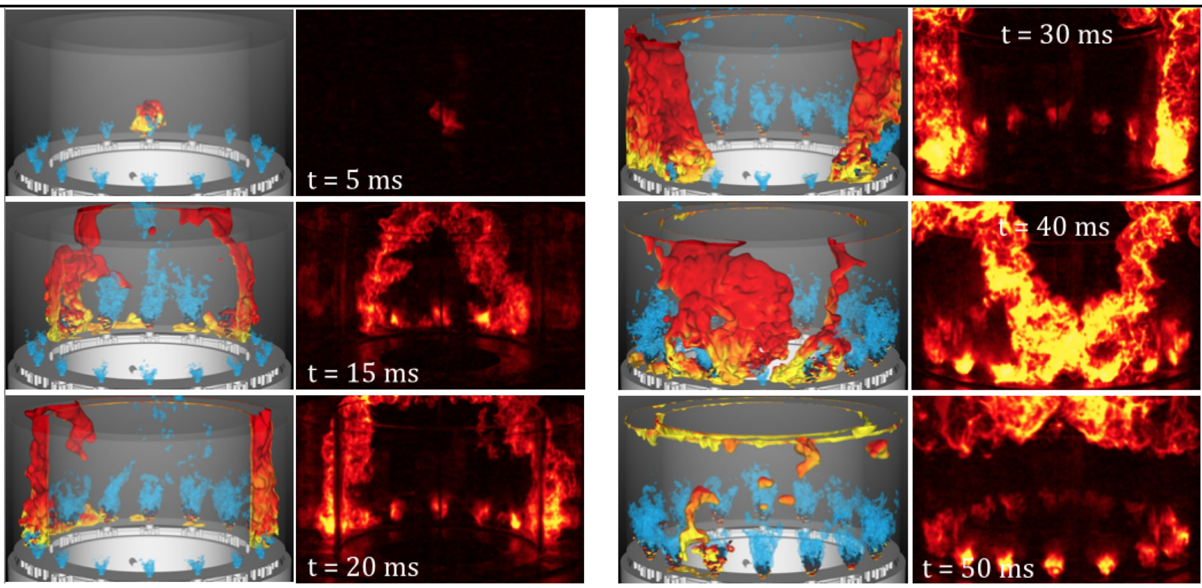

Comparison between experimental and numerical flame configurations for liquid n-heptane injection. $\phi = 0.8,\ \mathcal{P} = 79.8\,\mathrm{kW}$

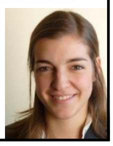

T. Lancien, D. Durox, K. Prieur, S. Candel and R. Vicquelin (2017) *J. Eng. Gas Turbines Power* 140(2), 021504.
Large Eddy Simulation of light-round in an annular combustor with liquid spray Injection and comparison with experiments

23

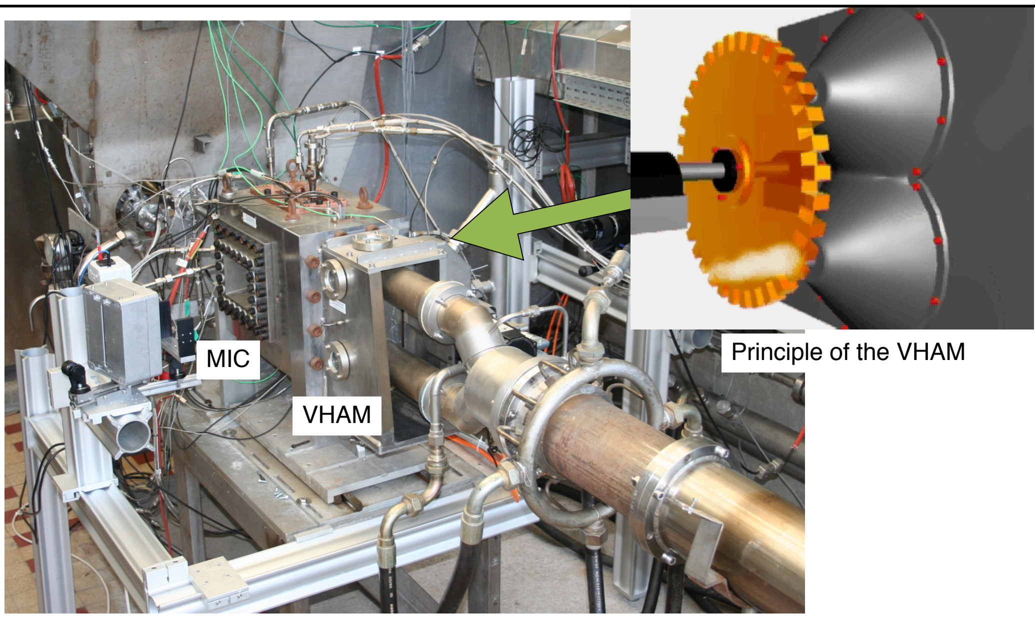

Multiple injector combustor (MIC) equipped with a Very High Amplitude Modulator (VHAM) mounted on the « Mascotte » cryogenic combustion testbench

24

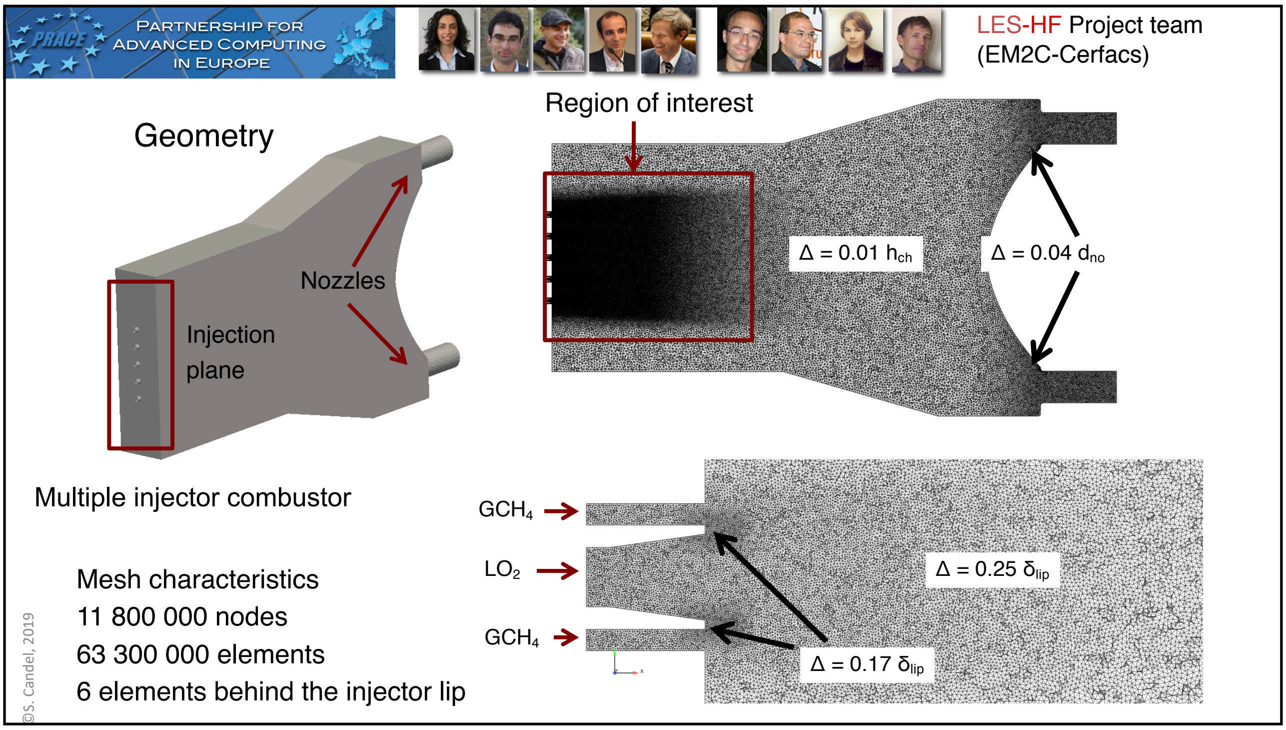
PARTNERSHIP FOR ADVANCED COMPUTING IN EUROPE
LES-HF Project team (EM2C-Cerfacs)
Geometry
Nozzles
Injection plane
Multiple injector combustor
Region of interest
Δ = 0.01 h_{ch}
Δ = 0.04 d_{no}
GCH_4
LO_2
GCH_4
Δ = 0.25 δ_{lip}
Δ = 0.17 δ_{lip}
Mesh characteristics
11 800 000 nodes
63 300 000 elements
6 elements behind the injector lip
©S. Candel, 2019

25

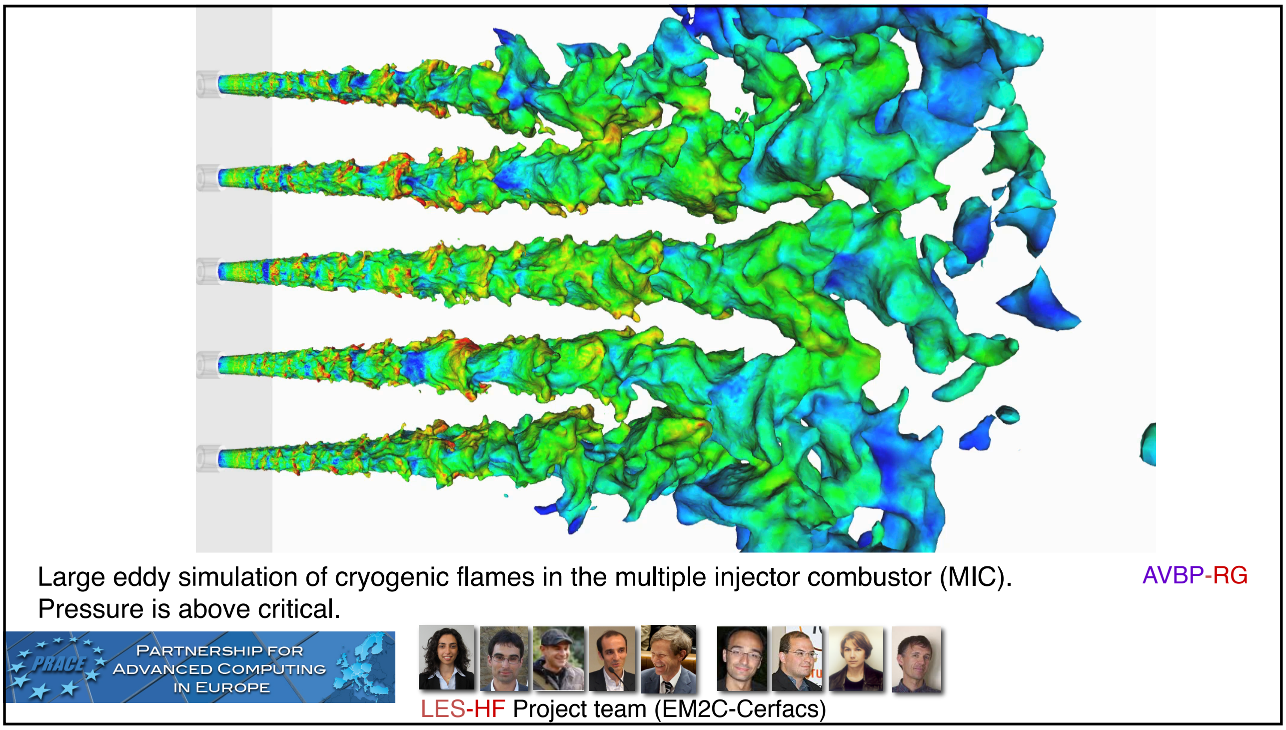
Large eddy simulation of cryogenic flames in the multiple injector combustor (MIC).
Pressure is above critical.
AVBP-RG
PARTNERSHIP FOR ADVANCED COMPUTING IN EUROPE
LES-HF Project team (EM2C-Cerfacs)

26

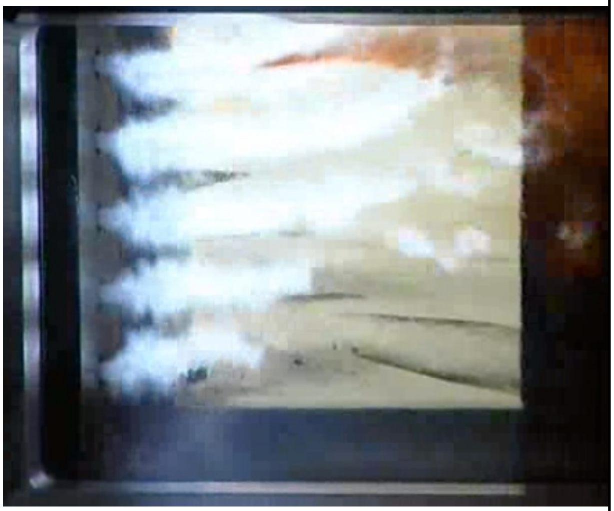

Cryogenic flames are developing in the absence of acoustic modulation

The transverse acoustic modulation induces a significant reduction in flame length

27

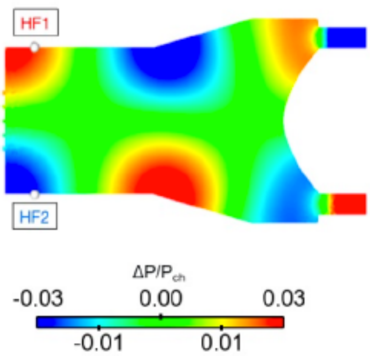

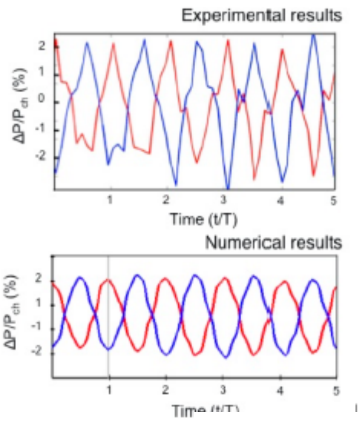

Experimental pressure signals

Simulated pressure signals

Structure modale obtenue dans la chambre au moyen d'une simulation numérique de la modulation par le VHAM

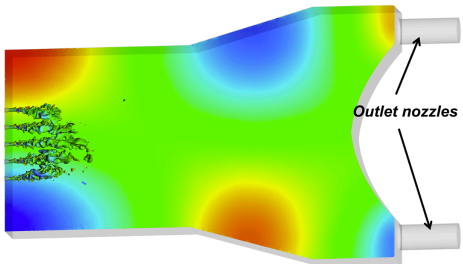

28

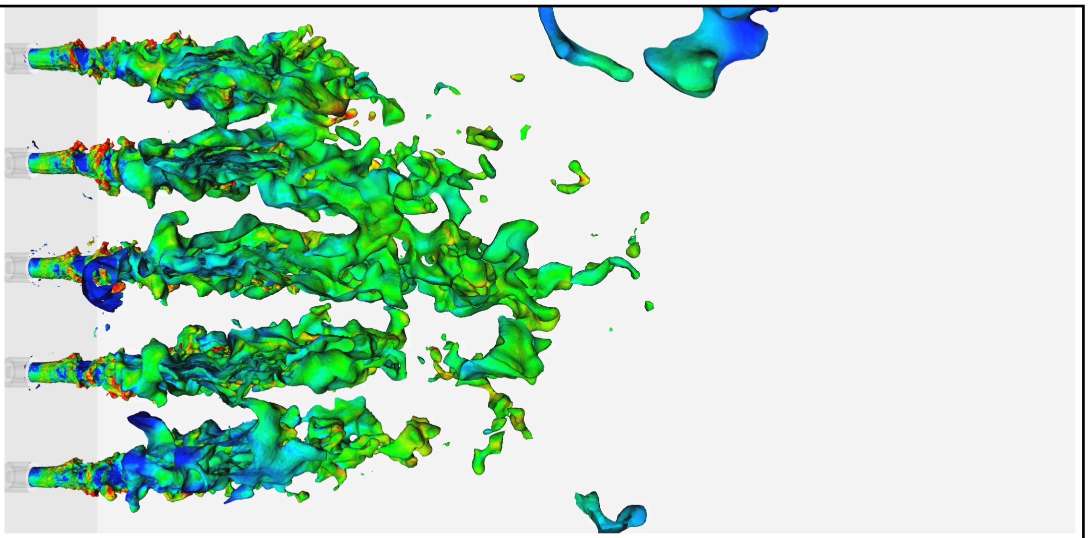

Large eddy simulation of cryogenic flames in the multiple injector combustor (MIC). Pressure is above critical. Flames interact with the 1T1L mode induced by the Very High Amplitude Modulator

AVBP-RG

PARTNERSHIP FOR ADVANCED COMPUTING IN EUROPE

LES-HF Project team (EM2C-Cerfacs)

29

Simulation of a cryogenic engine comprising 42 coaxial injectors (BKD)

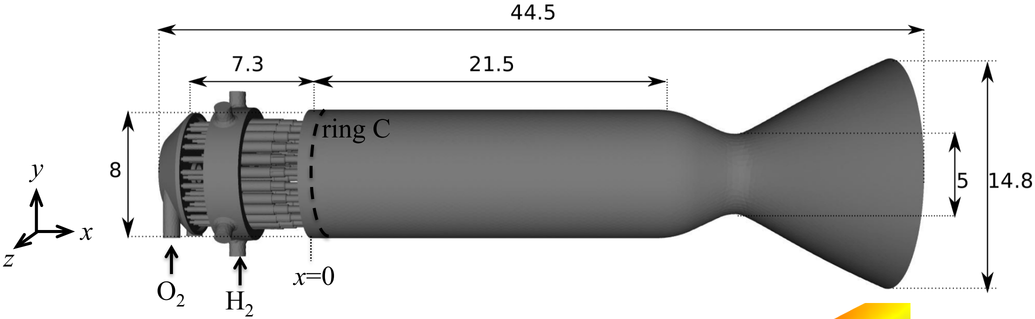

Nbr of elements
70 M
Mesh size
near the injector
lip $\Delta x = 50\mu m$

CPU time
on BlueGene Q
1M hours for 10ms

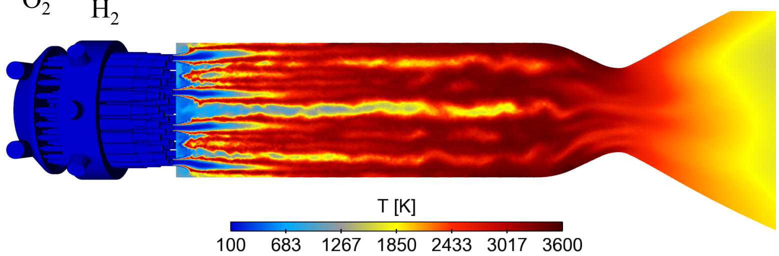

Temperature distribution in the engine in the absence of instability

A. Urbano, L. Selle, G. Staffelbach, B. Cuenot, T. Schmitt, S. Ducruix and S. Candel (2016) *Combustion and Flame*. 169, 129-140. Exploration of combustion instability triggering using Large Eddy Simulation of a multiple injector Liquid Rocket Engine.

A. Urbano, Q. Douasbin, L. Selle, G. Staffelbach, B. Cuenot, T. Schmitt, S. Ducruix and S. Candel (2017) *Proceedings of the Combustion Institute, 36.* Study of flame response to transverse acoustic modes from the LES of a 42-injector rocket engine.

30

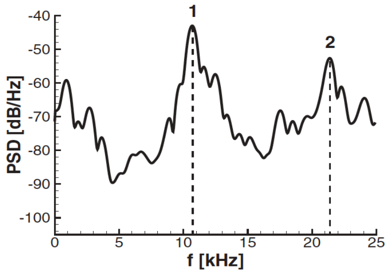

Power spectral density from simulation

(b) LP4-LES: $f_1 = 10,700$ Hz, $f_2 = 21,400$ Hz.

Power spectral density of a pressure signal in a regime of a high frequency instability (Operating point LP4)

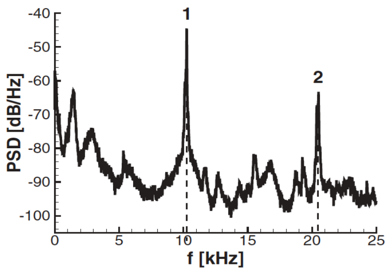

Measured power spectral density

(d) LP4-experiment: $f_1 = 10,260$ Hz, $f_2 = 20,500$ Hz.

A. Urbano, L. Selle, G. Staffelbach, B. Cuenot, T. Schmitt, S. Ducruix and S. Candel (2016) *Combustion and Flame*. 169, 129-140. Exploration of combustion instability triggering using Large Eddy Simulation of a multiple injector Liquid Rocket Engine.

31

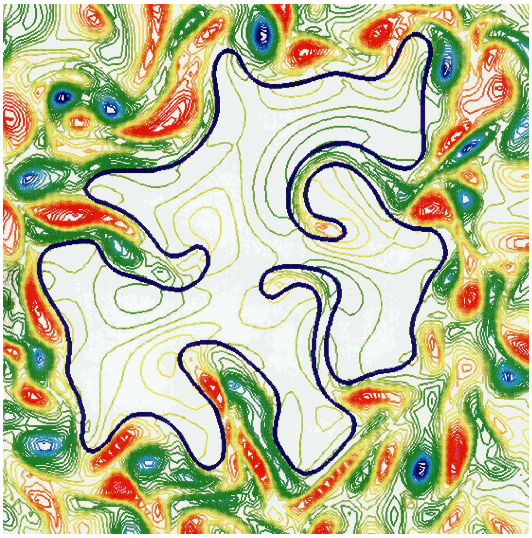

Combustion dynamics
Lecture 10d

S. Candel, D. Durox , T. Schuller

CentraleSupélec, EM2C lab, CNRS
Université Paris-Saclay

Tsinguha summer school, July 2021

1

Ignition dynamics

Ignition of a homogeneous reactor
Ignition under non premixed conditions
Light round in an annular combustor

2

Ignition of a homogeneous reactor

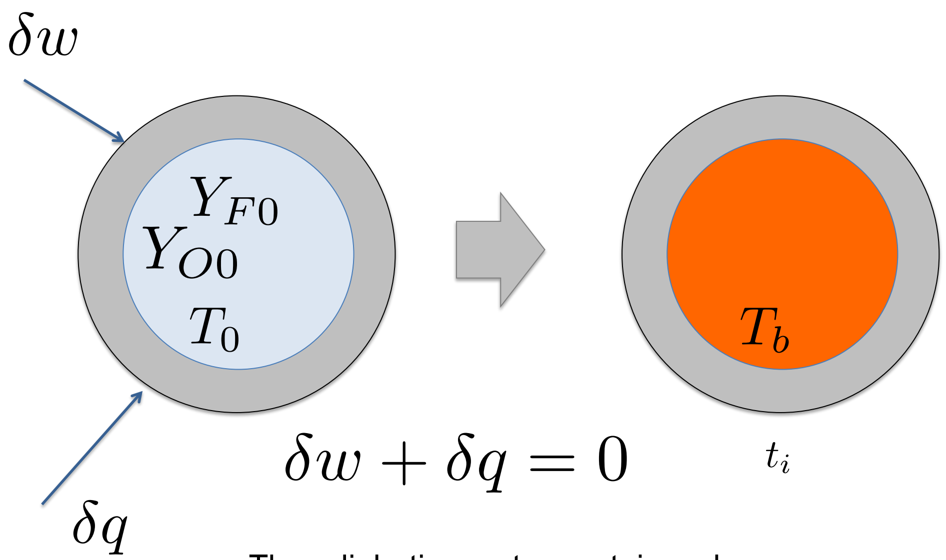

The adiabatic reactor contains a homogeneous reactive mixture at an initial temperature T_0 with initial mass fractions Y_{F0} *and* Y_{O0}

It is assumed that a single step reaction takes place

$$\nu'_F F + \nu'_O O \rightarrow P$$

with a reaction rate following Arrhenius kinetics

$$\dot{\omega} = B C_F C_{O_2} \exp(-\frac{E}{RT})$$

Species concentrations may be wriiten in terms of massa fractions

$$C_F = \rho Y_F / W_F, \quad C_O = \rho Y_O / W_O$$

The reaction rate becomes

$$\dot{\omega} = \frac{B\rho^2}{W_O W_F} Y_O Y_F \exp(-\frac{E}{RT})$$

The ignition is governed by a first order differential equation together with algebraic expressions for the fuel and oxidizer mass fractions

$$\rho c_v \frac{dT}{dt} = (-\Delta E)\dot{\omega}$$

$$\dot{\omega} = \frac{B\rho^2}{W_F W_O} Y_F Y_O \exp(-\frac{E}{RT})$$

$$Y_F = Y_{F0} - c_v \frac{\nu'_F W_F}{(-\Delta E)}(T - T_0)$$

$$Y_O = Y_{O0} - c_v \frac{\nu'_O W_O}{(-\Delta E)}(T - T_0)$$

An asymptotic analysis based assuming a large activation energy indicates that the perturbation of temperature with respect to the initial temperature is governed by the following differential equation

$$\frac{d}{dt}(\frac{T_1}{T_0}) = \frac{(-\Delta E)B\rho}{\varepsilon W_F W_O c_v T_0 Y_{F0} Y_{O0}} \exp(-\frac{E}{RT_0}) \exp(\frac{T_1}{T_0})$$

where $\varepsilon = RT_0/E$ is a small parameter

This expression features a characteristic time

$$t_i = \frac{RT_0}{E} \frac{c_v T_0}{(-\Delta E)B\rho} \frac{W_F W_O}{Y_{F0} Y_{O0}} \exp(\frac{E}{RT_0})$$

Inserting this definition in the differential equation for the temperature perturbation one finds

$$\frac{d(T_1/T_0)}{d(t/t_i)} = \exp(\frac{T_1}{T_0})$$

The temperature perturbation features a logarithmic behavior

$$\frac{T_1}{T_0} = -\ln(1 - \frac{t}{t_i})$$

When $t << t_i$ the perturbation in temperature is small. When t approaches t_i this perturbation increases without bound

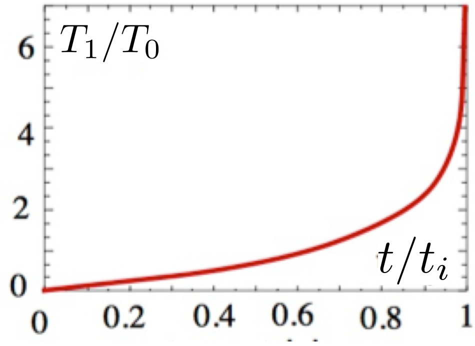

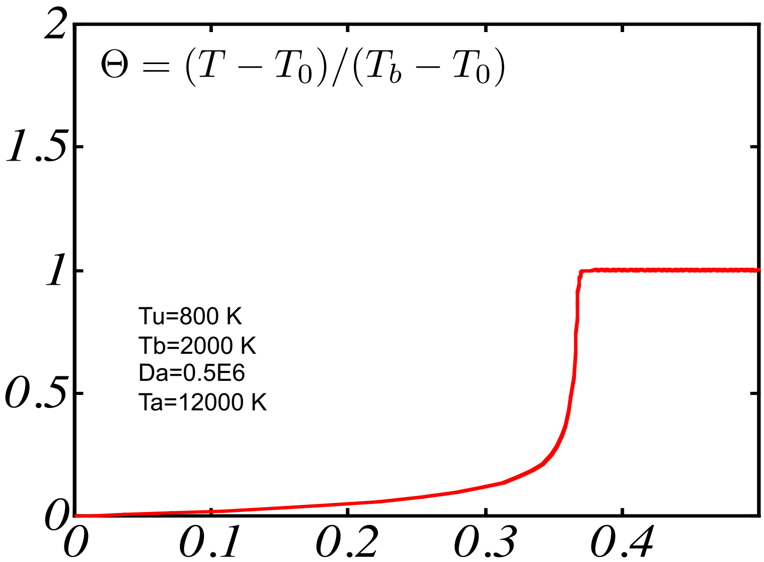

Temperature evolution as a function of time

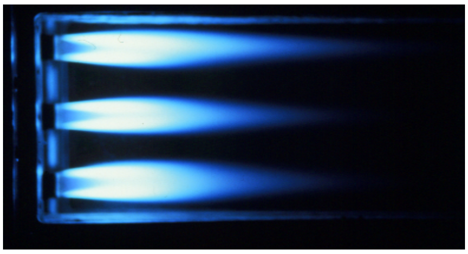

Stable operation

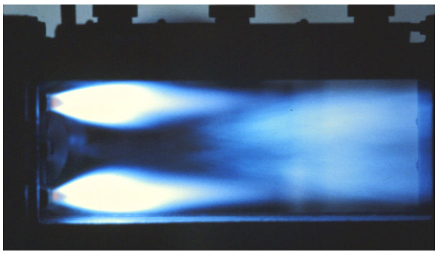

Extinction by pressure waves

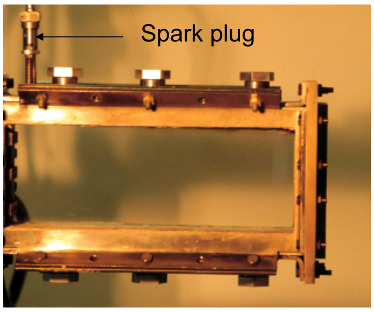

Combustor

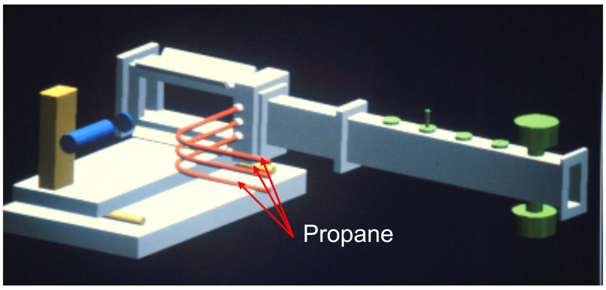

Non-premixed multiple injectorcombustor

Laser induced fluorescence of OH

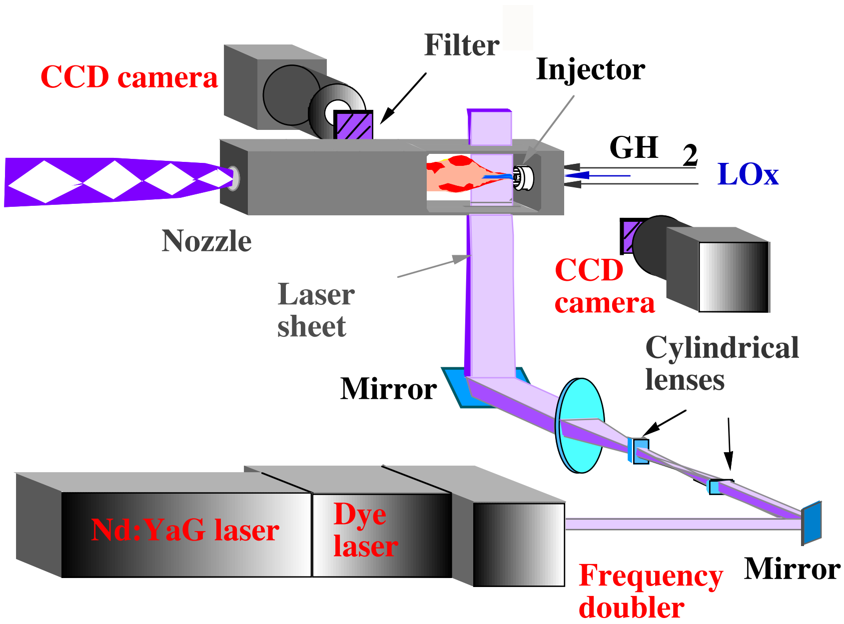

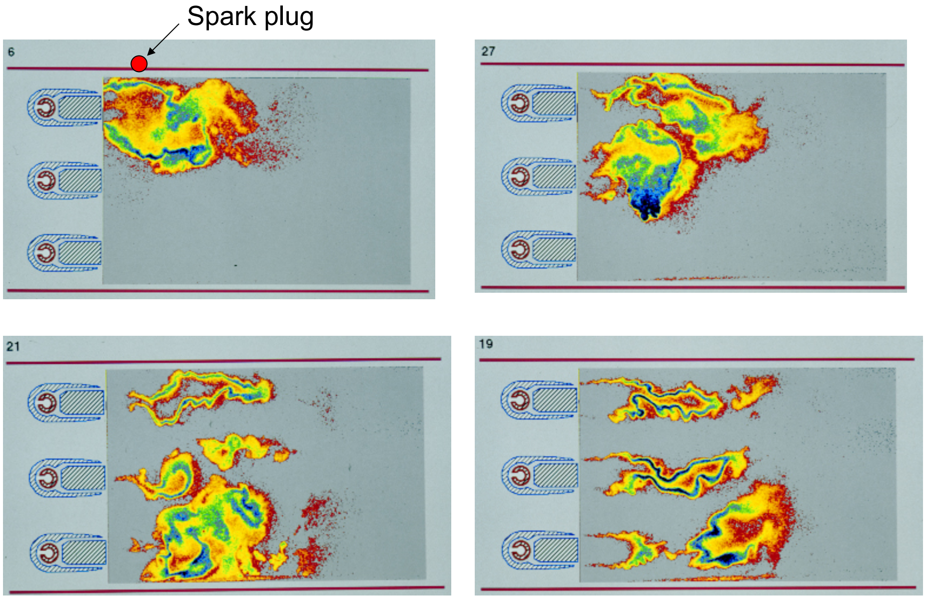

Ignition of the multiple injector combustor
(imaging by laser induced fluorescence of OH)

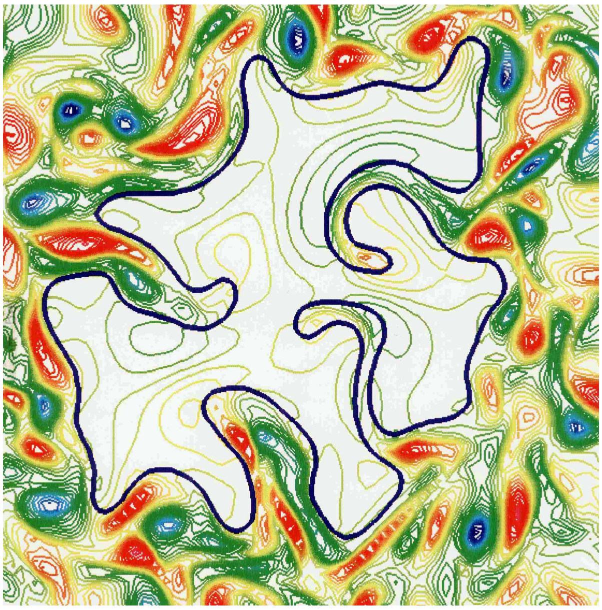

Direct simulation of ignition in homogeneous turbulence (T. Poinsot)

A pioneering LES of ignition in a gas turbine configuration

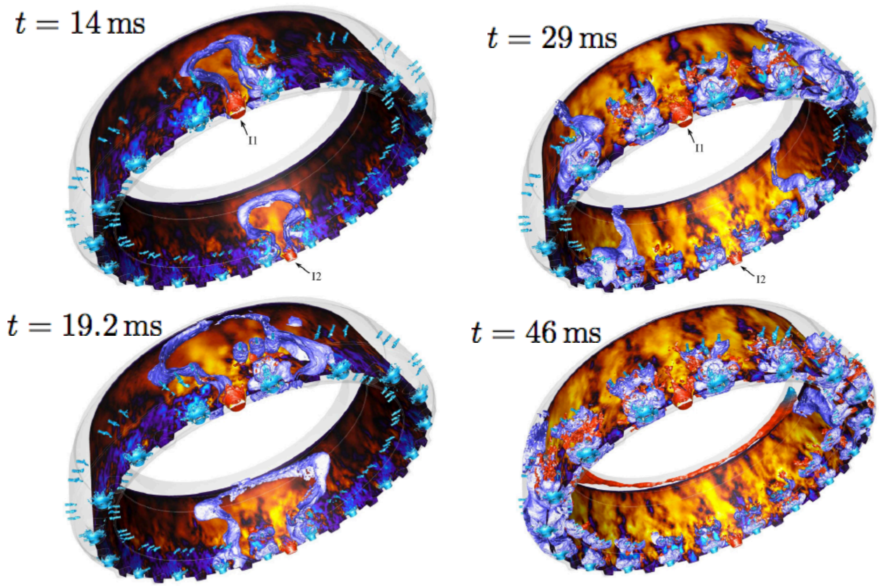

M. Boileau, G. Staffelbach, B. Cuenot, T. Poinsot and C. Bérat (2008) *Combust. Flame* 154, 2-22. LES of ignition in a gas turbine engine.

Ignition dynamics in annular combustors

CFM 56 turbofan

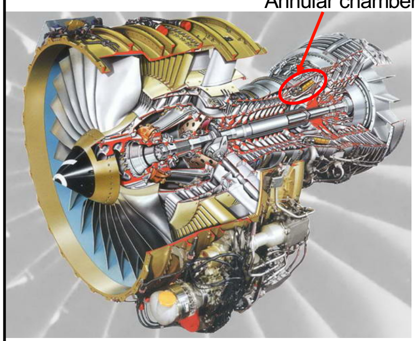

- Annular geometry
- Multiple swirled injectors
- Liquid phase injection (kerosine /air)
- High pressure

Annular combustor MICCA2

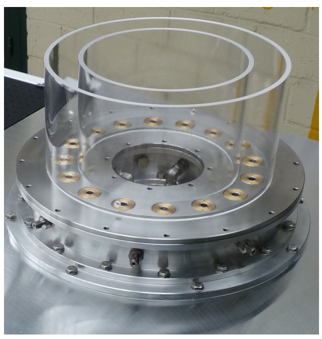

- Annular geometry
- Multiple swirled injectors
- Premixed (propane/air)
- Atmospheric pressure

Annular combustor MICCA-Spray

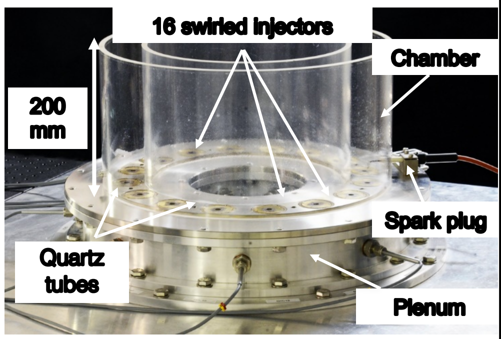

- Annular geometry
- Multiple swirled injectors
- Liquid injection (heptane/air)
- Atmopsheric pressure

Ignition dynamics in an annular combustor

High speed imaging

Frame rate

$$f_c = 1/6000\,\mathrm{s}$$

Exposure duration

$$\tau = 16.6\,\mu\mathrm{s}$$

Operating point

Bulk injection velocity

$$U_b = 12.2\,\mathrm{m/s}$$

Equivalence ratio

$$\phi = 0.76$$

Thermal power

$$P_{th} = 40\,\mathrm{kW}$$

J.F. Bourgouin, D. Durox, T. Schuller, J. Beaunier and S. Candel (2013) *Combust. and Flame*, **160**, 1398-1413. Ignition dynamics of an annular combustor equipped with multiple swirling injectors.

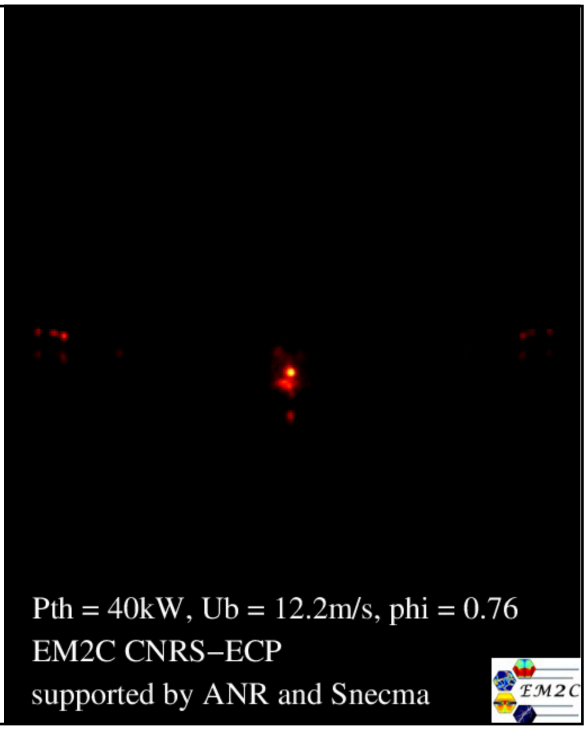

Light round ignition of the MICCA2 combustor

MICCA2 under nominal operation

J.F. Bourgouin, D. Durox, T. Schuller, J. Beaunier and S. Candel (2013) *Combust. and Flame*,160, 1398-1413. Ignition dynamics of an annular combustor equipped with multiple swirling injectors.

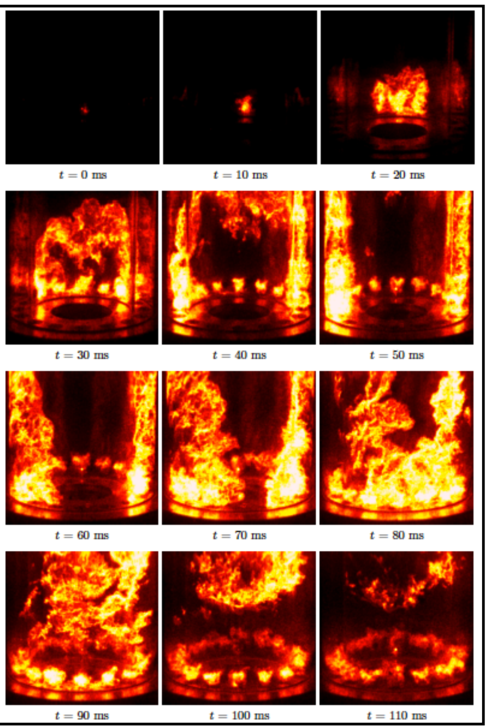

Light round ignition of the MICCA combustor. Experiment and simulation. $U_b = 18\,\mathrm{m\ s^{-1}}$

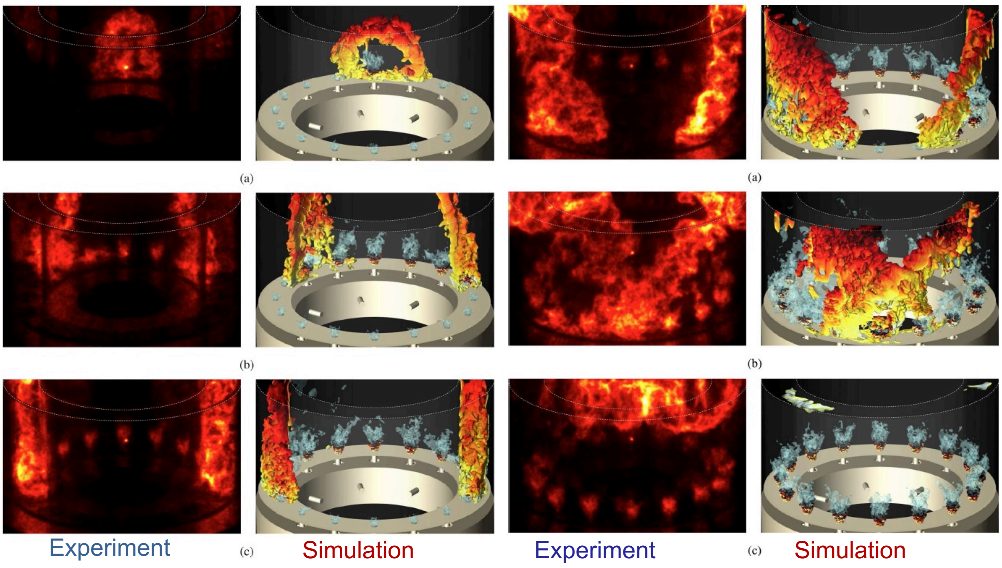

M. Philip, M. Boileau, R. Vicquelin, T. Schmitt, D. Durox, J.F. Bourgoin, S. Candel (2015) *Journal of Engineering for Gas Turbine and Power (ASME)* 137(3), 031501 Simulation of the ignition process in an annular multiple-injector combustor and comparison with experiments.

PARTNERSHIP FOR ADVANCED COMPUTING IN EUROPE

17

Light round ignition of the MICCA combustor. Experiment and simulation. $U_b = 24\,\mathrm{m\ s^{-1}}$

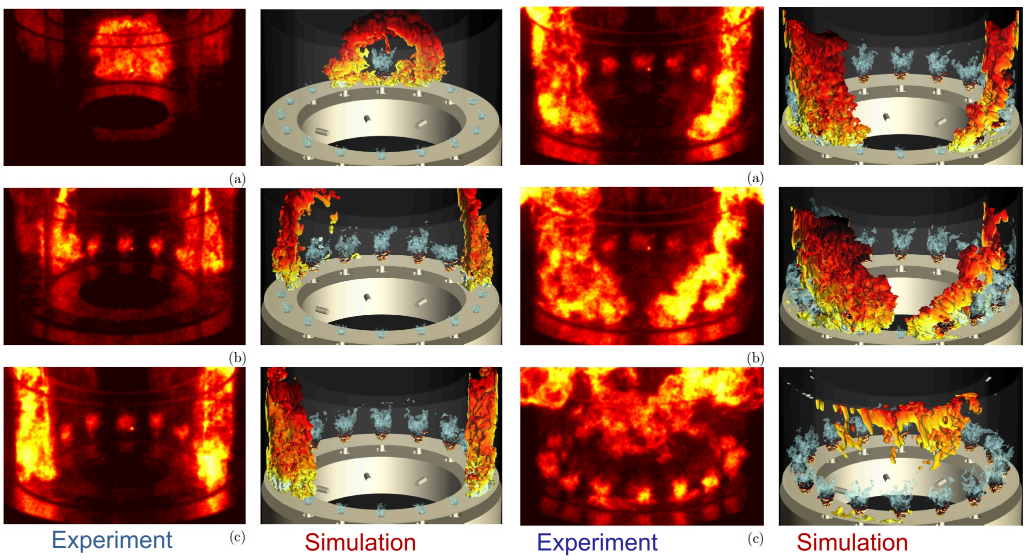

M. Philip, M. Boileau, R. Vicquelin, T. Schmitt, D. Durox, J.F. Bourgoin, S. Candel (2015) *Journal of Engineering for Gas Turbine and Power (ASME)* 137(3), 031501 Simulation of the ignition process in an annular multiple-injector combustor and comparison with experiments.

PARTNERSHIP FOR ADVANCED COMPUTING IN EUROPE

18

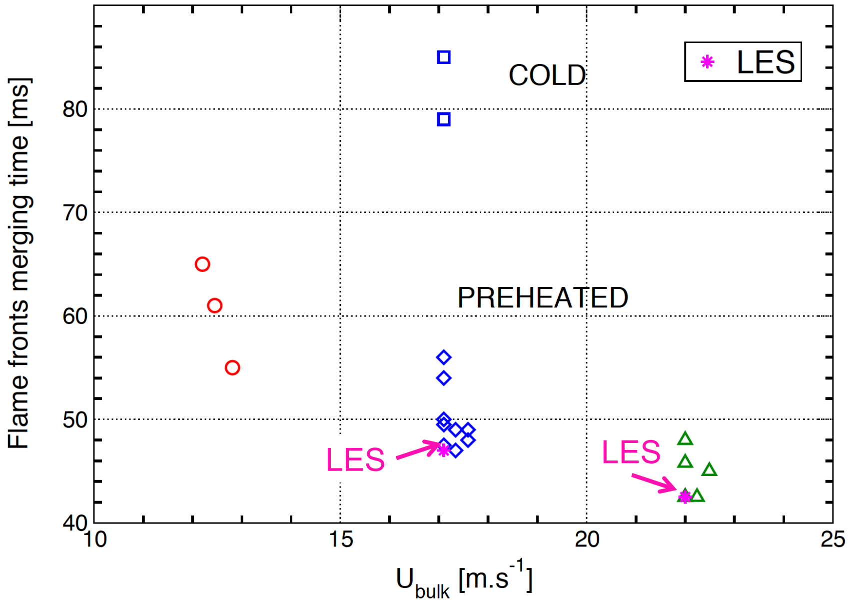

Flame fronts merging delay as a function of the bulk injection velocity. The magenta star symbols stand for the time lags determined from LES calculations

19

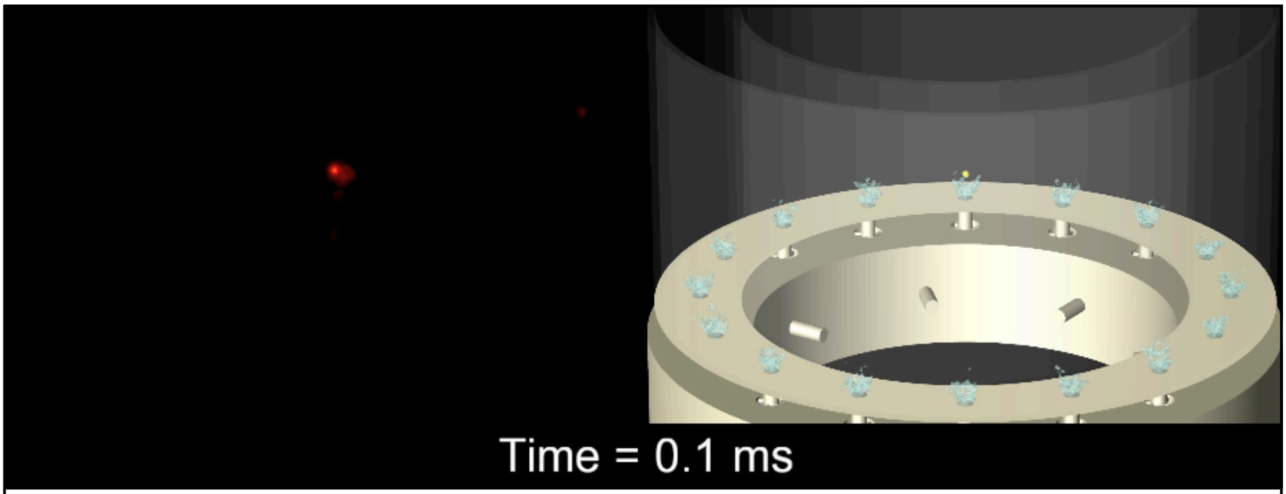

Experiment: light emission intensity from the flame represented in false colors

Large Eddy Simulation of the light round process

M. Philip, M. Boileau, R. Vicquelin, T. Schmitt, D. Durox, J.F. Bourgouin and S. Candel (2014) *Physics of fluids*, 26, 091106. Ignition sequence in a multi-injector combustor.

M. Philip, M. Boileau, R. Vicquelin, T. Schmitt, D. Durox, J.F. Bourgouin, S. Candel (2015) *Journal of Engineering for Gas Turbine and Power (ASME)* 137(3), 031501 Simulation of the ignition process in an annular multiple-injector combustor and comparison with experiments.

20

Light round ignition in MICCA-Spray

C_3H_8 Propane/air premixed

C_7H_{16} Heptane/air spray injection

$C_{12}H_{26}$ Dodecane/air spray injection

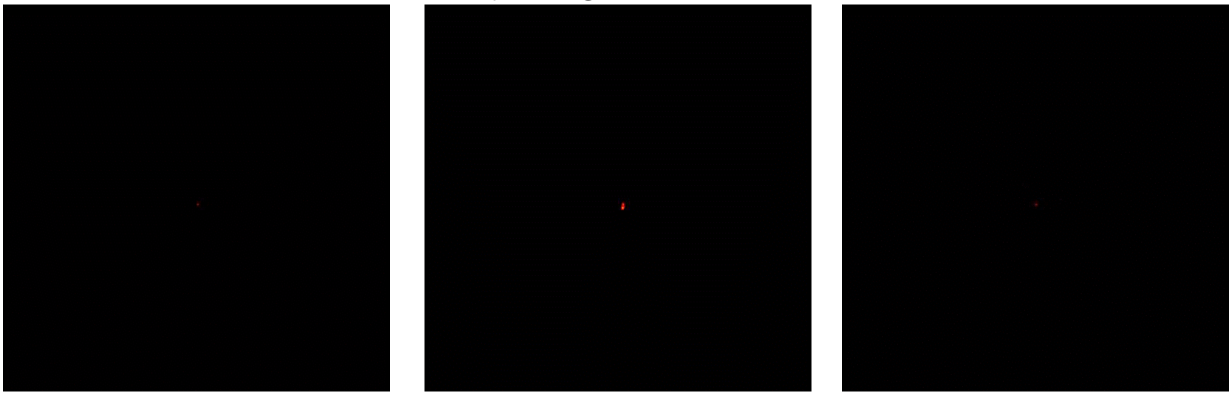

Filmed at 6000 fps, slowed down at 24 fps

K. Prieur, D. Durox, J. Beaunier, T. Schuller and S. Candel (2017) *Proceedings of the Combustion Institute.* 36, 3717-3724. Ignition dynamics in an annular combustor for liquid spray and premixed gaseous injection.

21

Flame and spray dynamics during the light-round process in an annular system equipped with multiple swirl spray injectors

Kevin Prieur, Daniel Durox, Guillaume Vignat, Thierry Schuller, Sébastien Candel

K. Prieur, D. Durox, G. Vignat, T. Schuller and S. Candel (2018) Flame and spray dynamics during the light-round process in an annular system equipped with multiple swirl spray injectors. *ASME Turbo-expo* ASME GT2018-78640 *Journal of Engineering for Gas Turbines and Power* JUNE 2019, Vol. 141 / 061007-11

université PARIS-SACLAY CentraleSupélec cnrs EM2C Agence Nationale de la Recherche ANR SAFRAN AEROSPACE · DEFENCE · SECURITY

22

Experimental Study of Ignition in Laboratory Scale Annular Combustors

Swirled Injector forms a Hollow Cone Spray C_7H_{16}/Air

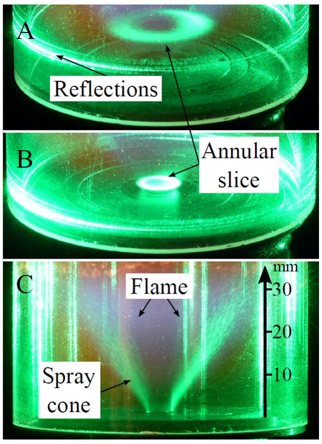

Impact of Fuel Volatility on the Light-Round Ignition Time in MICCA-Spray

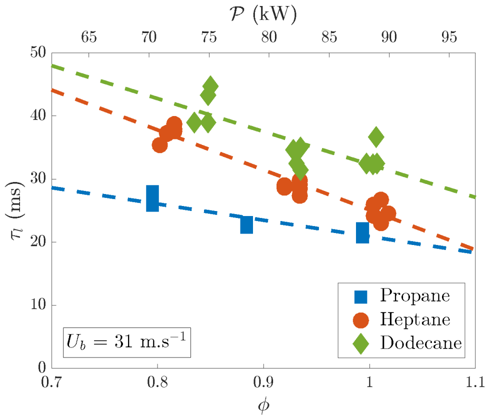

[1] Prieur, K, Durox, D, Beaunier, J, Schuller, T, Candel, S, *Ignition Dynamics in an Annular Combustor for Liquid Spray and Premixed Gaseous Injection,* **Proc Comb Inst**, 2016

23

MICCA: An Annular Laboratory Scale Combustion Chamber

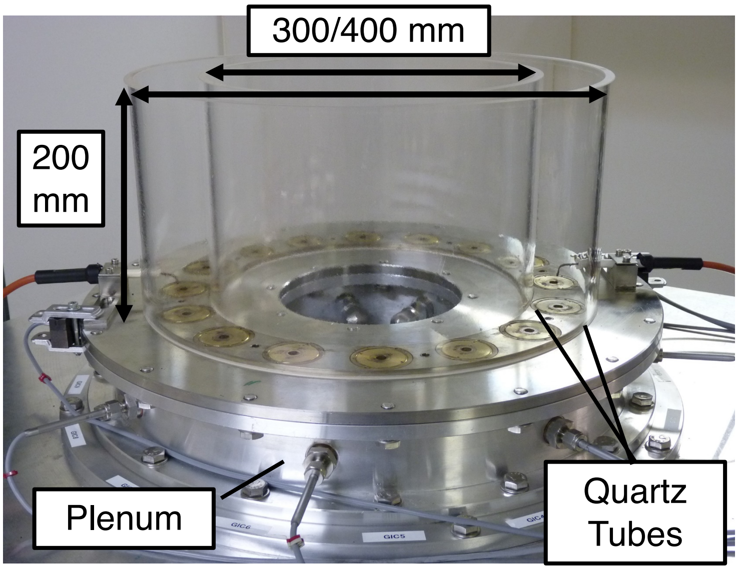

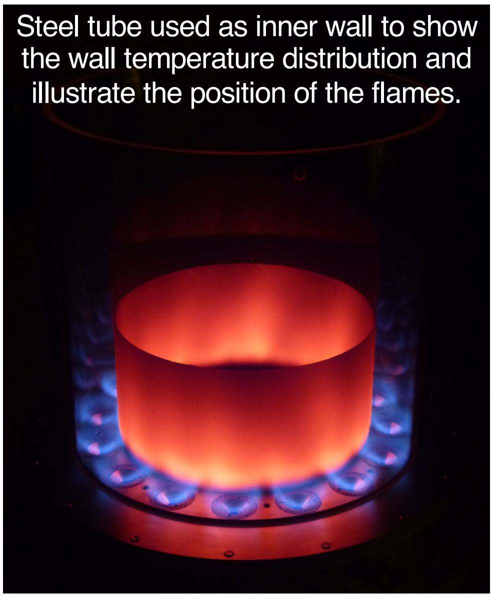

24

MICCA-Spray: An Annular Combustion Chamber with Swirl Spray Injectors

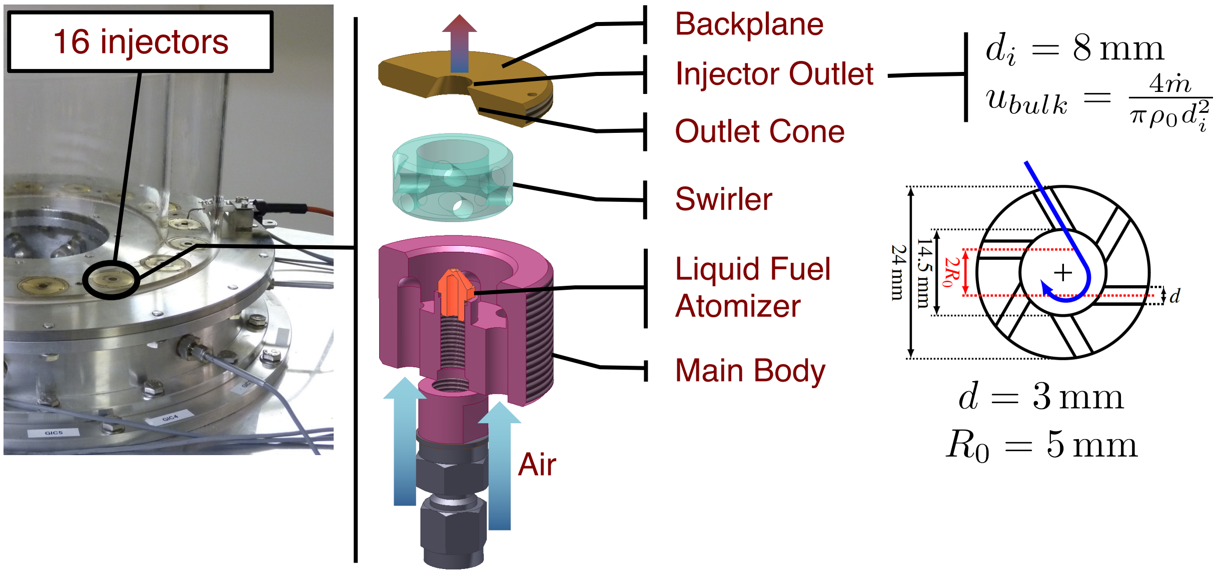

25

MICCA-Spray: An Annular Combustion Chamber

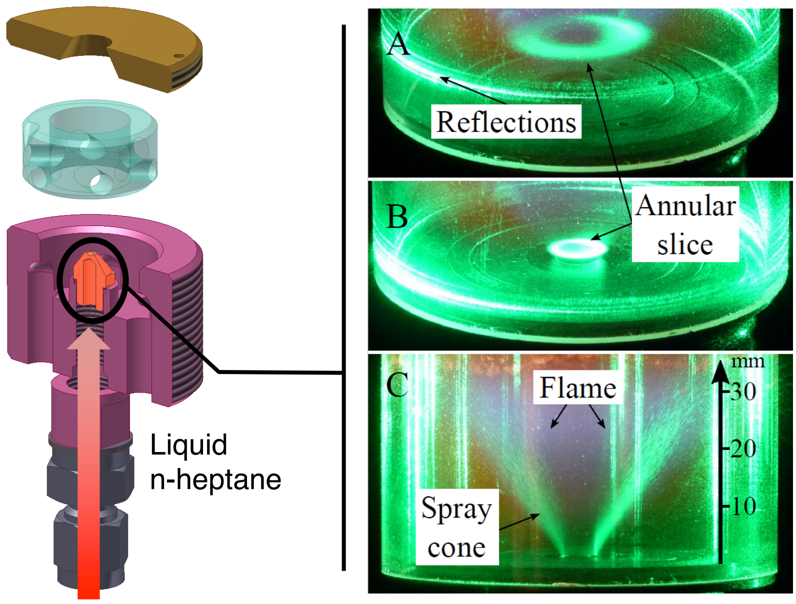

- Simplex atomizer
- Hollow cone spray
- n-heptane droplets
- $d_{32} = 27\,\mu\mathrm{m}$

A-B: horizontal laser sheet
C: vertical laser sheet

26

MICCA-Spray: Light-Round Process

n-heptane (liquid) / air

Equivalence ratio: 0.89

Bulk velocity: 31 m/s

Thermal power: 80 kW

Steps of the ignition process in an annular combustor

- Initiation of a hot gas kernel by the spark
- Expansion of the kernel leading to the ignition of the first injector
- Creation of two flame branches
- Propagation of these branches
- Flame merging

Phantom v2512
6 000 fps, 1280x800 pixels, Exposure $\Delta t = 166\ \mu s$
400 – 470 nm filter for CH* emissions

27

MICCA-Spray: Travelling Flame Branch

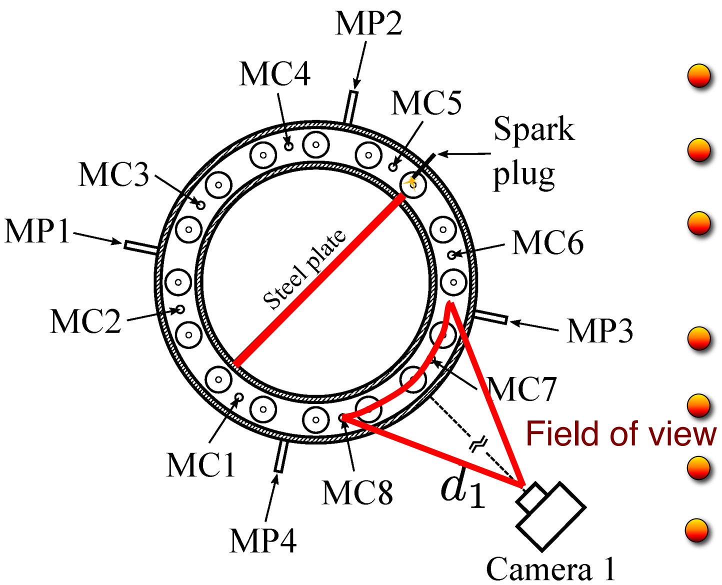

- Preheated combustor walls ($870\,\mathrm{K}$)
- Single spark plug ignition
- Central steel plate
  A single flame branch is filmed.
- n-Heptane (liquid) / Air
- $\phi = 0.89$
- $u_{bulk} = 31\,\mathrm{m\,s^{-1}}$
- $\mathcal{P} = 80\,\mathrm{kW}$

28

MICCA-Spray: Travelling Flame Branch

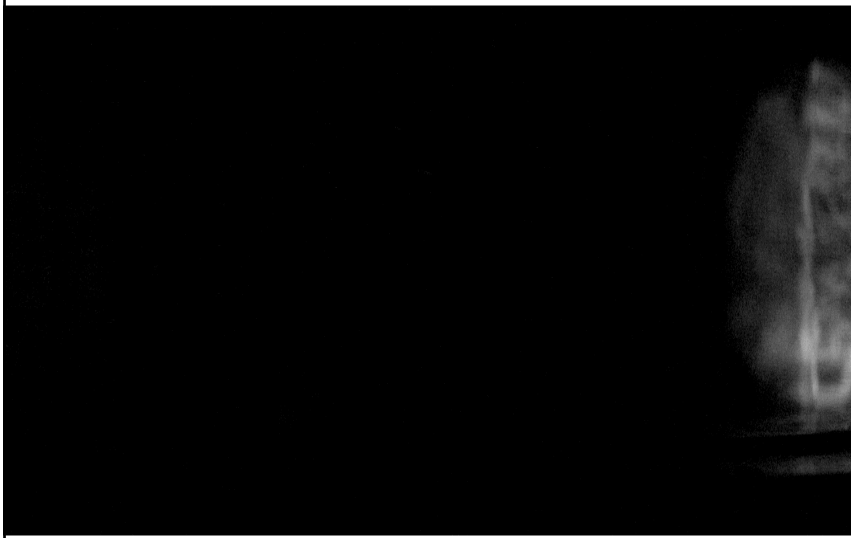

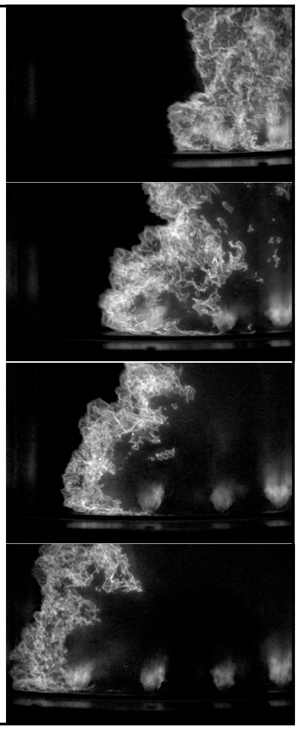

MICCA-Spray: Travelling Flame Branch

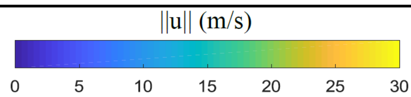

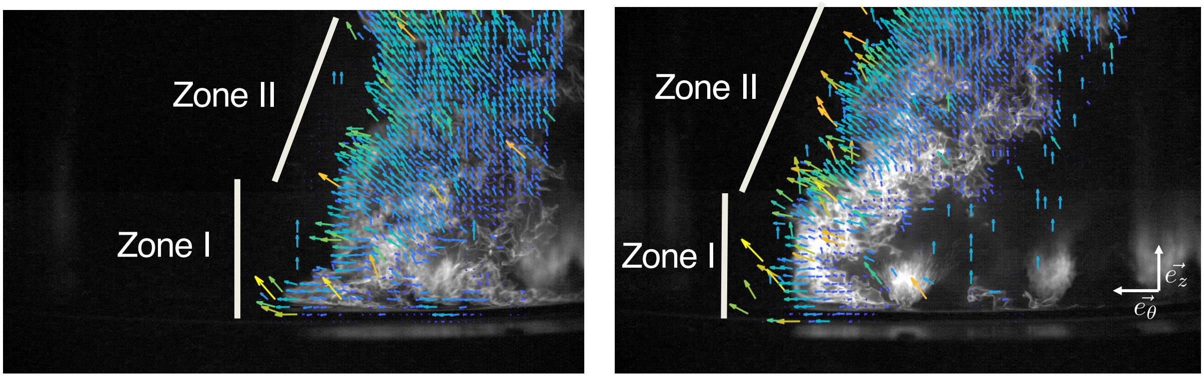

The volumetric expansion of the burned gases drives the movement of the flame.
Zone I: Close to the backplane, velocity mainly in the azimuthal direction,

$$v_\theta \approx 15 - 20\,\mathrm{m\,s^{-1}}$$

Zone II: Both azimuthal and axial components, $v_\theta \approx v_z$ and $\|v\| \approx 10 - 15\,\mathrm{m\,s^{-1}}$.

MICCA-Spray: Changes in Flame Shape during the Light-Round Process

MICCA-Spray: Changes in Flame Shape during the Light-Round Process

Direct CH* emission imaging

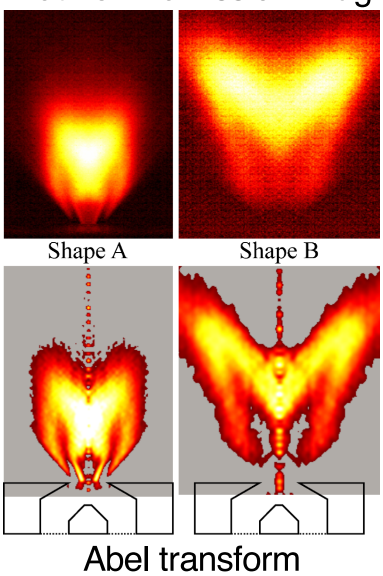

The ignition process is repeated several times.

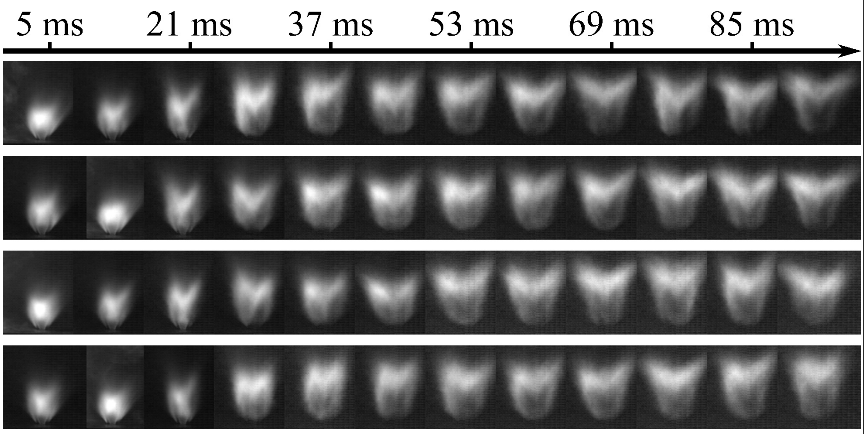

Transition from Shape A to Shape B in approximately $\tau_s = 40\,\mathrm{ms}$

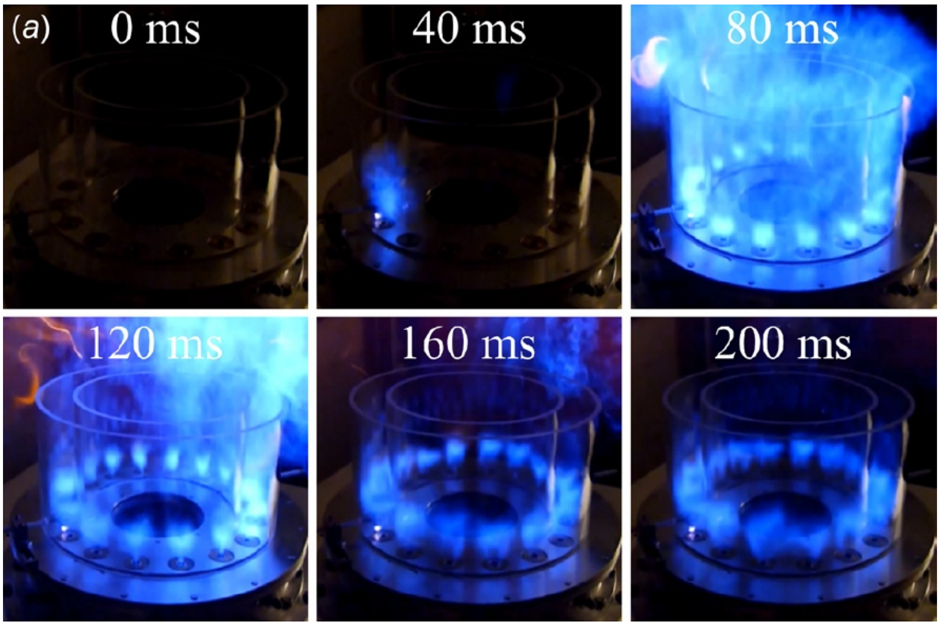

True-color low-speed images of the light-round in the MICCA combustion chamber under premixed propane-air conditions with $\phi = 0.76$ and $\mathcal{P} = 60$ kW.

33

SICCA-Spray measurements

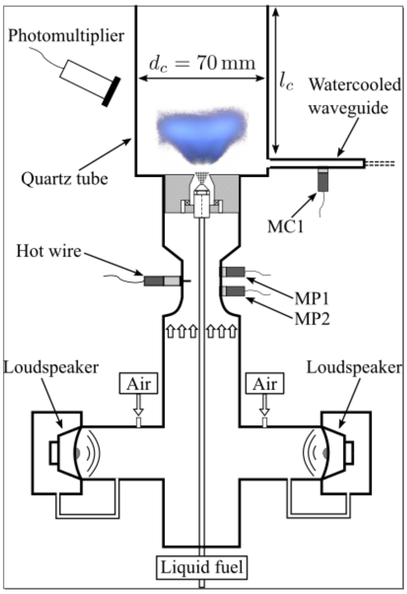

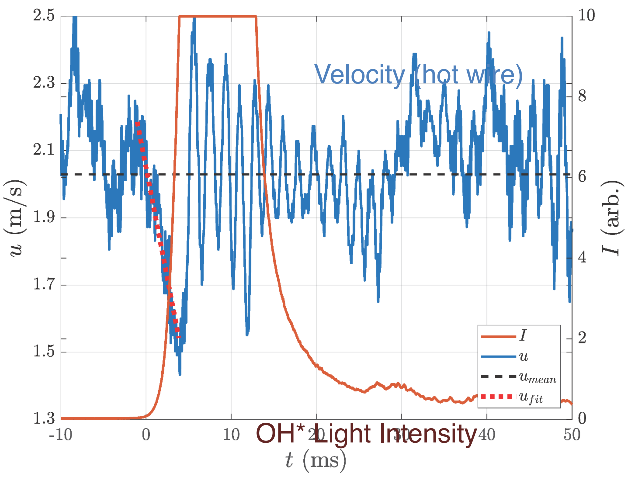

Velocity *u(t)* and flame luminosity *I(t)* signals during ignition of the single SICCA-Spray injector. The black-dotted line corresponds to the mean velocity at nominal operating conditions.

34

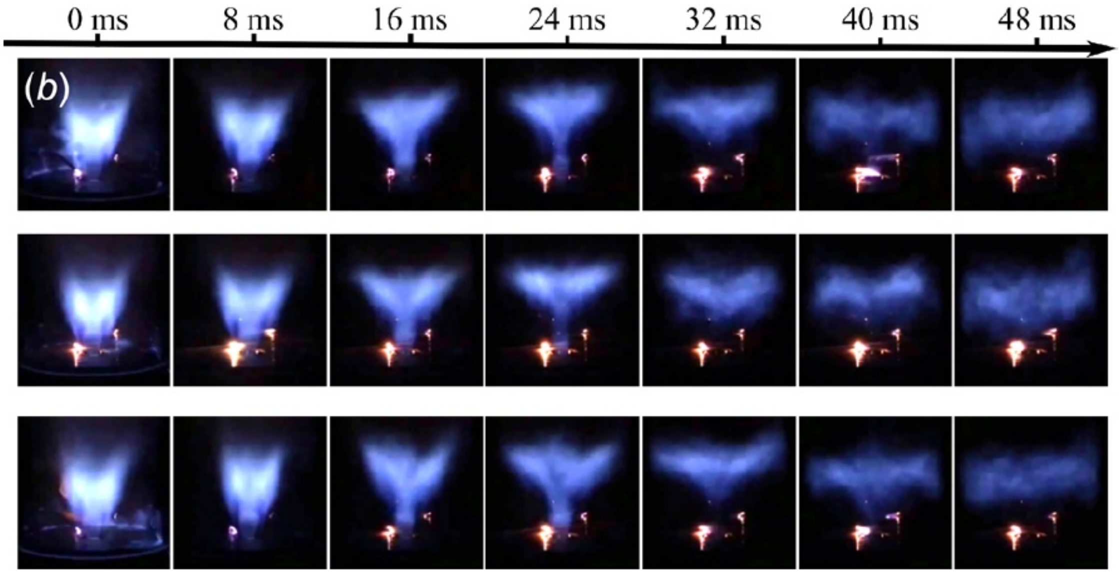

Three ignition sequences of the SICCA burner equipped with the premixed swirled injector with $\phi = 0.76$ and $\mathcal{P} = 3.75$ kW

Pressure perturbation associated with the rate of change of heat release is given by

$$\boxed{p'(\boldsymbol{r},t) = \frac{\gamma-1}{4\pi {c_0}^2}\int_V \frac{1}{|\boldsymbol{r}-\boldsymbol{r}_0|}\frac{\partial}{\partial t}\dot{Q}'(\boldsymbol{r}_0, t-|\boldsymbol{r}-\boldsymbol{r}_0|/c_0)dV(\boldsymbol{r}_0)}$$

The heat release occupies a compact region. One may use the heat release rate integrated over the whole region

$$p' \simeq \frac{\gamma-1}{4\pi c_0^2}\frac{1}{r}\frac{d\dot{Q}'}{dt}$$

In principle this expression is only valid in the farfield but it has been used under similar conditions with some success to estimate near field pressure perturbations (for example by Noiray et al)

To get the rate of change of heat release rate one uses

$$\Delta \dot{Q}' \simeq (80)\,(10^4)\ \mathrm{W} \qquad \Delta t = 4\,10^{-3}\ \mathrm{s}$$

(results of calculations by Thea Lancien)

$$\frac{d\dot{Q}'}{dt} \simeq \frac{(80)\,(10^4)}{(4)\,(10^{-3})} = 200\,\mathrm{MW\ s^{-1}}$$

$$p' \simeq \frac{0.4}{4\pi(340)^2}(2)(10^8)\frac{1}{r} \qquad p' \simeq 55.07\frac{1}{r}$$

For $r = 0.02$ m $\quad p' \simeq 2750\ \mathrm{Pa}$

The pressure disturbance induced by the rate of change of the heat release rate is of the order of 3000 Pa

Injector head loss

$$\Delta p = \frac{1}{2}\sigma\rho u_0^2$$

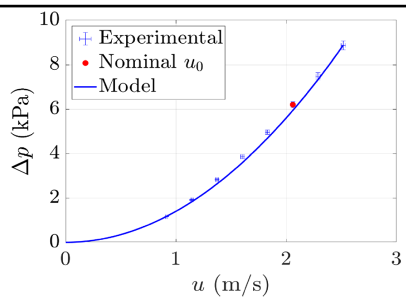

Pressure loss measurements in the SICCA-Spray burner as a function of the velocity at the hot-wire probe position. The value at the nominal operating conditions is indicated by a red dot

Model M1

$$\tau\frac{dv_*}{dt} + \frac{1}{2}v_*^2 = \frac{1}{2} + \frac{\Delta p'}{\sigma\rho u_0^2}$$

$$v_* = u/u_0$$
$$\tau = l/(\sigma u_0)$$

Model M2

$$\frac{1}{\omega_0^2}\frac{d^2v_*}{dt^2} + \tau\frac{dv_*}{dt} + \frac{1}{2}v_*^2 = \frac{1}{2} + \frac{\Delta p'}{\sigma\rho u_0^2}$$

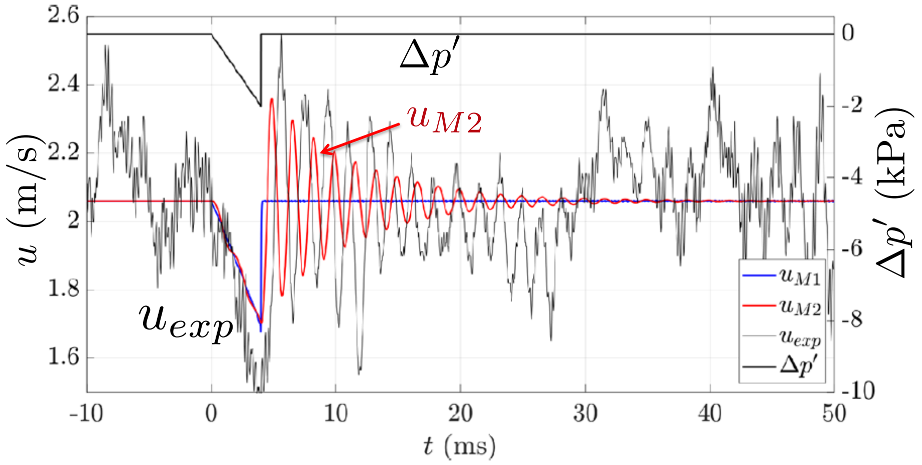

Velocity obtained at the hot wire position using model M1 (blue) and M2 (red). The velocity measured by the hot wire is shown as a thin black line. The pressure perturbation used for the present calculation is shown as a thicker black line on top, associated with the right axis.

K. Prieur, G. Vignat, D. Durox, T. Schuller and S. Candel (2018) Flame and spray dynamics during the light-round process in an annular system equipped with multiple swirl spray injectors. *ASME Turbo-expo* ASME GT2018-78640 *Journal of Engineering for Gas Turbines and Power* JUNE 2019, Vol. 141 / 061007-11

39